Improving the Performance of Polypropylene Matrix Composite Materials using Engineered Hemp Fibre Mats

A thesis

submitted in fulfilment

of the requirements for the degree

of

Doctor of Philosophy in Engineering

at

The University of Waikato

by

Tom Sunny

THE UNIVERSITY OF
WAIKATO
Te Whare Wānanga o Waikato

2021

Abstract

Projections of continuing demand for materials across the world is driving the development of more sustainable materials. The low energy consumption requirements, as well as recyclability found within the spectrum of natural fibre composites, has led to increased interest in improving these sustainable materials. Although the use of natural fibre composite materials has been documented in early civilisations, growing environmental concerns coupled with technological advancements have encouraged the expansion of their use in recent times. However, there are still significant issues, including their limited mechanical performance, that limit the ability to compete for future use. Amongst natural fibres, hemp fibres are an attractive alternative reinforcement to synthetic fibres due to their favourable mechanical properties as well as availability. Additionally, compared to other natural fibres, hemp fibres are more valuable for the bio-based economy due to its environmental benefits such as can be grown without pesticide and high yield of technical fibres. The hemp is cultivated in most of the EU countries.

However, to improve hemp fibre composites to further replace synthetic fibre composites, research is required. Presented in this thesis are experimental investigations on the properties of polypropylene matrix composites reinforced with hemp fibre mats produced using dynamic sheet forming (DSF) to align the short fibres used in the mats. The overall aim of this research was to improve the mechanical performance of hemp fibre mats produced using DSF and to assess the potential of these mats as reinforcement in polypropylene composites.

Two different alkali treatments were carried out on hemp fibres with the goal of producing fibre mats from high strength fibres using DSF, one at ambient and one at a higher temperature. The ambient temperature treatment was carried out using a solution of 5 wt% sodium hydroxide (NaOH), whereas the higher temperature treatment was carried out using a combination of 5 wt% sodium hydroxide and 2 wt% sodium sulphate (Na_2SO_3). The fibres were granulated either before or after the treatment and the effect of granulation was evaluated. Treated and untreated fibres were assessed using single fibre tensile testing, X-ray diffraction, scanning

electron microscopy (SEM), Fourier-transform infrared spectroscopy (FTIR) and thermogravimetric (TGA) analysis. It was found that the high temperature alkali treatment increased the tensile strength of the fibres by about 51 %, whereas the ambient temperature treatment decreased the tensile strength of the fibres to even lower than that of untreated fibres. Although granulation before or after the high temperature treatment had no significant effect on the tensile properties of the fibres, the fibres were found to have better separation when granulated after the high temperature treatment. Additionally, dynamic sheet forming (DSF) was found to be only possible with these better separated fibres for the production of aligned fibre mats.

An investigation was conducted into the effect of nozzle geometry in dynamic sheet forming (contraction ratio and exit shape) on the orientation (alignment) of fibres within the mats produced. Nozzles of different geometries were designed, 3D printed, fitted to the dynamic sheer former (the machine) and trialled to produce fibre mats. For the assessment of orientation, control samples, including highly aligned control sample and random mats, were produced. The alignment of fibres within hemp fibre mats was assessed using ImageJ (OrientationJ) and X-ray diffraction. Fibre orientations were quantified, mainly by means of coherency factors from image analysis of microscopic images using ImageJ and Herman's order parameter from analysis of results using XRD. These techniques were found to be in good agreement showing that the mats produced using DSF possess alignment with respect to the drum rotation direction (machine direction). Based on the literature, it was expected that nozzles with higher contraction ratios and circular exit shape would result in improved alignment of fibres within the mats compared to the nozzles with lower contraction ratio such as the current nozzle fitted to the machine. Although there was a trend of increasing fibre orientation for nozzles with the increase in contraction ratios, however, it was only significant for extreme cases (nozzles with the lowest and highest contraction ratios); the exit shape of a nozzle was found to have less influence on fibre orientation. A coherency factor of 0.23 and Herman's order parameter (f) of 0.464 was obtained for the mats made using the current nozzle in DSF compared to 0.11 and 0.139 for the random mats, respectively, indicating the potential of DSF to produce aligned fibre mats. Improvement attained for fibre orientation in this work is indicated by

the higher values of coherency factor (0.31 compared to 0.23) and Herman's order parameter (0.511 compared to 0.464) obtained for the fibre mats made using a high contraction ratio nozzle compared to those mats made using the current nozzle in DSF. The improvement was further supported by about 11 % increase in tensile strength for the composites with 30 wt% fibre mats made using the high contraction ratio nozzle compared to the tensile strength for those composites with fibre mats made using the current nozzle in DSF.

An investigation was conducted to assess the effect of surface treatments on fibre mats produced using DSF with the goal of improving the interface between the fibre and polypropylene. The fibre mats were treated with the addition of stearic acid (SA) or cellulose nanocrystals (CNCs). Untreated and treated fibre mats and composites made from these fibre mats were assessed using SEM, FTIR, Raman spectroscopy, swelling studies, water retention testing, TGA and tensile testing. The stearic acid treatment involved exposing mats to SA vapour, which reduced the hydrophilic nature of the fibre mats. It was found that improvements in tensile strengths in composites were obtained with the maleic anhydride polypropylene (MAPP) coupling agent and the stearic acid vapour treatment compared to composites with alkali only. The improvement with SA treatment was apparent only in composites without the MAPP coupling agent. The combination of SA and MAPP did not provide additive benefits in tensile strength of the composites. However, scanning electron microscopic images of their tensile fracture surfaces revealed more consistent interaction at the fibre-matrix interface with SA treated composites compared to the composite with only MAPP. This was also supported by the homogeneity in the tensile strength of composite samples indicated by the lower standard deviations with SA treatment. The CNC treatment involved a water-based spray and drying step, which increased the tensile strength of the fibre mats with 2 wt% CNC in water. In composites with 15 wt% fibre mats and with 2 wt% CNC treatment, the tensile strength and Young's modulus of composites significantly increased, by about 15 and 16 %, respectively. In contrast, composites with higher fibre contents (25 or 30 wt%) exhibited poor consolidation when CNC treated fibre mats were used. This poor consolidation is believed to related to CNC films formed between the fibres in the treated fibre

mats; these CNC films are likely to hinder the flow of polymer melt, resulting in insufficient wetting of fibres by the polymer.

In order to improve the mechanical performance of composites through high fibre content, different polymer sheet thicknesses and stacking arrangement were investigated. Generally, the strength and stiffness of fibre composites are expected to increase with increased fibre content, provided these composites have reasonable interfacial bonding between matrix and fibres, as the fibres are usually stronger and stiffer than the matrix. However, initial attempts to increase fibre content above 30 wt% resulted in declines of tensile properties of the composites. Scanning electron micrographs of tensile fracture surfaces of these composites revealed insufficient wetting of fibres by the matrix material. It was found that decreasing the overall thickness of fibre mats between two polymer sheets within the stacking arrangements of composites which decreased the travelling distance of polymer improved the fibre wetting through the composite and therefore improved the tensile properties. The strongest composite produced had a fibre content of about 60 wt%. At this fibre content, tensile strength and Young's modulus of the composites were found to be 3.0 and 6.9 times, respectively, higher than the control samples (PP/MAPP), while figures for flexural strength and flexural modulus were 3.4 and 3.6, respectively. The interface of the PP/hemp composites was assessed using a single fibre pull-out test. The composite was found to have an average interfacial shear strength of 8.7 MPa and a critical fibre length of 0.85 mm.

In conclusion, the investigation demonstrated that aligned short fibre mats could be produced from high strength hemp fibres using DSF. The performance of these fibre mats in composites can be improved in the following ways:

- Improving fibre orientation using a nozzle of high contraction ratio for dynamic sheet forming.
- Through altering surface properties using treatments such as stearic acid vapour treatment and spraying on cellulose nanocrystals, and
- Improving stacking arrangement/sheet thickness to allow high fibre content in composites while obtaining effective reinforcement and good fibre wetting and enhanced mechanical performance.

Acknowledgements

First of all, I would like to express my most respectful gratitude to my chief supervisor, Professor Kim Pickering, Associated Dean of Research (Division of Health, Engineering, Computing, & Science), for her invaluable advice, constant encouragement and patience throughout my PhD. I want to offer my sincere special thanks to Dr John McDonald Wharry, for being so supportive of my work. I would like to thank my co-supervisor, Dr Shen Hin Lim, for his support.

I am grateful to many other people who have assisted and supported me throughout my PhD journey.

I want to thank my parents, Sunny Joseph and Jancy Mathew, and my sister Dona Sunny, for their constant support, and all that they have provided me throughout my life. I would also like to express my gratitude to my parents-in-law and my brother-in-law for their constant emotional support.

The most special thank with love goes to my dear wife, Riya Tressa Augustian, who has been with me throughout this PhD, living every single minute of it, without whom I would not have completed my PhD journey. Also thanks to my new born daughter Hannah Clare Tom for being such a good girl.

Also, I want to thank all my family members, especially Riya, for their financial assistance.

And finally, I would also like to thank the technicians who helped for my research, especially Duncan, Jonathan, Helen, Chris, Yuanji, Ivan, Jenny and Anjana. Special thanks to Mary Dalbeth and Natalie Shaw for the administrative assistance. I am very grateful to other composite research group members, especially Maria, Humair, Safiya, Sandra, Xitan, Tim and Dr Christian for their constant encouragements and contributions to my studies.

Jeremiah 29:11 – *'For I know the plans I have for you, says the Lord, plans for welfare and not for evil, to give you a future and a hope'.*

Publications

Alkali treatment of hemp fibres for the production of aligned hemp fibre mats for composite reinforcement.

Tom Sunny, Kim L Pickering, Shen Hin Lim

Cellulose. Vol 27 Pages 2569-2582 Published 2020.

Fibre orientation distribution assessment of dynamically sheet formed hemp fibre mats by image analysis.

Tom Sunny, Kim L Pickering, Shen Hin Lim

Applied Mechanics and Materials, Volume 884, Pages 23-28 Published 2018.

Alignment of Short Fibres: An Overview.

Tom Sunny, Kim L Pickering, Shen Hin Lim

Proceeding In Processing and Fabrication of Advanced Materials – XXV. Conference held University of Auckland, New Zealand. Pages 617-625. Published 2016.

Table of Contents

List of Figures

List of Tables

Abbreviations and Symbols

NPFs	Natural plant fibres
NPFCs	Natural plant fibre composites
SNPF	Short natural plant fibre
GFRCs	Glass fibre reinforced composites
PP	Polypropylene
DSF	Dynamic sheet forming
ADF	Aligned discontinuous fibre
SNPFPCs	Short natural plant fibre polymer composites
SFRPCs	Short fibre reinforced polymer composites
NPFTC	Natural plant fibre thermoplastic composites
GMT	Glass-mat reinforced thermoplastic
HiPerDiF	High performance discontinuous fibre
MNS	Multiple nozzle system
UA	Ultrasonic alignment
SCORIM	Shear controlled orientation in injection moulding
MA	Maleic anhydride
MAPP	Maleic anhydride polypropylene
SA	Stearic acid
SP	Solution process
VP	Vapour process
NaOH	Sodium hydroxide
Na_2SO_3	Sodium sulphite
FTIR	Fourier transform infrared spectroscopy
NC	Nanocellulose
BC	Bacterial cellulose
CNC	Cellulose nanocrystals

CNF	Cellulose nanofibrils
BNC	Bacterial nanocellulose
IM	Injection moulding
CM	Compression moulding
FFT	Fast Fourier transform
XRD	X-ray diffraction
TGA	Thermogravimetric analysis
ASTM	American Society for Testing and Materials
SEM	Scanning electron microscopy
TS	Tensile strength
YM	Young's modulus
H	Hemp
MROM	Modified rule of mixtures
ISO	International Organisation for Standardisation
FWHM	Full width at half maximum
IFSS	Interfacial shear strength

Symbols

L_c	Critical fibre length
d	Fibre diameter
σ_f	Fibre tensile strength
τ_i	Interfacial shear strength
K_θ	Fibre orientation factor
σ_o	Characteristic stress
L_i	Sub-critical fibre length
L_j	Super-critical fibre length

v_i	Volume fraction of Sub-critical
v_j	Volume fraction of super-critical
k_{st}	Stress-transfer efficiency factor
I_C	Crystallinity index
σ	Tensile strength
E	Young's modulus
V	Volume fraction
V_f	Fibre volume fraction
Vm	Matrix volume fraction

1 Chapter One

Introduction

1.1 Overview of Composite Materials

In response to the demand of various manufacturing industries for low density and high performance structural materials at low cost, different composite materials have been developed [1]. Today, many industries, particularly aerospace, sports and automotive, are quite dependent on fibre reinforced polymer composites [2, 3]. The main potential advantage of fibre reinforced polymer composites, commonly known as polymer matrix composites (PMCs) over conventional structural materials is their low density, which results in higher specific properties of these composites when strong and stiff fibres are used. The higher specific properties are of great importance in moving components (e.g. transportation) where weight reduction can result in energy savings and reduced operating costs.

The reinforcement fibres in PMCs can be either synthetic (human-made) or natural and are often encapsulated in a more ductile matrix material. In most cases, the reinforcement is stronger and stiffer than the matrix. Natural fibres have been of increasing attention for the past couple of decades due to their advantages such as high specific properties at a low cost, low energy consumption and environmentally friendly when compared to traditional reinforcing synthetic fibres such as glass [4].

A composite material may have a metal, ceramic, intermetallic, polymer, carbon or cement matrix [5-7]. The matrix holds the fibres together, and transfers applied stresses from the composites to the fibres via the interface. The distinct constituents of a composite separated by an interface can be viewed on a microscopic scale.

The proportions and properties of the reinforcement and the matrix have a strong influence on the properties of the resulting composite. The strength characteristic of

the interface between the fibres and the matrix is also important in determining the properties of the composite. Subsequently, some other parameters which can significantly influence the properties of the composites are the size, shape, orientation distribution of reinforcement and the direction at which the force are being applied. When reasonable interfacial strength is established, generally, the volume fraction of constituents is regarded as an important parameter influencing the properties of a composite. Additionally, in order to suit the application, the volume fraction is a readily controllable manufacturing variable by which the properties of a composite can be altered [8].

The reinforcements in a composite can be fibrous or particulate. When compared to particulate reinforcements, the fibre reinforcements bring about greater improvements in various properties of the matrix material, especially strength and stiffness. Thus, the high performance fibre reinforcements are a greater focus of research in recent times [2, 9, 10]. Fibres such as carbon, aramid and glass are the commonly used synthetic fibres, with carbon and aramid used in composites that require high performance with extremely high tensile properties. Nevertheless, the most commonly used synthetic fibres in composites are glass fibres due to their lower cost and acceptable tensile properties. Natural fibres such as hemp, flax, jute and kenaf are the commonly used non-wood fibres in composites [2]. Increasing environmental awareness, coupled with the increasing demand for composite materials, has encouraged the use of natural plant fibres (NPFs) as reinforcement in PMCs, especially to replace synthetic fibres in applications where glass fibre is typically used. The focus of this research is on improving the performance of polymer composites made from natural plant fibres.

The reinforcing fibres used in composites can also be either in continuous or discontinuous forms. Research data largely reported on synthetic fibre composites revealed that composites reinforced with continuous fibres provided superior mechanical properties as the fibres can be easily aligned towards the loading direction [11]. However, discontinuous fibre composites are becoming more attractive with major benefits, including their low cost and ease of manufacture [12, 13]. In a composite, the reinforcement fibre carries most of the applied load, providing most of the stiffness and strength to the composite [14]. Thus, the selection

of fibres with reasonable mechanical performance is essential. Another important criteria to be considered with the selection of natural fibres is their local availability with long transport distances, increasing the overall energy consumption in the production of a composite [15]. In order to obtain an environmentally friendly composite, the selection of the matrix is also important, with biodegradability or recyclability as considerations. Generally, PMCs consist of either a thermoplastic matrix or a thermoset matrix. Thermosets cannot be re-melted once cured, whereas thermoplastics can be repeatedly melted, enabling recycling. Among thermoplastics, the most common matrices adopted for the natural plant fibre composites (NPFCs) are polypropylene (PP) and polyethylene (PE) as they are easy to process and simple to recycle [2].

1.1.1 Natural plant fibre composites

The natural plant fibres (NPFs) have undergone industrial uptake because of their favourable characteristics such as low density and cost. NPFs can be classified into two broad categories: wood and non-wood fibres [16, 17]. Non-wood fibres, such as flax and hemp, tend to be stronger than wood fibres, and along with their low density can in some cases, have comparable or higher specific tensile properties than glass fibres [16]. When compared to synthetic fibres, NPFs are renewable and have fewer concerns associated with health and safety during handling and manufacturing [18]. Additionally, when sourced from plants, the rapid growing NPFs, such as hemp, can be potentially considered carbon dioxide (CO_2) neutral. All plants utilise CO_2 when they grow and a similar emission of CO_2 occurs when the fibres are burned after their service life [10], whereas, processing synthetic fibres is energy-intensive and usually generates CO_2 [19]. Table 1.1 represents the specific properties comparison of hemp and glass fibres. As can be seen, hemp fibres have higher specific Young's modulus. Most of the interior parts in automobiles are mainly designed for low density and high stiffness [17], and hemp fibres are well-suited for this application [20]. Research findings have shown that the composites made of natural fibres perform better or were almost similar in terms of specific properties when compared to composites made of synthetic glass fibres [11, 21]. A detailed comparison between composites reinforced with the glass and natural fibres is further discussed in Chapter 2.

Table 1.1: Specific properties comparison of hemp and glass fibres [4, 17]

Property	Hemp fibres	Glass fibres
Density (g/cm^3)	1.48 -1.55	2.55
Tensile strength (MPa)	550 - 1110	1400 - 3000
Young's modulus (GPa)	58 - 70	70
Specific tensile strength (MPa per g/cm^3)	370 - 740	800 - 1400
Specific Young's modulus (GPa per g/cm^3)	39-47	29

A composite where polymers are reinforced with NPFs can be referred to as natural plant fibre composites (NPFCs). The natural plant fibre composites possess many advantages over conventional synthetic fibre polymer composites (SFPCs) such as lower density, lower cost, higher specific Young's modulus and are more sustainable as they can be processed with low energy consumption [16]. Excellent price-performance ratios with environmental sustainability benefits have resulted in increasing adoption of compression moulded natural fibre thermoplastic components in the European automotive industry [4]. A life cycle assessment study, which compared under-floor panels made from SFPCs with those made from NPFCs reported that the NPFCs were more attractive in terms of lower environmental impacts [12]. Although NPFCs have the potential for many engineering applications, further research is required to improve their durability (long-term performance), mechanical performance and fire retardance for successful commercialisation in more demanding applications [2, 4].

The applications of natural plant fibre composites in various industries are presented in Table 1.2. As mentioned before, most of the automobile interior parts are designed for weight reduction and stiffness [17], thus making natural fibre composites well-suited for automotive parts.

Table 1.2: Application of natural fibre composites in various industries [20, 22, 23]

Application (depends on manufacturers)	Industry	Manufacturers
Door panels, dashboard, instrument panel, seats back cover, linings (spare tire, boot)	Automotive	Audi, BMW, Daimler/Chrysler, Fiat, Ford, Opel, Peugeot, Renault, Rover, Saab, SEAT, Volkswagen, Volvo
Surfboard, skateboard, automotive interior parts	Sports /Automotive	Bcomp®
Furnishings for office and homes, modular house constructions	Furniture	FlexForm Technologies, Tech Wood International
Bio-based granulates	Casings for musical instruments/Automotive	Aqvacomp
Natural fibre pellets for injection moulding	Automotive/Non-automotive	HIB-Trim Part Solutions

1.2 Research Rationale

As with all composites, the mechanical performance of NPFCs not only depends on the properties of its constituents but also depends on the fibre orientation, distribution of fibres within the matrix as well as fibre/matrix interfaces and fibre content [15]. Previous research outcomes suggest the best mechanical properties are generally exhibited by the composites when the fibres are aligned to the loading direction [20, 24, 25]. There are various alignment techniques developed by researchers to manufacture aligned short fibre reinforced polymer composites, which will be discussed in detail in Chapter 2. Natural fibres can be fabricated to number of forms such as long yarns (produced by spinning processes), braided mats, woven and nonwoven mats, chopped-strand (with a binder) and chopped random-mats (no binder). However, literature reports that random mats are commonly used as they are low cost [26]. It has also been reported in the literature that to further reduce the

environmental impacts on the production of NPFs as reinforcements in composites, the key consideration would be to produce aligned NPF reinforcements without the requirement for energy-intensive spinning operations [12]. Research outcomes suggest dynamic sheet forming (DSF), a typical paper production method, has the potential for the production of short fibre mats with preferential alignment with respect to drum rotation direction [27, 28]. However, more research needs to be carried out to improve the production of DSF in order to improve the alignment of fibres within the fibre mats produced.

There are usually limited interactions between the hydrophilic natural fibres and hydrophobic polymer matrices, which commonly leads to their poor mechanical performance [29]. Additionally, weak fibre-matrix interface increase the moisture uptake of these composites, which affects their long-term performance [5]. For good interfacial bonding to occur, the matrix material must fully wet around the fibre. Thus, wettability of fibre by the matrix material should be considered as an important precursor to bonding. Extensive research has been carried out to improve the interfacial bonding between the fibre and the matrix, modifying the fibre surfaces by chemical or physical approaches and modifying the matrix by addition of a coupling agent. However, there are only limited works for thermoplastic reinforced with non-wood aligned fibre mats produced using DSF and these studies were conducted with polylactic acid (PLA) matrix [16, 27, 30-33]. Therefore, more research is required to develop composites with these aligned mats which could improve the mechanical performance of composites.

In the present study, research has been conducted to address some of the issues mentioned above. Alkali treated hemp and harakeke fibres have been reported as used for the production of DSF mats, [4, 16, 34] but the tensile strengths of these treated fibres were reduced compared to raw fibre due to the weakening of structural components [16, 27, 35, 36]. Therefore, a fibre processing approach producing short aligned hemp fibre mats from high strength fibres using DSF was introduced. Efforts were made to increase the performance of fibre mats produced using DSF as reinforcements in composites. The nozzles supplied for dynamic sheet forming commonly have a rounded-rectangular exit shape with a low contraction ratio. However, based on the literature, it was expected that nozzles with higher

contraction ratios [37-39] and a circular exit shape [40, 41] would result in mats with improved alignment of fibres and therefore lead to increased tensile performance of composites made from these mats in the alignment direction. Research has shown that treatment with stearic acid can be carried out via solution or vapour phase methods [42]. The most popular is by solution, which involves dissolving stearic acid in an appropriate solvent (most commonly in an ethyl alcohol solution) [5, 8]. However, the vapour phase treatment can be considered more environmentally friendly as there is no solvent involved. Although there is extensive research reporting for improvement of interfacial bonding through the use of selected fibre treatments and coupling agents [2, 4], no research has been carried out to assess stearic acid vapour treatment of fibre mats for reinforcement of composites. Different approaches are being used by researchers to modify natural fibre surfaces with nanocellulose: culturing cellulose producing bacteria in the presence of natural fibres, dipping natural fibres in a suspension containing bacterial cellulose followed by vacuum filtration, consolidation and drying to form the nonwoven mats. If successful, a basic spraying operation would offer greater potential for ease and improved time-effectiveness with in-line processing of mats. Additionally, studies were carried out to assess the effect of stacking arrangements and polymer sheet thicknesses for the production of composites in order to achieve high fibre content, thereby improving the mechanical performance of composites. These methods for improving the tensile properties of the composites were carried out though environmentally friendly methods.

1.3 Research Objectives

The current research aims to improve the performance of aligned fibre mats produced using DSF and to assess the potential of these mats as reinforcement in polypropylene composites. The specific objectives of the current work are summarised as follows:

1. To gain an understanding of natural fibre composites, and to gain an insight into techniques used to manufacture aligned short fibre composites.
2. To improve the mechanical properties and fibre separation of hemp fibres through chemical treatment in order to produce aligned fibre mats with high strength hemp fibres using dynamic sheet forming.

3. To improve the orientation of fibres within the mats produced using dynamic sheet forming.
4. To improve the performance of fibre mats by means of surface treatments (stearic acid vapour and cellulose nanocrystals) and to assess the effect of these treatments on the mechanical performance of composites.
5. To improve the mechanical performance of composites through high fibre contents.

1.4 Thesis outlines

This thesis is divided into eight chapters. Chapter 1 gives an introduction to the study, including research rationale, thesis objectives and an outline of the thesis. Chapter 2 presents relevant literature, including a short description of different methods used to manufacture short fibre composites. Chapter 3 covers the work done to produce high strength hemp fibres with better separation by means of alkali treatment. Chapter 4 investigates the effect of nozzle geometry on the orientation of fibres within the DSF mats. Fibre orientation was assessed using ImageJ and X-ray diffraction methods and the effect of fibre orientation on tensile properties are also discussed in this chapter. Chapter 5 covers the effect of stearic acid vapour and cellulose nanocrystal treatments on the mechanical properties of the composites. Chapter 6 investigates the effect of sheet thickness and stacking arrangement in the production of composites to achieve high fibre content in composites. The effect of fibre contents on the various mechanical properties the composites is also discussed. Chapter 7 draws the main conclusions of the studies. Finally, Chapter 8 suggests some recommendations and future works based on the findings of the study.

2 Chapter Two

Literature Review

2.1 Introduction

A major area of recent technological development has been that of natural plant fibre composites (NPFCs). Growing environmental concern and the pressure for sustainable development have encouraged the use of NPFCs as an alternative to conventional composites. The main constituents of NPFCs include plant fibres as the reinforcement and often polymer based matrix. Plant fibres are formed sustainably by photosynthesis and have gained significant importance because of their favoured characteristics such as low density, high specific strength, recyclability, low cost, environmental safety, low energy consumption and low hazard manufacturing [2, 4, 29]. Natural plant fibres (NPFs) are broadly classified as non-wood fibres and wood fibres, of which non-wood fibres, such as flax, hemp, jute, kenaf and harakeke (Phormium-tenax) are stronger. The matrix contains and holds the plant fibres in place and transfers the applied loads to them.

Plant fibres are lignocellulosic, and the presence of numerous hydroxyl groups make them hydrophilic in nature [29]. Polymeric matrices, although generally hydrophobic, are preferred for NPFCs due to their low density and ability to process at low temperatures [2]. Matrix selection is limited for NPFCs as the thermal stability of plant fibres is very poor above 200 °C, although under some conditions they can be processed at a maximum of 240 °C for short periods of time [43, 44]. Due to this limitation, polymers that can be processed below 200 °C are preferred as a matrix for NPFCs. The mechanical performance of natural fibres not only depends on fibre and matrix selection, but also on fibre length, fibre orientation, fibre dispersion, interfacial strength, and processing methods.

The combination of excellent price-performance ratios at low weight and environmentally friendly characteristics are making NPFCs increasingly popular in

the automotive and construction industries [31, 45]. Other than these industries, NPFCs are also found in aerospace, sports, office products, machinery, toys, funeral articles, packaging and cases for laptops and mobiles [4, 12, 46, 47]. However, moisture absorption, limited interfacial strength between the hydrophilic fibre and hydrophobic matrix, poor fire retardance and sub-optimal mechanical performance are limiting the applications of NPFCs. Therefore, further research needs to be carried out to extend the application range of NPFCs and to further replace synthetic fibres.

2.2 Natural Fibres

Natural fibres are commonly categorised as plant, animal or mineral fibres based on their origin. Cellulose, hemicellulose and lignin are the major components of plant fibres, whilst proteins such as collagen and keratin dominate in animal fibres. Mineral based fibres, mainly found within the asbestos group of minerals, are avoided nowadays due to health risks. Plant fibres are more popular than synthetic fibres due to their availability as they are grown in many countries and can be harvested in short periods and are a higher strength and stiffness (except silk which is expensive).

2.3 Types of Natural Plant Fibres (NPFs)

The majority of useful natural textile fibres are derived from plants, except wool and silk. Plant fibres are generally classified as primary plant fibres and secondary plant fibres. Some fibres, such as jute, hemp, kenaf, sisal and cotton are from plants grown for their fibre content, whereas other plant fibres such as pineapple, agave, and oil palm fibres arise as a by-product.

Plant fibres can be split as follows by botanical type [2]:

1. bast fibres (from the outer portions of stalks) such as jute, flax, hemp, ramie and kenaf
2. leaf fibres such as banana, sisal, agavae and pineapple
3. seed fibres such as coir, cotton and kapok
4. core fibres (from stalks) such as kenaf, hemp and jute
5. grass and reed such as wheat, corn and rice and
6. all other types such as wood and roots.

2.4 Selection of NPFs for Composites

To manufacture high performance plant fibre composites, it is very important to incorporate high strength reinforcing fibres. The mechanical properties of plant fibres depend upon many factors other than botanical type. These include chemical composition and structure, harvesting time, extraction method, treatment and storage conditions. Among the different types of plant fibres, bast fibres have the highest specific moduli and tensile strengths, which is considered to be mainly due to their higher cellulose content and their cellulose microfibrils aligned more in fibre direction [4]. Table 2.1 shows the mechanical properties of some NPFs.

Table 2.1: Mechanical properties of some of the NPFs [2, 4]

NPFs	Tensile strength (MPa)	Young's modulus (GPa)	Density (g/cm^3)	Specific tensile strength (MPa/gcm^{-3})	Specific Young's modulus (GPa/gcm^{-3})
Flax	345-1830	27-80	1.5	230-1220	18-53
Hemp	550-1110	58-70	1.5	370-740	39-47
Jute	393-800	10-55	1.3-1.5	300-610	7.1-39
Harakeke	440-990	14-33	1.3	338-761	11-25
Sisal	507-855	9.4-28	1.3-1.5	362-610	6.7-20

Hemp is one of the most utilised bast fibres. It exhibits high tensile strength ranging between 550 and 1110 MPa, specific Young's moduli ranging between 39 and 47 GPa/gcm^{-3} [4], and also environmentally friendly since it can be grown without pesticides and herbicides [48]. Hemp is being considered as a suitable NPF reinforcement for use in the present research because of its local availability and good mechanical properties.

2.4.1 Industrial hemp fibre

Industrial hemp is the term utilised for hemp grown for industrial use, selected such that it naturally attains a tetrahydrocannabinol (psychoactive chemical) content below 0.6 %. It is a fast growing annual plant, which has a height of up to 5 m (1.2-5 m) and stem diameter between 4 and 20 mm [2]. It has separate male plants and

female plants. Male plants are taller, more slender and with a small number of leaves surrounding the flowers. Female plants are characterised as shorter, stockier and have more leaves meeting at each inflorescence.

A dried hemp stalk is shown in Figure 2.1. Each dried stalk consists of a hollow core (called 'hurd') which contributes 65 to 70 % of the total weight. The bast fibre, of composite interest, is located between the hurd and epidermis, which contributes 25 to 30 % of the total dry weight of a stalk [5]. Apart from the aforementioned general classification of plant fibres, the bast fibres are of two types: primary and secondary bast fibres. Primary bast fibres are larger, stronger and contain more cellulose. The bast fibres are bonded together as fibre bundles. These can be separated into single fibres through treatments which will be discussed later. The average hemp fibre length and the average fibre width are 25 mm (5 to 55 mm) and 25 µm (10 to 51) µm, respectively [2].

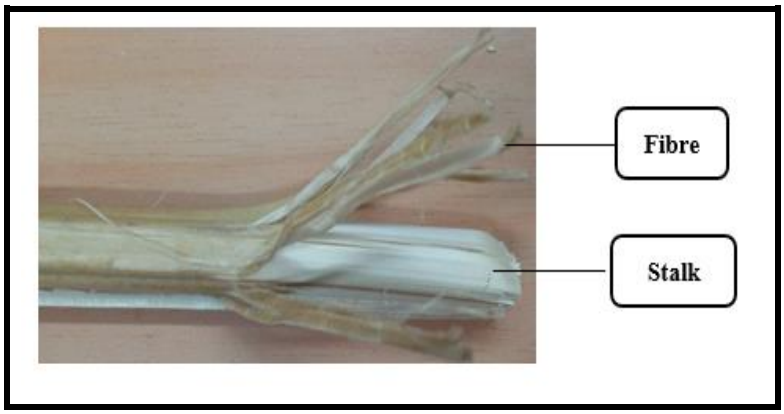

Figure 2.1: Dried hemp stalk.

Hemp has been used by humans for food, textiles, paper, fabric and fuel oil for thousands of years. Industrial hemp fibre applications include a wide range of composites for automotive, insulation materials and construction.

2.4.2 NPF chemistry and physical structure

Natural plant fibres consist primarily of cellulose, hemicellulose and lignin as the major constituents, with pectin and waxy substances as minor constituents. Cellulose forms the major network in a fibre. The chemical structure of cellulose is shown in Figure 2.2. Each repeating cellulose unit contains three hydroxyl groups (OH) [29].

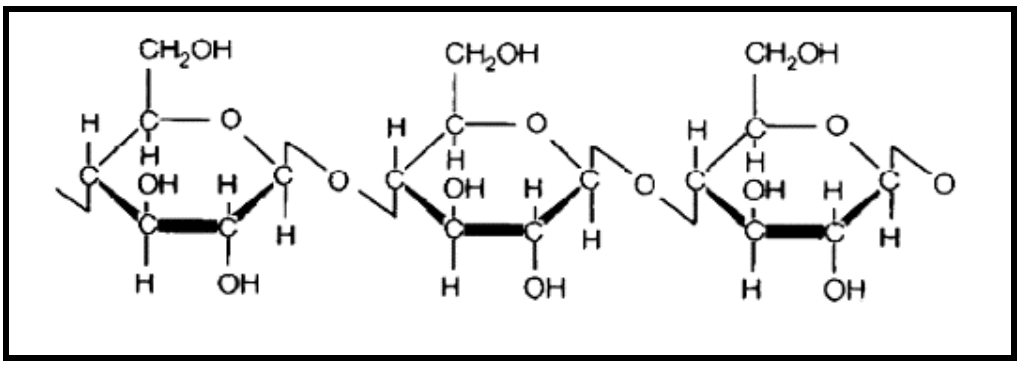

Figure 2.2: Chemical structure of cellulose [5].

Hemicellulose has a branched structure with short lateral chains as shown in Figure 2.3, containing different five and six carbon ring sugars such as xylose, mannose and galactose. It is hydrogen bonded to cellulose fibrils in plants. It is partly soluble in water because of its open structure containing many hydroxyl and acetyl groups [12] and can be removed with alkali solutions [49].

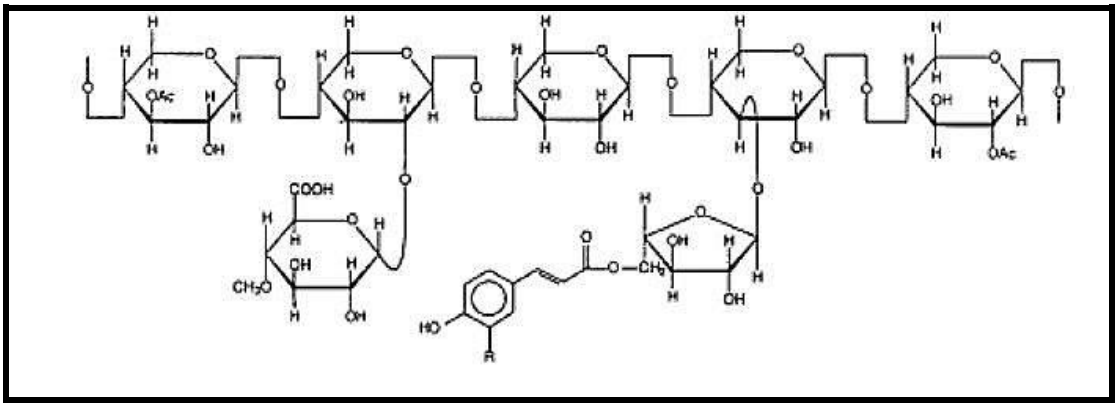

Figure 2.3: Chemical structure of hemicellulose [49].

Lignin is a complex hydrocarbon polymer and has an aromatic structure as shown in Figure 2.4. In the plant, lignin provides the structure and also a barrier for microbial attack. It has the least water absorption of the natural plant fibre components. However, lignin elimination can increase the tensile stiffness of the fibre and also allows effective stress transfer between natural plant fibres and matrices in NPFCs [50].

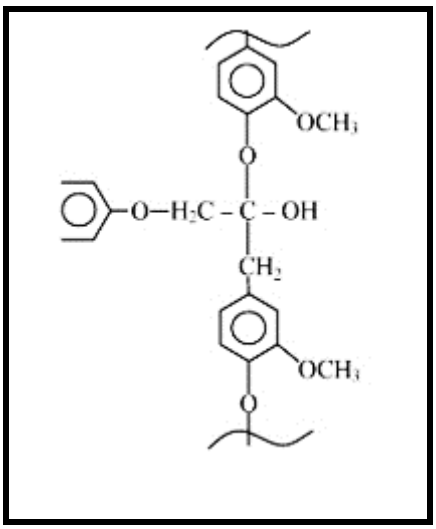

Figure 2.4: Chemical structure of lignin [29].

Pectin is a collective name for heteropolysaccharides. It consists of α-1, 4-linked galacturonic acid units, sugar units of various compositions and their respective methyl esters [5]. It can be easily hydrolysed at elevated temperatures. Waxy substances consist of different types of alcohols and affect the fibre/matrix adhesion [12, 44]. They can be easily extracted with organic solutions [44].

Moisture content in plant fibres varies from 5 and 10 % [51]. Plant fibres are hydrophilic in nature as there are many hydroxyl groups (OH) present in each fibre cell wall. When plant fibres are in contact with atmospheric moisture, the hydroxyl groups break and form hydrogen bonds with the water present. The hydrophilic tendency of plant fibres affects the mechanical performance of NPFCs, thereby limiting the applications of plant fibre composites. However, the moisture resistance can be improved by the reduction of hydroxyl groups from the fibre cell wall through various chemical treatments [4, 51, 52]. This will be discussed later.

Each natural plant fibre (regarded by biologists as a cell) has a complex layered structure which contains primary and secondary cell walls [29, 53], as shown schematically in Figure 2.5. Each cell wall is mainly made up of cellulose, hemicellulose and lignin. It consists of multiple layers of helically wound cellulose microfibrils in an amorphous matrix of lignin and hemicellulose [5].

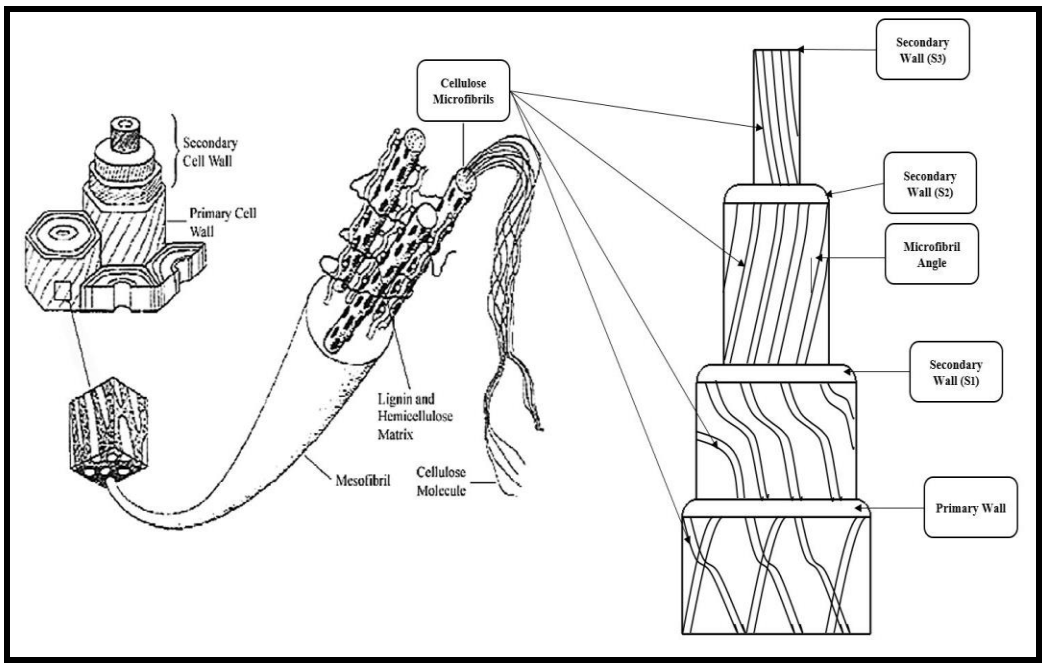

Figure 2.5: Schematic diagram of a NPF [54].

The cellulose content is higher in the secondary walls than the primary, but the hemicellulose content remains almost constant and the pectin content decreases. Hemicellulose is mainly responsible for biodegradation, moisture absorption and thermal degradation of the fibre because of its low resistance. Lignin is responsible for UV degradation [51]. The general factors that determine the properties of a particular fibre are the geometry of cellulose microfibrils (microfibril angles) and cellulose content [44].

2.5 Natural Plant Fibre Composites (NPFCs) and Factors Affecting their Performance

Nowadays, the international sales volume of polymer matrix composites is continuously growing [55]. Glass fibre is widely used as a reinforcement in polymer matrix composites because of its low cost, moderate strength and stiffness to weight ratio compared to high performance carbon and aramid fibres (Kevlar). However, glass fibres require burning of fossil fuels to provide the energy required for their production [5].

Environmental concerns have forced a considerable interest in making use of environmentally-friendly materials to produce eco-friendly products. Thus, the most important challenge for scientific research is the development of substitutes having

lower environmental impact. Carbon dioxide (CO_2) emissions due to the combustion of fossil fuels are the main cause of global warming [19]. Natural fibres possess the potential of reducing CO_2 emissions as well as the potential to replace glass fibres in polymer composites from applicative fields which do not require higher mechanical properties (such as packaging, cases, trays, gardening items) [19, 55]. Natural fibres are also more easily recycled than glass fibres; the common method for disposal of glass fibres is to discard in landfills, which is more expensive as well as harmful for the environment. NPFCs possess many advantages compared to conventional glass fibre reinforced composites as summarised in Table 2.2.

Table 2.2: Comparison between natural plant fibre composites and glass fibre composites [4, 19, 56]

Factors	NPFCs	GFRCs
Processing machinery damage	Low damage	Abrasive and increased wear
Health risk	Low	High
Recyclability of reinforcements	High durability and can be recycled several times without much reduction in strength	Hard to recycle compared to NPFs
End of life	Inexpensive and low environmental impact (potentially CO_2 Neutral)	More expensive and high environmental impact as end products dumped in landfills
Net energy consumption	Less energy required (30800 MJ/ton, 65% fibre)	Almost thrice the amount of energy required for NPFCs (81890 MJ/ton, 30% fibre)
Raw material cost	NPFs are cheaper	Expensive compared to NPFs
Reinforcements density	Low (35 to 40 % less weight compared to glass fibres)	High

Note the following: NPFCs-natural plant fibre composites and GFRCs- glass fibre reinforced composites.

Young's modulus values for NPFCs are competitive with glass fibre reinforced composites. However, the main challenges NPFCs still face is the incompatibility (limited interaction) between the fibre and the matrix. When a NPFC is exposed to moisture, water penetrates and establishes an intermolecular hydrogen bonds with fibres reducing the interfacial adhesion between the fibre and the matrix [53]. Therefore, research has to be carried out to produce high performance natural plant fibre composites, which could withstand a considerable amount of impact and exhibit moderate strength in comparison to glass fibre reinforced composites. The factors that have to be considered for obtaining high mechanical performance for NPFCs are discussed in the following sections.

2.5.1 Matrix selection

The matrix is important in a NPFC, as it holds the plant fibres together within the composite. It can protect the fibres from adverse environments (e.g. water, chemicals and impact properties) and transfers the applied load to the fibres. NPFCs include either a thermoset or thermoplastic polymer matrices [57].

Thermosets cannot be melted once cured, while thermoplastics can be repeatedly melted by the application of heat and solidify on cooling. This repeatability is one of the main advantages of thermoplastics, as they can be recycled without much affecting their physical properties. Some thermosets used as matrices include unsaturated polyester, epoxy and vinyl ester. Commonly used thermoplastics include polypropylene (PP), polyethylene (PE) and polystyrene (PS). The selection of matrices in NPFCs are normally limited to those that can be processed at less than 200 °C, although it is possible to use a maximum of 240 °C for a short duration [4, 44].

Thermoplastic matrices offer several advantages compared with thermosetting matrices. These include recyclability, easier control in processing, high impact resistance, low cost, greater resistance to moisture and some industrial solvents and flexibility in design (molecules in a linear chain can slide over each other) compared to thermoset matrices (cross-linked) [51, 58]. The properties of some of the common thermoplastics used are listed in Table 2.3.

Table 2.3: Properties of common thermoplastic polymers used in NPFCs [12, 59]

Thermoplastic polymers	Density	Water absorption (24h @h 20 °C)	Tensile strength (MPa)	Elastic modulus (GPa)	Izod impact strength (J/m)
Polypropylene	0.899 - 0.920	0.01 - 0.02	26 - 41.4	0.95 -1.77	21.4-26.7
Low Density Polyethylene	0.910 - 0.925	<0.015	40 -78	0.055- 0.380	>854
High Density Polyethylene	0.94 - 0.96	0.01- 0.2	14.5 – 38.0	0.4 -1.5	26.7-1068
Polystyrene	1.04 -10.6	0.03 - 0.10	25 - 69	4 -5	1.1

Polypropylene (PP) is the most widely used thermoplastic matrix in NPFCs, particularly for non-structural applications, because of its low density, low water absorption, excellent processability, good mechanical and electrical properties, good biological and chemical resistance, and good impact resistance and dimensional stability [4, 12, 56, 58-61].

2.5.2 Fibre length

Fibre length is a critical factor which affects the mechanical properties of short fibre reinforced polymer composites. For discontinuous fibres, the load applied to the composites is transmitted from the matrix to the reinforcement through a shearing action at the reinforcement-matrix interface. The effectiveness of load transfer depends upon critical fibre length (defined as the length at which the fibre can be fully loaded at its centre point as if it were continuous) or critical aspect ratio (defined as the minimum fibre aspect ratio in which the maximum allowable fibre stress can be achieved for a given load) which can be obtained by the equation below [54];

$$\frac{L_c}{d} = \frac{\sigma_f}{2\tau_i} \qquad (2.1)$$

where, L_c is the critical fibre length, d is the diameter of the fibre, σ_f is the tensile strength and τ_i is the interfacial strength. The length of the short fibres should be significantly greater than critical fibre length.

2.5.3 Fibre orientation

Fibre orientation is a major factor influencing composite performance; research, largely on synthetic fibre composites, supports that the highest strength and stiffness are achieved in composites when fibres are aligned in the loading direction [62]. Generally, with short natural plant fibre (SNPF) composites, randomly aligned fibre mats are used as reinforcements due to the biological limits of fibre length and the difficulty of aligning short fibre. However, there are a number of methods that have been developed for aligning short fibre, again largely employed for synthetic fibres. These methods can be broadly classified as wet processes and dry processes [63]. Generally, in the former, fibres are suspended in a liquid medium and are forced through a converging nozzle for fibre alignment along the fluid flow direction [64, 65] while in the latter, generally, dry fibres along with polymer powder are aligned by electric or pneumatic means to form the aligned fibre preforms. Although dry alignment methods attain faster production rates and control over orientation of fibres, the degree of fibre alignment obtained has been higher with wet alignment methods [13, 63, 64].

An overview of the main alignment techniques adopted to align short fibres along with a recently adopted alignment technique, i.e. dynamic sheet forming (DSF), which has been employed successfully to produce aligned natural fibre mat, are described in the following sections.

2.5.3.1 Discontinuous fibre alignment methods

2.5.3.1.1 Dry processes

The two main conventional short fibre alignment techniques used in the textile industry are carding, in which, rotating rollers, as shown in Figure 2.6a, guide the fibres to produce a fibre web and combing, where the rows of pins in the comb, as shown in Figure 2.6b, align the short fibres. These processes result in mats lacking homogeneous packing and sufficient alignment [65, 66].

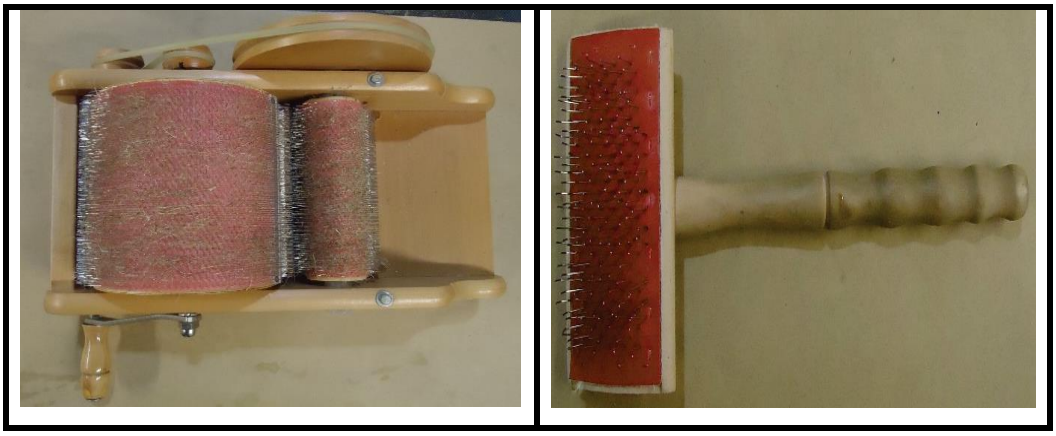

Figure 2.6: (a) Carding machine (b) Comb.

Alignment of short fibres electrically and pneumatically provides a higher production rate and a higher degree of alignment than carding and combing. Electric fields are used in the aligned discontinuous fibre composite process (ADF) [63]; short fibres coated with polymer powder are fed into an orienting electric field chamber via a vibratory feeder. The alignment of conductive fibres occurs in the direction of the electric field generated by electrodes. The aligned fibres, along with coated polymer powder, are then deposited on a moving belt, followed by exposure to heat which melts the polymer powder and joins the fibres together to form aligned ADF mats. Composites can be formed by compression moulding of ADF mats. The schematic diagram of ADF is shown in Figure 2.7. The ADF process depends on the conductivity of fibres and so are generally not relevant to short natural plant fibre polymer composites (SNPFPCs).

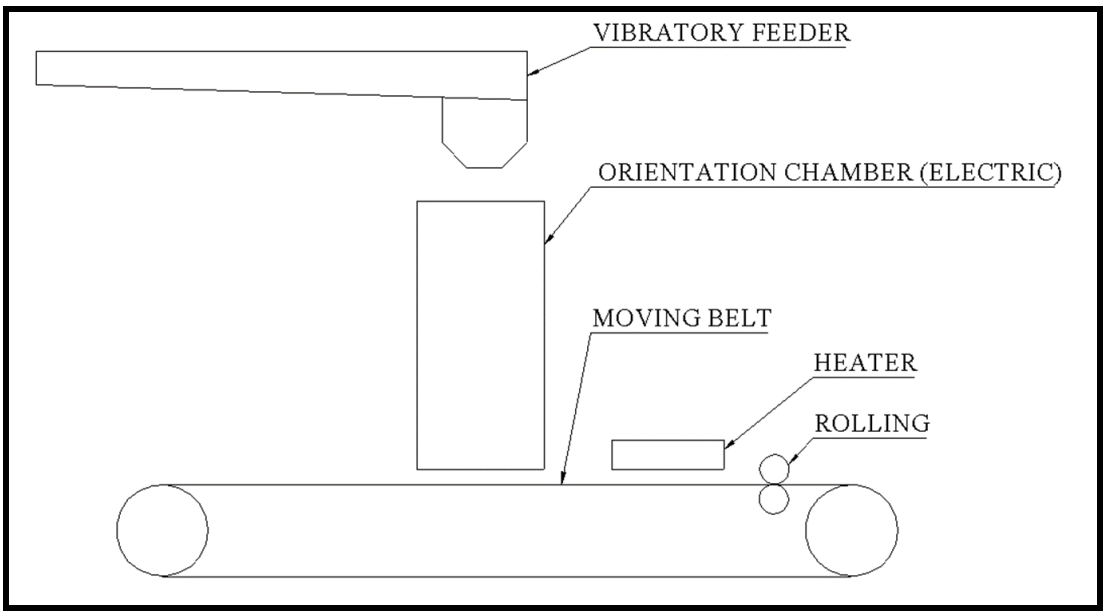

Figure 2.7: An overview of the ADF process.

The main pneumatic alignment method used is the glass-mat reinforced thermoplastic (GMT) technique. In this method, two orientation plates are used for the alignment of fibres as shown in Figure 2.8. A mixture of chopped glass fibres with thermoplastic powder are sprayed through a tube into the orientation plates. The orientated mixtures are then drawn towards a perforated steel plate, followed by heating of the mixture and applying compression to form GMT preforms [67].

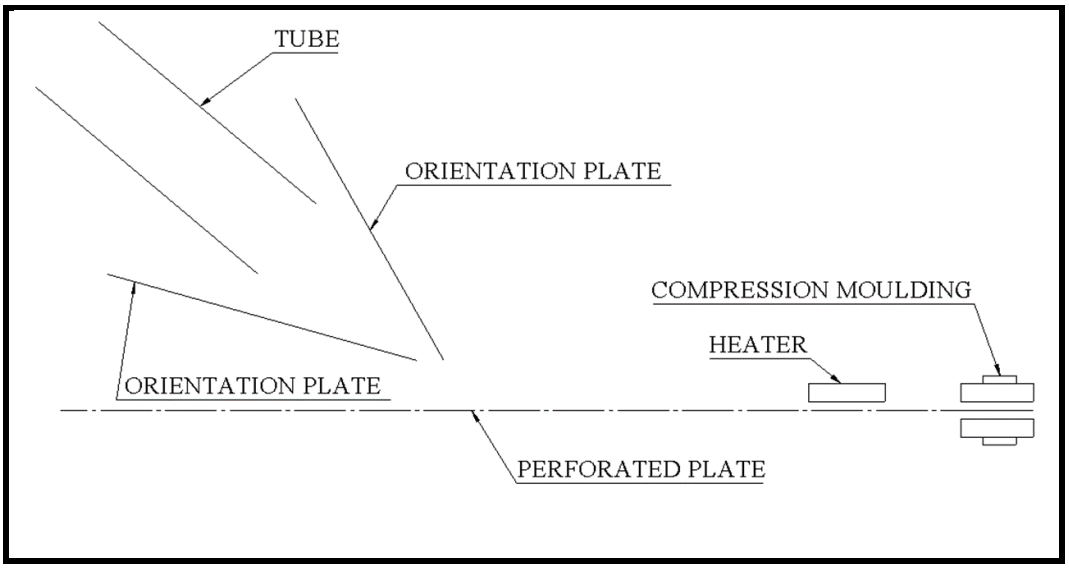

Figure 2.8: A Brief description of GMT.

Another pneumatic alignment process reported in the literature involves aligning fibres from a fibrous mass [68]. In this technique, a fibrous mass is laid on a screen. Then a high pressure pulsating compressed gas jet is discharged from the bottom of

the fibrous mass through a nozzle and a low pressure compressed gas is directed towards the fibrous mass through an opening provided in the middle portion of the apparatus. The pressure differences cause fibre separation and fibres to flow upwards. A specially designed conical annular vertical passage of the apparatus as shown in Figure 2.9 results in the alignment of fibres. The aligned fibres are collected at the top of the passageway on a porous closure.

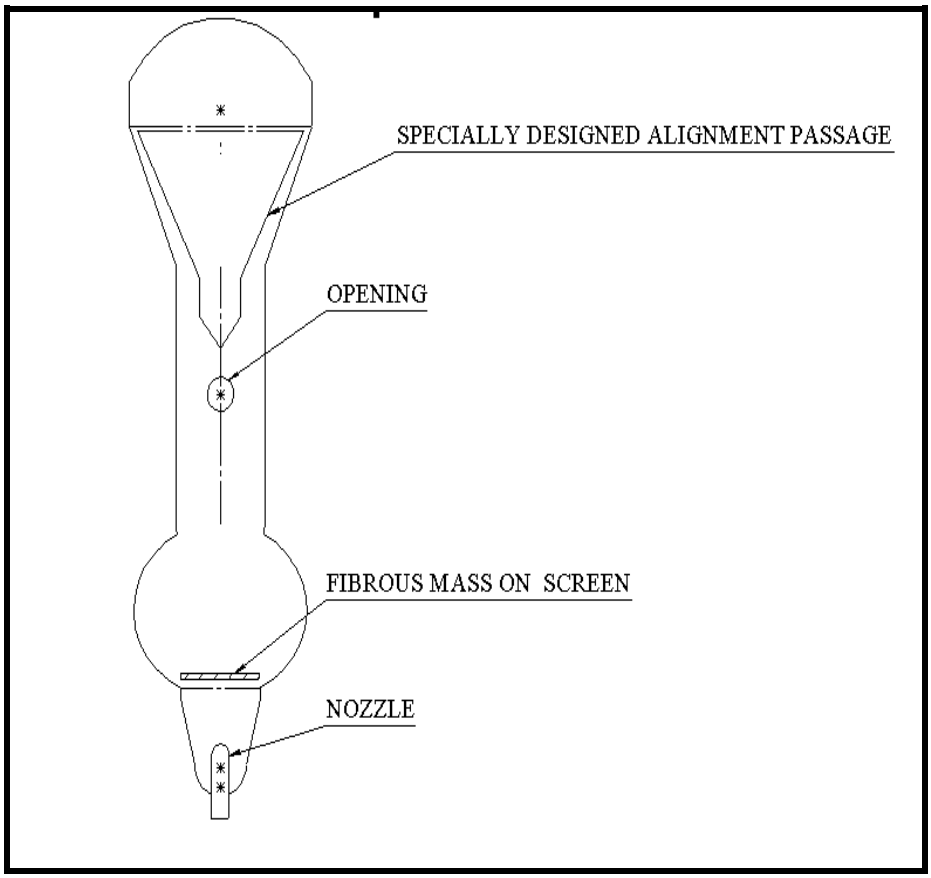

Figure 2.9: Apparatus for fibre alignment by pneumatic means.

2.5.3.1.2 Wet processes

Wet processes generally involve dispersion of short fibres in a liquid medium. There are two main mediums used by researchers: ammonium alginate solution and glycerine [41, 64, 66, 69]. Processing with ammonium alginate solution involves suspension of whiskers or fibres in this medium. The highly resulting viscid mixture is then extruded through an orifice (where the alignment occurs) into a precipitate bath. The gel filaments formed are wound onto a drum, followed by cleaning and drying [65, 69].

Processing with glycerine involves dispersion of short fibres in this viscous medium, which is made to flow through a reciprocating tapered nozzle (partial alignment of fibres), as shown in Figure 2.10, onto a flat gauze bed (wire mesh). The final alignment occurs as a result of fluid friction that occurs between the core layer and boundary layer thereby causing the fibre alignment towards the flow direction. Finally, the carrier fluid removal employing a vacuum was carried out with much care to prevent misalignment during removal [40, 66, 70]. Glycerine is used as a carrier fluid because of its low viscosity compared to alginate solution. The viscosity of the carrier medium affects the productivity by increasing the production time and the cost.

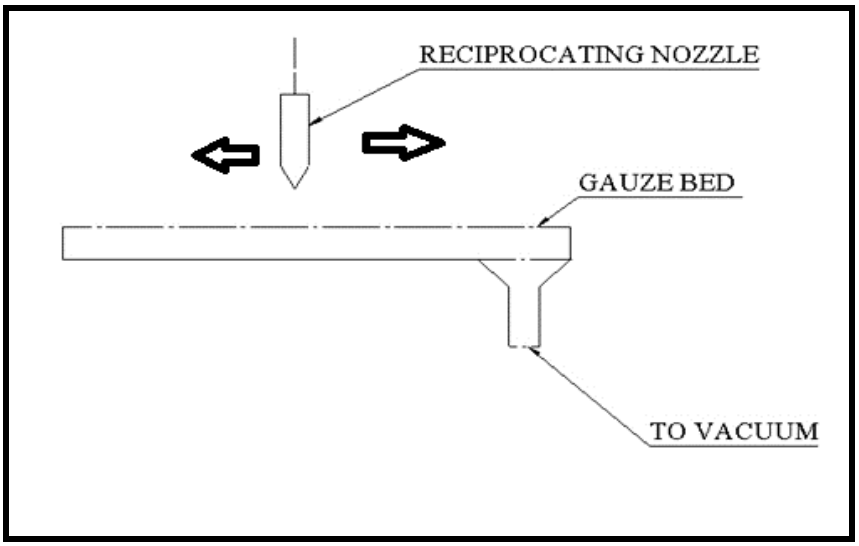

Figure 2.10: Viscous fluid technique.

Centrifugal alignment methods reduce the difficulty of removal of carrier fluids. Generally, in these techniques, aligned fibre mats are produced by discharging the fibre suspension through an aligning nozzle onto the inner permeable surface of a rotating cylinder, as schematically shown in Figure 2.11. This centrifugal rotation causes rapid removal of suspended fluid thereby retaining alignment [41, 71, 72]. Another related technique is the rotating vacuum drum method in which a rotating vacuum drum filter is employed to improve the fibre alignment [72]. The main drawback of the centrifugal technique is that it is a batch production method.

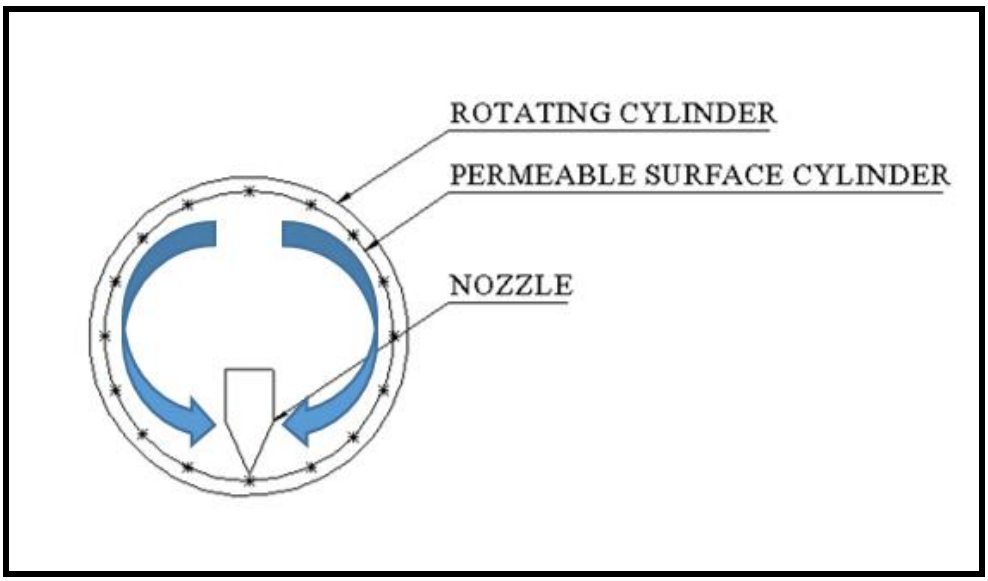

Figure 2.11: An indication of the centrifugal process.

A recent wet processing method to align short fibres to increase the production rate reported in the literature is the high performance discontinuous fibre method (HiPerDiF) [64] which produces a tape or tow type prepregs. In this method, the suspending fluid is water (less viscous compared to other conventional fluids). A nozzle, as shown in Figure 2.12, is used to discharge the fibre suspension to an orientation head. The orientation head has two parallel plates; one of the plates along with a moving belt, orients the fibre perpendicular to the suspension jet and the other acts as a guiding plate to prevent overflow of the short fibres. Suction of the carrier fluid through a vacuum maintains the fibre alignment on the perforated moving belt. Finally, the dried fibre is resin impregnated by the application of heat and pressure to form prepregs. The production rate can be increased with a multiple nozzle system (MNS). In a MNS, the middle plate acts as an orientation plate for the first unit and guiding plate for the second unit.

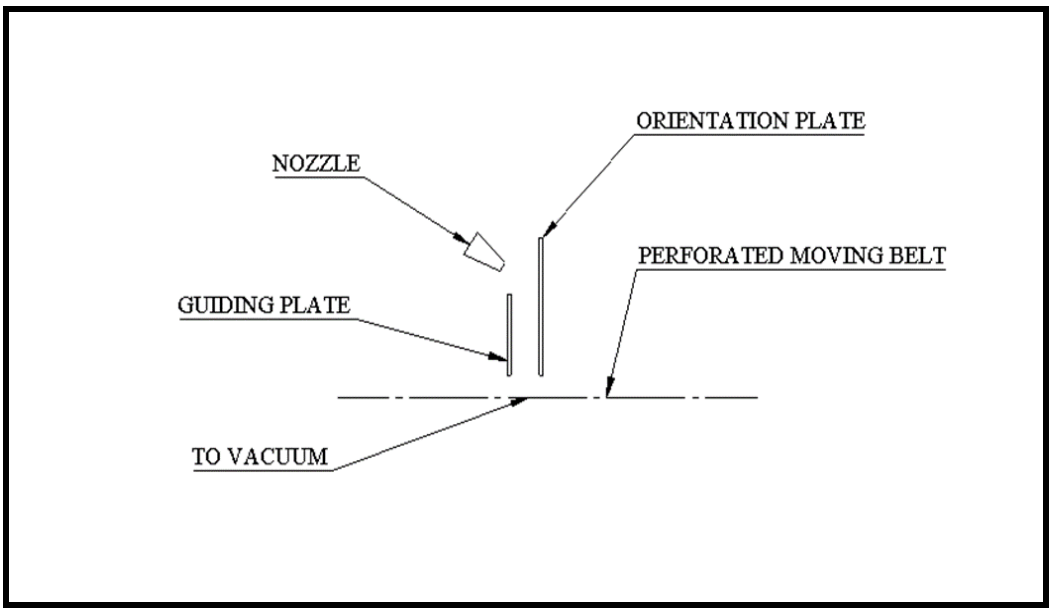

Figure 2.12: An overview of orientation head (HiPerDiF).

A method similar to the aforementioned centrifugal alignment methods is the dynamic sheet forming (DSF) which has been successfully employed to align short natural plant fibre. Generally, this method is used in paper production to align fibres. The equipment consists of a rotating drum as indicated in Figure 2.13, with a wire (screening fabric) on the inside surface. Initially, in this technique, a water wall is built up on the wire (acts as a fibre cushion) with a reciprocating nozzle (up and down) during the entire production [27, 73]. Once the required water wall is obtained, the aligned mats are produced by discharging the fibre suspension (water and short fibres) onto a rotating drum through a nozzle. The nozzle, in conjunction with the rotation of the drum maintains the fibre alignment.

In a dynamic sheet former, alignment of fibres is known to be influenced by the fibre suspension, nozzle geometry, jet-to-wire speed ratio and dewatering [37, 38, 40]. The present study focuses on nozzle geometry, and keeping all other variables constant. The nozzle geometry factors include the contraction ratio and the end shape of a nozzle. The role of a nozzle is to transfer the pipe flow of the suspension in the machine to a thin spanwise homogeneous jet where the fibres are uniformly dispersed onto the rotating drum [37, 38]. The nozzle not only helps in uniform dispersion, but also orientates the fibres towards the main flow direction. The nozzle geometry plays an important role in this uniform dispersion and orientation of fibres within the produced mats. It has been reported that the extensional flow due to the

sudden flow acceleration (change in velocity) from the contraction section of a nozzle creates a highly anisotropic distribution of orientation of fibres [39, 74-76].

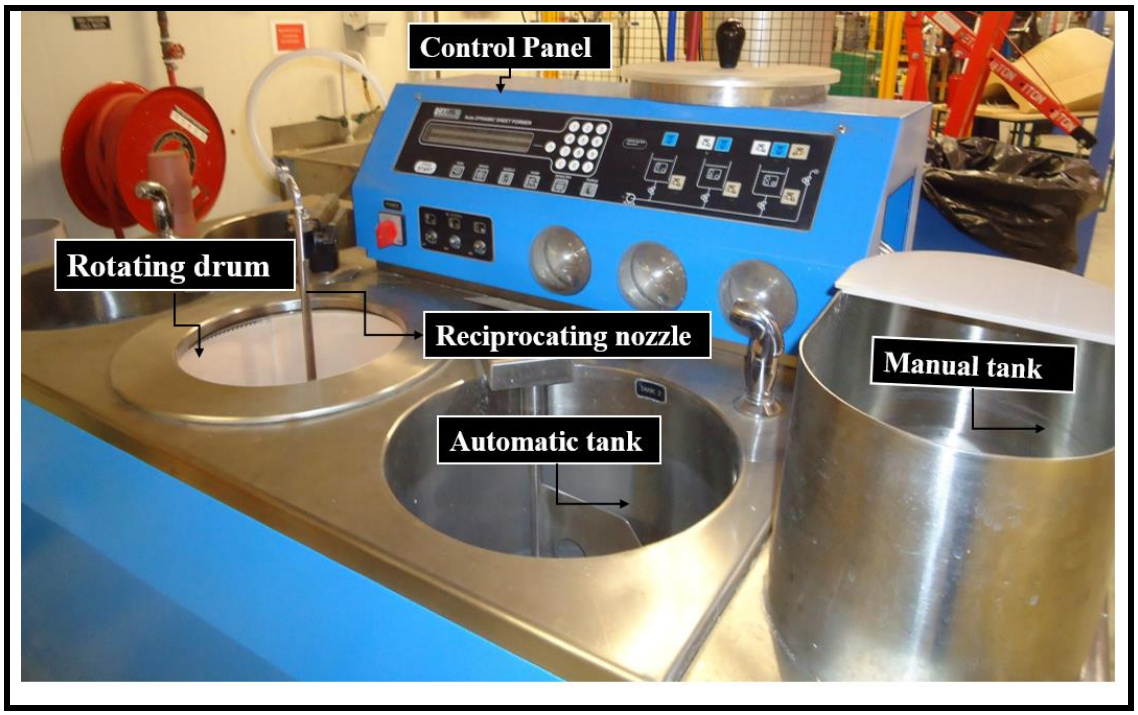

Figure 2.13: Dynamic sheet former.

At this point it is worth mentioning the rheology of fibre suspension for pipe flow and how the orientation distribution of fibres is affected by a nozzle. The rheology of a fibre suspension is dependent on the fluid the fibres are suspended in. Here, the suspending fluid is water. Pulp fibres suspended in water have a natural tendency to flocculate and form structures called flocs. The degree of flocs and alignment of fibres depend on flow characteristic of the fibre suspension. Extensive studies have been conducted to understand the rheology of fibre suspensions [77].

There are several flow regimes [37, 38, 75, 77] that occur during the flow of pulp suspensions through a pipe as illustrated schematically in Figure 2.14. These flow regimes may be categorised under three main flow regimes:

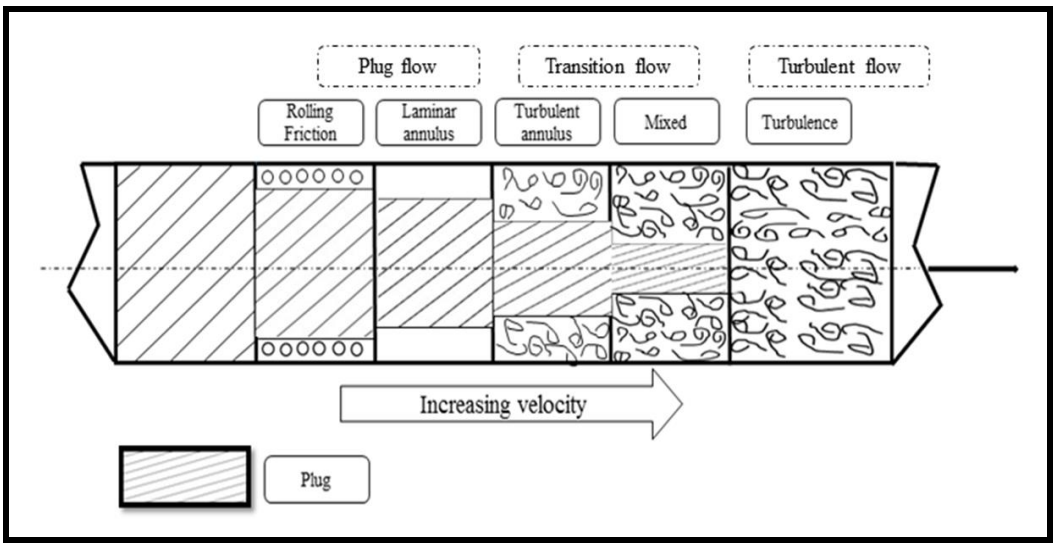

Figure 2.14: Various pipe flow regimes [77, 78].

I. Plug flow: Initially, where the plug-wall interactions dominate, the increasing velocity does not affect the pressure drop greatly due to the friction between the wall and the plug. Here, the velocity of the suspension across the cross-section of the pipe is constant. With further increasing velocity, the interactions between the wall and the outer surface of the plug cause single flocs to break off from the main pipe and roll along the pipe surface at a lower velocity than the plug. Then a stage occurs where the interactions between the plug and the wall cease and there arises plug flow and a thin clear water annulus region. Here, the flow condition is in laminar shear and the flow stresses deform the fibre network (plug) and the thickness of the water annulus increases with increased velocity.

II. Transition flow: Turbulence initiates in the water annulus region. Here, the permanent disruption of the plug begins. However, the plug is not fully affected.

III. Turbulent flow: - With further increase in velocity, the transition from mixed flow to fully developed turbulence occurs. It has been reported that reflocculation will occur rapidly if the turbulence intensity decreases.

The greater flexibility of natural fibres when wet compared to synthetic fibres allows them to rotate or bend as they are subjected to hydrodynamic forces. Generally, the main orientation of fibres is in the same direction as that of the flow. Most studies involving fibre orientation use the explanation of Jeffery [79] that an ellipsoid like

particle suspended in a Newtonian fluid experience simple shear flow [80]. Fibre orientation in a simple shear flow has been researched broadly in literature [39, 74, 79, 81]. It has been reported that in a simple shear flow, channel (pipe/nozzle or duct) width and thickness affect the alignment of fibres. If the channel is wide, although fibres near to the wall are aligned more towards the flow direction, at the centre, fibres are aligned perpendicular or random to the flow direction [74, 82]. In contrast, if the channel is thin enough, the core region slowly disappears due to the increasing tendency of the fibres in the suspension to flow towards the flow direction [74, 83].

As aforementioned, when the fibre mat is produced, the suspension from the pipe enters a nozzle. The main purpose of the nozzle is to distribute the fibre suspension uniformly across the full width of its exit cross-section and also orientates the fibres towards the flow direction. It should be noted that during the mat production, similar to the pipe flow, the suspension flow through a nozzle is subjected to variable flow characteristics that could result in complex fibre orientation distributions within a mat produced. The change in flow velocities through a nozzle can result in the formation of different flow characteristics [37, 84] that could cause anisotropic or isotropic distributions in the orientation of fibres within a mat produced.

A nozzle typically has a decreasing contraction section ending with a rectangular-round or circular exit cross-section. A contraction ratio is commonly defined as the ratio between the nozzle inlet area to the outlet area [85]. In DSF, the contraction section of the nozzle aids in transferring the pipe flow as a uniform homogenous jet to the rotating drum. It has been reported that the acceleration of flow in the contraction affects both the fibre flocs and orientation of fibres within a mat produced [37, 84]. This is due to the tendency of an ellipsoid-like particle, such as a fibre, to drift towards the flow gradient plane and align mainly towards the accelerated flow direction [86]. Due to the complexity of the flow, most of the researchers only provided speculative discussions on the possible reasons for the orientation of fibres towards the flow direction [37]. Some of the causes reported by researchers which could have influenced the fibre orientation in contraction due to the accelerated flow include the flow stresses, velocity gradients, fluid inertia, rate of strain of suspension in the flow direction (extensional flow) and relaminarisation (returning to laminar-like state) [74, 83]. It has been elsewhere reported that if a

turbulent boundary layer is accelerated by a strong favourable pressure gradient, relaminarisation could occur [74]. However, the velocity profile was not appropriate to conclude the relaminarisation. [83].

Overall, depending on the nozzle geometry or shape (mostly converging), it may be concluded that the fibre suspensions undergo both extensional (elongational) and shear flow (near the wall). During shear flow, there is a tendency for fibres to rotate towards the direction of shear, similarly, if the flow is extensional, the fibres rotate towards the direction of extension [87]. Thus, as the contraction ratio of a nozzle increases, the flow acceleration due to the contraction increases the tendency of fibres to strongly align the fibre towards the flow direction [76].

The current nozzle available with the dynamic sheet former is a rectangular-round nozzle (initially round and gradually decreasing with a more rectangular exit cross-section). It has been reported that a nozzle terminating with a circular shape could produce better alignment compared to those with slit nozzles [40]. Given the relationship between nozzle geometry and the alignment of fibres, more research is required to carry out for the improvement of the alignment of fibres within the mats produced.

2.5.3.1.3 Other alignment methods

Alignment of short fibres using an ultrasonic device is also reported in the literature [88]. In the ultrasonic alignment (UA) technique, alignment of short fibres in different matrix media occurs in response to the standing waves produced by two piezoelectric transducers placed at either side of the UA device. The standing waves align the fibres in its nodal position. The main drawbacks are low fibre volume fraction obtainable in composites using this method.

Injection moulding is one of the main processes used to manufacture short fibre reinforced polymer composites (SFRPCs). Alignment of fibres generally occurs due to interactions between different layers (skin and core layers) in the mould. The alignment of fibres follows the flow direction in boundary regions of the mould due to the friction exerted by the walls of the mould. The friction decreases towards the

central region where the alignment of fibres is transverse to the flow direction. There is a chance of occurrence of a shearing flow between the boundary region and central region which may improve the fibre alignment in the central region [5]. Shear controlled orientation in injection moulding (SCORIM) is a modification mainly used for aligning short fibres along the flow direction during injection moulding [81]. In this, macroscopic shears are generated with a device fitted between the mould cavity and nozzle of an injection moulding machine. This device consists of pistons which oscillate to produce macroscopic shear to solidifying melt inside the central-region of the mould, thereby improving alignment of fibres in this region.

A combination of injection moulding and compression moulding have been used by researchers to produce aligned short natural plant fibre polymer composites (SNPFPCs). Injection moulding was initially used to produce cylindrical rods of the short fibres with polymer matrices. Finally, those rods were aligned in a leaky mould followed by compression moulding to produce the aligned short fibre composites [89].

Additive manufacturing or 3D printing of polymer composites have the potential to print or fuse deposition modelling of aligned SFRPCs [4, 90]. Generally, in this method, extruded filaments of short fibres with polymer matrices are fed into a 3D printer to produce (or print) aligned SFRPCs [91]. For the filament extrusion for 3D printing, initially the matrix (pellets or powder) is melted and mixed with the fibre and forced out through a die. After solidifications, the mixture is granulated (8 mm). These granules are again extruded and forced through a circular die (3 mm). An electric spooling machine can be used to achieve consistent filament cross-section [92].

Among all aforementioned methods, the highest degree of fibre alignment reported in the literature is ± 3 ° (measured within the prepregs or composites produced) [64]. The two methods that have exhibited this range of fibre alignment are the HiPerDiF (67 % of the fibres with in this range) and rotating vacuum drum (60 % of the fibres with in this range). The performance in terms of alignment reported by electric field and pneumatic methods are ± 20 ° (70 % of the fibres with in this range) and ± 52 ° (majority of the fibres with in this range), respectively [62].

2.5.3.2 Potential benefits of dynamic sheet forming method

Various forms of short natural fibres are available, including randomly aligned mats, long yarns, braiding and woven textiles [93], but literature reports that generally randomly aligned mats are used as reinforcement in SNPFPCs as they are cheap compared to other forms [94]. However, work carried out at the University of Waikato has proved that the dynamic sheet forming method is a potential technique to produce aligned short fibre mats [4]. In that study, the occurrence of fibre orientation in harakeke mats was assessed by determining the ratio of transverse tensile strength to longitudinal tensile strength indicates a good degree of orientation. The ratio obtained was 0.3; when the ratio closes to zero point to the higher degree of alignment. It was also observed from the optical images and scanning electron micrographs that the fibre mats provide improved fibre dispersion in the composites. The composites produced with the harakeke fibre mats reinforced in epoxy resin and with hemp and harakeke fibres in polylactide polymers using compression moulding had exhibited higher tensile strengths and Young's modulus compared to random aligned short fibre mats [27, 73].

As aforementioned, dynamic sheet forming (DSF) is a promising method to produce aligned fibre mat with natural fibres. However, more research needs to be carried out to optimise the production of DSF in order to improve the alignment of fibres in the mats produced.

2.5.4 Fibre dispersion

To obtain good properties with NPFCs, it is essential to have good fibre distribution within the polymer matrix [5]. Poor dispersion of fibres is mainly due to the hydrophilic fibres in hydrophobic matrix. Chemical (e.g. alkali treatment) or physical (e.g. corona and plasma treatments) modifications of fibres separate the fibres from their bundles, ensuring good distribution and dispersion of fibres within polymer matrices. Dispersion can be improved by adjusting processing parameters such as temperature and pressure. Compatibilisers such as maleic anhydride polypropylene (MAPP) (improves interfacial bonding) and dispersing agents, such as stearic acid (SA) (reduces fibre-fibre attraction) have been used in PP to modify dispersion as well as fibre-matrix interfacial interaction, respectively [2, 4, 51, 95].

2.5.5 Porosity

Porosity (air filled cavities) is often an inevitable component in composite materials. This can be caused by the mixing and merging of two different materials [96]. Porosity acts as stress raisers in composites, affecting the overall performance. Therefore, much care should be taken during selection of processing methods for composites to minimise porosity as much as possible. Research has shown that the processing methods assisted with vacuum and compression are the best to reduce the porosity in composites [4].

2.5.6 Interfacial bonding between the fibre and the matrix

The strength of the interface has a large influence on composite properties which depends on the mechanism and amount of interaction. The mechanisms of interfacial bonding can be mechanical interlocking (rough fibre surface), chemical bonding (presence of chemical functional groups) and inter-diffusion bonding (interaction between atoms and molecules). There are possibilities of multiple bonding mechanisms occurring at an interface at the same time [4]. The interface strength also depends on the density of bonds. As already discussed, for NPFCs, there is usually limited interfacial bonding at the interface due to polar fibres and non-polar polymer matrices. This, in turn, affects the stress-transfer efficiency of NPFCs from the matrix to the fibre, thereby limiting the mechanical properties.

Most literature on interfacial bonding of NPFCs focuses on physical treatments, chemical treatments and coupling agents [2, 29, 34, 50, 53, 97-99]. The main objective in conducting these treatments is to improve wettability and potential for chemical bonding of the fibre surface with the matrix, thereby providing interfacial strength (effective stress transfer across the interface) [47].

Wettability of the fibre by the matrix is most essential for the matrix-fibre adhesion; which can be assessed from the surface energy of the fibre and the matrix. The surface energy of the reinforcements should be greater than that of the matrix for the occurrence of fibre-matrix adhesion [100]. However, NPFs, due to their hydrophilicity, absorb atmospheric moisture when exposed to the ambient

environment. This lowers their surface free energy which may even result in their surfaces possessing lower surface energy than that of matrices.

Coupling agents (also known as compatibilisers) act as a bridge between the fibre and the matrix and bond them together. Many studies have been carried out to achieve improved interfacial strength by different treatment methods on NPFCs. An overview of different treatment methods (physical, chemical, coupling agents and biological), used to improve interfacial bonding of NPFCs, is described in the following sections.

2.5.6.1 Physical methods

Corona, plasma and heat treatment are the three main physical treatment methods used on reinforcing fibre surfaces. Structural and surface properties of the fibres are altered by these methods, which mainly enhance the fibre-matrix interface via improved mechanical bonding [2]. However, these methods often require highly sophisticated equipment.

In corona treatment, surface modification of the fibre is due to a corona generated by the application of high voltage to sharp electrodes, resulting in ionisation at their vicinity, at low temperature and pressure. In addition, prolonged treatment times may result in a fibre with a significantly roughened surface, which enhances the bonding between fibre/matrix. This treatment improves wetting between fibres and matrices, which would improve the composite strength and stiffness [101, 102].

Plasma treatment involves charging the fibre surfaces in a vacuum chamber. Using this treatment, the interfacial shear strength has been increased by 200% in cellulose/linear low-density polyethylene composites [2].

Heat treatments affect both the physical and chemical composition of natural plant fibres. The cell wall undergoes pyrolysis when the processing temperature is too high, which often needs to be avoided [51]. Time, temperature and gas composition in the oven are the main controlling factors in this process. The advantages of the heat treatment are low cost and avoidance of chemicals. However, it is a difficult method to fully control and high precision is required to achieve the desired effects [2].

2.5.6.2 Chemical methods

Chemical treatments involve reactions between fibres and reagents, including alkali, acetyl, silane, benzyl, acryl, stearic acid, maleic anhydride, permanganate, peroxide, isocyanate, titanate, and zirconate [2, 4, 29, 43, 55]. The most popular treatments are alkali, acetyl and silane [4]. The majority of these treatments are aimed to modify surface chemistry. However, alkali treatment, which has been found to be the best method [103], is effective through a number of factors; NPFs treated with alkali have been seen to have benefits such as improved separation of fibres from fibre bundles, improved removal of unwanted surface constituents, increased tensile strength and stiffness, better thermal stability as well as improved interfacial adhesions compared to other common treatments [4, 31, 61, 97, 98, 104, 105].

2.5.6.2.1 Alkali treatment

Among different chemical treatments, the alkali treatment with sodium hydroxide (NaOH) is one of the most widely used treatments. This treatment removes hemicellulose, lignin, pectin, wax and fat from the NPFs. The removal of hemicellulose, lignin, pectin (cementing materials) from the NPFs results in fibre separation and enhances exposure of hydroxyl groups on the fibre surfaces, thereby improving interfacial bonding and fibre roughness and increasing thermal stability [4, 50, 98]. Modest treatments have been seen to bring about increased cellulose crystallinity which is considered to be because of removal of the abovementioned amorphous materials, whereas harsher treatments have been shown to convert crystalline cellulose to amorphous cellulose (Figure 2.15) and possibly result in chain scission [106].

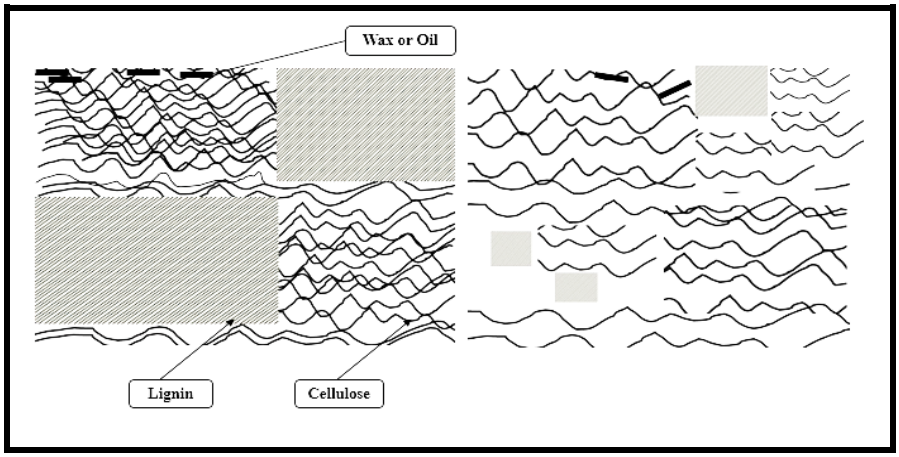

Figure 2.15: Change in crystalline cellulose structure before (left side) and after treatment (right side).

The chemical reaction reported by some researchers, which occurs between fibre cell wall and NaOH (sodium hydroxide), are represented in Figure 2.16. The hydroxyl (OH) groups in the fibre break down and react with water molecules (H-OH). The water molecules are thus driven out. The remaining reactive groups in the fibre (i.e. Fibre cell-O) may form Fibre-cell-O^-Na^+ groups between the cellulose molecular chains, which could significantly improve tensile properties of the fibres. However, alkali treatment is commonly carried out to remove the cementing materials.

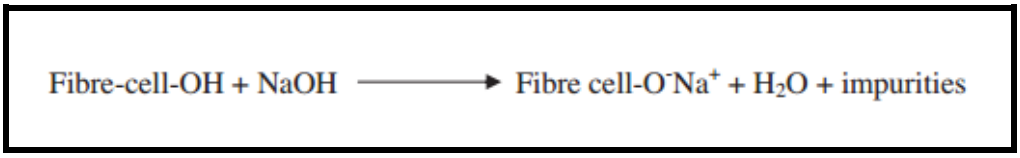

Figure 2.16: Chemical reaction between fibre cell and NaOH [29].

These alkali treatments have been carried out by different researchers in different ways including at ambient temperature (AT) as well as at high temperature (HT). AT treatments have many advantages, such as simplicity, low cost and can be easily carried out in large volumes, compared to HT treatment which requires fully controlled methods. Oushabi et al. investigated the effect of alkali treatment on date palm fibres with various concentrations of NaOH (0 wt %, 2 wt %, 5 wt %, 10 wt %) at 25 °C for one hour and found an increase in tensile strength of date palm fibres compared to raw fibres [107]. Mishra et al. reported that alkali treatment at 30 °C for one hour with 5 wt% NaOH concentration resulted in better strength for sisal/glass fibre polyester hybrid composites compared to 10 wt% NaOH [108]. Mohanty et al. carried out alkali treatment for sisal fibres at 30 °C with 5 wt% NaOH for one hour and reported a slight improvement in mechanical properties of sisal/polypropylene composites [109]. Table 2.4 lists some of the recent works on AT and HT alkali treatment of hemp fibres. As it can be seen, for different high temperature treatments significant improvement in average tensile strength was reported for hemp fibres treated with 5 wt% NaOH and 2 wt% Na_2SO_3 (sodium sulphate) at 120 °C with a holding time of 60 minutes compared to 10 wt% NaOH and untreated fibres [98].

Table 2.4: Some of the recent works on alkali treatment of hemp fibres or composites produced [27, 29, 31, 50, 73, 97, 98]

Methods of applications	Fibres or composites produced	Observations on properties of fibres or composites
Soaked hemp mats in 0.16wt% NaOH for 48 hours	Non-woven hemp mats in euphorbia resin	Increase in tensile strength of composites produced with treated fibre mats [110]
Immersed pre-dried hemp fibres in 5wt% NaOH solution for 30 minutes, *FSR- 1:20	Hemp fibre	Average tensile strength of the fibres increased [97]
Hemp fibres were soaked in 0 %, 4 %, 6 %, 8% and 10 % for 3 hours at room temperature. NaOH solutions were prepared in water ethanol mixtures.	Hemp fibre	All treatments reduced the tensile strength [111]
Hemp fibres were treated with 5wt% NaOH and 2wt% Na_2SO_3 solution in *SSCs at 120 °C for 60 minutes	Hemp fibre/polylactic acid	Interfacial shear strength increased as a result of alkali treatment, thereby improving mechanical properties of composites produced [30]
Hemp fibres were treated with 5wt% NaOH and 2wt% Na_2SO_3 solution in *SSCs at 120 °C for 60 minutes	Hemp fibre/epoxy	93 % of lignin was removed after the treatment. Improved tensile strength and Young's modulus of short fibre/epoxy composites [50]
Two different alkali treatments. In first method, fibres were treated with 10wt% NaOH to a maximum of 160^{o}C for 45 minutes in *SSCs, FSR - 1:6. In the second method, 5wt% NaOH and 2wt% Na_2SO_3 solution in *SSCs to a maximum of 120^{o}C for 60 minutes, FSR-1:7	Hemp fibre	5wt% NaOH and 2 wt%Na_2SO_3 treatment improved tensile strength and Young's modulus. Improved fibre separations of fibre bundles were also resulted with both methods of alkali treatments [98]
Three different alkali treatment; 5wt% NaOH, 10wt% NaOH, 5wt% NaOH and 2wt% Na_2SO_3, solutions in *SSCs at 160^{o}C for 30 min	Hemp fibre	5wt% NaOH and 2 wt%Na_2SO_3 improved fibre separation. Average tensile strength of the fibre reduced [31]

Note the following: *SSCs- stainless steel canisters and FSR- fibre to solution ratio.

Prior to DSF, good fibre separation is needed. Alkali treated hemp and harakeke fibres have been reported as used for the production of DSF mats [4, 16, 34], but the tensile strengths of these treated fibres were reduced compared to raw fibre due to the weakening of structural components [16, 27, 35, 36]. Therefore, further research is needed to develop processing parameters to improve fibre separation without reduction in tensile properties of fibres prior to DSF.

2.5.6.2.2 Acetylation

Chemical treatment of fibre with acetic anhydride is an effective method of reducing the innate hydrophilic nature of natural fibres. During acetylation treatment, the acetyl functional group (CH_3COO) reacts with the hydroxyl group of natural fibres forming ester bonds. This increase the hydrophobicity of treated fibres, thus improving dimensional stability of the composites [112]. It has also been reported in the literature that the treatment removes unwanted materials from the fibre surface resulting in a rough surface which enhances mechanical interlocking with the matrix [29, 43].

Kabir et al. [106] studied the effect of acetic anhydride treatment on hemp fibres and reported improved thermal stability at the temperature range of 250-350 °C. Zafeiropoulos et al. [42] found that the acetylation using acetic anhydride increased the surface free energy of the treated flax fibres. Bledzki et al. [113] studied the properties of treated flax fibres reinforced polypropylene composites and noticed an improvement in tensile, stiffness and flexural properties of the composites.

2.5.6.2.3 Silane treatment

Silanes are a range of chemicals with chains of SiH_4. The silane-based coupling agents are commonly used to modify fibre surfaces. They are hydrophilic compounds based on a silicon molecule with different organic groups attached [5]. These coupling agents can form as a bridge between the fibres and the matrix, which improves fibre-matrix adhesion. In the presence of water under acid catalysed conditions, silanols (Si-OH) are formed by the hydrolysable alkoxy group of silane. These silanols may react with the hydroxyl group of the fibres and/or with subsequent drying and condense themselves on the fibre surfaces forming a

macromolecular network [29, 114]. Hong et al. [115] reported that this treatment increased tensile properties of the jute-PP composites due to the improved adhesion in the interface.

2.5.6.2.4 Stearic acid treatment

The chemical formula of stearic acid (SA) is ($CH_3(CH_2)_{16}COOH$). Generally, stearic acid in ethyl alcohol solution is used to modify the fibre surface. The chemical reaction that could take place between stearic acid and NPFs is shown in Figure 2.17. The carboxyl group (-COOH) present in stearic acid can react with hydroxyl groups of the fibre to form an ester [29]. The esterification reaction reduces the number of hydroxyl groups in the NPFs available for bonding with water molecules, thereby reducing their innate water absorption tendency. The increase in fibre hydrophobicity reduces fibre-fibre interaction, whereby more dispersion of fibres is possible in polymer matrices compared to untreated fibres. It is also reported that this treatment can also remove some of the non-crystalline constituents from fibres (wax, oils) [29]. However, a solvent is required for this conventional treatment method.

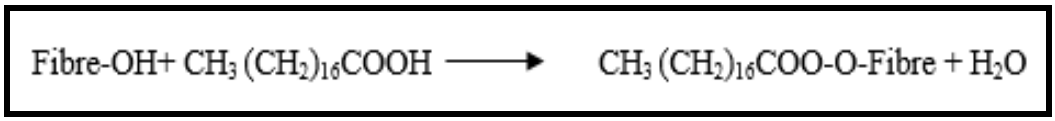

Figure 2.17: Proposed chemical reaction between fibre cells and stearic acid [29].

Another stearic acid treatment reported in literature, which eliminates the requirement of a solvent, is the vapour phase treatment. This treatment is carried out in a pre-heated oven. The fibres are placed on a fine mesh, directly above a stainless steel container containing stearic acid [42, 116]. Studies by Zafeiropoulos et al. [42, 116, 117] reported that stearic acid treatment by employing vapour process on flax fibres reduced their polar interaction ability. Further, it was reported that the stearic acid vapour phase treatment improved the interfacial stress transfer efficiency of flax fibre/isotactic polypropylene composites by the inter-entanglement of stearic acid chains with the matrix. Torres et al. [118] also reported increased interfacial shear strength for stearic acid treated sisal fibre in polyethylene matrix by 23 % compared to untreated fibres. Although stearic acid was detected on the treated fibre surfaces, no ester bond formation was revealed in FTIR. Different approaches to stearic acid treatment are summarised in Table 2.5.

Broda et al. [60] studied the formation and properties of polypropylene/stearic acid composite fibres and reported that stearic acid slows down the PP crystallisation creating a meso-phase in addition to the crystalline and the amorphous phases of pure PP. This could result in partial entanglement of long aliphatic tails of stearic acid into PP structure [60, 119]. It is also reported that a small portion of SA crystallises on to the polypropylene fibre surface [60]. Overall, stearic acid has the ability to act as a bridge between the natural fibre and polypropylene composites.

Table 2.5: Different approaches for stearic acid treatment [29, 42, 116-118, 120, 121]

Fibre - matrix composites	**Application methods**	**Outcomes**
	Solution Process	
Sisal/glass/LDPE	Stearic acid in ethyl alcohol solution-(1,2,3,4,5,6,7 % weight of fibre)-dropwise-continuous stirring	4 % exhibited maximum tensile strength, increased hydrophobic character of sisal fibre, good dispersion of fibres.
Banana/PP	Alkali treated fibres soaked in 1% alcohol, 1 h	Improvement in thermal stability
Jute and sisal fibres	Mixed 3% stearic acid in polymer melt (HDPE)	Tensile strength increased by 9 % and 5 % for HDPE/sisal and HDPE/jute fibre composites, respectively
	Vapour Process	
Flax fibre/PP	Dried fibres are placed on a mesh above stearic acid containing stainless steel container in a preheated oven. Duration of treatment and temperature are the controlling factors. (90,95,100,105 °C)/ (12,36,72 and 90 h)	At 105 °C and 36 h reduced water absorption tendency of fibre, improved stress transfer efficiency at the interface.

2.5.6.2.5 Nanocellulose treatment

The strength and stiffness of a NPF relates to the cellulose microfibrils. Depending on the fibre (source), the cellulose microfibrils range from 1 to 25 nm in width and 1 to 9 μm in length [122]. These thread like bundles of cellulose molecules contain amorphous and crystalline regions (Figure 2.18). The extraction of nano-meter diameter cellulose or nanocellulose from various sources (algae, sea animal, bacteria and plant biomass) includes multistage processes involving chemical and/or mechanical methods. Depending on the isolation method, the nanocellulose may be categorised into three types: cellulose nanocrystals (CNCs), cellulose nanofibrils (CNFs) and bacterial nanocellulose (BNCs) [123]. The CNCs are mainly obtained by controlled acid hydrolysis whereby the amorphous regions are hydrolysed resulting in cellulose crystals in nanometre size range. CNFs are produced by mechanical disintegration in which some of the interfibril hydrogen bonds or interfibril molecules break and form fibres of nanometre size in width and micrometre size in length. Unlike CNCs and CNFs, BNCs are synthesized by special bacteria. The properties of nanocellulose depend on the source and extraction conditions [124, 125]. Typical sizes of CNC range from 2 to 30 nm in width (diameter), whereas CNF range 20 to 30 nm in width [126]. On the other hand BNCs range from 50 to 100 nm in width and several micrometres in length [127]. CNCs are highly crystalline compared to CNFs due to the presence of amorphous cellulose material in CNFs.

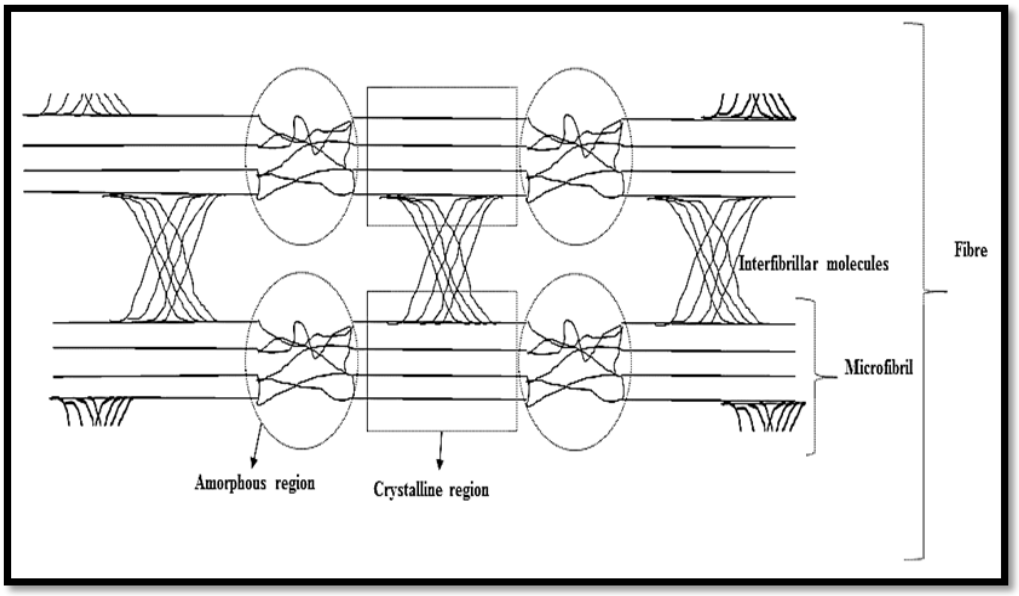

Figure 2.18: A schematic representation of a cellulose fibre with crystalline and amorphous regions.

Strong interactions are expected between the nanocelluloses and natural fibre due to the potential for hydrogen bonding between the hydroxyl groups present on their surfaces. It has been reported that CNFs could form entanglements and network structure throughout polymer matrices [128]. However, the highly fibrillated nature of CNFs could result in fibre agglomeration that could limit the reinforcement capability in polymer matrices compared to CNCs [126, 128]. Recent research has proved that nanocellulose can also be used as a binder to produce rigid and robust NPF preforms [129]. Various modification methods have been reported. One method is to deposit bacterial cellulose (BC) onto the surface of natural fibres. The coating of natural fibre with BC (biological growth) has been reported to improve the interfacial adhesion between the fibres and the matrix. However, this method requires long culturing times (around five days) and expensive reactors. Another method reported is the slurry dipping, in which the fibres to be modified are dipped into a suspension containing BC, followed by vacuum filtration, consolidation and drying [130]. It has been reported that BC binds the loose fibres in the natural fibre preforms and the composites with these preforms exhibited higher mechanical performances compared to composites without BC coating [129, 130]. It has also been reported that the hydrogen bonds formed upon the nanocellulose drying remain stable in water that prevented the disintegration of fibre preforms after being submerged in water [130]. However, all these methods are time-consuming and requires additional processing stages to produce a robust NPF preforms.

The mechanical strength of the dried hemp fibre mats produced using DSF is weak, with only friction holding the loose hemp fibres together. The strength of the mats can be improved using methods such as needle punching (inserting barbed needles and pulling fibres through the thickness of fibre webs to consolidate it into a mat) or spraying a polymer solution onto the fibre mats, although this requires substantial infrastructure or use of solvents [91, 129]. An alternative method reported in literature is a nanocellulose treatment. Nanocellulose (NC) with a highly crystalline structure has been considered to be used to modify the fibre-polymer matrix interface [123, 124, 130]. High surface area, aspect ratio, stiffness and strength, and sustainability of nanocellulose is making it popular in composite applications [131]. Additionally, the improved fibre-matrix adhesions obtained for some of the nanocellulose reinforced polymer composites [124, 127], prompt to assume that the interface can be improved with nanocellulose additions. However, more research is

required to perform this alternative treatment in a time-effective manner to upgrade the properties of DSF mats, thereby upgrading the properties of polymer matrix composites reinforced with these mats.

2.5.6.2.6 Coupling agents

Maleic anhydride (MA) grafted polymers are the most commonly used coupling agent for lignocellulosic fibres. As mentioned previously, coupling agent acts as a bridge between the cellulose fibres and the polymer matrices. MA functional group is generally grafted to the same polymer as the matrix to ensure better compatibility between the matrix and the coupling agent. Grafting MA to PP is common and considered the most successful coupling method to improve interfacial bonding in PP matrix NPFCs [2, 4, 29]. MA grafted polymer is used as an additive during processing. This improves wettability of the fibre as well as bonding thereby increasing mechanical performance of the composites. The chemical reaction, between maleic anhydride grafted polypropylene (MAPP) and the fibre surfaces are shown in Figure 2.19. MA functional groups interact with the fibre surface (OH groups) through covalent and hydrogen bonding. The long polymer chains of MAPP then combines with the unreactive PP matrix by means of chain entanglement [5].

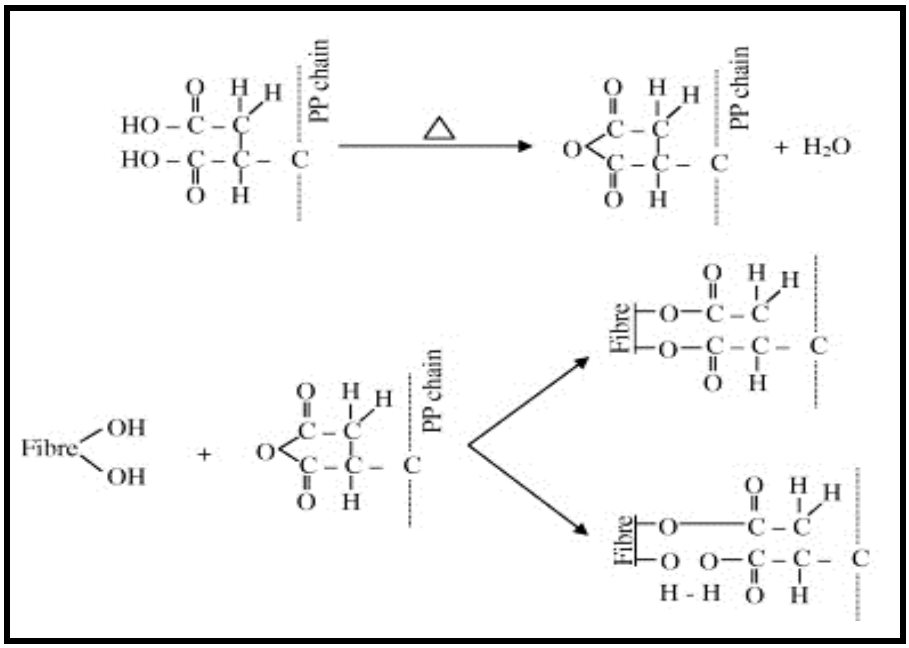

Figure 2.19: Chemical reaction between fibre cells and MAPP [29].

Increases in mechanical performance of natural plant fibre thermoplastic composites (NPFTC) with the inclusion of MAPP have been reported by many researchers [2]. It

has been previously reported that a MAPP (AC 950P, Honeywell International Inc., USA) to PP ratio of 7.14 g per 100 g was found to be an optimum MAPP content for short hemp fibre reinforced PP composite, above or below which the strength of the composites found to be reduced [5, 132].

2.5.6.3 Biological methods

Retting and fungal treatments are the most commonly used biological treatments for modifying natural fibres. Retting is a controlled degradation of plant stems, which separates bast fibres from their hurd, besides aid the fibre separations. Retting can be carried out using water or dew retting. In water retting, plant stems are immersed in water, whereas in dew retting plant stems are spread in the field to partially degrade [5]. Retting duration is very important as under retting can result in incomplete fibre separation and over-retting can weaken the fibres [5]. These treatments are carried out in aqueous environments and tend to be water polluting. Hence, it is not generally practised.

Fungal treatment involves an initial autoclave sterilisation of the fibres. Later, incubation of the fungi added fibres. Afterwards, they are washed and dried in an oven. Fungal treatment removes non-cellulosic contents such as wax from fibre surface by the action of enzymes [29]. It also roughens the fibre surface by removal of cellulose, hemicellulose, and lignin, thereby providing better interlocking for the matrices with the fibre surface [99].

2.5.7 Processing technologies (manufacturing technologies)

Common manufacturing processes of natural plant fibre thermoplastic composites (NPFTC) include injection moulding (IM), compression moulding (CM) and extrusion [47]. Properties of NPFTCs depend upon the manufacturing process and their processing parameters such as temperature, pressure and speed of processing [4]. These parameters should be prudently selected as the strength of NPFCs depends upon fibre length (which can reduce during processing), temperature (degradation above 200 °C), and orientation of the fibres obtained during the processing.

Thermoplastics usually in pellet form and chopped (short) plant fibres are the raw materials for injection moulding (IM). The raw materials are then fed through a feed hopper towards the heated compression barrel with a rotating screw. The rotation of

the screw with the application of heat transforms the polymer pellets into viscous fluid, which in turn mixes with the short fibres. The pressure developed by the screw mechanism pushes the viscous mixture through a sprue nozzle towards the mould cavity where it solidifies defusing the composite shape.

Compression moulding possesses potential advantages over other manufacturing processes; high reproducibility and low cycle time have made it popular [2, 4]. NPFTCs are produced with this process using flat thermoplastic prepregs and plant fibre mats, either randomly or aligned short or long fibres, stacked in the desired sequence in a mould before heat and pressure are applied.

Extruders commonly used in the plastic industry can be a single-screw or twin-screw [2]. In an extrusion process, thermoplastics (beads or pellets) are softened and a single or twin screw mixes it with plant fibres. The compression force exerted by the screw or screws pushes the mixture through a die. Improved dispersion of fibres has been shown to occur with twin screw extruders when compared to single screw extruders [4]. Composite granulates, continuous production of semi-finished products or components are produced by the extrusion process [2]. Compounding processes (blending of polymer matrices and natural fibre components, generally in the form of pellets) are gaining attention in the automotive industry [59].

Ideally, composites with high strength are produced by increasing the amount of reinforcement in the matrix. However, in injection moulding, the amount of fibre content in composites is limited to not more than 40 % of the total composite weight [4]. Here, the passage of fibres through narrow gates cause significant fibre attrition (size reduction) [47]. Comparison of the properties of injection moulded and compression moulded NPFCs shows that compression moulded parts exhibit better mechanical properties because of improved alignment, the longer reinforcement fibres and the higher fibre contents possible [2].

Previous studies have demonstrated that compression moulded polymer composites made with the mats produced using DSF exhibited higher mechanical performance compared to other short fibre processing techniques [4, 27, 73]. However, the maximum fibre content was limited to below 50 wt%, above which the tensile

properties were found to decrease. Therefore, more research is required to increase the fibre content in natural fibre composites, as composite strength increases with increasing fibre content.

2.6 Fibre Orientation Assessments

The orientation analysis, particularly in NPFCs, is challenging particularly due to the innate variability in the cross-section of natural fibres. Fibre orientation (alignment) is characterised statistically as fibre orientation distribution [133]. Many researchers characterised the fibre orientation by the optical section method [134] for which the composite samples are cut and polished in order to capture the micrograph of the fibres left on cross section [135]. However, this technique lacks accuracy as the elliptical marks in the cross sections are used to determine the fibre orientation. The use of radiography and computed tomography is also reported in the literature, but the low absorption index of the polymers makes the identification of fibre orientation more difficult [134]. Fibre orientation factor (K_θ) is also often reported in literature to indicate the degree of fibres aligned to the loading direction; (K_θ =1) for composites with highly orientated fibres. However, making and testing of composites is time consuming.

Image analysis has also been found to be a relatively fast method to assess and quantify fibre orientation. Xue et al. used Fast Fourier Transform (FFT) image analysis technique to determine the fibre orientation distribution of nonwoven flax mats and based on the profile of the peak determined orientation [136]. Orientation analysis employing ImageJ (NIH, USA) [137], an image analysis software via OrientationJ plug-in (EPFL, Switzerland), has been employed by some researchers to determine the distribution of governing fibre orientation angles [138-140]. However, ImageJ as an open-source software has more potential due to its availability compared to other image analysis software. Effective fibre orientation assessment using XRD has also been reported in the literature [141-143]. This X-ray diffraction (XRD) can provide mean diffraction patterns of the samples from which the preferred orientation of the crystalline component of the cellulose can be determined; to quantify the alignment of fibres with fibre mats [144].

In previous investigations into DSF mats made from hemp and harakeke fibres, the preferred orientation of fibres has been determined by analysis of optical microscopy images (either with visual observations [16] and ratio of transverse and longitudinal tensile strengths of the fibre mats [36]). Furthermore, composites with the DSF mats were tensile tested parallel and perpendicular to the main fibre alignment direction [36, 73], and estimation of fibre orientation factors from the tensile properties of the composites have also been reported in the literature [5, 16, 36]. However, testing of fibre mats or composites is time-consuming. And also, only limited literature discussing the assessment of orientation of natural fibres by image analysis can be found, with none for orientation assessment using XRD. Therefore, more research is required to make use of the available potential time-effective techniques that would be ideal for quantifying the degree of fibre alignment of natural fibre mats. The description of these assessment methods are provided in the following sections.

2.6.1 Fibre orientation assessment using ImageJ

OrientationJ plug-in is based on structure tensor; a matrix derived from the gradient of an image. For the assessment of every input image (images can be either optical or scanning electron microscopic), this software utilises a cubic B spline-interpolation by computing the continuous spatial derivatives in x and y directions (Figure 2.20a and 2.20b). A histogram with these parameters provides information on general distribution of fibres and predominant orientation angles corresponding to maximum intensity or frequency of pixel orientations [138-140]. The structure tensor for each pixel is represented as, a 2 x 2 matrix as shown below [9].

$$J = \begin{matrix} < fx, fx > w & < fx, fy > w \\ < fx, fy > w & < fy, fy > w \end{matrix} \qquad (2.2)$$

Where fx and fy are partial spatial derivatives of the image $f(x, y)$ and w is the observation window. This structure tensor decomposition provides eigenvalues (λ_{max} and λ_{min}) and eigenvectors by which this plug-in features local orientation, coherency and energy of every pixel of an image. The eigenvalues of the structure tensor provide information regarding the distribution of gradients within *w*, through parameters energy (E) and coherency (C). Through these values, one can determine the local predominant orientation (θ) corresponding to the alignment of the largest eigen vector (Figure 2.20c) of the structure tensor.

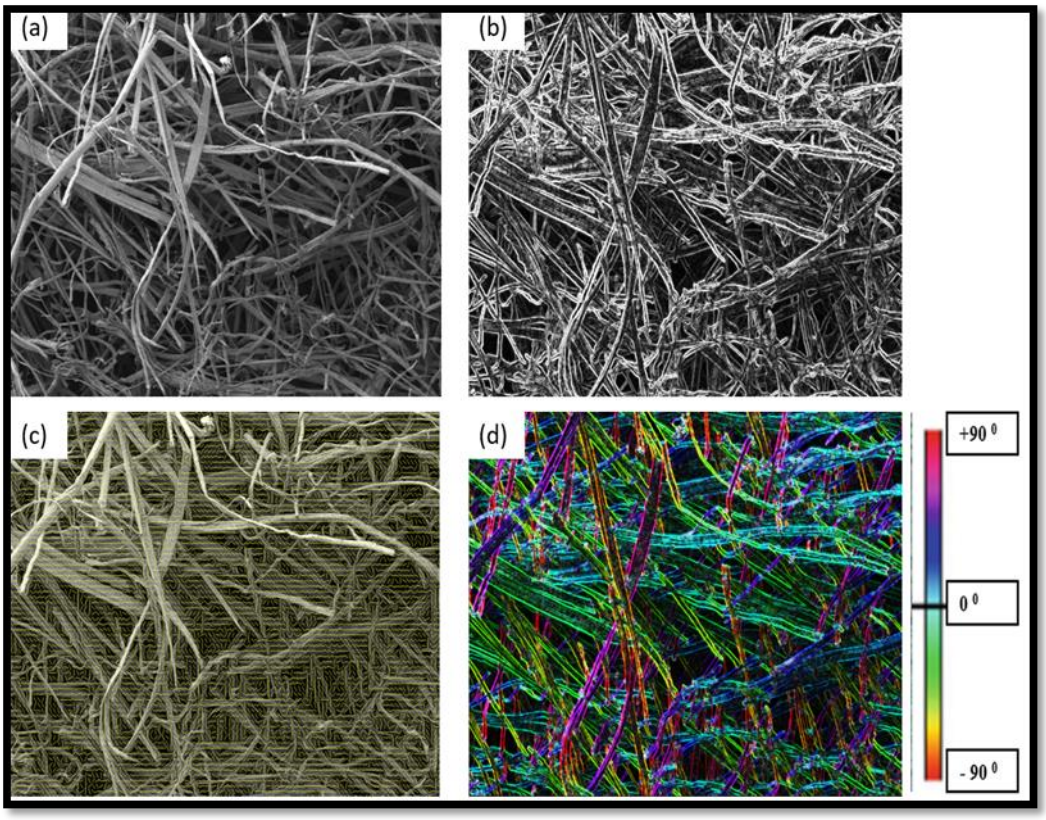

Figure 2.20: (a) Original image (a DSF mat) (b) Image showing the fibre edges (c) Image showing vectors on original image (d) Colour coded image showing orientation of fibres. (All the images were processed using ImageJ)

The local dominant orientation in the considered region (local window) is given by [139, 145],

$$\theta = \frac{1}{2}\arctan\left(2\frac{< fx, fy > w}{< fy, fy > w - < fx, fx > w}\right) \qquad (2.3)$$

The energy and the coherency are defined as the trace of the structure tensor, and the ratio between the difference and sum of the largest (λ_{max}) and smallest (λ_{min}) eigenvalues respectively. Generally, aligned structures possess higher energy values and coherency close to 1 (C is bounded between 0 and 1) [139, 146]. Qualitative visual representations (colour coded maps) of orientation (Figure 2.20d) are also possible in OrientationJ with HSB mode; Hue-angle of orientation, Saturation-coherency and Brightness-input image.

2.6.2 Fibre orientation assessment using XRD

X-ray diffraction technique is useful in revealing detailed information about the crystallographic structure of solid materials [147]. Most solids are crystalline in nature, but crystal orientations are not always present. Figure 2.21 shows the schematic illustration of preferred orientation and random orientation in a polycrystalline material. As aforementioned, the DSF has the potential to orient most of the fibres within the produced mats towards the flow direction, which is the preferred orientation. Thus, the fibre mats produced using DSF are very often textured with a strong preferred orientation. Therefore, XRD can be used to quantify the texture in the specimen as samples are with systematic orientation.

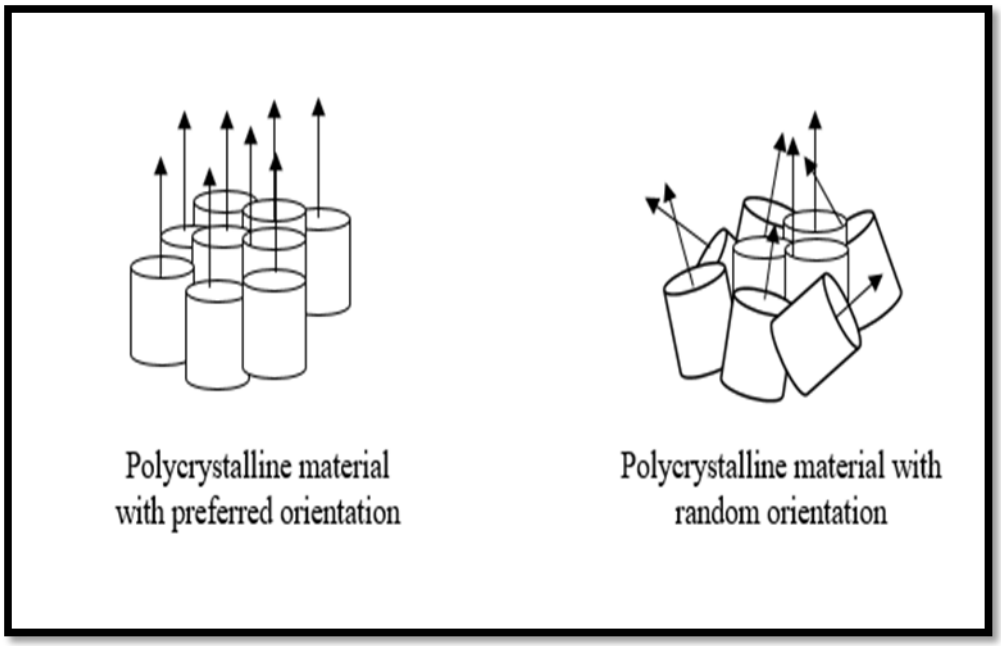

Figure 2.21: Schematic illustration of orientation.

2.7 Composite Tensile Properties Predictions

From a perspective of fibre length, the fibre reinforced composites may be classified as continuous and discontinuous fibre composites. A number of theoretical models have been developed and reported in literature to give good approximations, they are often used to predict strength of continuous fibre composites. Most of the strength prediction models are based on the assumption that fibres are continuous and are aligned axially to the direction of applied load [5]. Commonly, in the prediction models, both fibre reinforcement and matrix are assumed to be elastic and the strain

in the fibre and the matrix are assumed to be the same [32]. However, it should be noted that in discontinuous fibre composites, the tensile properties of the composites are governed by a number of factors such as fibre length, fibre orientation, dispersion of fibres within the matrix materials, stress transfer between the fibre and the matrix [32]. Therefore, when the fibres are discontinuous equations given by the Rule of Mixtures are generally not obeyed. Additionally, NPFCs diameter variation along the length of the fibres is also a significant factor. Some of the simple mathematical prediction models used for the present study are briefly described in this section.

The parallel and series Rule of Mixture models are commonly applied to represent the upper and lower bounds for tensile properties of axially aligned short fibre composites. According to this model, tensile strength and Young's modulus can be calculated using the equation:

$$\sigma_C = \sigma_f v_f + \sigma_m v_m \tag{2.4}$$

$$E_C = E_f v_f + E_m v_m \tag{2.5}$$

where σ, E and v are the tensile strength, Young's modulus and volume fraction of fibres, respectively. The subscripts *c*, *f* and *m* indicate composite, fibre and matrix, respectively in this work. The equations 2.4 and 2.5 are commonly known as the parallel model, whereas the series model (perpendicular to fibre alignment direction) is shown by the equations 2.6 and 2.7.

$$\sigma_C = \frac{\sigma_m \sigma_f}{\sigma_m v_f + \sigma_f v_m} \tag{2.6}$$

$$E_C = \frac{E_m \sigma_f}{E_m v_f + E_f v_m} \tag{2.7}$$

The Hirsch model, as shown by the equations 2.8 and 2.9, is based on a combination of the above mentioned parallel and series models. Hence, this model can be applied to discontinuous fibre composites. An empirical fitting parameter, x is introduced in this model, which can be considered as an indication of the stress-transfer efficiency between the fibre and the matrix whilst considering alignment of fibres, fibre length and stress amplification at fibre ends. The value of x can be varied from 0 to 1 to give the best fit.

$$\sigma_c = x(\sigma_f v_f + \sigma_m v_m) + (1-x)\sigma_c = \frac{\sigma_m \sigma_f}{\sigma_m v_f + \sigma_f v_m} \qquad (2.8)$$

$$E_c = x(E_f v_f + E_m v_m) + (1-x)\frac{E_m \sigma_f}{E_m v_f + E_f v_m} \qquad (2.9)$$

The Haplin-Tsai model has been previously reported to be used by several researchers to determine the strength of polymeric blends consisting of continuous and discontinuous phases [148]. It has been reported that this model can be used for predicting the tensile properties of discontinuous fibre composites orientated either in longitudinal or transverse direction [16]. This model is a semi-empirical model with the shape fitting parameter ς. This shaping fitting parameter is to fit the model to experimental data depending on the fibre geometry and the loading direction (longitudinal or transverse). According to this model, tensile strength can be predicted as follows:

$$\sigma_c = \sigma_m \left(\frac{1 + \varsigma \eta v_f}{1 - \eta v_f}\right) \qquad (2.10)$$

$$Ec = \mathrm{E_m}\left(\frac{1 + \varsigma\eta^{*} v_{\mathrm{f}}}{1 - \eta^{*} v_{\mathrm{f}}}\right) \tag{2.11}$$

where:

$$\eta = \left(\frac{\frac{\sigma_f}{\sigma_m} - 1}{\frac{\sigma_f}{\sigma_m} + \varsigma}\right) \tag{2.12}$$

$$\eta^{*} = \left(\frac{\frac{\mathrm{E}_f}{\mathrm{E}_m} - 1}{\frac{\mathrm{E}_f}{\mathrm{E}_m} + \varsigma}\right) \tag{2.13}$$

such that η is the relative strength of the fibre and the matrix. The shape fitting parameter ς for circular cross-section is given by:

$$\varsigma = \frac{2l}{d} \tag{2.14}$$

where, l is the length of the fibre in the direction of loading and d is the diameter of the fibre.

The Haplin-Tsai model was modified further [149] in order to account for the amount of fibre incorporated into the matrix as well as fibre arrangement as shown by the equations:

$$\sigma_C = \sigma_{\mathrm{m}}\left(\frac{1 + \varsigma\eta v_{\mathrm{f}}}{1 - \eta\psi v_{\mathrm{f}}}\right) \tag{2.15}$$

$$E_C = \mathrm{E_m}\left(\frac{1+\varsigma\eta^* v_\mathrm{f}}{1-\eta^*\psi v_\mathrm{f}}\right) \quad (2.16)$$

where:

$$\psi = 1+\left(\frac{1-\Phi_{max}}{\Phi_{max}{}^2}\right)v_f \quad (2.17)$$

where Φ_{max} is the maximum fibre packing fraction based on the relevant fibre arrangement and have values 0.785, 0.907 and 0.82 for a square, a hexagonal array, random packing arrangements of fibres, respectively. η and ς can be determined by equations 2.12 and 2.14, respectively.

Cox's model is amongst the earliest models to predict the tensile properties of discontinuous fibre composites. According to this model, the tensile properties of short fibre composites can be predicted similar to the Rule of Mixture, but by including a factor that would account for the effectiveness of load transfer from the matrix to the fibre. This model gives the tensile properties of the composites using the equations:

$$\sigma_C = \sigma_f v_f\left(1-\frac{tanh\left(\frac{\beta l}{2}\right)}{\frac{\beta l}{2}}\right)+\ \sigma_m v_m \quad (2.18)$$

$$E_C = E_f v_f\left(1-\frac{tanh\left(\frac{\beta l}{2}\right)}{\frac{\beta l}{2}}\right)+\ E_m v_m \quad (2.19)$$

where

$$\beta = \left(\frac{2\pi G_m}{E_f A_f \ln \frac{R}{r}} \right)^{\frac{1}{2}} \qquad (2.20)$$

where r, G_m, l are the radius of fibre, shear modulus of matrix and length of the fibre, respectively. And A_f and R are the area and centre to centre distance of the fibres.

For square packed fibres,

$$R = r \left(\frac{\pi}{4 v_f} \right)^{\frac{1}{2}} \qquad (2.21)$$

If (βl/2) is large, the value of reinforcement effectiveness reduction factor approaches unity and the reduction factor tends to zero when the value is small.

Krenchel further modifies the Cox model to take into account the orientation of fibres by incorporating a factor for fibre orientation, K_θ. The orientation factor has a value of unity for axially aligned fibre composites: 0.2 for randomly orientated fibre composites and 0.375 for planar random configuration [150, 151].

Kelly-Tyson modified the rule of mixture for fibres parallel to loading direction to predict the tensile properties of axially aligned discontinuous fibre composites depending on whether the average length of the fibres is above or below critical length of the fibre(L_c). The minimum length at which the stress in the fibre reaches the fibre tensile strength is termed as the critical fibre length(L_c). This can be determined experimentally. The most common techniques used to determine are the pull-out test or a fibre fragmentation test [5, 152] where the critical length of the fibre can be determined using the following equation:

$$\frac{L_c}{d} = \frac{\sigma_f}{2\tau_i} \qquad (2.22)$$

where (σ_f) average fibre strength, (d) average fibre diameter and (τ_i) the interfacial shear strength. It is clear that improvement of τ_i results in lower L_C.

According to this model, a stress transfer efficiency factor, k_{st} was introduced into the basic Rule of Mixture equation and determines the stress transfer efficiency from matrix to fibres. The equations 2.4 and 2.5 were further modified as

$$\sigma_C = k_{st}\sigma_f v_f + \sigma_m v_m \qquad (2.23)$$

$$Ec = k_{st}E_f v_f + E_m v_m \qquad (2.24)$$

with k_{st} was determined using the following equation,

For $L < L_C$, $k_{st} = \frac{L}{L_C}$ or

For $L > L_C$, $k_{st} = 1 - \frac{L_C}{2L}$

The Bowyer-Bader model proposed a model based on the Kelly-Tyson modified Rule of Mixtures, which predicts the tensile strength of short fibre composites by considering the sum contributions of different fibre lengths (sub-critical and super-critical fibre length, as well as that of matrix.

To enable the strength prediction of composites containing fibres orientated in different directions, a simple numerical fibre orientation factor (K_θ) was fitted to the Rule of Mixture equation to account for the distribution of orientation:

$$\sigma_C = \sigma_f v_f k_\theta k_{st} + \sigma_m v_m \qquad (2.25)$$

$$Ec = E_f v_f k_\theta k_{st} + E_m v_m \quad (2.26)$$

As mentioned before, in the Kelly-Tyson model the average fibre length is used. Instead of this, the effect of fibre length distribution on composite tensile properties was taken into account in the Bowyer-Bader model:

$$\sigma_C = k_\theta \left\{ \sum_i \left[\frac{v_i \sigma_f L_i}{2L_c} \right] + \sum_j v_j \sigma_j \left[1 - \frac{L_c}{2L_j} \right] \right\} + \sigma_m v_m \quad (2.27)$$

where, L_i and L_j are the sub-critical and super-critical fibre length respectively, and v_i and v_j, are the volume fractions of these sub-critical and super-critical fibre lengths, respectively.

2.7.1.1 Limitations associated with strength prediction models

Table 2.6 displays the models used for the present study and some of the assumptions associated with each of these composite strength prediction models. All the models used in the present study (Table 2.6) assume that the fibres within the composites are anisotropic. But, this is very unlikely for natural fibres as they are expected to be weak in the transverse direction and strong in longitudinal (fibre-axis) direction [5]. The models also assume that the fibres are cylindrically shaped. However, the hemp fibres (natural fibres) are not perfectly cylindrical. Thus, the strength prediction models consider only the in-plane failure associated with natural fibres; they do not consider fibre strength distributions associated with the fibres. Moreover, each model assumes that the composite is void-free. This could lead to the inaccuracies of predicted strength as the voids formed at the interface between the fibres and the matrix can act as stress raisers and influence the performance of composites.

Most composite manufacturing processes leads to complex fibre orientations, which can complicate data analysis and comparisons with experimental and theoretical predictions [153, 154]. Fibre orientations within a composite are not easy to measure as the fibres are obscured by the matrix and cannot be clearly viewed in three

dimensions. Thus, the fibre orientation factors in most models are given as fitting factors and are derived indirectly from experimental tests, rather than being measured or evaluated based on fibre orientation distributions within the composites [155].

Table 2.6: Main models and the associated assumptions used for the prediction of tensile strength of the composites [32, 156]

Models	Main assumptions
Parallel and Series Rule of Mixture Model	• Reinforcing fibres have perfect interfacial bonding with the fibre and the matrix. • Iso-strain conditions exist for fibre and matrix.
Hirsch's Model	• Fitting parameter (X); between 0 and 1, fitted empirically to experimental data. 'X' can be supposed to represent the stress transfer between the fibre and the matrix, considering fibre orientation, fibre length, and stress amplifications at fibre ends.
Halpin-Tsai Model	• Shaping fitting parameter (ς); to fit this model to experimental data depending on the fibre geometry and loading direction.
Modified Halpin-Tsai (Neilsen) Model	• Introduced further a factor Ψ; to enable better prediction by considering the fibre arrangement as well as fibre content.
Cox Model	• The applied load is assumed to be transferred from the matrix to the fibres by means of shear forces. • Perfect interfacial bonding between fibre and matrix perfect. • Included a factor to account for the effectiveness of load transfer at the interface.
Modified Cox (Krenchel) Model	• Introduced further a fibre orientation factor, K_θ – has value 1, 0.2 and 0.375 for axially, random and planar random configuration for fibre-reinforced composites, respectively.

Kelly –Tyson Model	• No fibre-matrix debonding occurs. • No voids present in the composites. • Composites properties are same as those of neat matrix (PP) properties. • Similar assumption to the Cox model in terms of load transfer, but further assumed the stress increases linearly with distance from the fibre ends up to the yield stress, at which the stress at the interface is assumed to be constant until iso-strain conditions exist of which fibre stress levels and the shear stress at the interface is 0. • Critical fibre length (L_c) is considered; the minimum length at which the stress in the fibre can reach the fibre tensile strength. • L_c – determined using SFPO testing. • The tensile properties of the composite depend on a fibre stress transfer factor, $K_{st.}$ This factor determines stress transfer efficiency from matrix to fibre depending on whether the average fibre length is above or below L_c.
Modified Kelly –Tyson Model	• Similar to above, fitted further a fibre orientation factor (K_θ). The common values for the factor are as given in modified Cox model.
Bowyer-Bader Model	• Take into consideration the sub-critical and super-critical fibre length distributions in composites. • No fibre-matrix debonding occurs. • No voids present in the composites. • An orientation factor, K_θ may be applied to account fibres not orientated to the loading direction. K_θ - independent of strain and is same for all length of fibres. • The interfacial stress transfer is independent of the loading angle.

2.8 Chapter conclusions

Generally, fibre reinforcements are either in continuous or discontinuous form. Continuous fibre reinforced composites perform better because the fibre continuity allows easy alignment in the preferred direction compared to short fibres [71]. However, discontinuous fibre reinforced polymer composites are becoming more attractive, with major benefits including the ability to manufacture complex structural parts due to their higher ductility in all directions [64, 71]. Commonly, randomly orientated preforms are used as reinforcement in short (discontinuous) natural fibre composites (SNPFCs) due to the difficulty in aligning short fibres. However, mechanical performance can be improved by the alignment of fibres in the main loading direction. Generally, for orientation of fibres, two main approaches are used: dry and wet processes. Of these, a higher degree of orientation has been reported for wet processes. Dynamic sheet forming, a wet process, mostly used in paper production has proven to be an effective way to produce mats with reasonable alignment. However, more research needs to be carried out to optimise the fibre mats production to improve the potential use of these mats in polymer matrices.

3 Chapter Three

Alkali treatment of hemp fibres for the production of aligned hemp fibre mats using dynamic sheet forming

3.1 Introduction

The main objective of this study was to produce aligned hemp fibre mats from high strength hemp fibres using dynamic sheet forming (DSF). Alkali treatment of hemp fibre was carried out at ambient and high temperatures. The alkali treatments used are modifications of selected alkali treatments from the literature that report improved tensile strength for NPFs [5, 157]. The data obtained for the tensile strengths of the hemp fibres were statistically analysed using Weibull statistics.

3.2 Materials and Methodology

3.2.1 Materials

Industrial hemp fibre was obtained from Moffett Orchards Ltd., New Zealand. The bast fibres were hand separated from the stalks. The chemicals used for the experiments were sodium hydroxide (NaOH) and sodium sulphite (Na_2SO_3) supplied by Sigma Aldrich, New Zealand.

3.2.2 Alkali treatment

High temperature (HT) and ambient temperature (AT) alkali fibre treatments were carried out on pre-dried hand separated hemp fibres. For ambient temperature treatment, fibres were granulated using an 8 mm mesh in a laboratory scale Castin granulator and then immersed in 5 wt% sodium hydroxide (NaOH) solution in a glass beaker as shown in Figure 3.1a, for one (AT/one hour) or two hours (AT/two hours) with a fibre to solution ratio of 1:8. The temperature inside and outside the

beaker was measured using a thermometer. The measured room temperature was between 20.5 and 22 °C, whereas the temperature inside the beaker ranged from 30.5 °C at the start of the treatment to 24 °C at the end of the treatment. For high temperature treatment, fibre and a solution of 5 wt% NaOH and 2 wt% Na_2SO_3 with a fibre to solution ratio of 1:8 were placed in stainless steel canisters (SSCs) (Figure 3.1b). These canisters were then positioned inside a laboratory scale pulp digester controlled by a proportional-integral-derivative (PID) system as displayed in Figure 3.1b, which was set to operate with a time-temperature profile as shown in Figure 3.2. Granulation was either conducted before or after treatment. The fibres were washed with clean water and filtered through a sieve after the treatments at least six times, before being dried in an oven at 80 °C for 48 h.

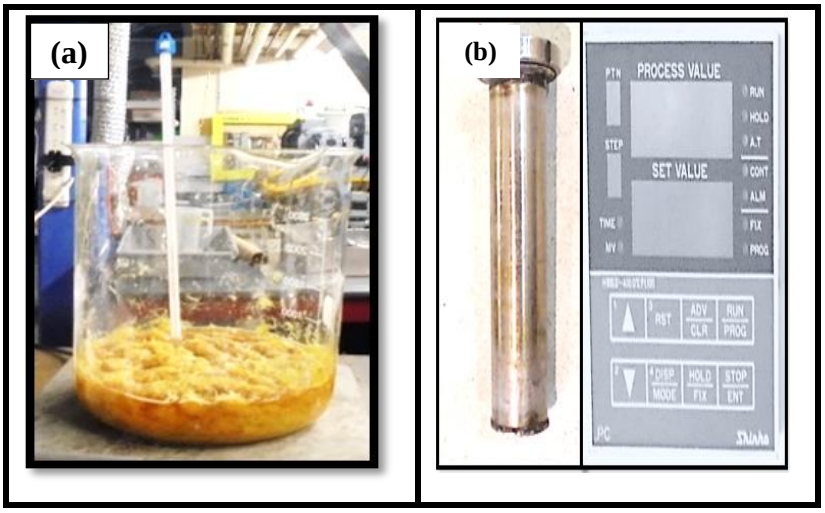

Figure 3.1: (a) Set up used for the AT treatment (b) SSC and PID system used for the HT treatment.

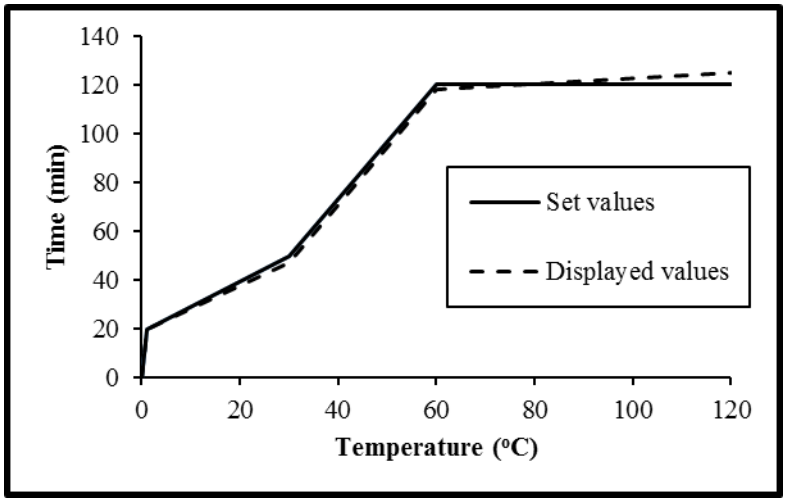

Figure 3.2: Time-temperature profile used for the HT treatment.

3.2.3 Single fibre tensile testing

The ASTM D 3379-75: Standard Test Method for Tensile Strength and Young's Modulus for High-Modulus Single-Filament Materials [158] was followed to determine the tensile strength and Young's modulus of untreated (UT), AT/one hour treated, granulated before HT treated and granulated after HT treated hemp fibres. The untreated fibres were soaked in water for around 10 days to remove dirt from the fibre surface. Two-millimetre thick cardboard was used for mounting tabs with a gauge length of 2 mm as schematically represented in Figure 3.3. Selected single fibres were adhered to the mounting tabs by the application of polyvinyl acetate (PVA) glue.

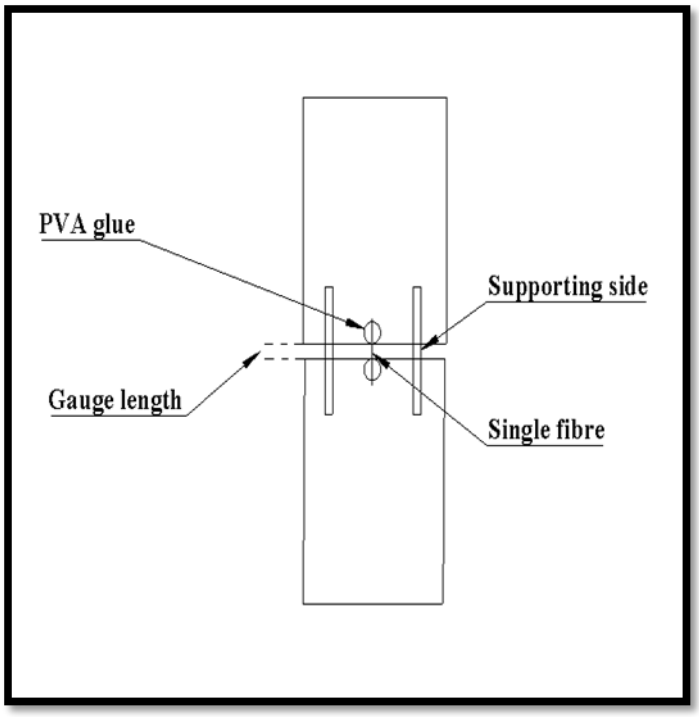

Figure 3.3: Schematic representation of a mounting tab used for tensile testing of single fibre.

For the measurement of single fibre diameter, optical images were captured of single fibres as shown in Figure 3.4, by means of an Olympus BX60F5 optical microscope fitted with a Nikon camera. The diameter was measured at five different points along each fibre (as hemp fibres have variable diameters across their length) and average values were used for the calculations.

The single fibres were then tensile tested using an Instron-4204 universal testing machine after burning off the supporting sides using a hot wire cutter. The test was carried out at a rate of 0.5 mm/min with a 10 N-load cell. Thirty samples were tested for each treatment and system compliance was determined experimentally to obtain Young's moduli according to the procedure described in ASTM D 3379-75. For this, mounting tabs with gauge lengths of 5, 10 and 15 mm were also prepared.

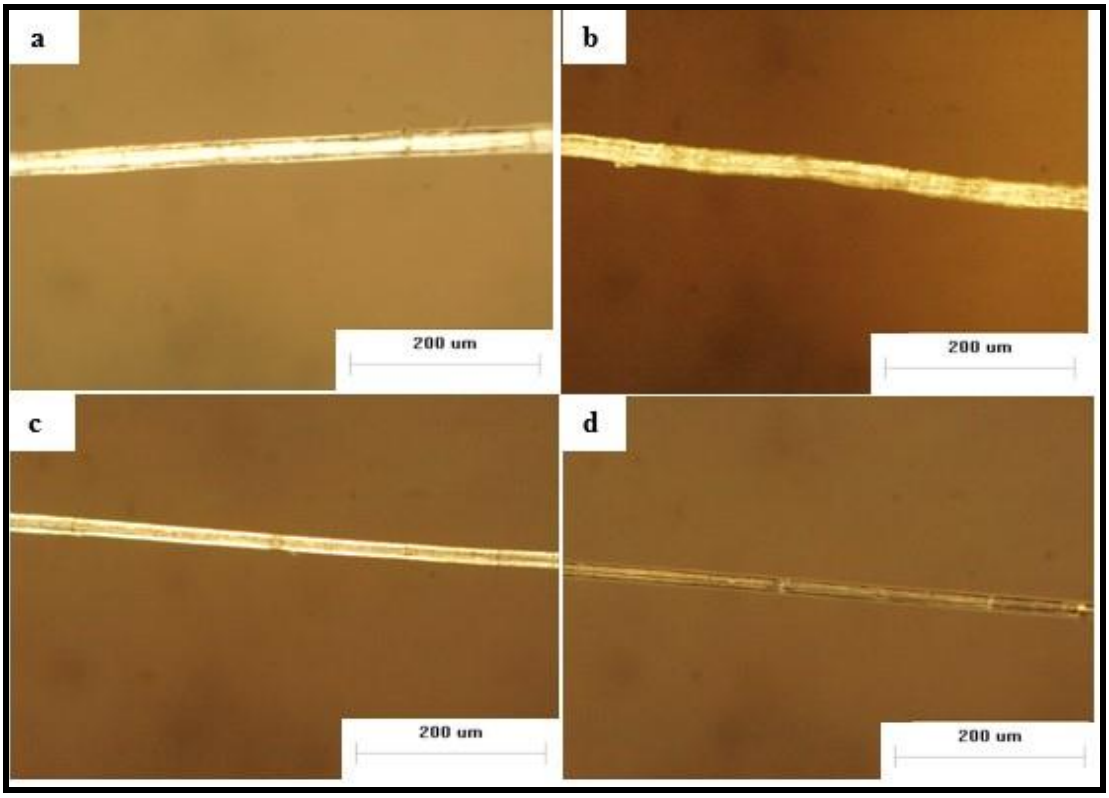

Figure 3.4: Single hemp fibre as observed under optical microscope: (a) UT, (b) AT/one hour, (c) granulated before HT and (d) granulated after HT treated hemp fibres.

The Weibull distribution is commonly used to analyse the strength variation for natural fibres [31, 132, 159, 160]. Here, the rearranged two-parameter Weibull cumulative distribution expression [132, 159], as shown below, was used to analyse data obtained for different single fibre testing statistically.

$$lnln\left(\frac{1}{1-P_f}\right) = wln\sigma - wln\sigma_o + lnL \qquad (3.1)$$

where w is the Weibull modulus (shape parameter) and σ_o characteristic strength (scale parameter). These parameters are important as they describe the distribution of the fibre failure strength where w describes the variability, a low value of w indicates high variability and σ_0 is the stress at which the probability of failure of unit length is 0.632 (1-exp (-1)) [160]. A Weibull plot of $lnln\left(\frac{1}{1-P_f}\right)$ versus $ln\sigma$ provides a straight line with gradient w and intercept σ_o at $lnln\left(\frac{1}{1-P_f}\right) = 0$.

3.2.4 Scanning electron microscopy of hemp fibre surfaces

A Hitachi S-4100 SEM was used to obtain micrographs of fibres. Before this, carbon tapes were employed to mount the samples on aluminium stubs and were then sputter coated with platinum to make them conductive.

3.2.5 X-ray diffraction

XRD spectra were obtained using an EMPYREAN diffractometer system (PANalytical). For the measurements, the fibres were chopped and pressed into a disk using a cylindrical steel mould. The scanning range was between 5^o and 45^o by employing CuKα radiation (λ=1.54 nm) with a voltage and current of 45 mV and 40 mA respectively. Crystallinity index (I_c) of the fibres was calculated using the Segal method [161]:

$$I_c = ((I_{22.7} - I_{18.3})/I_{22.7})\ \text{X100} \qquad (3.2)$$

where I_{200} is the maximum intensity of the (200) lattice diffraction peak of cellulose I, and I_{am} is the minimum intensity of diffraction at an angle at 18.3° representing amorphous content [132].

3.2.6 Fourier transform infrared spectroscopy

A PerkinElmer Spectrum One spectrometer was used to obtain infrared spectra of untreated, AT/one hour treated and granulated after HT treated hemp fibres. Hemp fibre samples were ground to fine powder using a Retsch MM400 ball mill. The ground powder for each sample was then mixed and compressed with KBr (potassium bromide) using a hydraulic press by applying 8 tonnes/cm^2 pressure to prepare corresponding sample disc for FTIR analysis.

3.2.7 Thermogravimetric analysis

Thermal gravimetric analysis (TGA) of untreated, AT/one hour treated and granulated after HT treated hemp fibres was carried out using a PerkinElmer simultaneous thermal analyser STA 8000. Data were obtained at a rate of 10 °C/min with a heating range of 40 °C to 500 °C and a static airflow at 20 ml/min.

3.2.8 Fibre mat production

Aligned fibre mats (Figure 3.5a) were produced using a dynamic sheet former built by Canpa, Canada (Figure 3.5b). To produce fibre mats, fibre suspension (approx. 5g in 10 litres of water) was made. This suspension was then pumped by the dynamic sheet former through a reciprocating nozzle onto a rotating drum covered with a wire mesh which acts as a cushion for the deposited fibre [4]. The alignment of the fibres is in accordance with the nozzle and rotation of the drum. A total of 45g of fibre was used for production of each mat. For the production of fibre mats using DSF, well-separated fibre is required to avoid blocks mainly in the flow hoses through which the fibre suspension is discharged onto the rotating drum from the suspension tank.

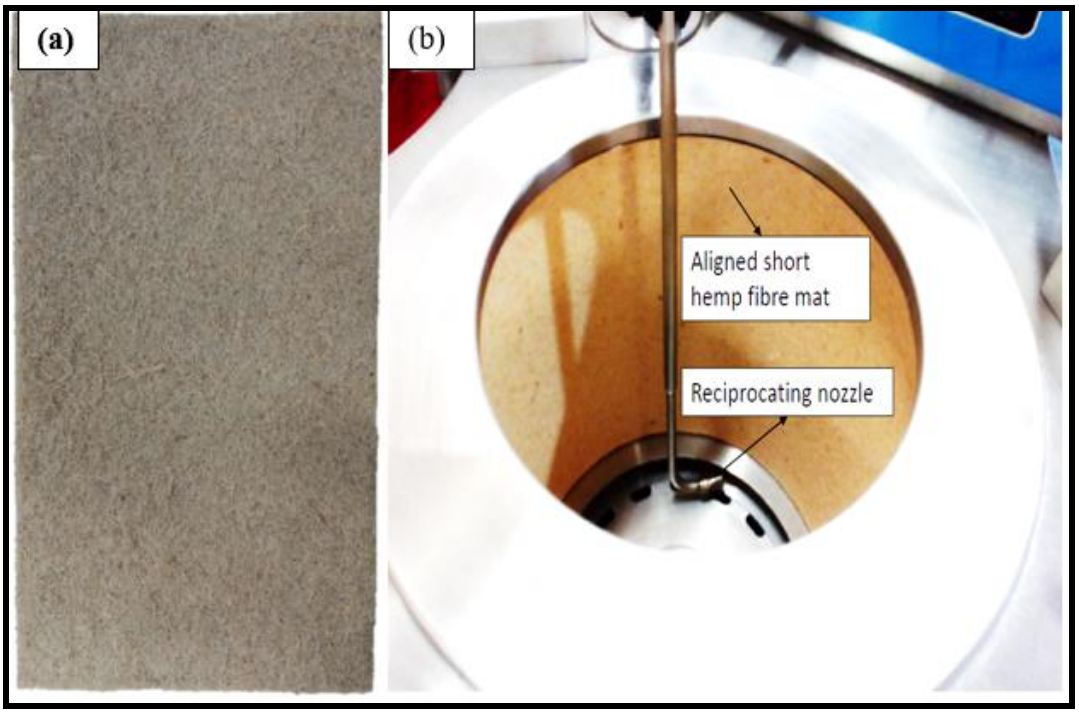

Figure 3.5: (a) Aligned short hemp fibre mat (b) Dynamic sheet former.

3.3 Results and Discussion

3.3.1 Tensile properties of fibres

Hemp fibres have a complex layered structure, containing primary and secondary cell walls. These cell walls consist of many layers of helically wound cellulose microfibrils. The main factors that determine the mechanical properties of different plant fibres are cellulose content, microfibrillar angle, defects and treatments [44].

Table 3.1 displays the diameters, maximum load and mechanical properties of untreated and treated fibres obtained in this work. As can be seen, the HT alkali treatment (granulated before and after HT) resulted in more fibre diameter reduction compared to the AT treatment. It has been found that reduction in fibre diameter is due to the removal of hemicellulose and lignin [29, 103, 111, 157]. Although no specific studies were carried out to measure the hemicellulose or lignin content in this work, it has been reported elsewhere that hemicellulose breakdown occurs easily in a high temperature environment than at low temperature and the addition of Na_2SO_3 assists NaOH in the removal of lignin [5]. It was found that HT treatment removed sufficient hemicellulose and lignin from the fibres to give good fibre separation, whereas similar separation was not observed for the fibres with AT treatment.

Table 3.1: Mechanical properties of hemp samples. Standard deviations are shown in parentheses. Number of fibres tested for each batch = 30.

Hemp samples	Fibre diameter/μm	Maximum load /N	Average tensile strength /MPa	Young's modulus /GPa
UT	30.3 (10.6)	0.30 (0.14)	517 (355)	7.4 (4.7)
AT/one hour	29.9 (6.7)	0.30 (0.18)	436 (236)	6.4 (2.7)
Granulated before HT	21.4 (4.3)	0.25(0.08)	781 (428)	12 (4.4)
Granulated after HT	22.4 (5.8)	0.28(0.13)	833 (577)	12.3 (7.3)

From the tabulated results, it can be seen that the HT alkali treated fibre exhibited higher average tensile strength and Young's modulus compared to UT and AT alkali treated fibres, whereas the average tensile strength and Young's modulus exhibited

by the AT alkali treated fibre were lower than for UT fibre. This suggests that the resulting structures of the treated fibres depend on the alkali treatment used. When compared to UT fibres, the average tensile strength and Young's modulus of the fibres improved by about 51 and 62 %, respectively. The increase in average tensile strength for HT alkali treated fibre compared to UT fibre is thought to be due to the removal of weak components (non-strengthening components) evidenced by the fibre diameter reduction after the treatment. The removal of weak components from the fibre cell walls can lead to close packing of cellulose chains and possibly a decrease in the microfibrillar angle. This close compaction could have enhanced the adhesions between cellulose microfibrils, thereby providing better tensile properties for HT treated fibres towards the loading direction compared to UT treated fibres [31]. As can be seen in Table 3.1, although the diameter of AT alkali treated fibre reduced after the treatment compared to UT fibre, the tensile properties of the fibre were reduced even below that of UT fibre. The decrease in tensile properties associated with the fibre is thought to be due to the degradation of the crystalline cellulose chains in the microfibrils or bonding between cellulose microfibrils as affected by the AT treatment [31, 162].

Student's t-test (statistical hypothesis test) was carried out for comparing HT alkali treated fibres with different granulation sequence and it was found that the sequence of granulation had no significant effect on tensile properties of the fibres.

Weibull modulus, Weibull characteristic strength and experimental average tensile strength are displayed in Table 3.2. As expected, the characteristic strength has the same trend as that of average tensile strength. Bearing in mind that natural fibres commonly possess much larger variability in physical, chemical and mechanical properties compared to synthetic fibres [31], low Weibull modulus representing a high distribution of fibre strength was expected, as seen here. The Weibull modulus for the fibres varied from 1.68 to 2.05. These values are comparable with those reported in the literature for cellulosic fibres [16, 132].

Table 3.2: Comparison of Weibull parameters with experimental tensile strength for hemp samples

Hemp samples	Weibull modulus/ w	Characteristic strength/MPa, σ_0	Average tensile strength /MPa
UT	1.68	576	517
AT/one hour	1.92	478	436
Granulated before HT	2.05	869	781
Granulated after HT	1.74	928	833

3.3.2 Cellulose crystallinity index (I_c)

Crystallinity index indicates the degree of crystallinity of cellulose [163, 164]. The X-ray diffraction profiles (curves) of UT, AT/one hour, AT/two hours and granulated after HT treated hemp fibres are shown in Figure 3.6. The I_c values were calculated from maximum and minimum intensities of diffraction for each profile which are around $2\theta = 22.7^{o}$ and $2\theta = 18.3^{o}$, respectively and are displayed in Table 3.3.

Table 3.3: Crystallinity index for hemp samples

Hemp samples	Crystallinity index/I_c
UT	64.87
AT/ One Hour	71.16
AT/ Two Hours	61.68
Granulated after HT	80.65

As can be seen in Table 3.3, alkali treatments improved the I_c values except for AT/two hours. The higher I_c value of HT alkali treated fibre compared to the UT fibre would be expected due to the removal of non-crystalline materials and possibly better packing of cellulose chains within the fibre [5]. Although the I_c value of AT/one hour alkali treated fibres was higher compared to UT fibre, as discussed earlier the tensile strength of this fibre was lower than that of UT fibre. This suggests that chain scission could have overridden the influence of increased crystallinity [16, 30, 50, 97]. It has been reported elsewhere that the degradation rate of cellulose in

alkali is influenced by fibrillar morphology; a more ordered physical structure impedes degradation [165]. This supports the production of better-packed cellulose chains with HT treatment which would have impeded the diffusion of alkali reducing cellulose degradation compared to AT alkali treated fibres.

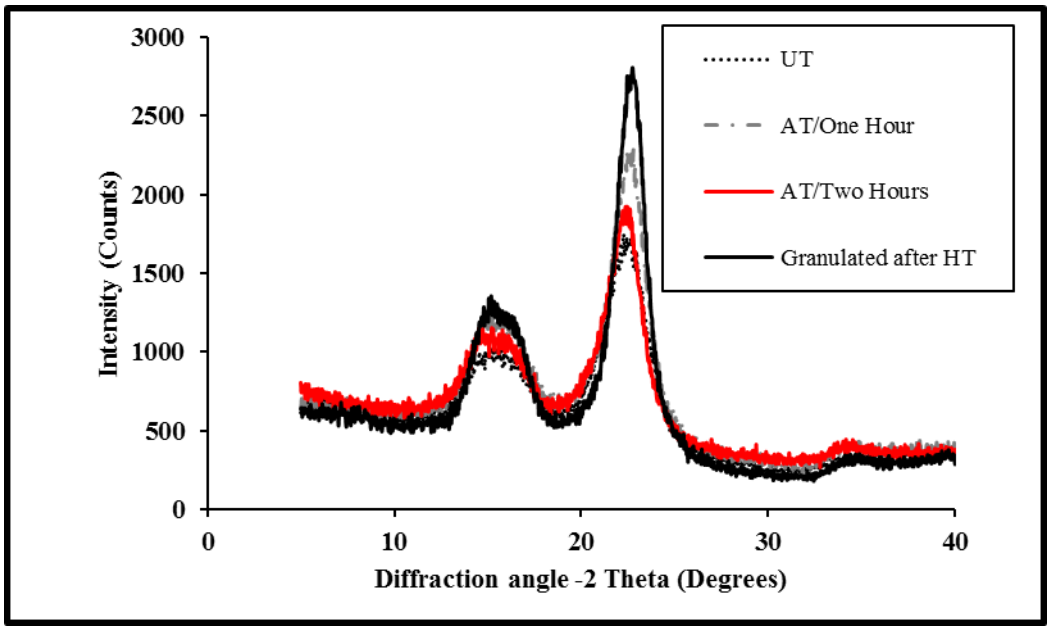

Figure 3.6: X-ray diffraction curves for untreated, atmospheric temperature treated and high temperature treated fibres.

3.3.3 Fourier transform infrared spectroscopic analysis

Peaks (Figure 3.7) in the regions 1730-1740 cm^{-1} and 1200-1300 cm^{-1} indicate the hemicellulose and lignin components through the presence of C=O linkages [166, 167]. Peaks at 1737 cm^{-1}, 1252 cm^{-1} and 1201 cm^{-1} for the UT fibres became smaller for the AT alkali treated fibres and were not visible for HT alkali treated fibres. Reduction of peak heights supports alkali treatment removed hemicellulose and lignin, with more removal occurring in HT alkali treated fibres compared to AT alkali treated fibres [50, 106, 166, 168-170]; the peak at 1232 cm^{-1} corresponding to the C-O stretching vibration of lignin reduced after the alkali treatments. Similarly, the smaller peaks in the range between 1280 cm^{-1} and 1330 cm^{-1} for HT alkali treated fibres compared to AT alkali treated and UT fibres further support that HT treatment removes more hemicellulose than AT alkali treated fibres [157]. The intensity of peaks between 1630 cm^{-1} and 1650 cm^{-1} slightly increased after alkali treatment,

which may be due to water molecules formed by the reactions between sodium hydroxide and cellulosic hydroxyl groups [171].

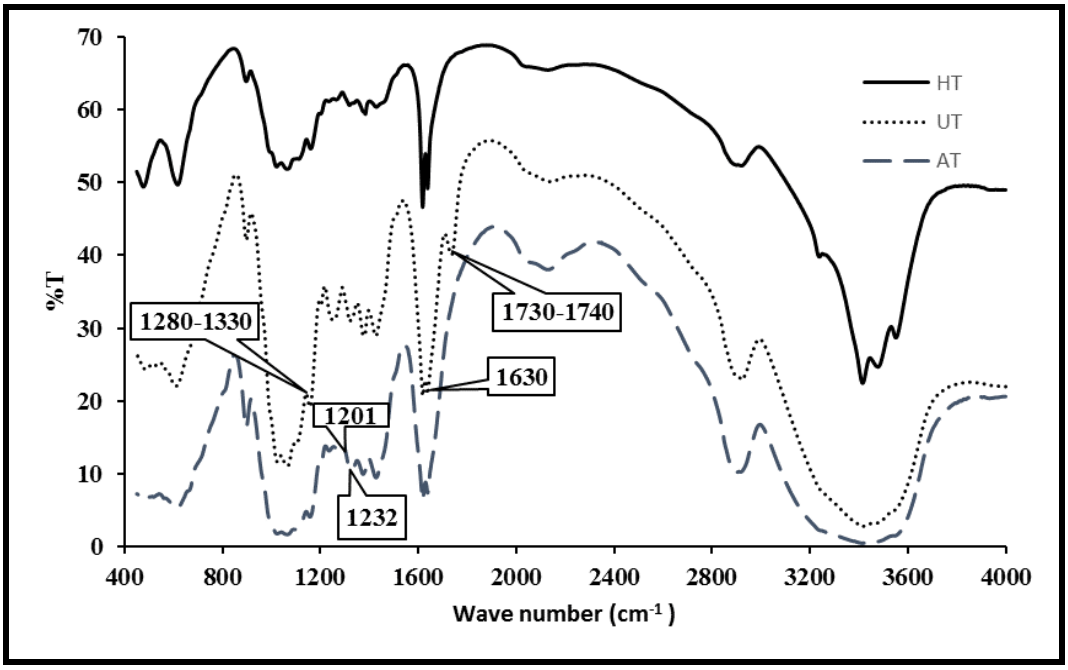

Figure 3.7: The FTIR spectra of untreated, AT/one hour treated, and granulated after HT treated fibres.

3.3.4 Thermogravimetric analysis (TGA)

Typically for NPFs, there are three main stages of degradation where most of the weight loss occurs: between 50 and 100 °C due to evaporation of moisture in the fibres, between 200 and 350 °C due to hemicellulose decomposition and between 300 and 500 °C (450 °C) mainly due to degradation of lignin and cellulose [172-174].

Figure 3.8 and Figure 3.9 show the TGA thermograms and weight loss summary for UT fibres and AT and HT alkali treated fibres. From Figure 3.9, it can be seen that the initial 10 % weight loss occurred only at 297 °C and 329 °C for the AT and HT alkali treated fibres respectively compared to 288 °C for UT fibres supporting the overall improved thermal stability of the fibres. The improved thermal stability of the fibres is likely to be due to thermally unstable components (hemicellulose and pectin) being removed from the fibres due to alkali treatment [5], with more removal occurring with HT alkali treatment compared to AT treated fibres as supported by FTIR analysis. As the temperature further increased above 360 °C, the weight loss was lower for UT fibres compared to treated fibres, which may be due to a stable

lignocellulose complex formed at higher temperatures that prevented this lignin-rich fibre from further weight loss above 360 °C [35]. In addition, at higher temperatures, it was found that the weight percentage loss was higher for HT alkali treated fibres compared to AT alkali treated fibres (Figure 3.9). This higher weight percentage loss for HT alkali treated fibres above 360 °C up to 450 °C supports that the greater removal of lignin from the fibre was by HT alkali treatment compared to AT alkali treatment [5, 16].

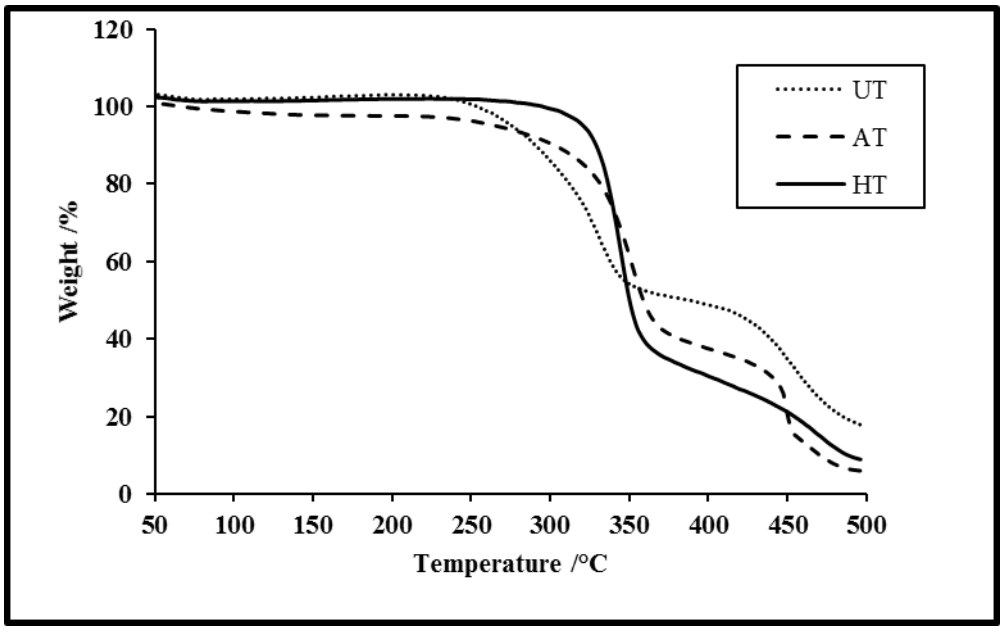

Figure 3.8: TGA thermograms for UT, AT/one hour treated, and granulated after HT treated fibres.

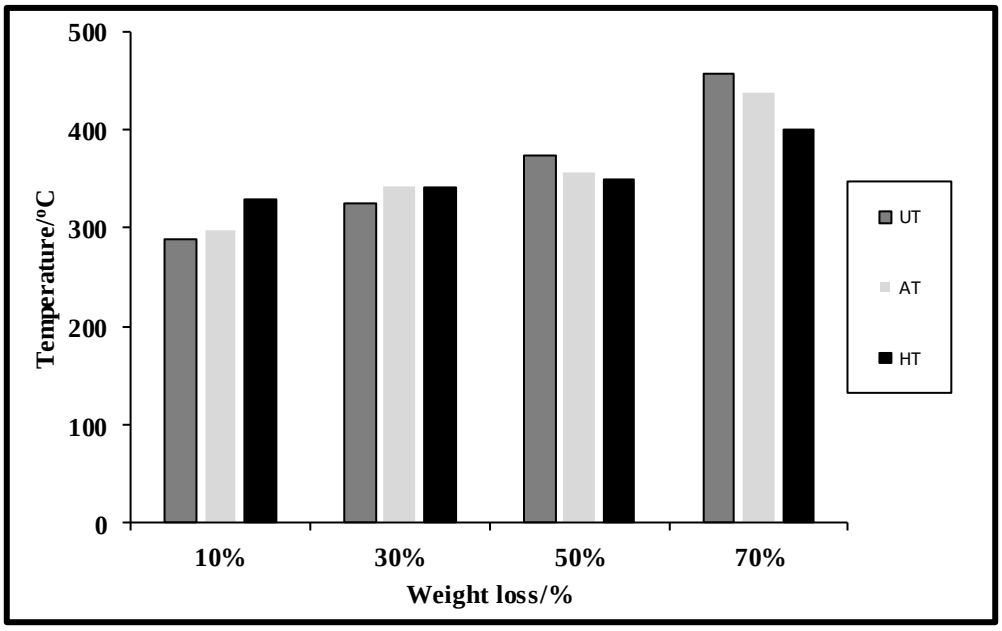

Figure 3.9: Weight loss summary for different samples.

3.3.5 SEM microscopy of hemp fibre

Figure 3.10 shows the SEM micrographs of hemp fibre. As can be seen in Figure 3.10a, the UT fibres are mostly bundle form; substances known to include lignin, pectin, hemicellulose and other non-strengthening components are localised on their surfaces [16]. Alkali treated hemp fibres appeared to have undergone some degree of fibre separation known to occur due to the removal of some of these components (Figure 3.10b, 10c and 10d). However, it was found that the AT treatment resulted in very little separation of fibres compared to the HT alkali treatment (Figure 3.10b). It was also found that the fibres granulated after HT alkali treatment were more separated compared to the fibres granulated before HT alkali treatment, which is evident from Figure 3.10d compared to Figure 3.10c.

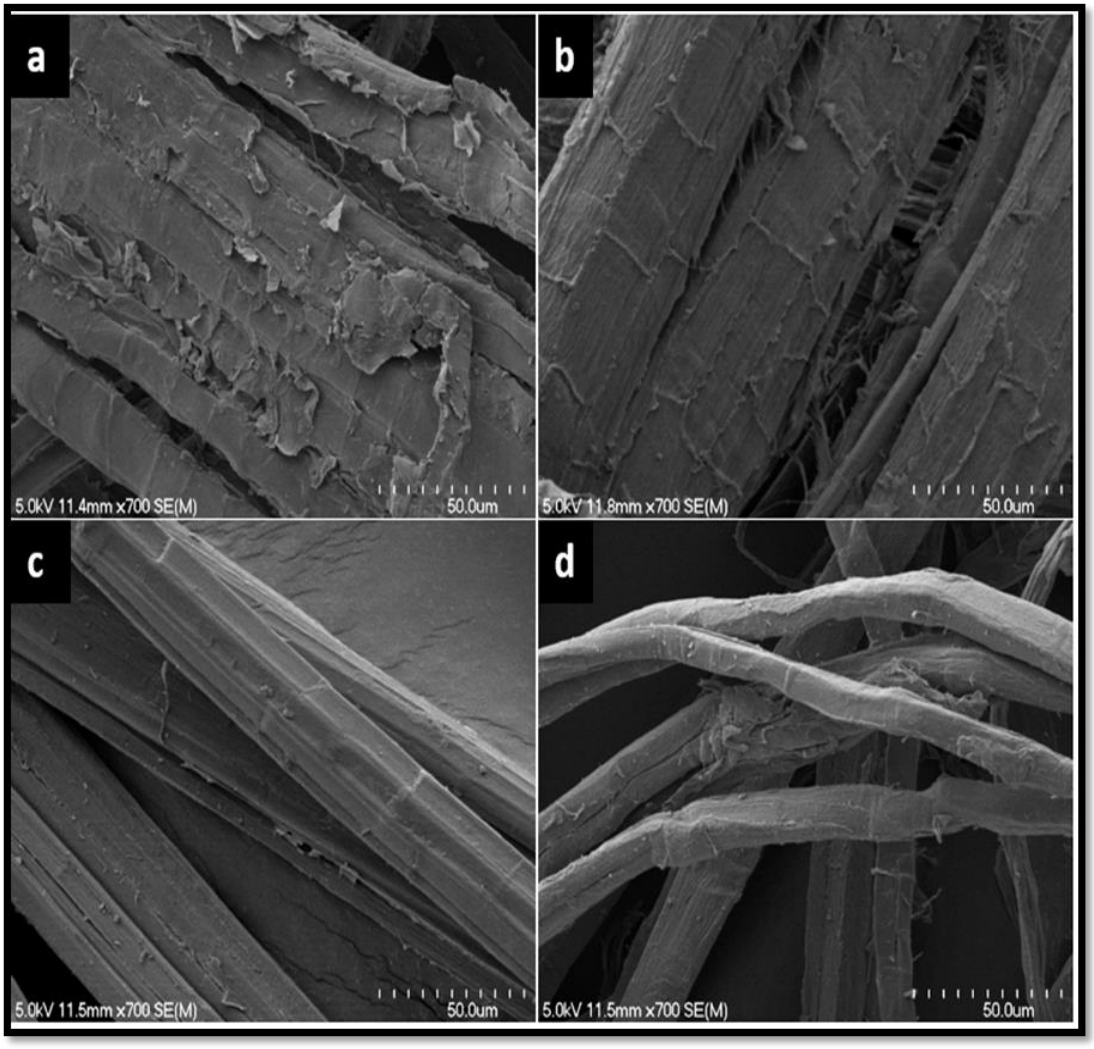

Figure 3.10: SEM images of hemp fibre surfaces (a) UT fibre (b) AT/one hour alkali treated fibre (c) Granulated before HT alkali treated fibre (d) Granulated after HT alkali treated fibre.

3.4 Chapter Conclusions

The high temperature treatment at 120 °C using 5 wt% NaOH and 2 wt% Na_2SO_3, with a fibre to solution ratio of 1:8, improved the tensile strength and Young's modulus of hemp fibres by 51 % and 62 % respectively compared to untreated fibre. In contrast, tensile strength and Young's modulus of ambient temperature treated hemp fibre were lower than that of untreated fibres by 16 % and 14 % respectively. SEM, XRD, FTIR and TGA analyses support that the high temperature treatment removes more non-strengthening components from the fibres compared to ambient temperature treatment. Improvement of fibre strength with high temperature alkali treatment compared with the reduction of fibre strength obtained with ambient temperature alkali treatment along with increased crystallinity index for fibre after the higher temperature treatment suggest better packing of cellulose chains occur for high temperature treatment providing better resistance to cellulose degradation. Overall, significantly aligned short hemp fibre mats from high strength hemp fibres was produced using DSF.

4 Chapter Four

Effect of nozzle geometry on the performance of polypropylene matrix composites reinforced with aligned hemp fibre mats

4.1 Introduction

The main objective of this study was to improve the orientation of fibres within the mats produced using dynamic sheet forming. This chapter describes the work carried out to assess the effect of nozzle geometry (contraction ratio and exit shape) on orientation for the dynamic sheet forming. The orientation of fibres within the mats produced was assessed using ImageJ (OrientationJ) and X-ray diffraction. Composites were produced with selected fibre mats (fibre mats produced using lowest and highest contraction ratio nozzles) and were tensile tested to assess the effect of orientation. Details of materials used, the methods and analysis of results are included in this chapter.

4.2 Materials and Methodology

4.2.1 Materials

The hemp fibres that underwent high temperature alkali treatment (HT) as described in Chapter 3 were used to produce fibre mats. Polypropylene random copolymer SKRX3600 supplied by Clariant (New Zealand) Limited, with a melt index of 18 g/10 min and with a density of 0.9 g/cm^3 was used as the matrix. The coupling agent used was A-C 950P maleic anhydride polypropylene (MAPP) supplied by Honeywell International Inc., USA. VeroWhite resin was used for 3D printing.

4.2.2 Nozzle design details and manufacturing

In a dynamic sheet former, alignment of fibres is known to be influenced by the fibre suspension, nozzle geometry, jet-to-wire speed ratio and dewatering [37, 38, 40]. The

present study focuses on nozzle geometry and keeping all other variables constant. The nozzle geometry factors include the contraction ratio and the end shape of a nozzle. The contraction ratio of each nozzle was calculated as the ratio of the cross-sectional area at the inlet to that at the exit [75]. The current nozzle used for dynamic sheet forming is a rectangular-round exit nozzle with a low contraction ratio. Based on the literature, it was expected that nozzles with higher contraction ratios [37-39] and a circular exit shape [40] would result in improved alignment of fibres within the mats produced compared to the current nozzle fitted to the machine.

Nozzle details, including the nomenclature used, are given in Table 4.1. The length of each nozzle was 30 mm. The entrance of each nozzle was circular in shape with an inlet diameter of 10 mm that continued for a length of 10 mm from where the contraction section (commonly known as throat) of each nozzle begins. Among the nozzles, all circular (or round) and two rectangular-round (R35 and R24) exit nozzles were with a converging boundary profile from the contraction section towards the exit as can be seen in Figure 4.1a. The other two rectangular nozzles (R56 and R46) were with slight diverging profiles from the contraction section towards the exit. However, it should be noted that, regardless of the converging or diverging profile, all the nozzles had a smaller exit area compared to the inlet area. Figure 4.1b shows the schematic representation of the current nozzle (a rectangular-round exit nozzle) used for dynamic sheet forming. Figure 4.1c shows the photograph image of all the 3D printed nozzles used for the present study. The 3D printer used was Objet30 - Stratasys.

The volumetric flow rate (Q) of the DSF, i.e. the amount of water discharged from the manual tank of the dynamic sheet former through the flow hoses onto the rotating drum (without nozzle) in one minute, was measured and found to be an average of 3.9 l/min, i.e. 6.52 x 10^{-5} m^3/s. Then, mean flow velocity of the suspension in m/s at the exit of each nozzle was calculated using the equation below.

$$v = \frac{Q}{A} \qquad (4.1)$$

where 'v' is the flow velocity, 'Q' volumetric flow rate and 'A' inlet or exit area of each nozzle.

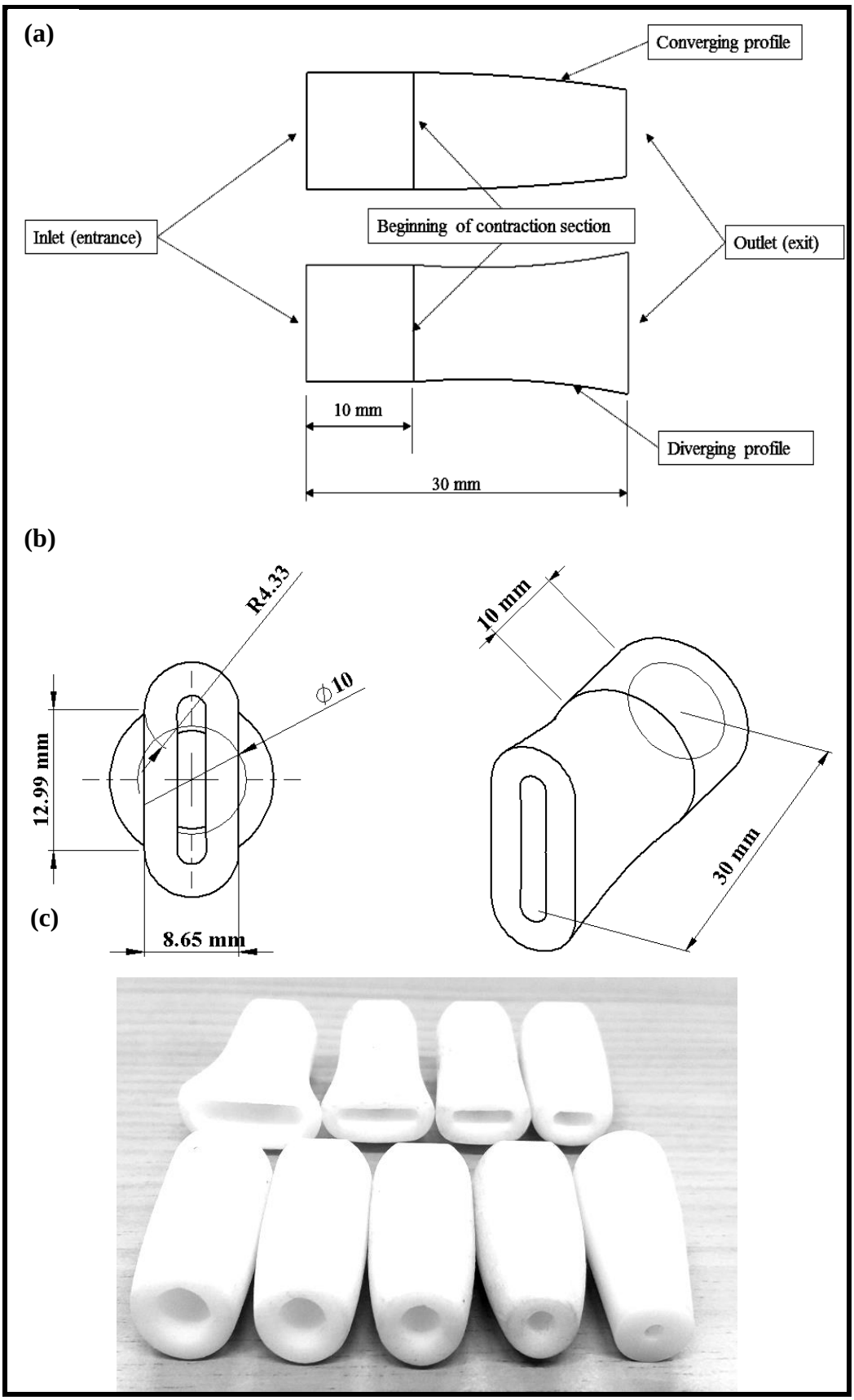

Figure 4.1: (a) Schematic representation of converging or diverging profiles of nozzles (b) Current nozzle (R46) used in dynamic sheet forming and (c) 3D printed nozzles used for the present study. Note the following: all the dimensions include the wall thickness of 3 mm.

Table 4.1: Nozzle details

Nozzles	Inlet area/ mm^2	Exit area/ mm^2	Contraction ratio	Flow velocity at the entry of each nozzle, m/s	Flow velocity at the exit of each nozzle, m/s
R56	↑	56	1.40	↑	1.16
R46		46	1.70		1.42
R35		35	2.24		1.86
R24		24	3.23		2.72
C46	79	46	1.70	0.83	1.42
C35		35	2.24		1.86
C25		25	3.13		2.61
C10		10	7.50		6.52
C6	↓	6	14.22	↓	11.81

Note the following: In the abbreviations 'R' and 'C' refer to exit shape rectangular-round and circular, respectively. The number following 'R' refers to the exit area of a nozzle; rectangular-round represented by R and circular represented by C.

4.2.3 Production of fibre mats

The aligned fibre mats (Figure 4.2a) were produced by dynamic sheet forming. The production details are described in Section 3.2.8. All nozzles listed in Table 4.1, were trialled for the production of mats. The mats produced were then cut into sizes of 150 x 300 mm and then oven-dried at 80 °C for 48 hours.

For comparison purposes in alignment assessment, two control samples were prepared. Highly aligned control sample (Figure 4.2b) was prepared by carefully wrapping hemp fibre bundles (hemp bundles) around a rectangular aluminium piece in the DSF rotation direction. The random control sample, i.e. the random mat (Figure 4.2c) was formed by hand. For this, the fibre suspension (10 g fibres in 10 litres of water) was poured onto a screen with very fine holes where the water flows

out through the screen and the fibres were deposited onto the screen surface, forming a mat. The mat was then removed and oven dried at 80 °C for 48 hours.

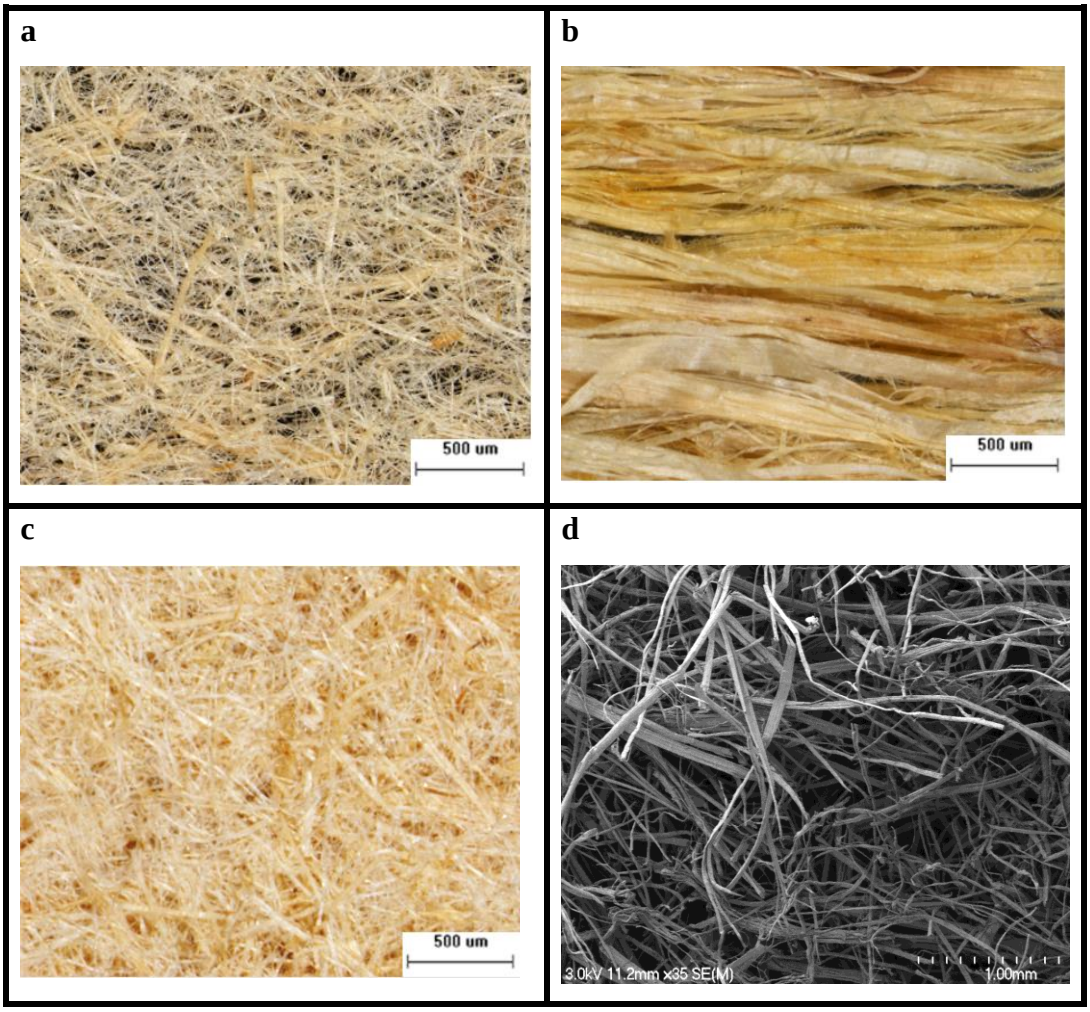

Figure 4.2: (a), (b), (c) Optical microscopic images of fibre mats produced using dynamic sheet forming (DSF), highly aligned control sample and random mat, respectively, (d) Scanning elctron microscopic images of fibre mats produced using DSF.

4.2.4 Assessment of orientation

4.2.4.1 Orientation assessment of fibre mats using ImageJ

Assessment of orientation (alignment) of fibres were carried out using ImageJ and X-ray diffraction. All the optical microscopic images were captured using a Wild M3B stereomicroscope attached with Nikon Digital DS-SMc camera and scanning electron microscopic (SEM) images were captured using a Hitachi S-4000 Field Emission scanning electron microscope operated at 5 kV. Prior to the SEM analysis, mats were mounted onto an aluminium stub using a carbon tape and sputter coated with platinum. For the image analysis using ImageJ (OrientationJ) [140, 175], both optical (Figure 4.2a, 4.2b and 4.2c) and scanning electron microscopic (Figure 4.2d)

images of fibre mats produced using DSF were separately assessed. The principles behind this Image analysis tool are provided in the Section 2.6.1. The fibre orientation distribution profiles obtained using the OrientationJ plug-in were interpreted using three approaches: the predominant orientation peaks and the coherency factors, the ratio between maximum and minimum frequencies, and the full width at half maximum (FWHM). Twenty five images were analysed for each batch.

4.2.4.2 Orientation analysis using X-ray diffraction

For the assessment of orientation of fibres using XRD (spectra were obtained using an EMPYREAN diffractometer system (PANalytical) fitted with a Cu Kα X-ray tube), each sample was prepared, as shown in Figure 4.3. The sample was then placed parallel and perpendicular to the X-ray beams for three minutes 2θ scan in transmission modes ranging from 5 ° to 45 ° using a current and voltage of 40 mA and 40 mV. The scanned signals were detected and recorded to provide the characteristic peaks using an X-ray detector. From these scans, the most intense diffraction plane was chosen (200) for all the samples; defined by 2θ = 22 °- 23 °. The sample was then subjected to a phi (Φ) scan (rotating the sample around 360 °) for six minutes with 2θ fixed at the top of the (200) plane to obtain the azimuthal diffraction profile. For the calculation, azimuthal diffraction profile of each mat was normalised with the minimum intensity of diffraction as is common in literature [147, 176]. Three analysis approaches (methods) were used to interpret the azimuthal intensity profiles of each mat: ratio of maximum to minimum peak intensity, Herman's order parameter (f) and degree of ordering (π). Two samples were measured for each batch.

Herman's order parameter (f) and the degree of ordering (π) were calculated using the equations displayed below [143]

$$f = \frac{3 < cos^2\gamma > -1}{2} \qquad (4.2)$$

where,

$$< cos^2\gamma > = 1 - 2 < cos^2\theta > \qquad (4.3)$$

$$< cos^2\theta > = \frac{\int I(\Phi) cos^2(\Phi) \sin(\Phi)\, d\Phi}{\int I(\Phi) sin(\Phi)\, d\Phi} \quad (4.4)$$

$$\pi = \frac{180 - FWHM}{180} \quad (4.5)$$

where, FWHM is the full width at half maximum. A program was written in MATLAB in order to obtain the FWHM.

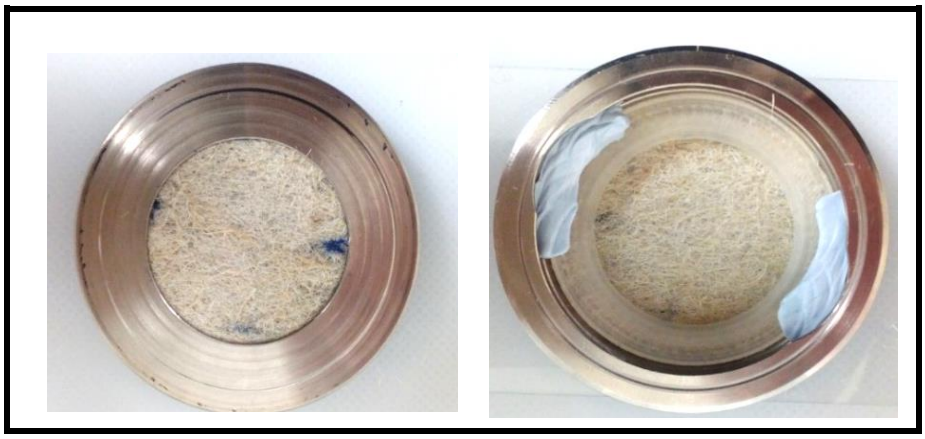

Figure 4.3: Photographs of a sample prepared for XRD analysis. Note the following: top view (left) and bottom view (right).

4.2.5 Production of PP/MAPP sheets

PP blended with MAPP (7.14g MAPP/100g PP) were formed into sheets using a ThermoPrism TSE-16-TC twin screw extruder attached with a sheet die (coat-hanger type) as shown in Figure 4.4. The design fundamentals of the extrusion coat-hanger type sheet die can be found in the literature [177]. The five heating zones at the extruder barrel temperatures were set at 145 °C (feed entrance), 160 °C, 155 °C, 160 °C, 170 °C (feed exit). The twin screws were operated at 45 rpm (revolutions per minute) maintaining torque less than 40 %. The produced sheets after allowing to cool down to room temperature were cut to 150 x 90 mm to allow them to fit in a compression mould. The sheets were then stored in sealed polyethylene bags.

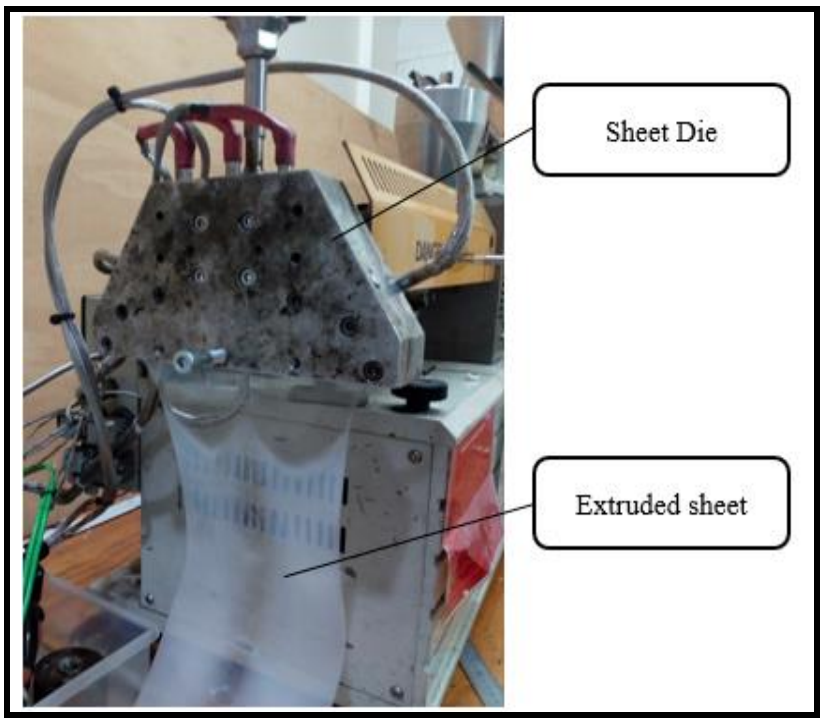

Figure 4.4: Blending PP and MAPP as sheets using a ThermoPrism TSE-16-TC twin screw extruder.

4.2.6 Fabrication of composites

The PP/MAPP sheets and the fibre mats were weighed and arranged in stacks between two Teflon sheets (to prevent adhering to the mould) for the production of composites.

Table 4.2 shows the stacking arrangements of fibre mats and the PP/MAPP sheets with relative numbers of each based on the targeted weight percentage of fibre mats. Stacks were heated and pressed in a hot press same as that of PP/MAPP samples (at 170 °C for 5 minutes at 1 MPa). Since the fibre mats was easily distorted, the consolidation of PP/MAPP sheets with the fibre mats should be carried out carefully. It was ensured that PP/MAPP sheets were fully melted before slowly applying pressure. Insufficient melting is believed to distort fibre mats, which could reduce composite mechanical performance. After hot pressing, the mould was removed from the hot press and allowed to cool down to room temperature with a weight on the top of the mould (a steel block of 10 kg). Composite samples were then taken out and weighed. The final fibre weight percentage was determined from knowing the weight of fibre mats placed in the mould. All samples were then stored in sealed polyethylene bags. The stacking arrangements of polymer sheets and fibre mats in the mould were according to the literature [16].

Table 4.2: Arrangements of PP/MAPP sheets and fibre mats inside the mould

Samples**	No. of PP* sheets	No. of fibre mats	Targeted fibre wt% (approx.)	Fibre wt%	Arrangements of PP* and fibre mats from bottom to top of the mould	Fibre loading direction
PP/MAPP	4	0	0	0	4PP	-
R46-15 C10-15 R46-15-P# C10-15-P#	4	3	15	15.7 14.5 15.5 15.6	1PP*/1MAT/1PP*/ 1MAT/1PP*/1MAT/ 1PP*	Parallel or Perpendicular
R46-30 C10-30	3	6	30	29.2 29.3	1PP*/3MATS/1PP*/ 3MATS/1PP*	Parallel

Note the following: P# - fibre mat perpendicular relative to DSF rotation direction and PP* = PP/MAPP. **In the abbreviations 'R and C' refer to the hemp composites in which the mats were produced using a rectangular-round and circular exit cross section nozzles, respectively. The first number following 'R or C' refers to the exit cross section area of the nozzle and the final number following 'R or C' refers to the targeted weight percentage (wt %) of fibres.

4.2.7 Tensile testing of composites

All the samples were cut into tensile test pieces of approximately 150 x 15 mm [16, 31] and their edges were ground using a fine abrasive paper to give a smooth and uniform sections for the testing. Procedures detailed in ASTM D 638-03; Standard Test Method for Tensile Properties of Plastics was followed for testing the specimens. In advance of tensile testing, all the samples were conditioned at 23 °C ± 3 °C and 50 % ± 5% relative humidity for at least 48 hours. An Instron-4204 tensile testing machine fitted with a 5 kN load cell was used for the testing. The gauge length of the specimens was 80 mm. An Instron 2630-112 extensometer with a gauge length of 50 mm was attached to the central part of the test specimen for the measurement of strain. The specimens were tested at a cross-head speed of 1 mm/min. A total of five samples were tested from each batch. The specimens without fibres were tested only to maximum stress point because of excessive necking, whereas specimens with fibres were tested to failure.

4.3 Results and Discussion

4.3.1 Production of fibre mats using different nozzles

As aforementioned, different nozzles were trialled for the production of fibre mats using DSF. An example of a complete mat produced using DSF is shown in Figure 4.5. The production of mats was successful using all the nozzles (Table 4.3), except R56 and C6. Instead of a complete mat, the use of R56 nozzle resulted in fibre flocs or clumps (Figure 4.6) onto the rotating drum, believed to be due to the relatively very large exit area of this nozzle compared to other nozzles (Table 4.1). The large exit area of a nozzle can lead to low flow velocity (Table 4.1) of fibre suspension through the nozzle, resulting in fibre clumps. It has been previously reported that at low flow velocities, the fibre suspension behaves like a plug flow, where fibre-fibre interactions are dominant, resulting in fibre flocs. As the flow velocity increases and reaches a sufficient range, the fibre-fibre interactions become insignificant due to the flow stresses, and permanent disruption of the plug (fibre-flocs) occurs [38, 76, 84]. It has also been previously reported that the flow characteristics of a fibre suspension depend on the flow velocity [37]. In contrast to R56, the fibres were found to frequently clogging up inside the C6 nozzle, believed to be due to the relatively very small exit area of this nozzle compared to other nozzles (see Table 4.1). This suggests that, with the current operating variables for DSF, further well-separated fibres (small size fibres) are required for the successful production of fibre mats when using nozzles with very small exit areas.

Table 4.3: Production of fibre mats using different nozzles

Nozzles	Complete mat
R56	No
R46	Yes
R35	Yes
R24	Yes
C46	Yes
C35	Yes
C25	Yes
C10	Yes
C6	No

Figure 4.5: A complete hemp fibre mat produced using DSF, (approx. 1000 x 300 x 0.80 mm).

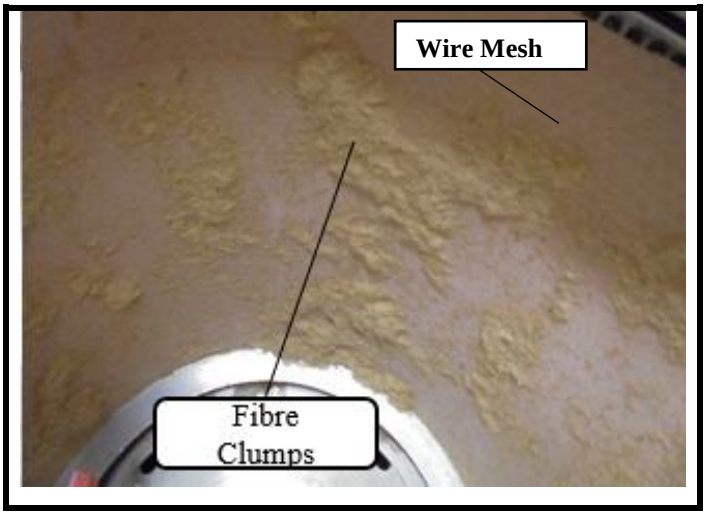

Figure 4.6: Fibre clumps formed on the wire mesh covering the rotating drum of the dynamic sheet former.

4.3.2 Orientation assessment of fibre mats using ImageJ

4.3.2.1 Using optical microscopic images

Figure 4.7 shows the fibre orientation distribution profiles obtained for the mats and fibre bundles (highly aligned control sample) using OrientationJ plug-in available with ImageJ software. Commonly, the orientation is indicated by the predominant peak of an orientation distribution profile [138, 139]. As can be seen in Figure 4.7, the profile obtained for the random mats (the mats in which the fibres are mostly at random angles) appeared to have a relatively small broad peak (almost a flat curve). In contrast, the profiles obtained for the fibre bundles and fibre mats appeared to have a relatively sharp predominant peaks around 0 ° (± 8 °). These predominant peaks around the preferred direction (0 °) for the mats produced using DSF compared to the almost flat profile (or a small peak around 40 °) of random mats support the

potential of dynamic sheet former to produce aligned short fibre mats. However, the profiles obtained for the mats produced using DSF were relatively wider indicating that the orientations of fibres within the mats are distributed in different directions with a significant proportion of fibres aligned to the preferred direction [85, 86].

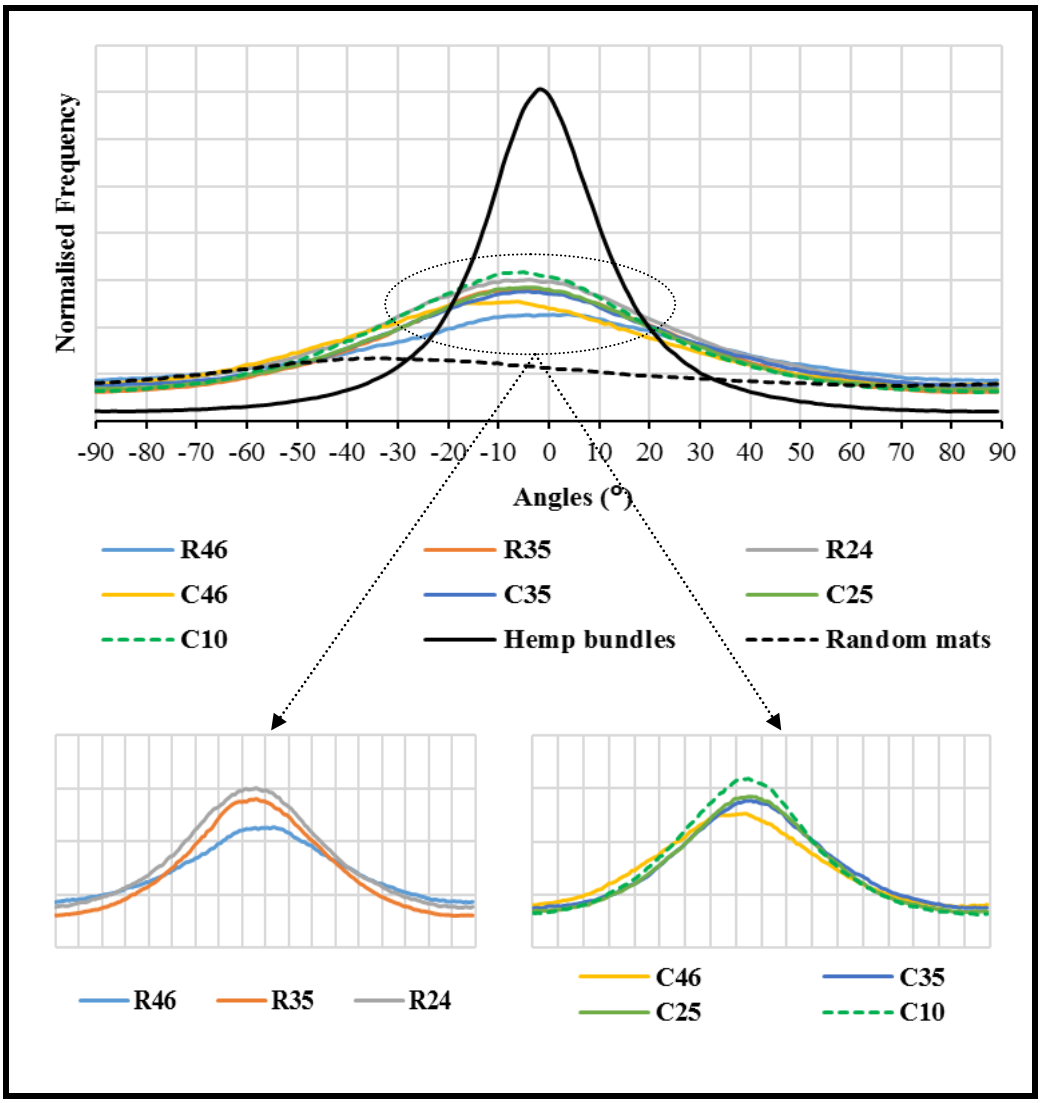

Figure 4.7: Graphs representing fibre orientation distribution profiles obtained for the hemp fibre mats made using DSF with different nozzles and control samples. Optical microscopic images of the fibre mats were used for the analysis.

In addition to the calculation of predominant or preferred orientation of fibres in an image, the OrientationJ program also calculated a 'coherency factor' to that orientation [178]. This factor is calculated based on the amount of pixels that are in line in a particular direction and is bound between 0 and 1; with 0 and 1 indicating isotropic and anisotropic orientations, respectively [179]. The coherency factors generated by OrientationJ plugin are represented in Table 4.4. As can been, the

highest coherency factors were obtained for the fibre bundles followed by the fibre mats produced using DSF and the random mats.

Among the fibre mats produced using DSF with different nozzles, there was a trend of increasing fibre orientation for nozzles with increasing contraction ratio as indicated by the increasing predominant orientation peak heights (Figure 4.7) and coherency factors (Table 4.4), but it was only significant for extreme cases (lower versus higher contraction ratios). Also, the exit shape of a nozzle was found to have less influence on fibre orientation as there was no significant differences (confirmed by Student's t-test) in fibre orientation between the mats made with nozzles of similar contraction ratios (R46, C46 and R35, C35). When compared to the current nozzle (R46), coherency factor was found to increase by about 35 % with the C10 nozzle. These results indicate that the exit shape of a nozzle is less significant for fibre orientation in DSF. Previous studies have reported that in a simple shear flow, nozzle exit area largely affects the alignment of fibres. If the nozzle exit area is large, although fibres near to the wall are aligned towards the flow direction, at the centre, fibres are aligned perpendicular to the flow direction. In contrast, if the nozzle exit area is small, the core region slowly disappears and increases the tendency of the fibres in the suspension to align towards the flow direction [74, 82, 83]. It has also been reported that fibre suspension experiences extensional flow due to the sudden flow acceleration (change in velocity of suspension) by the contraction section of a nozzle and can result in more alignment of fibres towards the flow direction [39, 74-76].

Qualitative visual representations of orientation distribution (colour coded maps of local angles) are also available with OrientationJ in HSB mode: Hue-the angle of fibre orientation, Saturation-coherency and Brightness-input image [137, 175]. The colour coded maps obtained for the highly aligned control sample, the random mat and the selected mats (R46, C10) produced using DSF, are shown in Figure 4.8. The data visualisations are in good agreement with the data acquired for the orientation distribution profiles. As can be seen, apart from the fibre bundles, the fibre mats made with the C10 nozzle (Figure 4.8d) revealed more orientated fibres towards 0 ° compared to the random mat (Figure 4.8b) and the fibre mats made with the R46 nozzle (Figure 4.8c).

Table 4.4: Coherency factors generated by OrientationJ plugin, the calculated frequency ratio and FWHM of the fibre orientation distribution profiles using optical microscopic images

Samples*	Contraction ratio	Average coherency factor	SD	Average max/min frequency ratio	SD	FWHM	SD
Random mats	-	0.11	0.04	1.80	0.21	-	-
Fibre bundles	-	0.36	0.12	25.9	8.83	25.00	0.98
R46	1.70	0.23	0.03	2.42	0.53	73.88	7.09
R35	2.24	0.24	0.04	3.10	0.89	69.40	6.27
R24	3.23	0.26	0.04	3.12	0.85	67.60	6.71
C46	1.70	0.21	0.06	2.76	0.82	70.96	8.22
C35	2.24	0.23	0.04	2.79	0.72	70.60	7.16
C25	3.13	0.26	0.05	3.12	0.93	67.68	6.53
C10	7.50	0.31	0.02	3.43	1.05	67.88	7.08

Note the following: *the abbreviations represent the fibre mats produced using dynamic sheet forming with different nozzles. SD = standard deviations. FWHM = full width at half maximum.

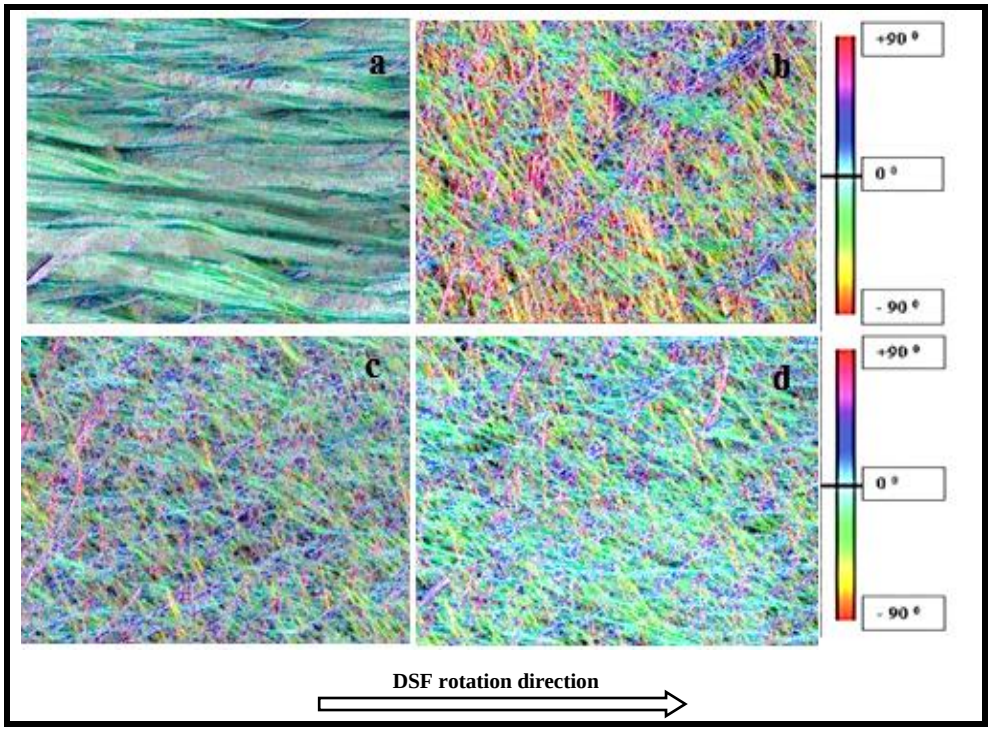

Figure 4.8: The colour-coded maps obtained with OrientationJ for: (a) Fibre bundles (b) Random mats and (c), (d) Fibre mats produced using R46 and C10 nozzles, respectively.

The frequency ratio, i.e. the ratio of maximum to minimum frequency, for the aforementioned fibre orientation distribution profiles are also provided in Table 4.4. The reported average frequency ratio could be considered as an indication of degree of orientation of fibres within a mat. Among the mats produced using DSF with different nozzles, the mats made with the C10 nozzle exhibited the highest average frequency ratio. The nozzles of similar contraction ratio but with different exit shapes (i.e. rectangular-round or circular) were also compared based on the average frequency ratio and no significant differences were observed.

The full width at half maximum (FWHM) is commonly used to describe the width of a peak at the mid-height position [180]. Generally, a profile with low FWHM indicates a high degree of orientation. The FWHM obtained using a Gaussians fit for each fibre orientation distribution profile (see Figure 4.7), except for the random mats are also presented in Table 4.4. The flat profile for the random mats made FWHM difficult. Unsurprisingly, the lowest FWHM was shown for the fibre bundles. Among the fibre mats produced using DSF with different nozzles, a decreasing trend for FWHM was shown with increases in contraction ratio of nozzles. However, statistical analysis (Student's t-test) did not support significant differences between these results.

4.3.2.2 Using scanning electron micrographs

Figure 4.9 shows the scanning electron micrographs (SEM) of hemp fibre mats produced using DSF with different nozzles. As can be seen, it is hard to have clear visual differences between distributions of orientations of fibres within the mats. The micrographs of selected fibre mats (R46 and C10) were assessed using OrientationJ. The data obtained was analysed using the three aforementioned approaches. The results were relatively consistent with that found for OrientationJ analysis with optical microscopic images. Figure 4.10 represents the fibre orientation distribution profiles of these mats. The predominant orientation peak height was higher for the fibre mats made with the C10 nozzle compared to the R46 nozzle. Qualitative visual representation of fibre orientation distribution within these mats can be seen in Figure 4.11. As expected, the scanning electron micrographs provided better visual distinction of orientation of fibres within the selected mats compared to the optical microscopic images (Figure 4.8c and 4.8d compared to Figure 4.11). Table 4.5

displays the generated coherency factor, calculated frequency ratio and FWHM of the fibre orientation distribution profiles for these mats. The trends were similar to the results obtained for the optical microscopic images of these fibre mats.

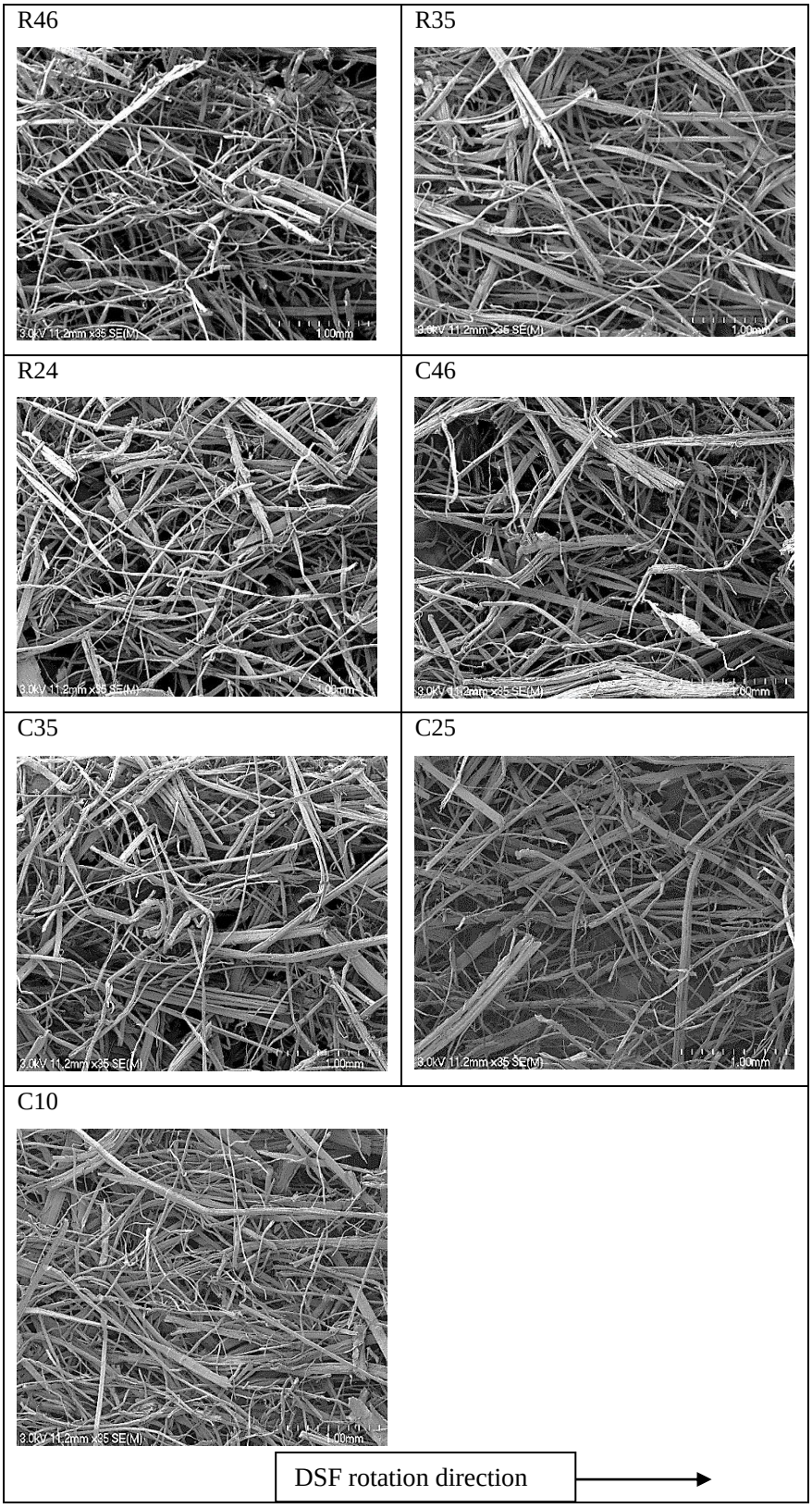

Figure 4.9: Scanning electron micrographs of fibre mats produced using DSF with different nozzles.

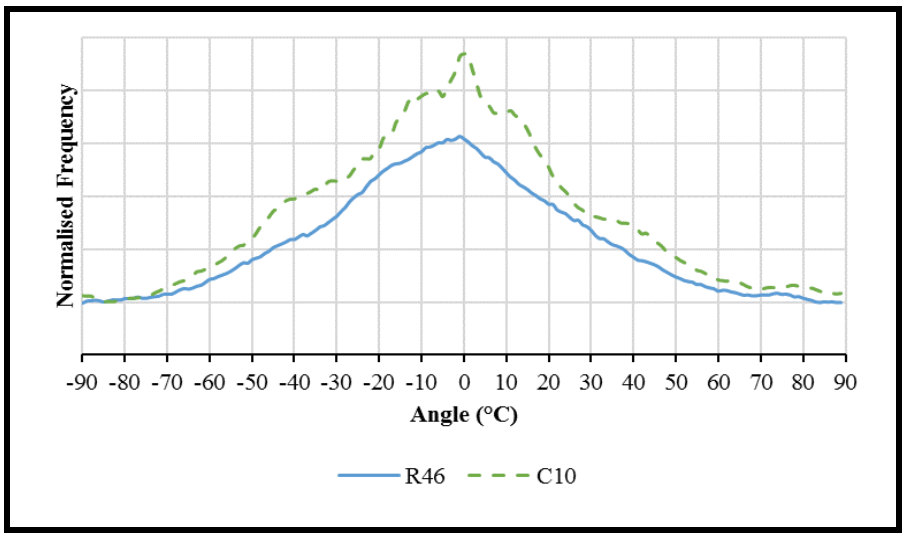

Figure 4.10: Graphs representing fibre orientation distribution profiles obtained for the fibre mats made using DSF with selected nozzles (R46 and C10). Scanning electron micrographs of the fibre mats were used for the analysis.

Table 4.5: Coherency factors generated by OrientationJ plugin, the calculated frequency ratio and FWHM of the fibre orientation distribution profiles using SEM images

Samples	Contraction ratio	Average coherency factor	SD	Average frequency ratio	SD	Average FWHM	SD
R46	1.7	0.24	0.02	4.38	0.78	68.67	6.02
C10	7.5	0.29	0.01	5.76	0.54	20.33	3.79

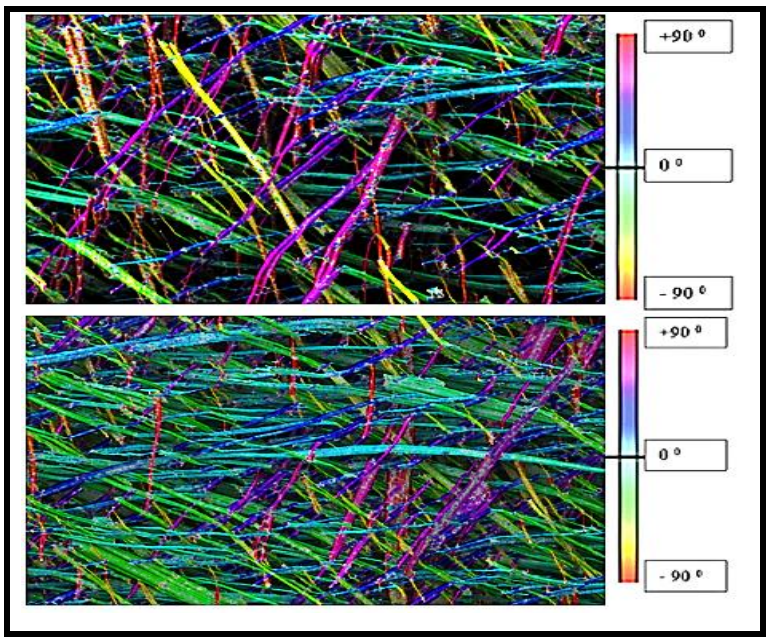

Figure 4.11: Colour coded maps obtained for the scanning electron micrographs of the selected fibre mats using OrientationJ plugin (R46-top and C10-bottom).

Overall, the trend of increasing fibre orientation for nozzles with increasing contraction ratio was more consistent with the fibre orientation distribution profiles and the frequency ratio approaches compared to the FWHM approach.

4.3.3 Orientation analysis using X-ray diffraction

Generally, the cell walls of natural plant fibres (NPFs) consist of primary and secondary cell walls (S1, S2, and S3 layers). The long and thin microfibrils dominate the secondary cell walls. These microfibrils are made up of cellulose, which is mainly responsible for the tensile strength of the fibres. Typically, native cellulose consists of crystalline and alternating amorphous regions [144]. Figure 4.12 shows the 2θ profiles: the raw diffraction pattern and resultant diffraction pattern of a hemp fibre mat. The raw diffraction pattern data (raw data) is a combination of crystalline and amorphous contributions. The amorphous background was estimated from this raw data by fitting a power trend line to the data points from the regions (indicated by orange colour in Figure 4.12) outside of the main crystalline cellulose peaks. The estimated background was then subtracted from the raw data. For all the samples, the most intense diffraction plane was (200) plane of cellulose I. The selected (200) plane was then monitored during scans where the fibre mats on the sample holder were rotated around the phi (Φ) axis [176], resulting in an azimuthal diffraction profile for each mat.

Figure 4.13 shows the azimuthal diffraction profiles of the selected fibre mats produced using DSF and random mats. As can be seen, the azimuthal diffraction profiles for the mats produced using DSF indicate that the (200) crystal planes had preferred orientation distribution around 90 and 270 °. In contrast, there were many peaks distributed over 360 ° for the random mats, suggesting no clear preferred orientation of the (200) crystal planes. This again supports the potential of dynamic sheet former to align fibres along the preferred direction. It was found that the fibre mat made with the C10 nozzle exhibited a more preferred orientated azimuthal diffraction profile compared to the fibre mats made with R46 nozzle.

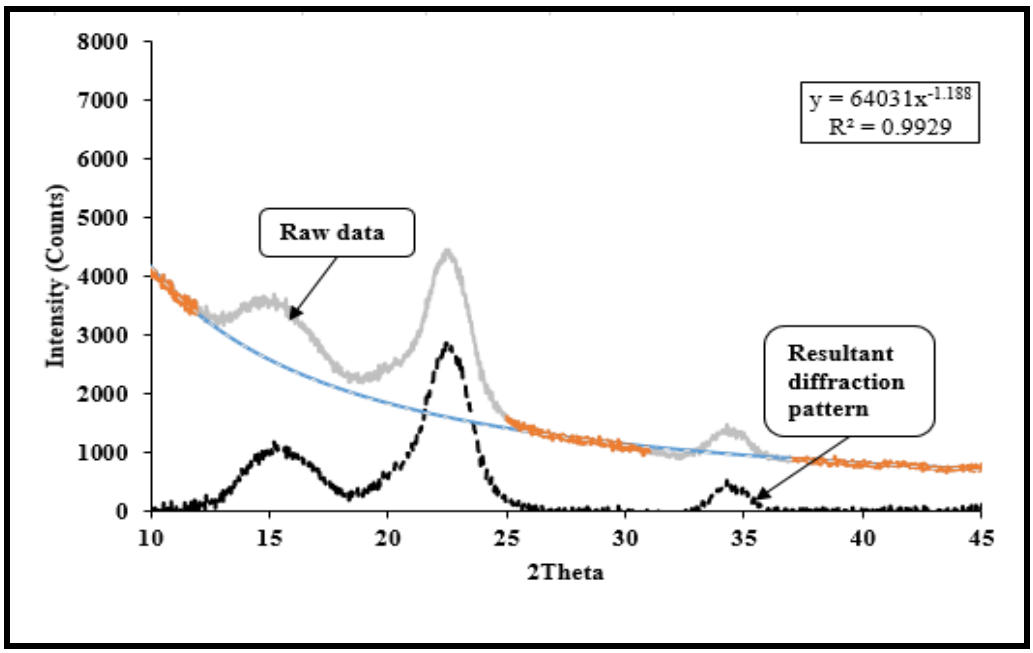

Figure 4.12: X-ray diffraction pattern of a hemp fibre mat using Cu Kα radiation.

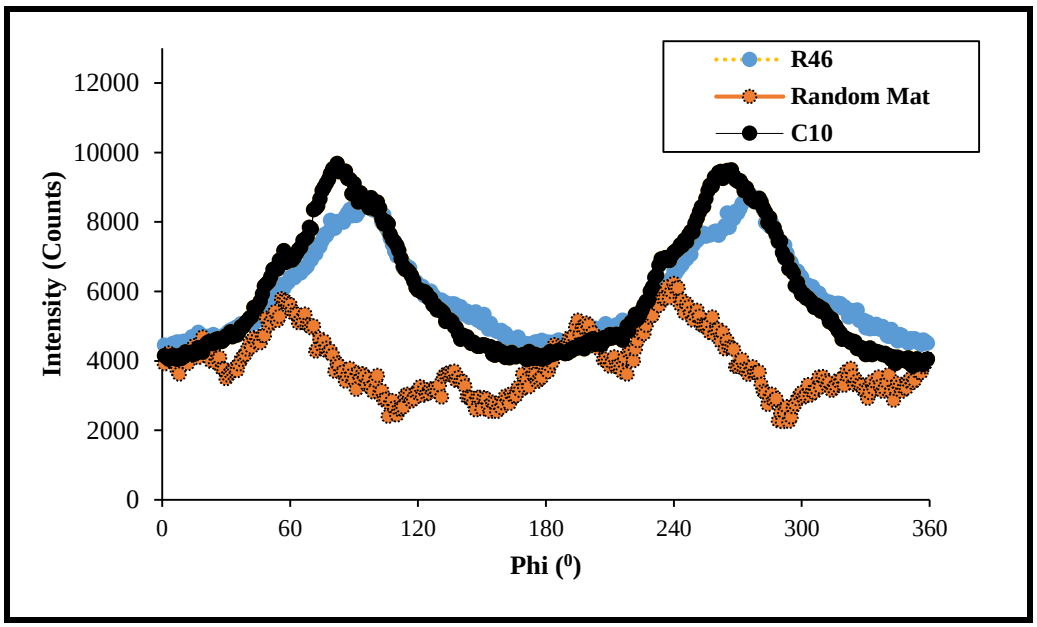

Figure 4.13: Azimuthal diffraction profiles for the selected fibre mats and random mats.

The peak intensity ratio, i.e. ratio of maximum to minimum intensity of azimuthal diffraction profiles, was calculated, and the average values plotted for each mat are provided in Table 4.6. The average intensity ratio indicated an increasing trend with increasing contraction ratio. However, a significant difference (confirmed by Student's t-test) was found only between the fibre mats made with the C10 and R46 nozzles. Also, no significant differences were observed between nozzles with similar contraction ratio but with a different exit shape, i.e. rectangular-round or circular.

It has been reported that Herman's order parameter (f) can be used to quantify the degree of orientation of the cellulose chain axis relative to some other axes of interest. Generally, f =1 for completely aligned and f = 0 for randomly orientated [142]. Herman's order parameters (f) calculated for different processed azimuthal diffraction profiles are summarised in Table 4.6. In good agreement with the ImageJ results, more pronounced orientation of fibres was observed for the mats made with the C10 nozzle as indicated by the highest Herman's order parameter. Unsurprisingly, the lowest (f) value was observed for random mats indicating a very low degree of orientation.

The full width at half maximum (FWHM) and degree of ordering (π) calculated for the azimuthal diffraction profiles of the fibre mats are also presented in Table 4.6. Generally, a low FWHM of azimuthal diffraction profile indicates a high degree of orientation [141]. The FWHM and degree of ordering indicated an increasing trend with increasing contraction ratio, however, were found to be statistically insignificant using the Student's t-test.

Table 4.6: XRD assessment of orientation of fibre mats: average intensity ratio and Herman's order parameter, FWHM and degree of orientation.

Samples*	Contraction ratio	Average intensity ratio	SD	Herman's order parameter	SD	FWHM	SD	Degree of Orientation (π), %
Random mats	-	1.346	0.135	0.139	0.094	-	-	-
R46	1.70	1.904	0.064	0.464	0.033	58.2	2.1	67.67
R35	2.24	1.988	0.079	0.446	0.047	57.9	1.3	67.83
R24	3.23	1.994	0.052	0.402	0.016	57.2	1.5	68.22
C46	1.70	1.952	0.142	0.504	0.042	58.1	1.9	67.72
C35	2.24	2.070	0.264	0.455	0.018	57.7	1.1	67.94
C25	3.13	2.122	0.098	0.418	0.039	57.1	1.6	68.28
C10	7.50	2.278	0.156	0.511	0.005	53.1	0.7	70.50

Note the following: *the abbreviations represent the fibre mats produced using different nozzles.

4.3.4 Evaluation of composites

Figure 4.14 shows typical stress-strain curves for composites made with selected fibre mats (selected based on the orientation analysis) along with that for PP/MAPP (the control sample) for comparison purposes. The composites containing fibre content of approximately 15 wt% were tested parallel and perpendicular to the main fibre alignment direction (the preferred direction). As can be seen, the control samples extended in a ductile manner to high strain without fail, whereas the incorporation of fibres caused the samples to fail in a brittle manner without much noticeable yielding.

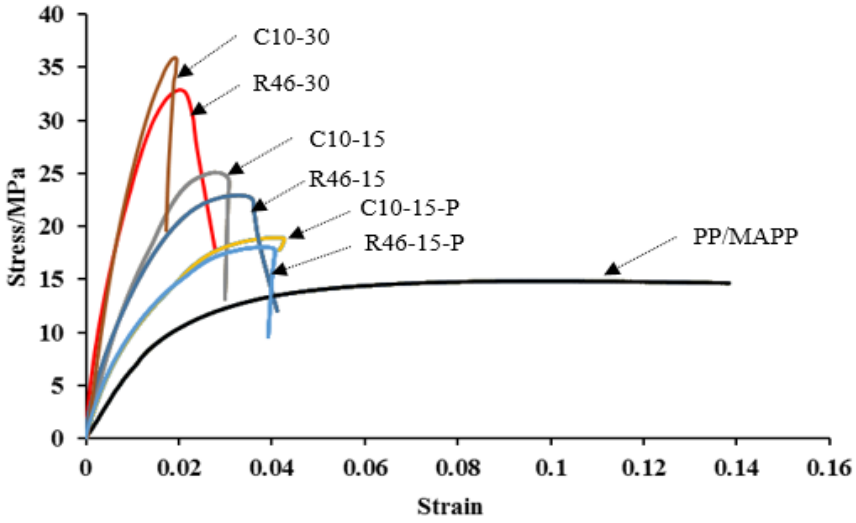

Figure 4.14: Typical stress-strain curves for PP/MAPP and composites reinforced with approximately 15 and 30 wt% fibre loaded parallel and perpendicular to main fibre alignment direction.

Figure 4.15a represents the tensile strength of fibres as a function of fibre content and loading direction for the composites. Composite tensile strength was normalised with weight percentages of fibres (

Figure 4.15b) to account the variability in tensile strengths of composites based on the slight variations of fibre content. From the results, it can be seen that, for the composites tested parallel to the main alignment direction, the tensile strength increased with an increase in fibre content. The tensile strengths for the composites made with 15 and 30 wt% fibre mats produced using the highest contraction ratio nozzle, C10, significantly increased to 23.08 and 35.64 MPa, respectively; these were approximately 5 and 11 % higher than the respective composites made with the

fibre mats produced using the current nozzle, R46. Increased tensile strengths obtained here is believed to be due to the improved fibre orientation.

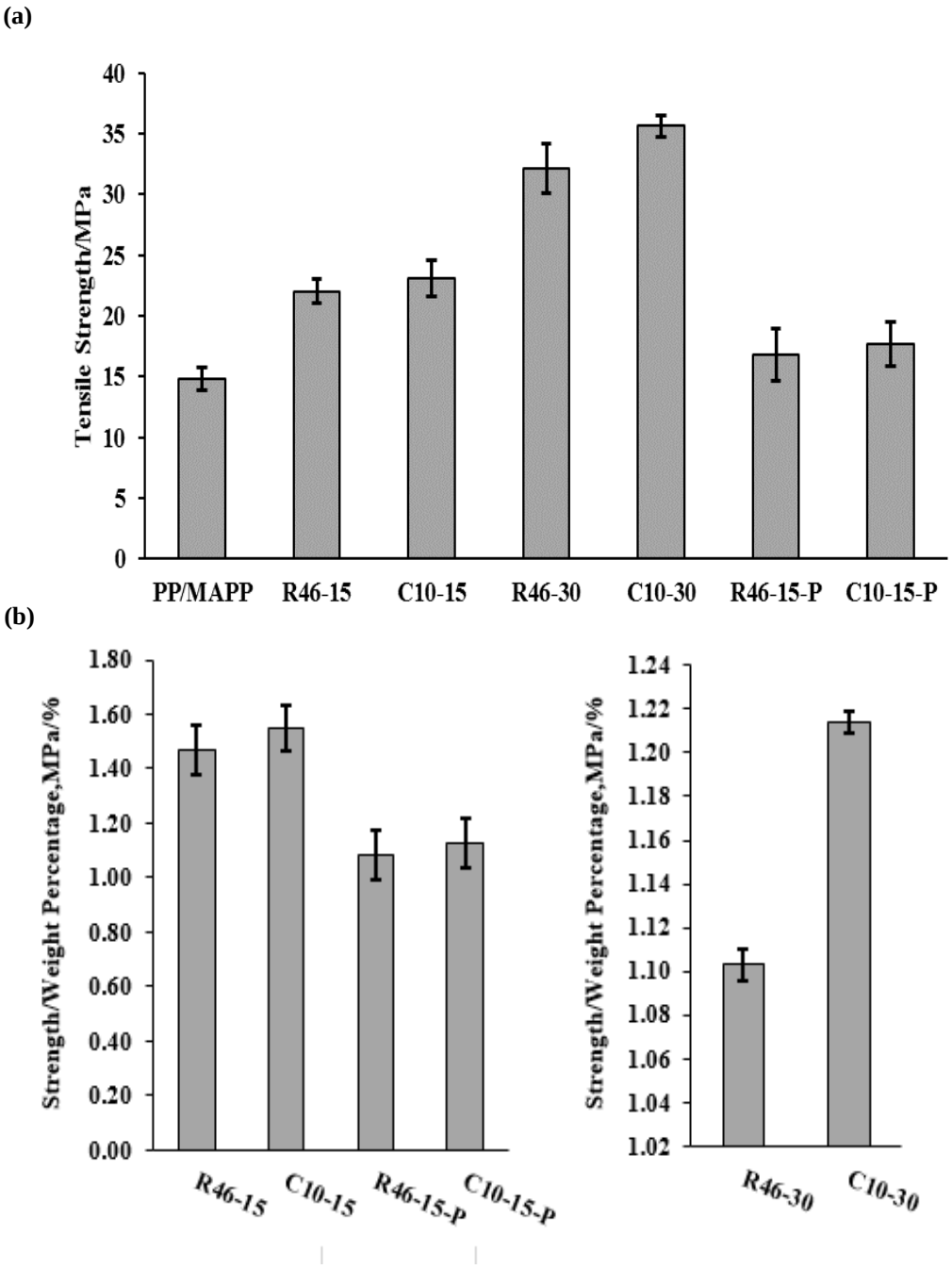

Figure 4.15: Graphs representing: (a) Tensile strength and (b) Tensile strength/weight percentage* of various composites tested. Weight percentage = weight percentage of fibres.

Unsurprisingly, the composites tested perpendicular to the main alignment direction exhibited lower tensile strengths compared to those composites tested parallel. In the main fibre alignment direction, composite properties are known to be strongly dependent on fibre properties and the fibre-matrix interface. However, in the

perpendicular direction, properties are more dependent on the fibre-matrix interface and the matrix [16, 181]. Furthermore, in this direction, the diameter of the fibre is very small relative to the critical fibre length to bring about tensile load in the fibre [16]. Moreover, it is most likely that the fibre strength is lower in this direction due to the orientation of microfibrils which has shown to provide high strength when aligned parallel to the fibre direction [35].

Figure 4.16a and 4.16b represent Young's modulus and Young's modulus/weight percentage of fibres as a function of fibre content and loading direction for the composites. As expected, Young's modulus of PP/MAPP increased with the inclusions of the fibres. This is due to the fact that fibre possesses higher Young's modulus (see Table 3.1) than PP/MAPP. Similar to the tensile strength, Young's modulus of composites tested parallel to the main fibre alignment direction were higher compared to those composites tested perpendicular. According to the Student's t-test, there are no significant increases in Young's modulus of composites made with fibre mats produced using the C10 nozzle compared to the composites made with fibre mats produced using the R46 nozzle. However, the averaged test results suggest that Young's modulus of the composites made with fibre mats produced using the C10 nozzle are slightly superior.

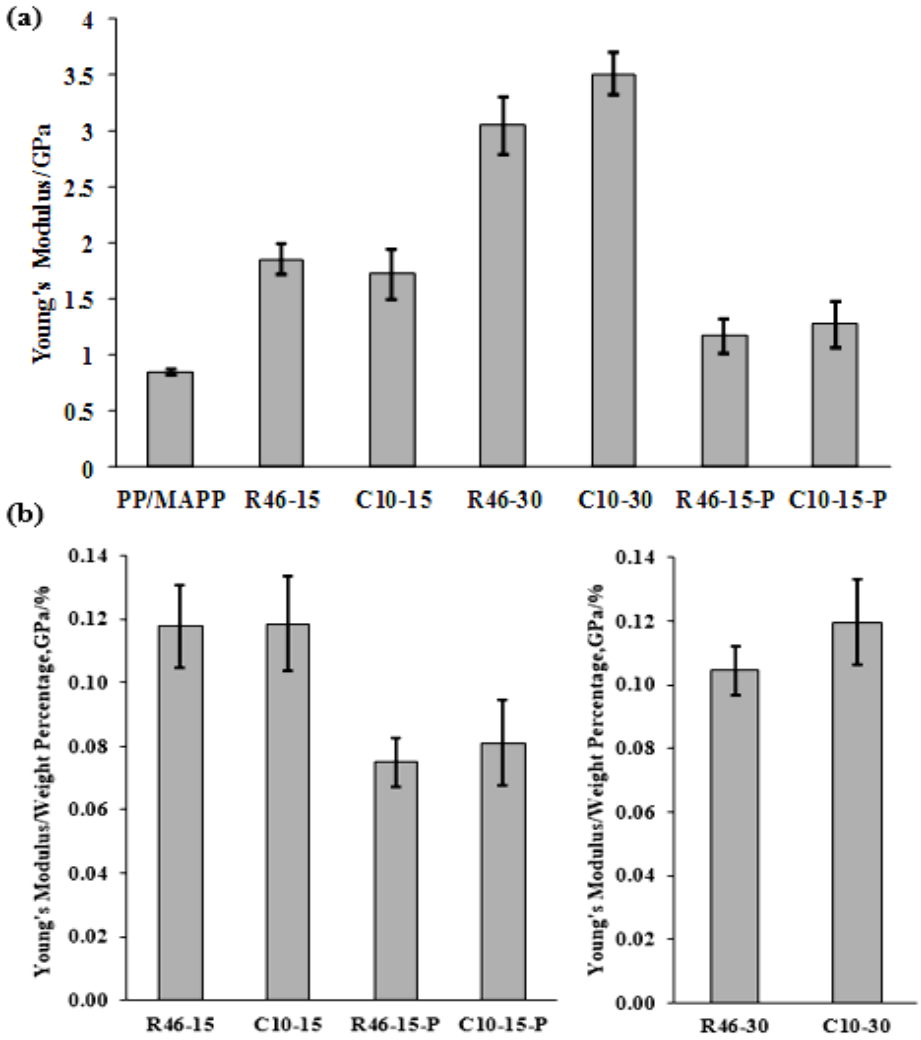

Figure 4.16: Graphs representing: (a) Young's modulus and (b) Young's modulus/weight percentage* of various composites. Weight percentage = weight percentage of fibres.

4.4 Chapter Conclusions

Nozzles with different geometries were used to produce hemp fibre mats using dynamic sheet forming. The orientation of fibres within these mats was investigated using ImageJ and X-ray diffraction analyses. It appears that both techniques were in good agreement, showing that dynamic sheet forming has the potential to produce aligned short fibre mats. In the results, although there was a trend of increasing fibre orientation for nozzles with increasing contraction ratio, it was only statistically significant for extreme cases (lowest versus highest contraction ratios of the nozzles which successfully produced sheets); exit shape of a nozzle was found to have less influence on fibre orientation. Improved fibre orientation obtained for dynamic sheet forming was indicated by higher values of coherency factor (0.31 compared to 0.23)

and Herman’s order parameter (0.511 compared to 0.464) for the fibre mats produced using the highest contraction nozzle compared to those mats produced using the lowest contraction ratio nozzle (the current nozzle). The improved fibre orientation was further supported by an 11 % increase in tensile strength for the composites made with 30 wt% fibre mats produced using the highest contraction ratio nozzle compared to the respective composites made with the fibre mats produced using the current nozzle, R46. Overall, the orientation of fibres within mats produced using dynamic sheet forming has been improved.

5 Chapter Five

Effect of surface treatments of aligned hemp fibre mats on the performance of polypropylene matrix composites

5.1 Introduction

The main objective of this study was to improve the performance of fibre mats produced using DSF. The hemp fibres that underwent a high temperature (HT) alkaline treatment, as described in Chapter 3, were used for the production of fibre mats using DSF. Further treatments with stearic acid and cellulose nanocrystals were carried on these fibre mats separately and assessed. Composites were made with different fibre contents up to a maximum of 30 wt%. This chapter describes the work carried out to assess the effects of stearic acid and cellulose nanocrystal treatments on the performance of polypropylene reinforced with treated fibre mats. This chapter is divided into two parts:

I. Effect of stearic acid vapour treatment on the properties of fibre mats produced using DSF and their potential use in polypropylene matrix composites.

II. Effect of cellulose nanocrystal treatments on the properties of fibre mats produced using DSF and their potential use in polypropylene matrix composites.

5.2 Part I: Materials and Methodology

5.2.1 Materials

Stearic acid, in powder form, with molecular weight of 284.48 g/mol was purchased from Merck Schuchardt, Germany. The materials used for the production of the fibre mats and composites are described in Chapter 4.

5.2.2 Fibre mat production

The method used for the production of fibre mats was similar to that described in Section 3.2.8.

5.2.3 The stearic acid vapour treatment

Prior to stearic acid (SA) vapour treatment, the fibre mats to be treated were dried overnight at 80 °C. The SA treatment for the mats was carried out using a vapour process. A predetermined 4 g of stearic acid was spread onto an aluminium tray. The fibre mats to be treated were left on a wire mesh that was temporarily fitted to the top of the tray, as shown in Figure 5.1. The set up was entirely covered using an oven bag and sealed, and then placed in a preheated oven at 105 °C for 36 h; the treatment time and temperature were selected from a previous study that reported improved stress transfer for NPFCs [42]. After the treatment, the mats were removed from the mesh and then oven dried at 50 °C for 12 h. The weight percentage gain from the treatment was calculated based on the dry weight of the untreated fibre mats.

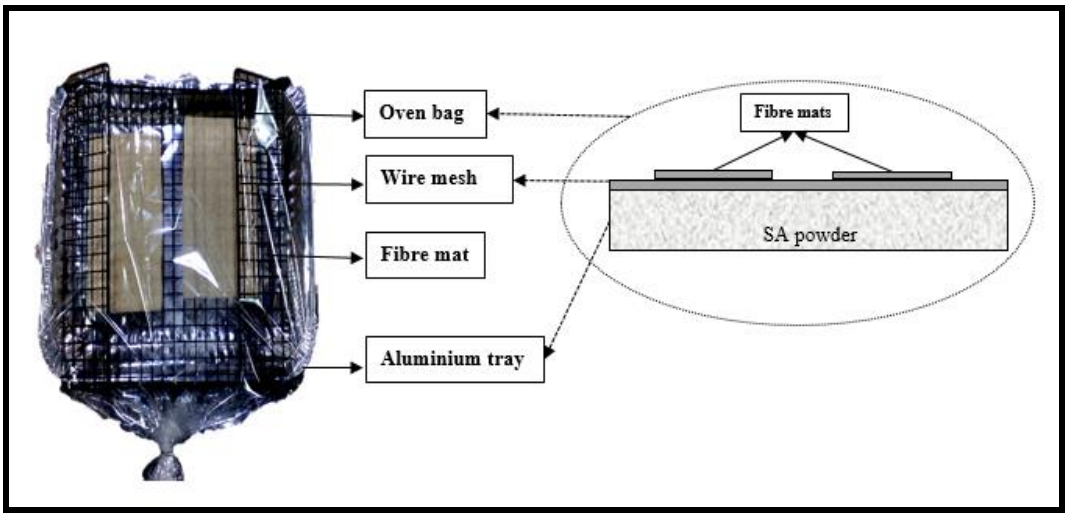

Figure 5.1: Setup used for the stearic acid (SA) vapour treatment.

5.2.4 Production of PP/MAPP sheets

The method used for the production of PP/MAPP sheets was similar to that described in Section 4.2.5

5.2.5 Assessment of fibre mats and composite morphology

The fibre mat surfaces and the microstructure of the tensile fracture surfaces of the samples were assessed using a Hitachi S-4100 field emission scanning electron microscope operated at 5 kV. All samples were mounted on aluminium stubs using carbon tapes and then sputter-coated with platinum to make them conductive before observation.

5.2.6 Fourier transform infrared spectroscopy

A PerkinElmer Spectrum One spectrometer was used to obtain the infrared spectra of the samples. The fibre mat samples were ground to fine powder using a Retsch MM400 ball mill. The ground powder for each sample was then mixed and compressed with KBr (potassium bromide) using a hydraulic press to form a disc for FTIR analysis. Neat stearic acid was also analysed.

5.2.7 Water retention value test

The fibre mat surfaces were characterised by measuring the water retention value (WRV), following a method previously reported for characterising fibre surfaces with stearic acid treatment [95]. For the test, 500 mg of fibre mat was placed in a test tube with 3 ml of distilled water and shaken for 10 minutes. The mat was manually taken out from the test tube and then the wet weight of the mat (w_1) was measured. The mats were then dried in an oven at 105 °C for 24 h to obtain the dry weight of the mat (w_2). Three replicate samples were tested for each batch and average values are reported. The following equation has been used to determine the water retention value:

$$\text{WRV} = \frac{(w_1 - w_2)}{w_2} \qquad (5.1)$$

5.2.8 Contact angle measurement

Neat PP and PP/MAPP sheets and fibre mats were assessed for contact angle. A simple custom experimental set up, as schematically shown in Figure 5.2, was constructed which allowed the measurement of contact angle with reasonable precision [182]. The images for analysis were captured using a digital mobile camera. A cardboard box was employed for shielding the liquid droplet (distilled water) from air contaminants and stray light. Additionally, a commercial lamp along with a filter paper (diffuser) was positioned behind the liquid droplet for uniform lighting. Measurements were carried out on samples of dimensions 25 x 25 mm at room temperature. The measurements were repeated for three times for each batch.

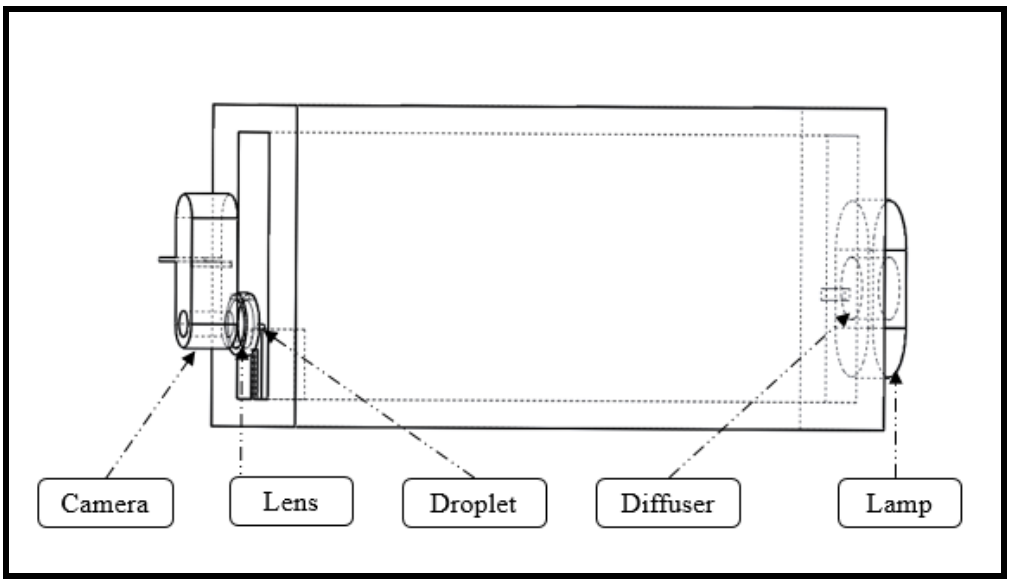

Figure 5.2: Schematic diagrams of contact angle measurement set up.

5.2.9 Production of composites

Composite processing was conducted according to the method described in Section 4.2.6. Composites with fibre contents of approximately 15 and 30 wt% were prepared for this work. An example of a moulded composite is shown in Figure 5.3. Neat PP samples were also produced for comparison purposes. Stacks of neat PP samples were heated and pressed in a hot press same as that of PP/MAPP samples (at 170 °C for 5 minutes at 1 MPa).

Figure 5.3: Hemp composites with 30 wt% fibre content fabricated by compression moulding.

5.2.10 Tensile testing of composites

Tensile testing of composites was conducted according to the method described in Section 4.2.7. Details and abbreviations of the samples used can be seen in Table 5.1. Five samples for each batch of composites were tested.

Table 5.1: Abbreviations used for PP, PP/MAPP and composite samples

Sample	Abbreviation
Neat Polypropylene	PP
PP blended with MAPP coupling agent (the control)	PP/MAPP
PP matrix composite reinforced with alkali-treated hemp	PP/H#
PP matrix composite reinforced with alkali-stearic acid-treated hemp	PP/H#/SA
PP/MAPP matrix composite reinforced with alkali-treated hemp	PP/MAPP/H#
PP/MAPP composite reinforced with alkali-stearic acid-treated hemp	PP/MAPP/H#/SA

Note the following: 'H' refers to hemp fibre and the '#' following 'H' is equal to the nominal weight percentage of fibres in composites. For instance, H15 = 15 wt% hemp fibre in composites.

5.2.11 Thermogravimetric analysis

3 mg and 15 mg samples were taken from each type of fibre mat and composite, respectively and analysed using a PerkinElmer STA 8000 as described in Section 3.2.7.

5.2.12 Swelling studies

Swelling studies were carried out to evaluate the interaction between the fibre and matrix in composites. The test was conducted according to the method reported in the literature [16]. Toluene was used as the solvent for immersion. Prior to the immersion of samples with nominal dimensions of 30 x 5 x 3 mm, the dry weights (initial weights, *w*) of three replicate samples were measured. The samples were then immersed in the solvent at room temperature for 48 hours. After immersion, the samples were taken out and wiped with a soft cloth. Then the weight of solvent absorbed was recorded and average values have been reported. The swelling index of the composite is calculated using the following equation [183]:

$$\text{Swelling Index}, \% = \frac{A_s}{w} \; x \; 100 \qquad (5.2)$$

where A_s - the amount of solvent absorbed.

5.3 Results and Discussion

5.3.1 Microscopic evaluation of hemp fibre surfaces

SEM micrographs of hemp fibre surfaces are shown in Figure 5.4. As can be seen in Figure 5.4a, the untreated fibres (UT) are in fibre bundle forms. In contrast, high temperature alkali treated fibres (HT) appeared to have undergone separations from their bundle forms (Figure 5.4b) due to the removal of localised components on their surfaces, revealing a rough texture with a large number of grooves (Figure 5.4c) [4, 31]. It appears that the stearic acid vapour treatment (HT/SA) smoothed the fibre surfaces (Figure 5.4d compared to Figure 5.4c). Furthermore, it may be seen that the fibre surfaces appeared to be covered by a thin layer. This thin layer could be attributed to the presence of stearic acid, which has been deposited on the fibre surfaces. Similar observations have been reported elsewhere [42, 116].

To further investigate this deposition, the fibres treated with alkali only and further treated with stearic acid were separately exposed to electron beams under high magnification for the same exposure time (5 s). Three replicate samples were tested. An interesting observation was that the stearic acid treated fibres appeared to have undergone less damage than that of the alkali only treated fibres (Figure 5.4f compared to Figure 5.4e). This is thought to be due to the presence of stearic acid, which could have hindered the damage.

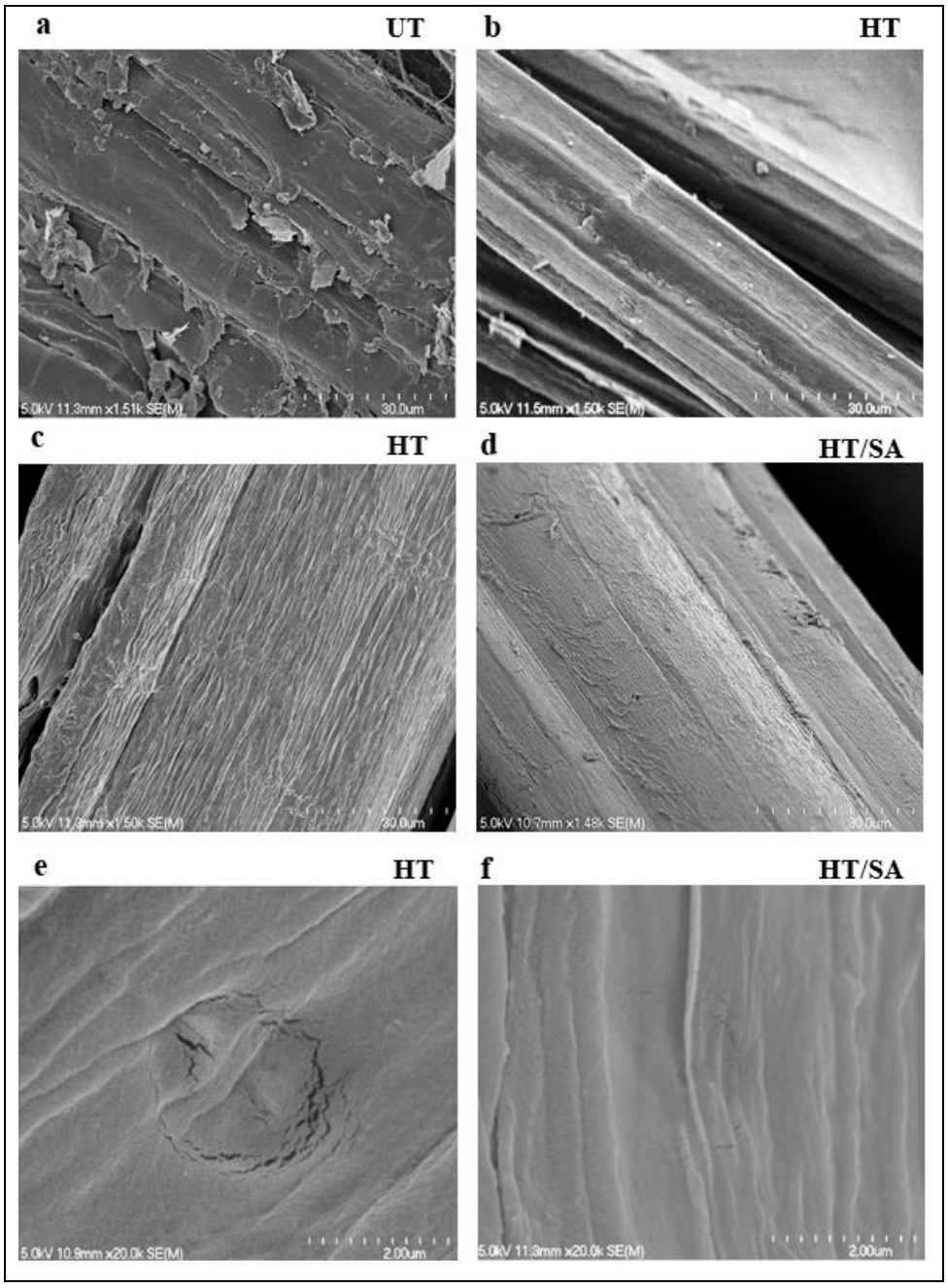

Figure 5.4: Scanning electron micrographs of fibre mats: (a) Untreated (UT), (b), (c) and (e) fibres treated with alkali only, HT and (d) and (f) fibres further treated with stearic acid, HT/SA. Note the following: HT - high temperature, SA - stearic acid, HT/SA - both HT alkali and SA treated.

5.3.2 Fourier transform infrared spectroscopy

Detailed comparison of spectra of untreated (UT) and fibres treated with alkali only (HT) have been provided in Section 3.3.3. Figure 5.5 shows the spectra of fibre mats without stearic acid (HT) and with stearic acid (HT/SA) and neat stearic acid. A few minor differences can be seen between the spectra of the fibre mats. In the spectra of neat stearic acid, high intensity peaks were detected at 1705, 1470, 1300, 1733 and 1228-1235 cm^{-1}, which are commonly assigned in literature to the carboxylic acids. [117, 184]. A few minor differences can be seen between the spectra of the fibre mats; the two peaks related to the stretching vibrations of CH_2 groups at 2850 and 2920 cm^{-1} [184, 185] were more pronounced in the spectra of fibre mats with stearic acid than those without stearic acid supporting the presence of stearic acid on the fibre surfaces. Assessment of whether reaction between stearic acid and the fibre had occurred was conducted, for which peaks would expected to appear at around 1733 (C=O) and 1000-1300 (C-O) cm^{-1} [186]. However, such peaks were not noticeable in the spectra of fibre mats with stearic acid treatment. These observations were similar to the work reported for flax fibres treated with stearic acid vapour [117]. The absence of ester functional groups peaks from the spectra could be due to the very low levels of stearic acid deposited on the fibre surfaces; the weight percentage gain in the fibre mats obtained after the SA treatment was around 0.54 % and so the presence of ester bonding between stearic acid and the fibre was inconclusive.

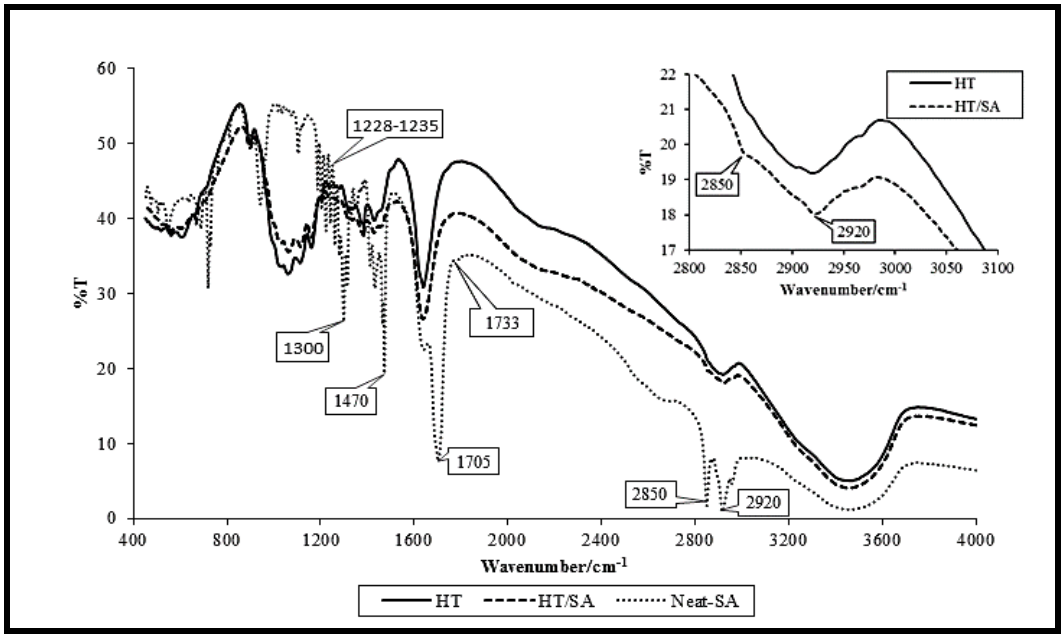

Figure 5.5: FTIR-spectra of: fibre mats with alkali treated fibres only (HT), fibre mats further treated with stearic acid (HT/SA), and neat stearic acid. Note the following: HT - high temperature and SA - stearic acid.

5.3.3 Water retention values

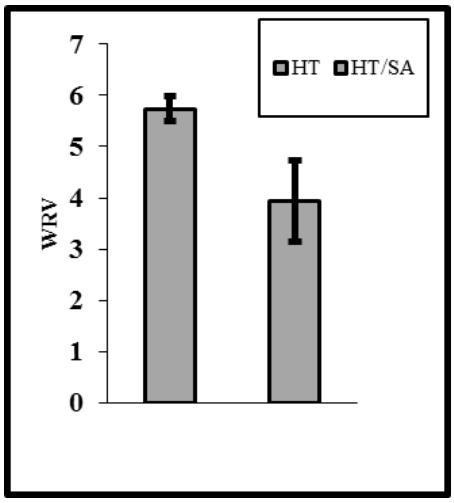

Figure 5.6: Water retention values of fibre mats: fibre mats treated with alkali only (HT), fibre mats treated further with stearic acid (HT/SA).

Figure 5.6 represents the average water retention values (WRVs) obtained for the alkali treated fibre mats only (HT) and fibre mats further treated with SA (HT/SA). As can be seen, the water retention value was significantly lower for the SA treated fibre mats compared to the fibre mats without SA. This indicates that the fibre surfaces become less hydrophilic with the deposition of stearic acid. The long hydrocarbon chain of SA (18 carbon atoms) could have provided protection of fibres from water since it is itself quite hydrophobic [42].

5.3.4 Contact angle measurements

The outcomes of all measurements made for contact angles of neat PP and PP/MAPP sheets and fibre mats without (HT) and with SA treatment (HT/SA) are presented in Table 5.2. As expected, the neat PP films exhibited the characteristics of hydrophobic surfaces with a contact angle of 116 °C. When PP was blended with MAPP, a significant decrease in the contact angle (88 °) was observed. This is most likely due to the polar functional group (MA group) available on the surfaces of PP/MAPP sheets as a result of blending [5]. It has been previously reported that the availability of polar functional groups on the film surfaces influences wettability by water [187]. Unsurprisingly, the test liquid (water) drop spontaneously spreads onto to the fibre mats (see Figure 5.7b, left). In contrast, the water droplets were stable on the fibre mat surfaces that underwent the SA treatment (Figure 5.7 b, right). This could be due to the thin layer deposited on the fibre mat surfaces (see Section 5.3.1) as a result of the SA treatment. This thin layer could have changed the innate

hydrophilic characteristics of fibre mat surfaces to hydrophobic, resulting in a high contact angle of 126 °.

Table 5.2. Summary of contact angle measurements. Standard deviations are shown in parentheses. CA = contact angle

Samples	CA-Left/°	CA-Right/°	Average CA
Neat PP	115.8 (3.6)	117.0 (3.2)	116.4 (3.4)
PP/MAPP	86.8 (1.9)	89.9 (1.9)	88.4 (1.9)
HT	0	0	0
HT/SA	126.3 (1.5)	127.3 (5.1)	126.8 (3.3)

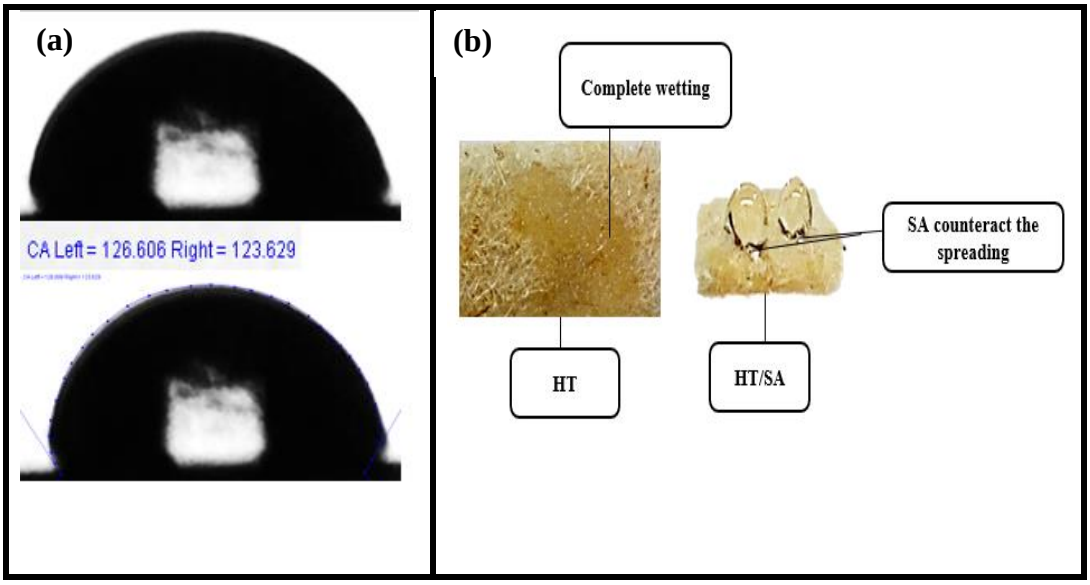

Figure 5.7: (a) A sample image of water droplet used in the measurement of CAM (b) Photograph images fibre mats without and with the SA.

Overall, from SEM, FTIR, weight percentage gain, WRV and contact angle measurements it may be concluded that stearic acid is present on the fibre surfaces and is more likely to be in the form of thin layers.

5.3.5 Tensile properties of composites

Figure 5.8a represents the tensile strengths of neat PP, PP/MAPP (the control) and various composites tested. Composite tensile strengths normalised by the weight percentage of fibre is shown in Figure 5.8b to confirm the change in tensile strength for composites due to SA addition. It was found that the tensile strength of neat PP was not significantly affected with the addition of MAPP as confirmed by a

Student's t-test, although the average tensile strength suggests a slight increase. Table 5.3 represents the percentages of improvement obtained in the average tensile strengths of composites from fibre inclusion, further fibre mat treatment (SA treatment, but not MAPP), coupling agent (MAPP) and the combination of SA and MAPP, along with those values for composites with alkali treated fibre mats only (no MAPP and no SA) for comparison. As can be seen, the inclusion of fibres into neat PP increased the tensile strengths of composites significantly.

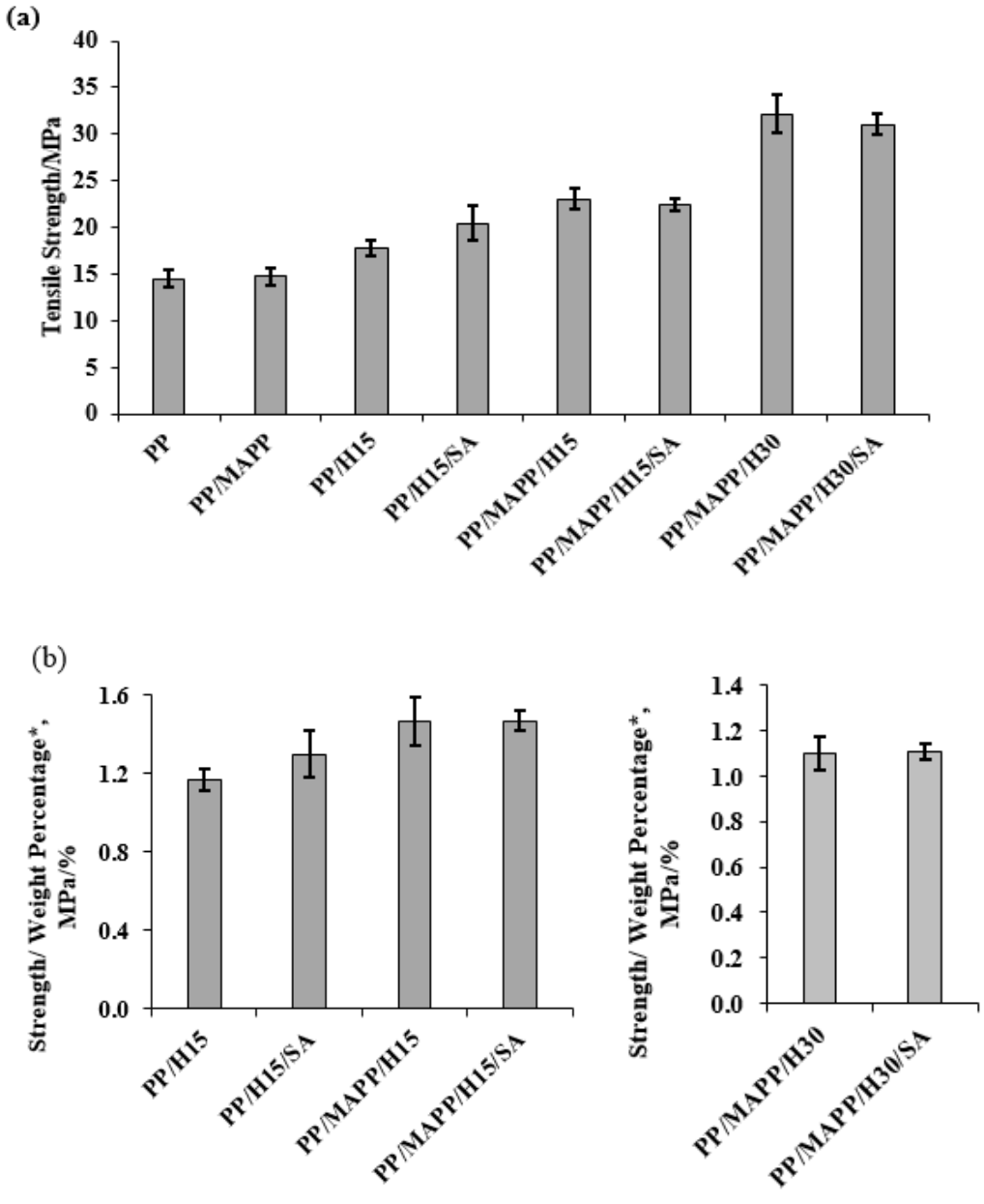

Figure 5.8: (a) Tensile strength of composites as a function of various treatments (b) Tensile strength/weight percentage* of the composites. Table 5.3: Percentage improvement in tensile strengths of composites over composite with alkali treated fibre mats only

Sample	Average tensile strength/MPa	Improvement/%
PP/H15	17.7	-
PP/H15/SA	20.4	15.3
PP/MAPP/H15	23.1	30.5
PP/MAPP/H15/SA	22.9	29.4

The improvement in tensile strengths for composite with fibres treated with SA (but not MAPP) from various studies seen in the literature is believed to be due to improved compatibility resulting fibre wetting by the matrix [42, 116, 117]. As aforementioned, the fibre surfaces appeared to be less hydrophilic after the SA treatment. Thus, the treatment could have facilitated better interfacial compatibility between the fibre and the matrix than the composites with fibres with alkali treatment only [188, 189]. The possible interactions between the fibre surfaces, stearic acid and the matrix are shown in Figure 5.9a. The SA could react with available OH groups on the fibre surfaces to form ester bonds [190]. There are chances of partial entanglements of aliphatic chains of SA with the polymer chains of the matrix (PP) [8, 22]. Furthermore, the stearic acid molecules present on the fibre surfaces may reduce volatiles such as moisture from being adsorbed onto the fibres. The volatiles can desorb easily at the processing temperature of NPFCs, resulting in voids leading to the poor fibre-matrix interfaces [23].

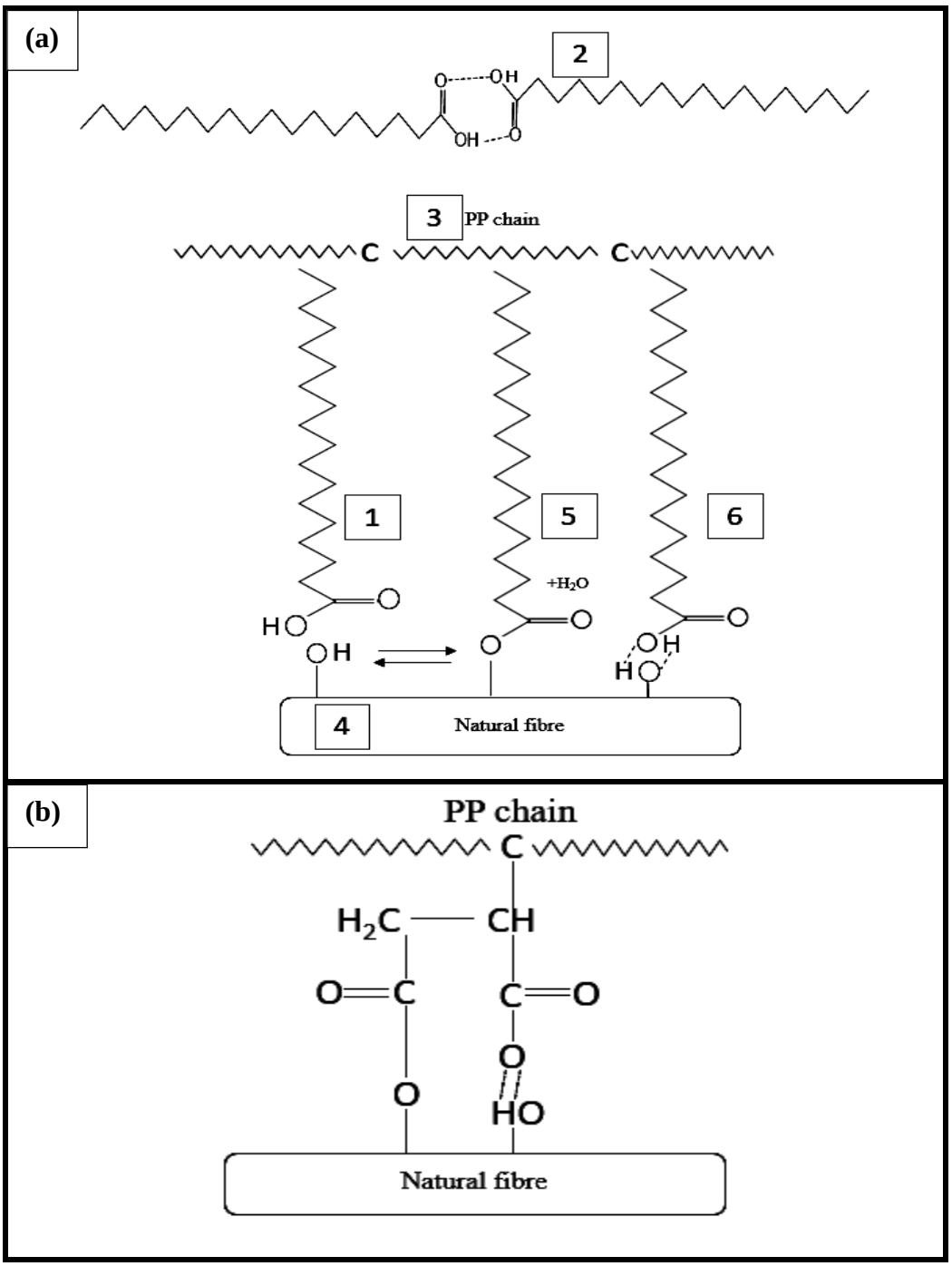

Figure 5.9: (a) Possible interactions of stearic acid, natural fibre and PP (1 - neat SA, 2 - SA dimer, 3 - neat PP, 4 - natural fibre surfaces, 5 - ester bond formed with fibre surfaces, 6 - potential of hydrogen bonding), (b) Possible interactions between maleic anhydride of MAPP and OH groups on the natural fibre surfaces.

The highest improvement obtained here for tensile strength of composites coupled with MAPP can be attributed to the greatest improvement for interfacial shear strength between the fibre and the matrix, which have facilitated better stress transfer through strong bonding to the fibres. This is due to the anhydride group (MA monomers) available with the MAPP which can react strongly through strong

covalent ester-linkage plus potential hydrogen with the hydroxyl group present on the fibre surfaces (Figure 5.9b). Additionally, the long polymer chains of MAPP can interact with the PP by means of chain entanglement. Thus, the MAPP coupling agent acting as a bridge between the matrix and the fibres, improving the fibre-matrix adhesions, leading to the improved tensile strengths for the composites compared to the composites treated with alkali only.

Although the composites with the combination of SA and MAPP did not show any additive benefits for tensile strengths, interestingly, the standard deviations obtained for the tensile strengths of the composites were smaller compared to composites coupled with MAPP. This indicates that, at the fibre/matrix interface, the MA monomers of MAPP react strongly with the available hydroxyl group (OH) on the fibre surfaces and stearic acid deposited on the fibre surfaces is more likely to facilitate for better fibre wetting by the matrix, making interactions more consistent.

Figure 5.10a shows Young's modulus for neat PP, PP/MAPP and all composites tested. Similar to the tensile strength, Young's modulus of the composites was normalised by the fibre weight percentage as shown in Figure 5.10b. As for the tensile strength, the addition of MAPP did not significantly affect Young's modulus of neat PP. As can be seen, only slight improvement in Young's modulus for composites with stearic acid treated fibre mats and composites coupled with MAPP and the combination of SA and MAPP is obtained.

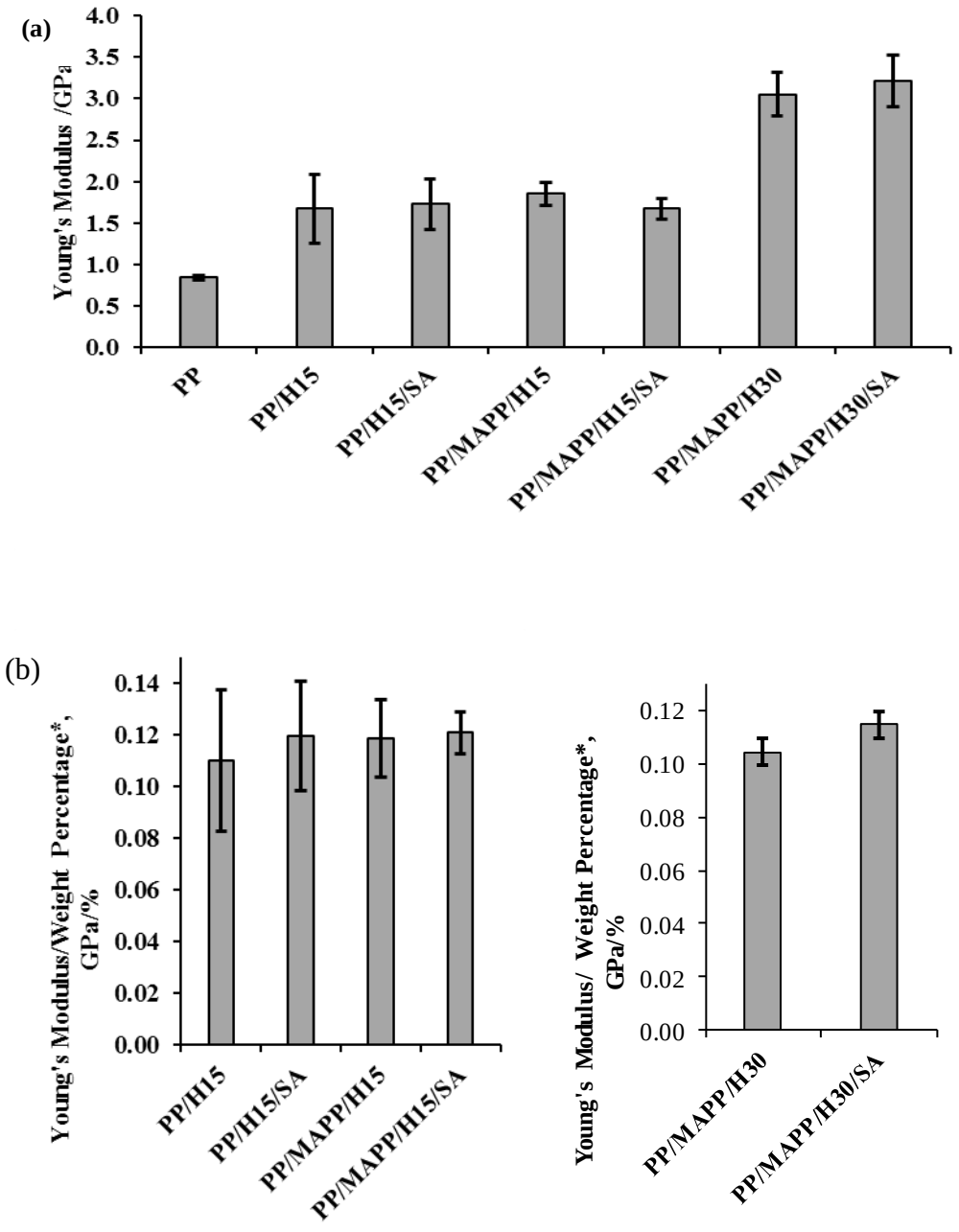

Figure 5.10: (a) The Young's modulus of PP/hemp composites as a function of various treatments (the composites were approximately 15 and 30wt %) (b) Young's modulus/weight percentage* of composites. Weight percentage* = weight percentage of fibre mats with or without SA.

Figure 5.11 shows stress versus strain curves for the composites. The composites with alkali treated fibre mats only failed at lower stress and larger strain compared to other composites. In contrast, the composites with stearic acid treated fibres only, composites coupled with MAPP and with the combination of SA and MAPP improved the load-bearing capacity (stress), indicating improved interfacial

adhesions with further treatment and when coupled with MAPP and with the combination of SA of MAPP.

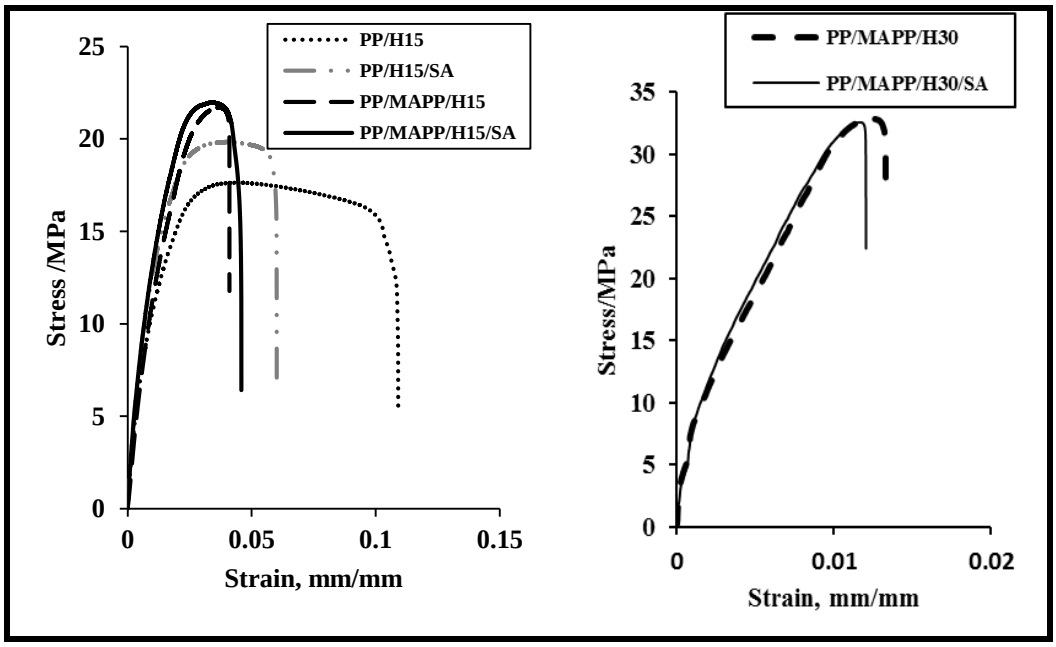

Figure 5.11: Stress-strain curves for composites with fibre contents of approximately: (a) 15 wt% (b) 30 wt%.

Scanning electron micrographs of tensile fractured surfaces for composites with alkali treated fibre mats only, composites with SA treated fibre mats and composites coupled with MAPP and the combination of SA and MAPP are shown in Figure 5.12a to 5.12d. As can be seen, the composites with alkali treated fibre mats only (Figure 5.12a) appeared to have large holes, showing a very weak fibre/matrix interfacial adhesion. There is a large number of unbroken fibres sticking out of the fracture surfaces indicating, much fibre pull-out due to inadequate fibre wetting by the matrix. In contrast, it can be seen in Figure 5.12b that the composites with SA treated fibre mats slightly improved the fibre/matrix interfacial adhesion. The further treatment with SA could have provided better access for PP matrix to impregnate around the fibres. Although these composites showed better fibre/matrix interfacial adhesion compared to those composites with alkali treated fibre mats only, there are still large protruding fibres and gaps between the fibres and the matrix.

It can be seen in Figure 5.12c that the addition of coupling agent (MAPP) greatly improved the fibre/matrix interfacial adhesion. There is less evidence of fibre pull-

out, and the matrix looks as if to have adhered strongly to the fibre surfaces, indicating good fibre wetting. Very few short fibres can be observed at the interface as the majority of the fibres are covered up by the matrix. It can also be seen that the composites with the combination of SA and MAPP (Figure 5.12d) appeared to have almost similar fibre/matrix interfacial adhesions.

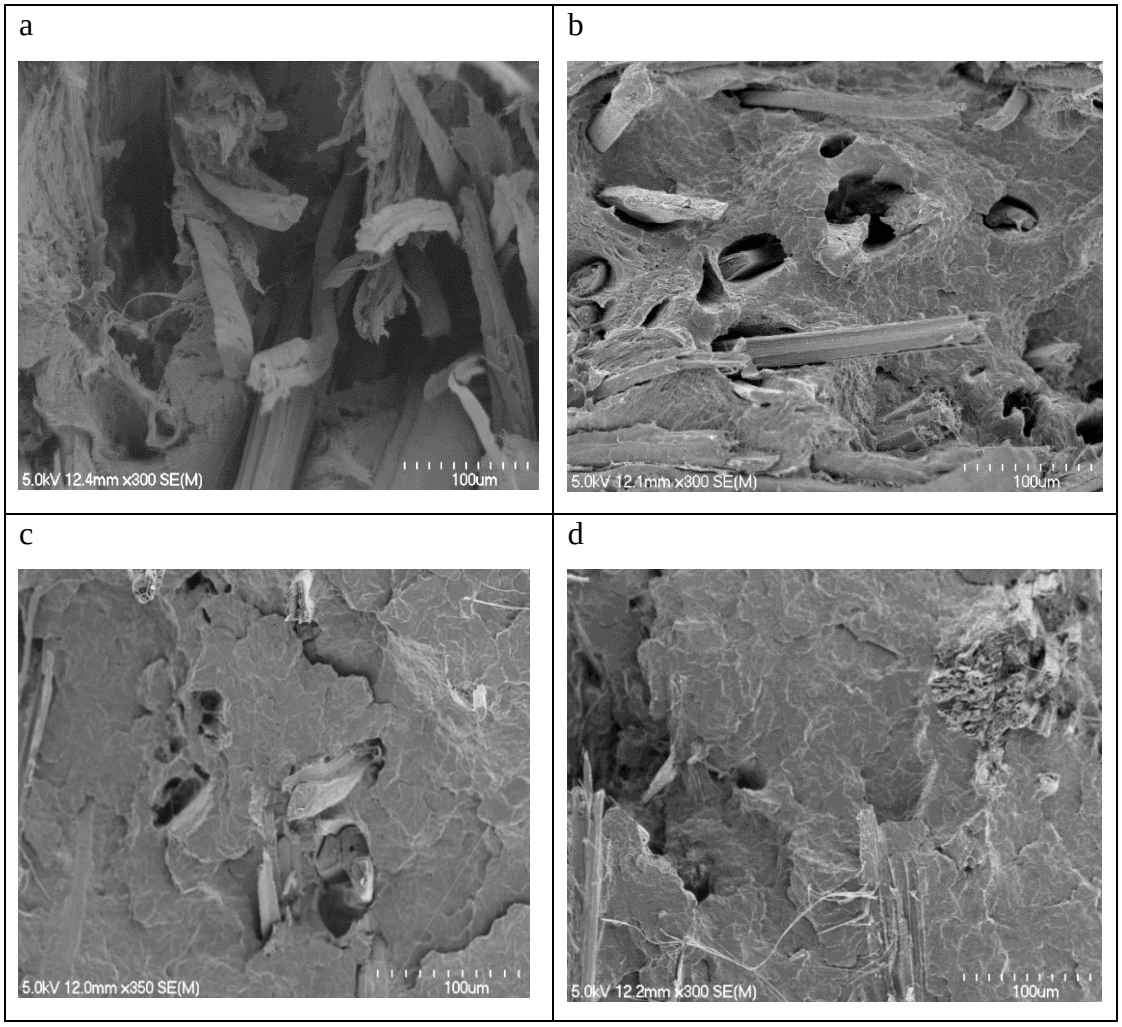

Figure 5.12: SEM images of tensile fracture surfaces for composites: (a) with alkali treated fibre mats alkali only (b) with fibre mats further treated with SA, (c) with coupling agent MAPP and (d) with the combination of SA and MAPP.

5.3.6 Thermogravimetric analysis of fibre mats and composites

The TGA curves for the fibre mats without (HT) and with SA treatment (HT/SA) are shown in Figure 5.13a. The fibre weight was maintained for the fibres without and with SA treatment until declines at around 328 °C and 332 °C, respectively. Above 380 °C, the fibres without SA treatment lost almost 93 % of their initial weight, whereas fibres with SA treatment lost only 86 % of their initial weight. These

indicate that the thermal stability of the fibres has slightly improved after the SA treatment. A similar finding has been previously reported; the SA vapour treatment had a profound effect on the thermal stability of the fibres [188]. The consistent improvement in thermal stability of SA treated fibres above 380 °C could be due to the presence of SA on their surfaces. It has also been reported elsewhere that above 380 °C, under air, the presence of SA could reduce the oxidative decomposition of charred residue [191]. However, as the thermal degradation of cellulosic materials is a complex phenomenon, more research is required to make clear why the stearic acid vapour treatment improved the thermal stability of the fibres.

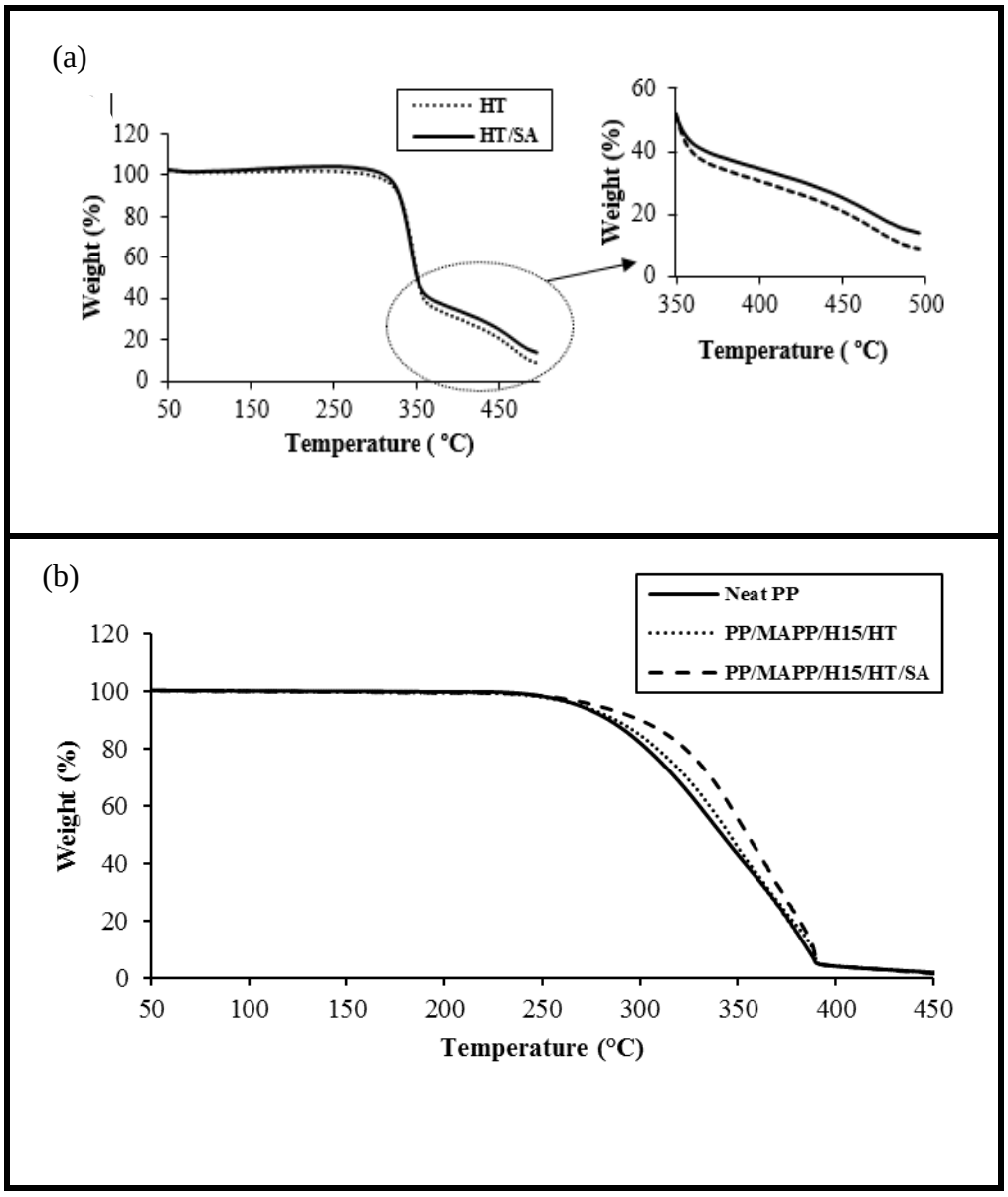

Figure 5.13: TGA analysis of (a) fibre mats and (b) composites.

TGA curves for neat PP, composites with the coupling agent (without SA) and with the combination of SA and MAPP are shown in Figure 5.13b. The thermal degradation of neat PP and the composites initiates at around 260 °C. The initial 10 % of the weight loss occurred for neat PP around 280 °C, whereas the weight loss occurred only at 295 °C and 310 °C for the composites with MAPP only and combination of SA and MAPP treatment, respectively. When compared to neat PP, the increased thermal stabilities of the composites are likely to be due to the presence of thermally more stable fibres. It has been previously reported that the incorporation of fibres could immobilise the free radicals formed as a result of the initiation of polymer degradation, improving the thermal stability of composites [192]. Similar observations where PP matrix reinforced hemp composites displaying higher degradation temperatures compared to neat PP has been previously reported [193]. The slight improvement in thermal stability for the composites with the combination of SA and MAPP compared to composites with MAPP only could be due to the presence of SA.

5.3.7 Swelling studies

For composites reinforced with fibres, the interfacial strength between the fibre and the matrix could be correlated to the swelling index [16]. This is related to the presence of voids at weak interfaces, commonly promoting solvent uptake [194, 195]. As can be seen in Figure 5.14, the swelling indices for composites with SA only, composites with MAPP and the combination of SA and MAPP were lower compared to those composites with alkali only, supporting a further improvement for interfacial strength obtained. The composites coupled with MAPP had the lowest swelling index followed by composites with SA only. Swelling index for the composites with combination of SA and MAPP was slightly lower compared to the composites with MAPP only. However, this reduction was found to be insignificant (confirmed by Student's test).

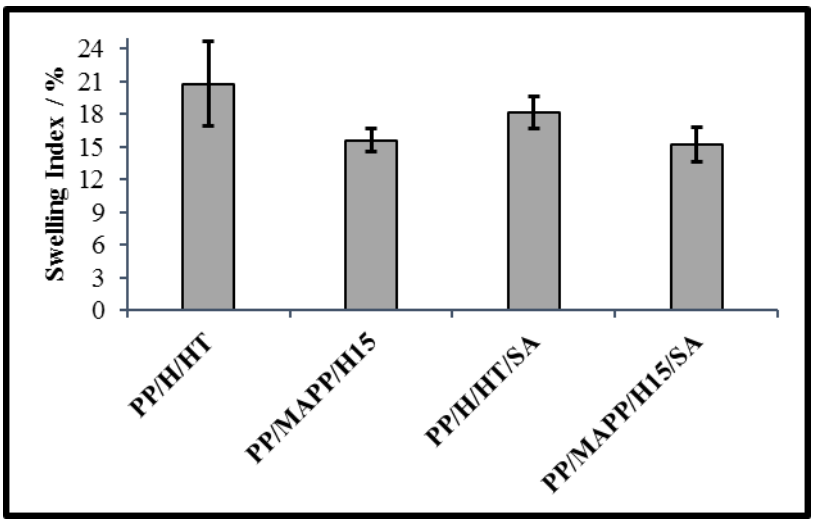

Figure 5.14: Swelling index for hemp composites (fibre content of 15 wt%). Immersion of samples was 48 h.

5.3.8 Part 1 - Conclusions

For the stearic acid vapour treatment, the weight percentage gain (0.54 %) of the fibres after the treatment indicates that stearic acid is most likely to affect only the surfaces, not the bulk. Scanning electron micrographs of the fibre surfaces revealed that the treatment smoothed fibre surfaces. Furthermore, after the treatment, there were traces of material covered on the fibre surfaces, indicating that the stearic acid is most likely to be deposited on the surfaces as a thin layer. This was further supported by the improved thermal stability obtained for the fibres after the treatment. The drastic increase in water contact angle for the fibres treated with stearic acid indicates that the treatment strongly reduces their polar interaction ability.

The composites with maleic anhydride polypropylene coupling agent exhibited the highest tensile strength. In the absence of maleic anhydride polypropylene coupling agent, the composites with stearic acid treated fibres appeared significantly stronger (15 %) than the composites with alkali treated fibre mats only. This indicates that stearic acid could act as a coupling agent to improve the strengths of the composites, but not as effective as maleic anhydride polypropylene. Although the composites made with a combination of stearic acid and maleic anhydride polypropylene did not exhibit any additive benefits for tensile strengths, there was a noticeable reduction in the standard deviations in tensile strength values between the test samples. This indicates potentially more reliable wetting of fibres by the matrix with the addition of

stearic acid. Stearic acid, being low cost and renewable, could be a viable alternative to MAPP in applications where maximising strength is not the only parameter being optimised. Additionally, the stearic acid vapour treatment could be considered, as this treatment required only a small amount of stearic acid and can be carried out without needing to use a solvent. Overall, the stearic acid treatment reduced the polar interaction ability of the fibre mats, thereby making these fibre mats relatively more compatible with the PP matrix.

5.4 Part II - Materials and Methodology

5.4.1 Materials

Commercial cellulose nanocrystals (CNCs) as a dry powder was purchased from Celluforce (Canada). The materials used for the production of the fibre mats and composites are described in Chapter 4.

5.4.2 Cellulose nanocrystals treatment (CNC)

Two CNC suspensions were investigated: one with 1 wt% CNC and the other with 2 wt% CNC in water. To prepare each CNC suspension, a predetermined amount of CNC was added to distilled water and heated up to 70 °C (Figure 5.15a). The mixture was continuously stirred for half an hour, maintaining a temperature range of about 60 to 70 °C until it formed a homogeneous suspension. This suspension was then allowed to cool down to room temperature before being transferred into a small container. The treatment was carried out by spraying. Figure 5.15b shows the spraying system used for the treatment. The set up to held the small container containing CNC suspension and a commercially available trigger spray attachment.

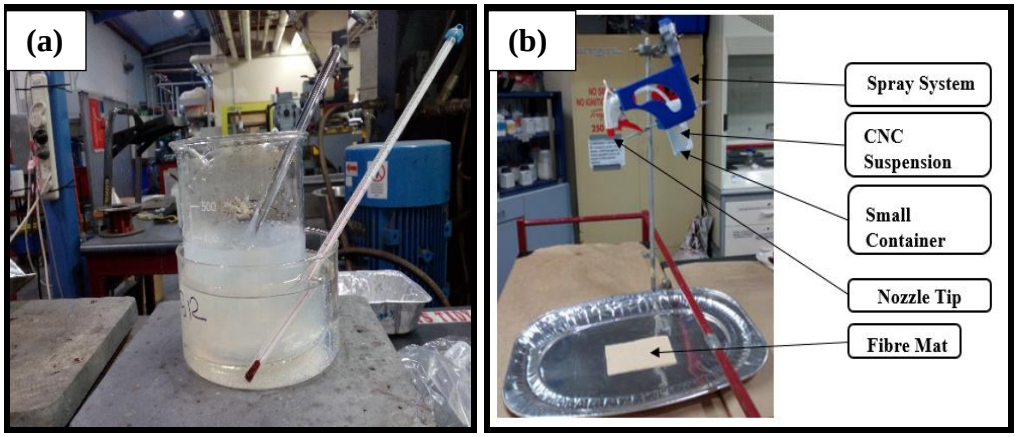

Figure 5.15: (a) CNC solution preparation (b) CNC treatment.

Based on preliminary trials, while spraying, the distance between the spray nozzle tip and the fibre mats was maintained as 450 mm to provide good coverage for CNC suspension onto the mats. Five sprays were made on each side of the mat. After spraying on both sides, the mats were oven-dried for 3 h at 105 °C. This approach delivered 0.088 g (± 0.006) and 0.190 g (± 0.007) of CNCs onto the fibre mats with 1

and 2 wt% CNC treatments, respectively. After oven drying, the mats were stored in sealed polyethylene bags.

5.4.3 Fourier transform infrared spectroscopy (FTIR)

The fibre mats were ground to fine power using a Retsch MM400 ball mill. All the samples were mixed and compressed with potassium bromide by applying a pressure of 8 tonnes/cm^2 to prepare the sample discs for the analysis. A PerkinElmer Spectrum One spectrometer was used to obtain infrared spectra of pure CNC, fibre mats without (CNC0) and with CNC treatments (CNC1, CNC2). A total of 20 scans were taken for each sample with transmission mode from 4000 to 400 cm^{-1}.

5.4.4 Raman spectroscopy

The samples to be analysed were placed on an aluminium foil and the laser power was set to 20 % of maximum. Raman spectra were acquired using a PerkinElmer RamanStation 400R spectrometer equipped with an air-cooled CCD detector. Raman spectra of pure CNC, fibre mats without (CNC0) and with CNC treatments (CNC1, CNC2) were obtained. Each spectrum was acquired as the sum of five repeats of 20 s exposure on the same location on the sample.

5.4.5 X-ray diffraction

XRD spectra were obtained using an EMPYREAN diffractometer system (PANalytical) fitted with a Cu Kα X-ray tube. The fibre mats for analysis were prepared as described in Section 4.2.4.2. Fibre mats without (CNC0) and with CNC treatments (CNC1, CNC2) were analysed.

5.4.6 Production of PP/MAPP sheets

PP blended with MAPP were formed into sheets using a Labtech 1201-LTE20-44 twin-screw extruder. The 11 heating zones of the extruder barrel were set at 155 °C (feed entrance), 165 °C, 165 °C, 165 °C, 165 °C, 170 °C, 170 °C, 170 °C, 170 °C, 170 °C and 170 °C (at exit). The rotating screw speed was set to 45 rpm. The sheets produced were cut to 150 x 90 mm. In order to reduce the thickness of these polymer sheets, they were pressed between two aluminium plates inside a hot press. The plates were lined with Teflon® sheets to avoid polymer sheets adhering to the plates. The time, applied pressure and temperature were 5 min, 1.5 MPa and 140 °C, respectively. After cooling down to room temperature, the polymer sheets were cut

to the size of the mould (150 x 90 mm) used for the production of composites and stored in sealed bags.

5.4.7 Fabrication of composite materials

Composite processing was conducted according to the method described in Section 4.2.6. Table 5.4 represents the stacking arrangements and the abbreviations used for composites. It should be noted that the composites containing fibre content of about 25 wt% with 2 wt% CNC was heated at 170 °C for 5 minutes and pressed at 1 MPa (H25CNC2) or 2 MPa (H25CNC2*).

Table 5.4: Abbreviations used for PP/MAPP and composite samples

Samples	Targeted fibre wt%	Stacking arrangements	Thickness of polymer sheets used/mm	Production process of polymer sheets
PP/MAPP	-	4PP*	0.56	Extrusion
H15CNC0 H15CNC1 H15CNC2	15	1PP*/1MAT/1PP*/1MAT/1PP*/1MAT/1PP*	0.56	Extrusion
H25CNC0# H25CNC2# H25CNC2*#	25	1PP*/1MAT/1PP*/1MAT/ 1PP*/1MAT/1PP*/ 1MAT/1PP*/1MAT/1PP*/ 1MAT/1PP*	0.29	Extrusion + Pressed between two aluminium sheets
H30CNC0 H30CNC0# H30CNC1 H30CNC1# H30CNC2 H30CNC2#	30	1PP*/3MATS/1PP*/ 3MATS/1PP*	0.56	Extrusion
		1PP*/2MATS/1PP*/2MATS/ 1PP*/2MATS/1PP*	0.29	Extrusion + Pressed between two aluminium sheets

Note the following: In the abbreviations, 'H' refers to hemp fibre and the number following 'H' is equal to the nominal weight percentage of fibres in composites. CNC0 = composites without CNC, CNC1 = composites with 1 wt% CNC treated fibre mats, CNC2 = composites with 2 wt% CNC treated fibre mats. # = composites made with polymer sheets thickness of 0.29 mm.

5.4.8 Assessment of fibre mats and composites

A Hitachi S-4700 scanning electron microscope, operated at 5 kV, was used to examine the surfaces of fibre mats and the fracture surfaces of composites. Prior to SEM observation, all samples were mounted on an aluminium stub using carbon tape and coated with platinum.

5.4.9 Tensile testing of fibre mats and composites

Tensile testing of fibre mats was based on Tappi standard T 404cm-92. An Instron-4204 universal testing machine fitted with a 10 N load cell and a crosshead speed of 1 mm/min was used for the testing. Ten strips of 150 x 20 mm were cut from the fibre mats for each direction, longitudinal and transverse to the rotation direction of DSF (fibre alignment direction). The mats were conditioned at 23 ± 1 °C and 50 % ± 2 % for 48 hours, prior to testing. Average tensile strengths for each direction were calculated and are reported as the breaking load divided by the width of the strip. The orientation of fibres within the mats were also quantified from this testing; when the fibres in the mats are randomly orientated TTS (transverse tensile strength) to LTS (longitudinal tensile strength) ratio is close to 1, whereas when the fibres are unidirectional orientated, the ratio approaches 0 [178]. Tensile testing of composites was conducted according to the method described in Section 4.2.7.

5.4.10 Thermogravimetric analysis (TGA)

Thermogravimetric analysis of the composites without CNC (H15CNC0) and with (H15CNC2) treatment was carried out using a PerkinElmer simultaneous thermal analyser STA 8000 instrument. A scanning range of 40 to 500 °C with a constant heating rate of 10 °C/min and air flow at 20 ml/min were used to obtain the data.

5.4.11 Swelling studies

The details of swelling studies are similar to that described in Section 5.2.12.

5.5 Results and Discussion

5.5.1 Microscopic evaluation of fibre mats with and without CNCs

The surfaces of fibre mats with and without CNCs were observed by means of a scanning electron microscope (SEM). As can be seen in Figure 5.16a, there appeared to have large number of grooves on the surfaces of fibres without CNC, revealing a rougher texture as commonly seen in literature for alkali treated fibres [4] (detailed in

Section 3.3.5). Figure 5.16b clearly shows the presence of rod-like CNCs on the fibre surfaces. It appears that a thin layer of CNCs films are covering the fibre surfaces. The CNCs deposited were measured using ImageJ software [137] and found to have average sizes of 15 (± 6.6) nm in width and 226 (± 66) nm in length. These dimensions are consistent with that previously reported for cellulose nanocrystals supplied from the same manufacturer [196]. Strong interactions between CNCs and natural fibre surfaces are expected due to the affinity of cellulosic materials through hydrogen bonding [122, 197]; a large number of hydroxyl groups available on the CNCs and the fibre surfaces promotes the potential for hydrogen bonding between them.

Figure 5.17a to 5.17e show the scanning electron micrographs of fibre mats without (CNC0) and with CNCs (CNC1 and CNC2). The fibre mats without CNC appeared to have many gaps between the fibres (Figure 5.17a). In contrast, the fibre mats with CNCs appeared to have thin films formed between the fibres. Also, increase in CNC content (from 1 to 2 wt%) was found to fill more gaps between the fibres (Figure 5.17b compared to Figure 5.17c). The films formed between the fibres within the mats indicated the potential of CNCs to act as binders to hold loose fibres together. The films formed between the fibres could also be an indication of the self-organising capability of CNCs [122]. It appears from the micrograph that the films formed between the fibres consisted of several stacks of thin CNC films (Figure 5.17e).

The CNC was delivered by the manufacturer as powder form and are likely to be prepared from wood pulp by sulfuric acid hydrolysis [196]. It is well-known that sulfuric acid hydrolysis could have yielded CNCs with negatively charged surfaces, enabling them to disperse uniformly in water due to the electrostatic repulsions [198]. The fibre mats after the treatments were oven dried at 105 °C for 3 hours. During the drying process, the evaporation of the suspending fluid (water) takes place, resulting in deposition of CNCs onto the fibre surfaces and formation of thin films between the fibres. It has been previously reported that the most notable property of CNCs is the ability to self-assemble and form as a film while water evaporating from a CNC suspension spreads onto a substrate [199]. However, it is less likely that the CNCs

were formed as a uniform film throughout the mat as the CNC treatment was carried out by spraying.

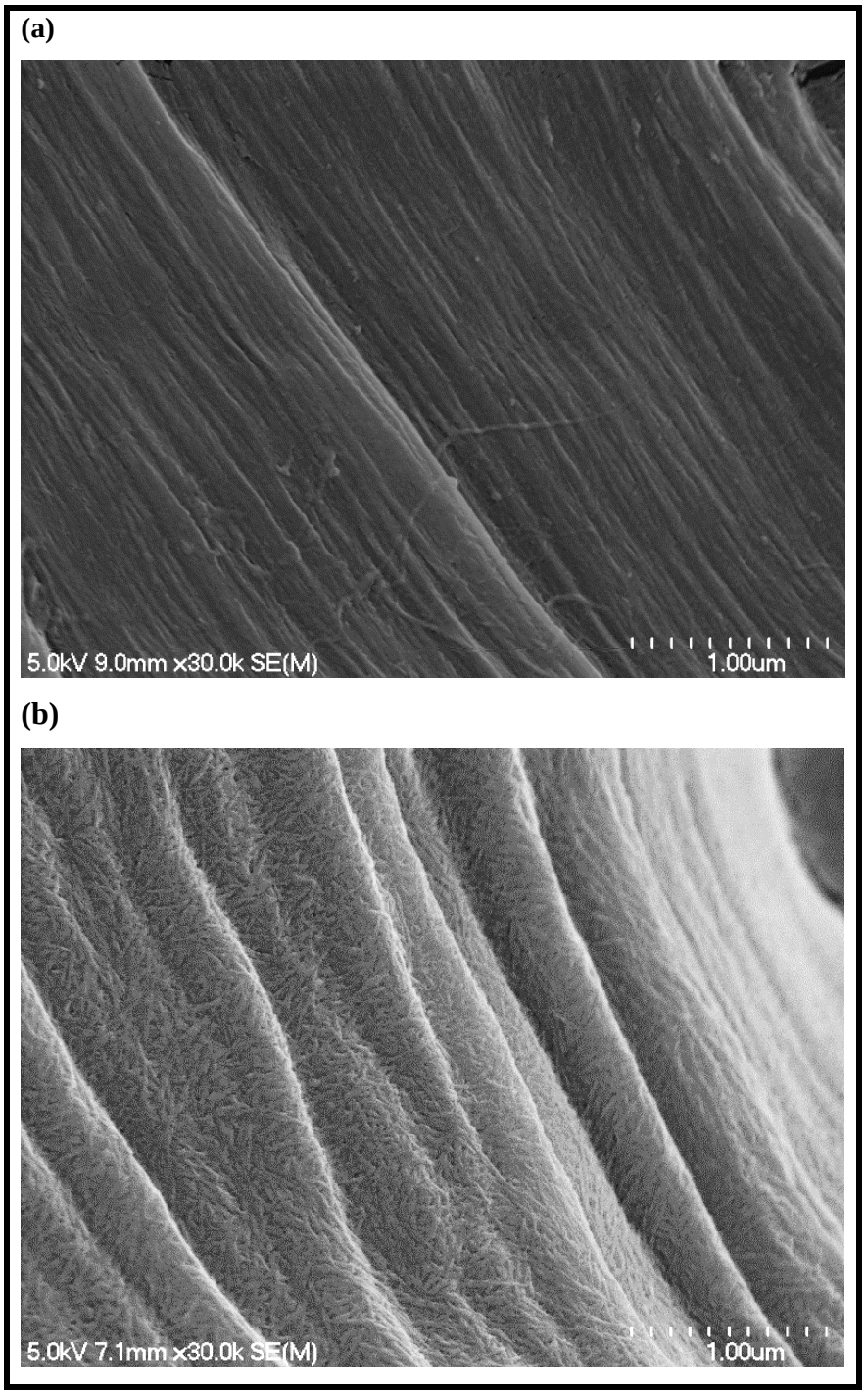

Figure 5.16: Scanning electron micrographs of fibre surfaces: (a) without (CNC0) and (b) with CNC treatment.

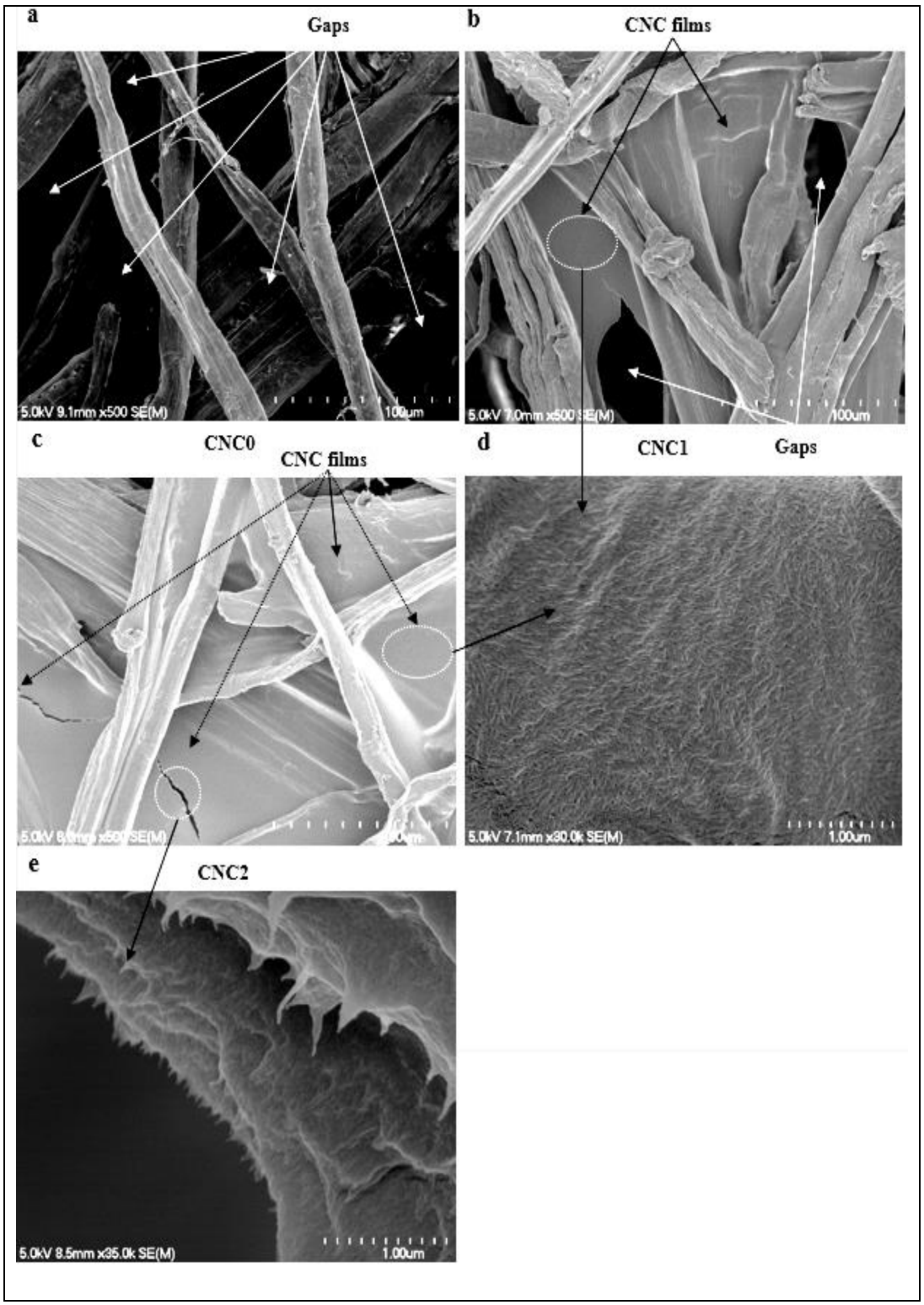

Figure 5.17: Scanning electron micrographs of fibre mats without (CNC0) and with CNC (CNC1 and CNC2) treatments.

5.5.2 Fourier transform infrared spectroscopic analysis

Fourier transform infrared spectroscopic analysis was carried out to understand the chemical composition of pure CNC and fibre mats with and without CNC treatments. The spectra of the samples analysed are shown in Figure 5.18. The peaks in the range

3300-3400 cm^{-1} show the spectra of all samples can be attributed to the stretching vibrations of the hydroxyl groups and reflect the hydrophilic nature of cellulosic materials [200]. The peak around 2900 cm^{-1} corresponds to the stretching vibrations of C-H groups of cellulose [201, 202]. Although this peak appeared in the spectra of all samples, slightly higher peak intensity was shown for pure CNC compared to the fibre mats with or without CNC indicating the highly crystalline nature of pure CNCs [203, 204]. The peak at 1430 cm^{-1} corresponds to the CH_2 bending vibration. The intensity of this peak appeared very sharp for the pure CNC followed by fibre mats with CNC treatment. It has been previously reported that the higher the intensity of this band, the higher the degree of crystallinity of the sample [204]. The peaks around 1638 cm^{-1} are commonly attributed to the bending vibration of hydroxyl groups [201] and was present in the spectra of all samples. The peaks appeared in the range 1330-1360 cm^{-1} in the spectra of all samples correspond to the bending vibrations of C-OH groups [171]. The peaks at 1238, 1058 and 896 cm^{-1} are associated with the C-H groups bending, CH stretching and bending vibrations of cellulose, respectively [205] and were present in the spectra of all samples. However, the intensity of these peaks appeared strong for pure CNC followed by fibre mats without CNC or with CNC treatments. The peaks appeared in the range 900-1500 cm^{-1} [204] were very strong for pure CNC followed by the fibre mats with CNC and without CNC. These results strongly indicate the presence of high crystalline CNCs on the fibre mats. The decreases in intensities of peaks in this range indicate reduction in the degree of crystallinity [204].

The strong peaks at 850 cm^{-1} [206] and 1163 cm^{-1} [200] in the spectrum of pure CNC indicate the presence of sulfate groups (SO_2 groups). The formation of sulfate ester groups as a result of sulfuric acid hydrolysis has been previously reported [206]. It is well known that the presence of SO_2 groups reduce the thermal stability of CNC [200, 206-208]. The disappearance of this peak from the spectra of CNC treated fibre mats indicates that the fibre mats are free of sulfate groups. This could be due to oven drying of the mats at 105 °C for 3 h [196]. It has been previously reported that oven drying at 105 °C for only 5 min removed 75 % of sulphur content from CNC films as a result of desulfation (the loss of negatively charged sulfate ester groups and their replacement by OH groups) [196, 209].

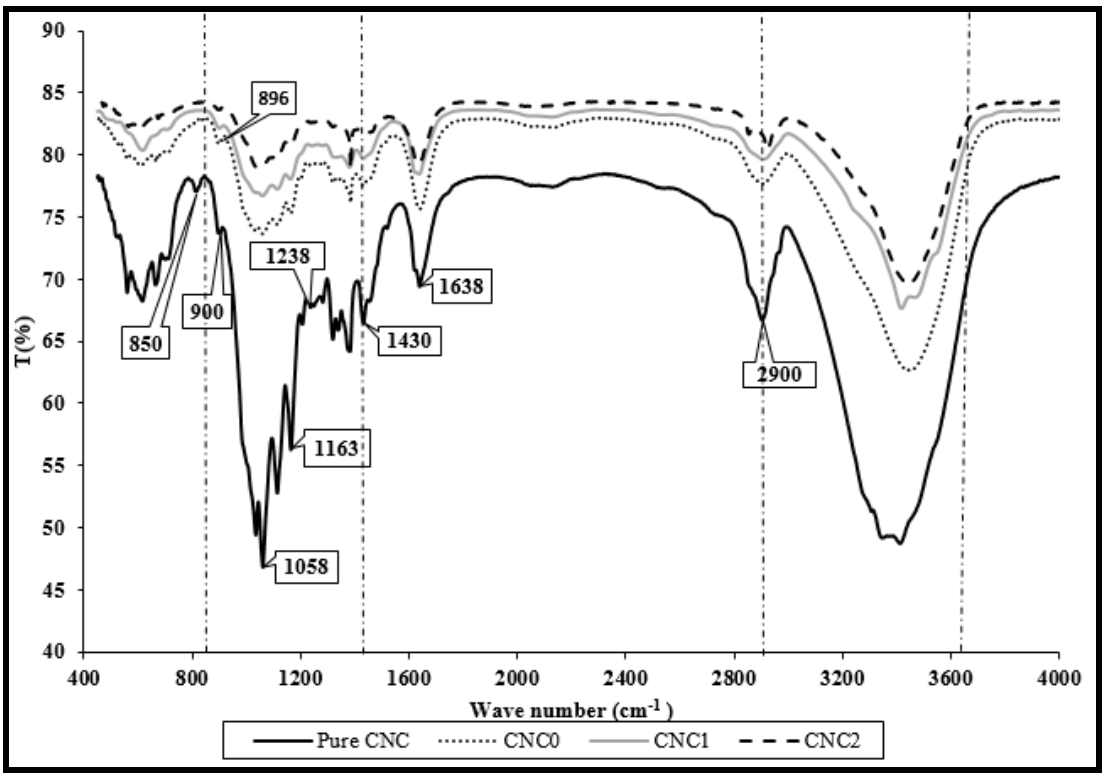

Figure 5.18: FTIR spectra of fibre mats without (CNC0) and with CNC treatments (CNC1 and CNC2) and pure CNC.

5.5.3 Raman analysis

Raman analysis was carried out to confirm the removal of sulfate groups from the spectra of CNC treated fibre mats. Raman spectra of pure CNC, the fibre mats with and without CNC treatments can be seen in Figure 5.19. When compared to the fibre mats without CNC treatment, the intensity of cellulose peaks at 1098 cm^{-1}, 1120 cm^{-1}, 1374 cm^{-1} and 2900 cm^{-1} appeared sharper for pure CNCs and fibre mats with CNC treatments, supporting the presence of CNCs on the fibre mats [210].. The characteristic peaks associated with the S-S bond of sulfur appeared in the range 400-500 cm^{-1} in the spectrum of pure CNC confirm the presence of SO_2 groups in CNCs [211]. The absence of these peaks from the spectra of CNC treated fibre mats indicated the removal or reduction of sulfate groups of CNCs. Also, the peaks in the range 1050-1200 cm^{-1} related to SO_2 groups appeared very weak or absent in the spectra of CNC treated fibre mats further supports that the fibre mats were mostly free of SO_2 groups [212].

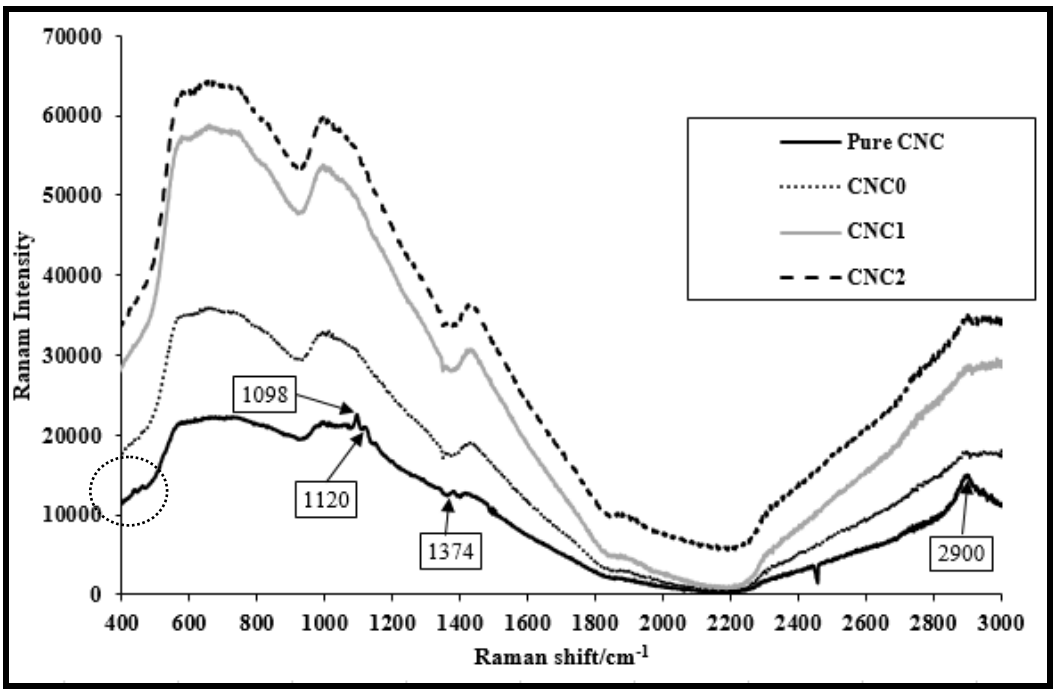

Figure 5.19: Raman spectra of fibre mats without and with CNC treatments and pure CNC.

Overall, the combination of FTIR and Raman spectroscopy results indicated that the CNC treated fibre mats were largely free of sulfur groups or these techniques were not able to detect the sulfate groups due to the very low levels present.

5.5.4 Cellulose crystallinity index (I_c)

The major peaks for crystalline phases of most cellulosic fibres are generally observed at about 2θ = 15, 17, 22.7 and 35 ° (denoted as 'a', 'b', 'c' and 'd', respectively) as shown in Figure 5.20, representing the (110), ($1\bar{1}0$), (200) and (400) crystallographic planes, respectively of cellulose I [5, 16]. As expected, the major crystalline peak (200) of cellulose for the fibre mats without or with CNC treatments appeared at about 2θ = 22.7 °. In order to calculate the crystallinity index, the intensity of diffraction of the amorphous material (I_{am}) was taken at 2θ = 18.3 ° (denoted as 'e' in Figure 5.20), where the intensity is minimum. It should be noted that the crystallinity index is commonly considered for comparison instead of describing absolute crystallinity [50]. As can be seen in the results presented in Table 5.5, the crystallinity index of the fibre mats was increased by CNC treatments. Such behaviour is expected with the applied treatment, as highly crystalline CNCs are

deposited onto the fibre surfaces. It can also be seen that increasing the CNC content slightly increased the crystallinity index of the fibre mats.

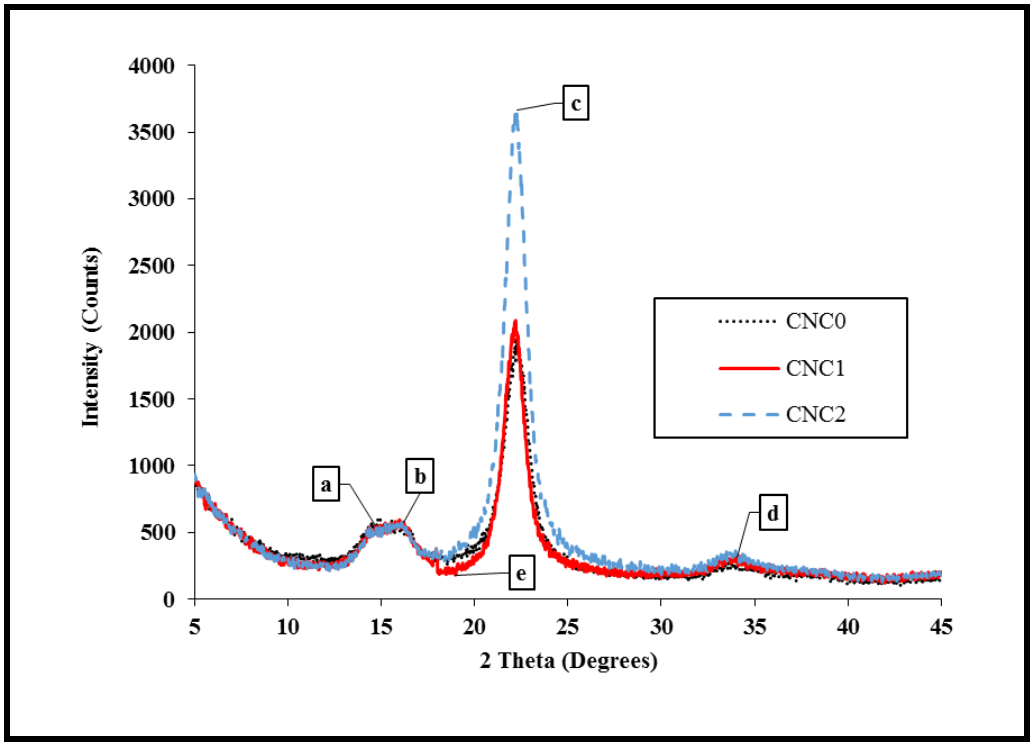

Figure 5.20: X-ray diffraction curves of fibre mats without and with CNC treatments used in calculating crystallinity index (I_c).

Table 5.5: Crystallinity index (Ic) of hemp fibres without and with CNC treatments

Samples	I_{am} (18.3 °)	I_{200} (22.7 °)	Crystallinity index (%)
CNC0	1963	255	87
CNC1	2086	181	91
CNC2	3664	290	92

5.5.5 Fibre mat assessment

Table 5.6 displays the average tensile strengths and the ratio of transverse tensile strength to longitudinal obtained for the 2 wt% CNC treated fibre mats. The strength was calculated by dividing the maximum load required to break the mat by its width, as the cross-section area of the fibre mats is not well defined [36, 130]. Although attempts had been made to obtain the tensile strength of the fibre mats without any

CNC addition and with 1 wt% CNC, it appeared that they were very weak and also below the accuracy limits of the equipment. This is due to the fact that only friction is holding the loose fibre together [129, 130] even though the wet processing (DSF) would have helped the fibres to consolidate and form as mats. It appears that even the use of 1 wt% CNC was not enough to promote the fibre-fibre stress transfer. The fibre mats treated with 2 wt% CNC tested parallel to the fibre orientation direction attained an average tensile strength of 0.11 kN/m. This indicates that the CNC could act as binders to hold the loose fibres together within the mats, thereby improving the fibre-fibre stress transfer within the mats. It has been previously reported that the ratio between transverse tensile strength (TTS) to the longitudinal tensile strength (LTS) indicates the degree of fibre orientation [36]. The ratio TTS/LTS for the fibre mats was 0.39 (± 0.27). The ratio of 0.39 found in this work indicates a good degree of fibre alignment within the fibre mats produced using DSF.

The weight percentage gains in fibre mats with respect to the CNC treatments are shown in Figure 5.21. The maximum weight gain was found to be approximately 4 wt% when treated with 2 wt% CNC.

Table 5.6: Tensile strengths of fibre mats with 2 wt% CNC treatment

*LTS (kN/m)	*TTS (kN/m)	TTS/LTS
0.11 (0.04)	0.03 (0.02)	0.39 (0.27)

***LTS –longitudinal tensile strength, *TTS – transverse tensile strength. All the values in parenthesis are the standard deviations. Ten mats were tested in each direction.**

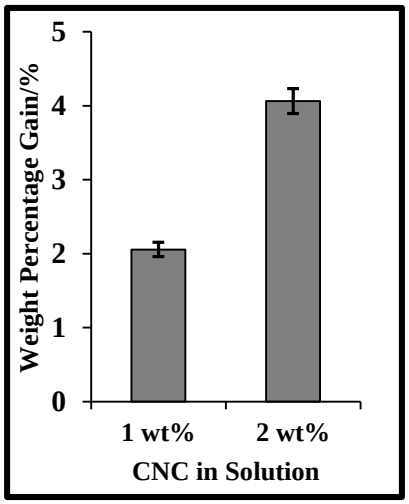

Figure 5.21: Weight percentage gain in the fibre mats with respect to the CNC treatment.

5.5.6 Tensile properties of composites

The average tensile strengths of various composites and the control (PP/MAPP) samples are represented in Figure 5.22a with composite tensile strengths normalised by the weight percentage of fibres are shown in Figure 5.22b. The tensile strengths of all composites were higher than that of the control. At a fibre content of 15 wt%, the average tensile strength of composites with 1 and 2 wt% CNC treated fibre mats increased to 23.57 and 26.51 MPa, respectively; these were approximately 2.1 and 14.8 % higher than the respective composites without CNC treated fibres mats. However, the increase of composite tensile strengths was found to be statistically significant (Student's t-test) only with the inclusion of 2 wt% CNC treated fibre mats. The normalised graph (Figure 5.22b) was used to ensure that the increases in composite tensile strength was due to CNC addition and not due to variability in the precise fibre content [130]. The improvement in composite tensile strength with CNC treated fibre mats is thought to be due to the addition of high strength nanocellulose. Additionally, the large surface-to-volume ratio of CNCs could have facilitated more surface contact with the polymer matrix improving fibre wetting and thereby, the tensile strength for composites [213]. It has been previously reported that the introduction of high strength and high modulus nanocellulose into composites could enhance the tensile strength and Young's modulus of the composites [129, 131, 208, 213, 214].

In the absence of CNCs, it can be observed that an increase in fibre content significantly increased the composite tensile strength. In contrast, at high fibre contents, the incorporation of CNC treated fibre mats were found to significantly decrease the composite tensile strength (except 1 wt% CNC at the fibre content of 25 wt%, no significant differences) relative to the respective composites without CNC treated fibres mats. Decline in composite tensile strengths at higher fibre and CNC contents compared to the composites without CNCs indicates that the CNC films formed between the fibres (see Figure 5.17) within the mats is mostly likely to act as barriers, resulting in very poor fibre wetting by the matrix. A further decrease in the tensile strengths for the composites (H25CNC2 compared to H25CNC2*) was observed with the increase in the amount of pressure applied during compression moulding; 1 MPa to 2 MPa, although increasing pressure was expected to improve the fibre wetting. It is worth mentioning at this point that no reliable data was

acquired from the tensile strength of composites with a fibre content of 30 wt% containing CNCs (for both 1 and 2 wt%) due to very poor consolidation (see Figure 5.23). For composites containing fibre content of approximately 30 wt%, there was no significant difference in tensile strength between composites (H30CNC0 and H30CNC0[#]) made with different polymer sheet thicknesses (0.56 or 0.29 mm).

(a)

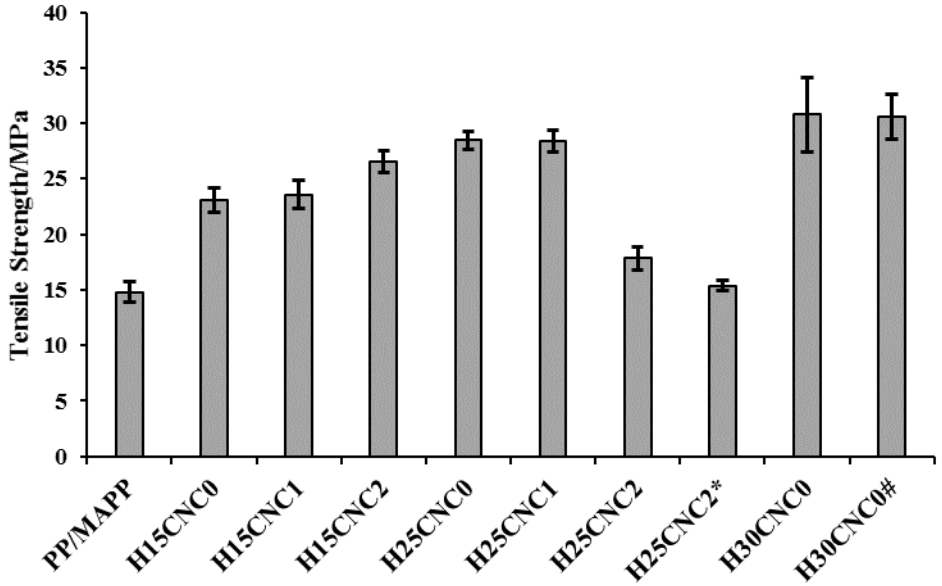

(b)

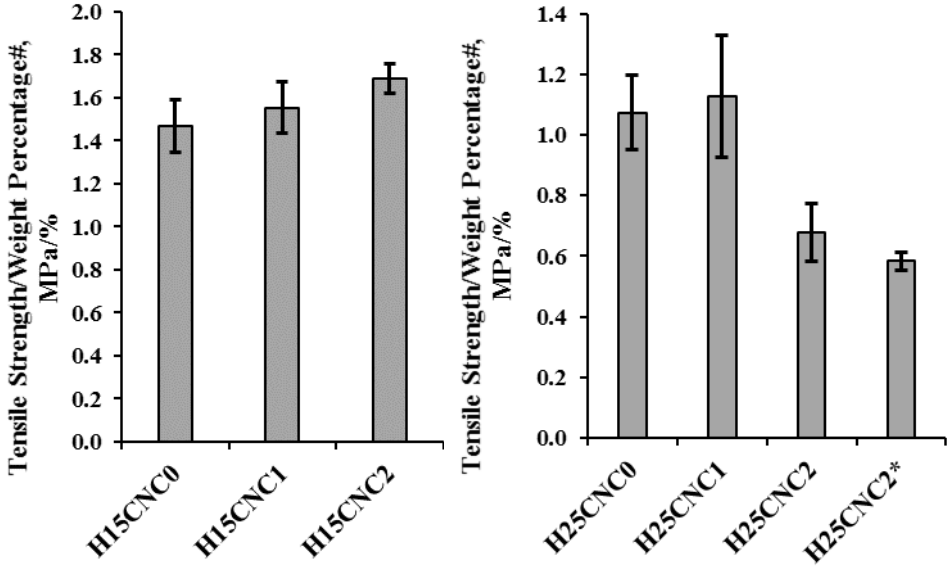

Figure 5.22: (a) Tensile strengths of PP/MAPP and various composites tested (b) Tensile strength/weight percentage[#] of composites (normalised).

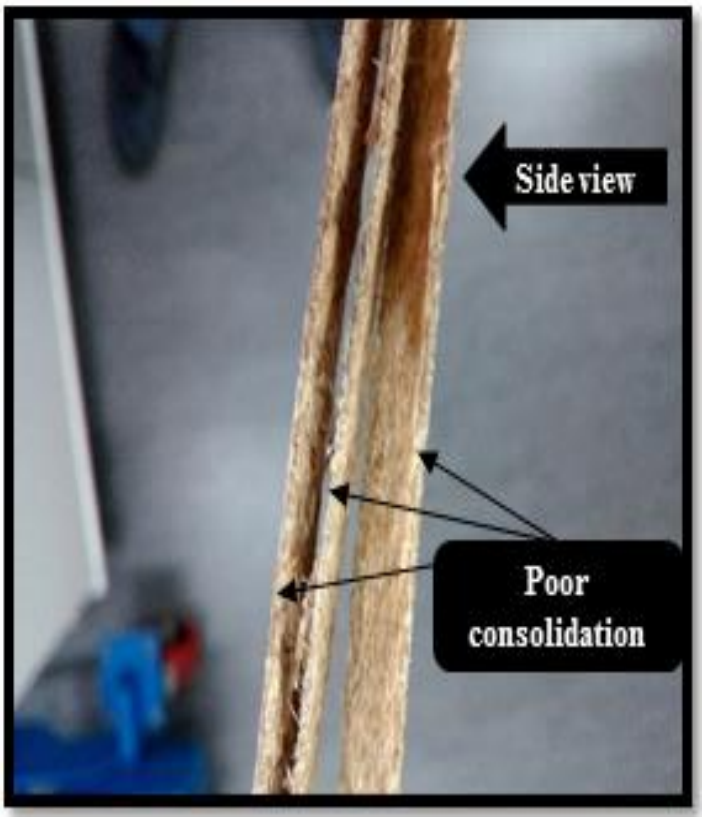

Figure 5.23: A side cross-section image of 30 wt% composite with CNC sample (cut-edge) displaying poor consolidation.

The Young's modulus of various composites and the control (PP/MAPP) samples are represented in Figure 5.24a. The composite Young's modulus normalised by the weight percentage of fibres is shown in Figure 5.24b. A similar trend as that of tensile strengths were observed for the Young's modulus of the composites. When compared to composites without CNC, an increase by about 16 % was noticed for the composites with 2 wt% CNC (at fibre content of 15 wt%) supporting the increase of interfacial adhesions between the CNC treated fibre mats and the PP/MAPP matrix. Figure 5.25 shows the stress-strain curves for the composites with and without CNC treatments. The stiffness of the composites increased with increasing CNC contents, but the failure strain decreased.

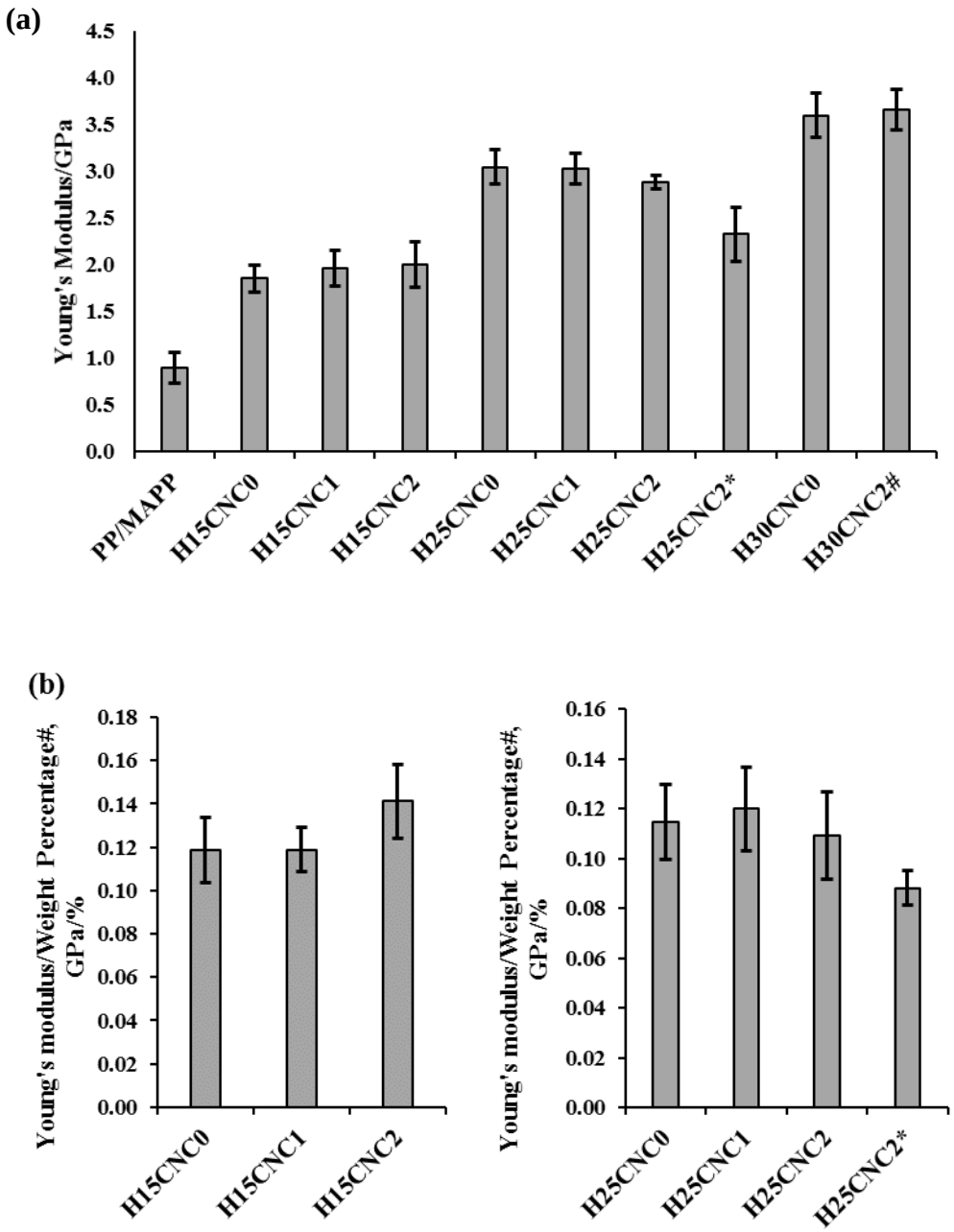

Figure 5.24 (a) Young's modulus of PP/MAPP and various composites (b) Young's modulus/weight percentage[#] of composites (normalised).

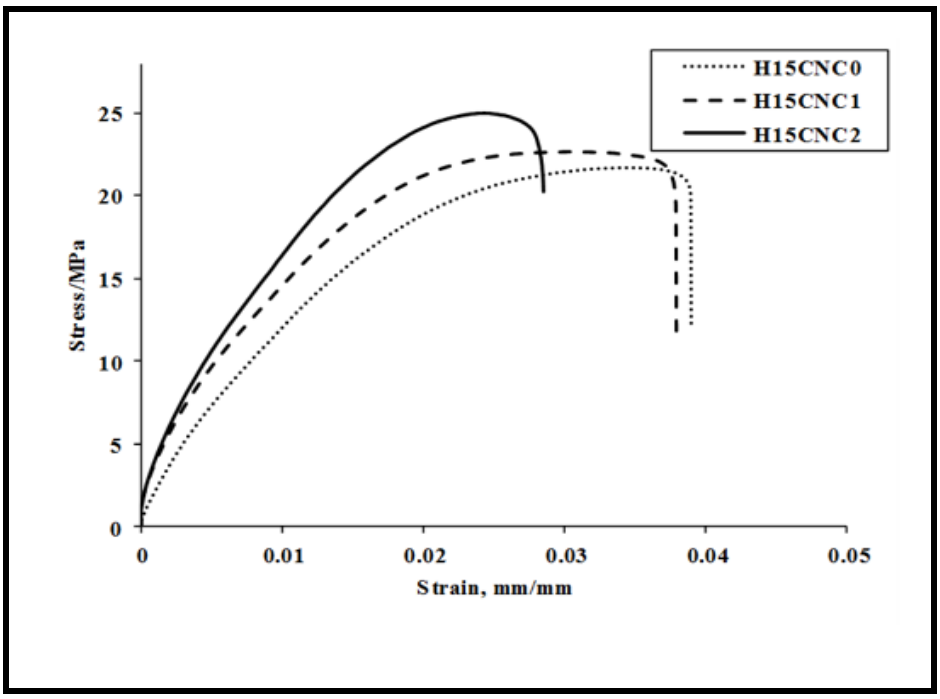

Figure 5.25: Stress-strain curves of 15 wt% composites with and without CNC treated fibre mats.

The scanning electron micrographs of the tensile fracture surfaces of composites without and with CNC treated fibre mats can be seen in Figure 5.26a to 5.26f. The fracture surfaces of the 15 wt% composites with CNC treated fibre mats appeared rougher compared to those composites without CNC treated fibre mats (Figure 5.26a and 5.26d compared to Figure 5.26b, 5.26c and 5.26e). This indicates that the addition of CNCs had improved the fibre-matrix interfacial adhesions. It has been previously reported that the failure mode is more like matrix and fibre tearing as the interfacial shear strength increases [215]. The addition of CNCs (due to its high aspect ratio) possibly enlarged the contact area between the treated fibre mats and the PP/MAPP matrix, thereby potentially improving the interfacial adhesions [131]. However, composites with high fibre and CNC contents have shown very poor fibre wetting (Figure 5.26f), suggesting that the CNC films formed between the fibres most likely to restrict the flow of the molten polymer through the composites. It is well known that for the formation of good interfacial adhesion between the fibres and matrix in a composite, the molten matrix material should ideally flow around and fully wet the fibres. Poor fibre wetting results in weak fibre-matrix interfaces with defects such as fibre pull-out and voids, which act as stress raisers, thus reducing the overall mechanical performance of composites [2, 4, 127].

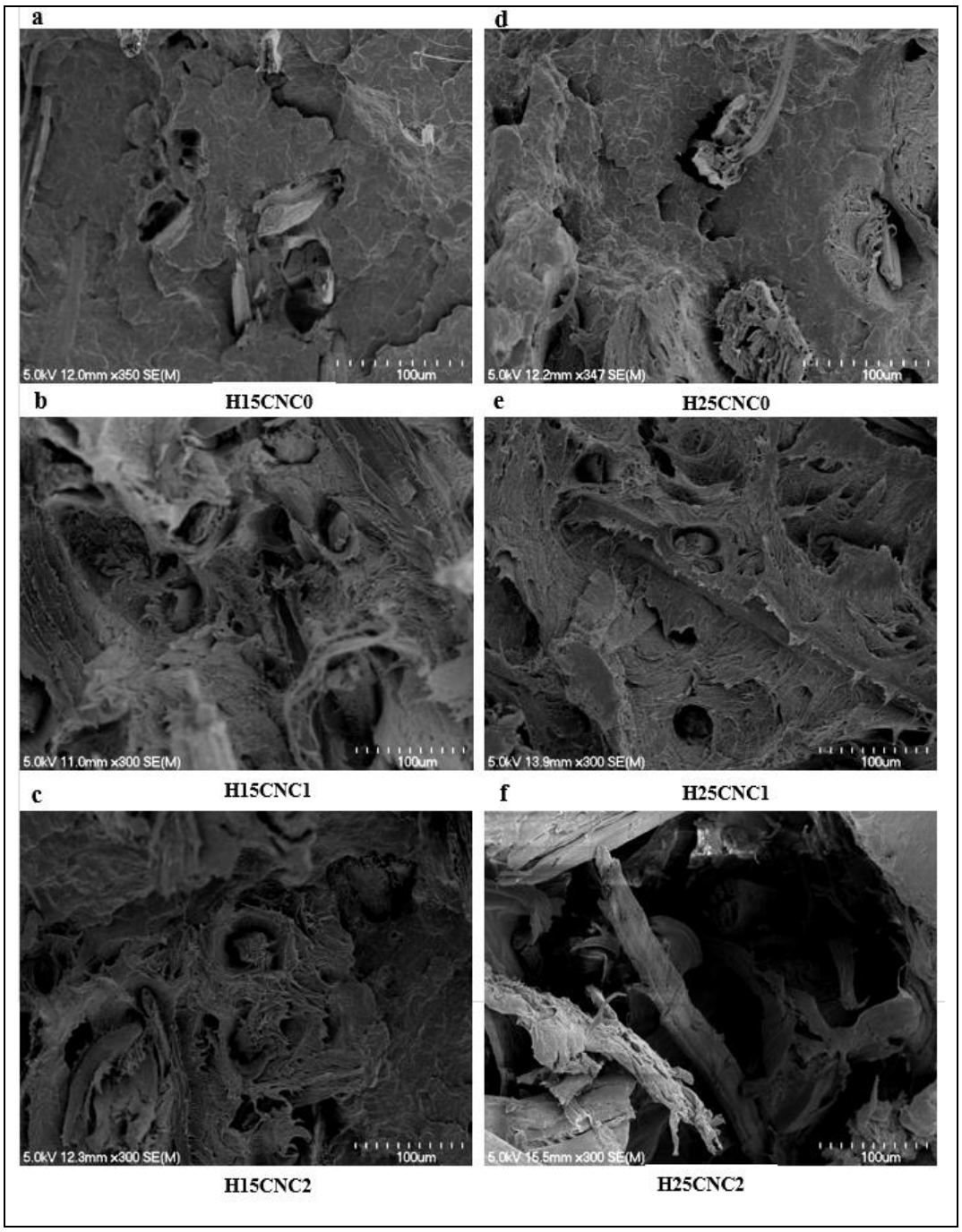

Figure 5.26: Scanning electron micrographs of tensile fracture surfaces of composites with and without CNC treated fibre mats.

5.5.7 Thermogravimetric analysis (TGA)

Thermogravimetric curves for composites with and without CNC are shown in Figure 5.27. Both composites started losing mass around 260 °C. Above 260 °C up to a temperature of 360 °C, a slight increase in the thermal stability for the composites with CNC was observed. The apparent increase in the thermal stability of the composites is thought to be due to the presence of CNCs. It has been previously

reported that the presence of inherently high thermally stable nanocellulose in composites could effectively hinder the heat flow to composites, thus inhibiting the thermal degradation process to higher temperatures [208]. It has also been reported that improved interfacial interaction between the fibres and the matrix could also delay the thermal decomposition [102, 129].

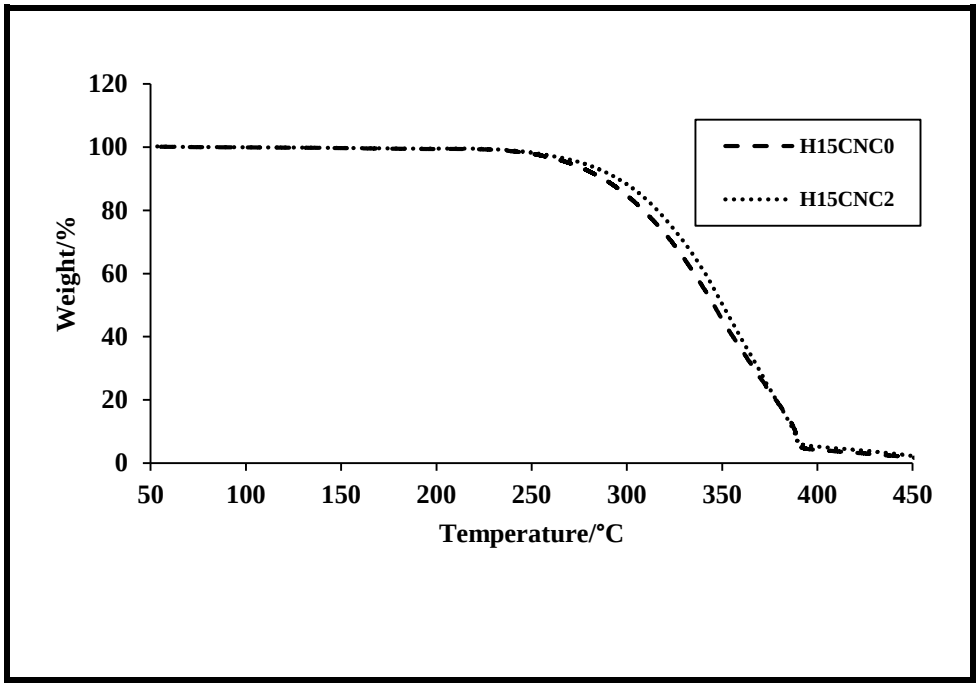

Figure 5.27: TGA curves for composites with and without CNC treated fibre mats (heating rate of 10 °C/min and air flow at 20 ml/min).

5.5.8 Swelling studies

As can be seen in Figure 5.28, the composites with 2 wt% CNC treated fibre mats had the lowest swelling indices. This further supports that the presence of CNCs improved the interfacial adhesion between the treated fibre mats and the PP/MAPP matrix. It has been previously reported that the coating of natural fibres with nanocellulose increases the surface energy of the fibres due to its highly crystalline nature, thus resulting in improved fibre wetting with polymer materials [216, 217].

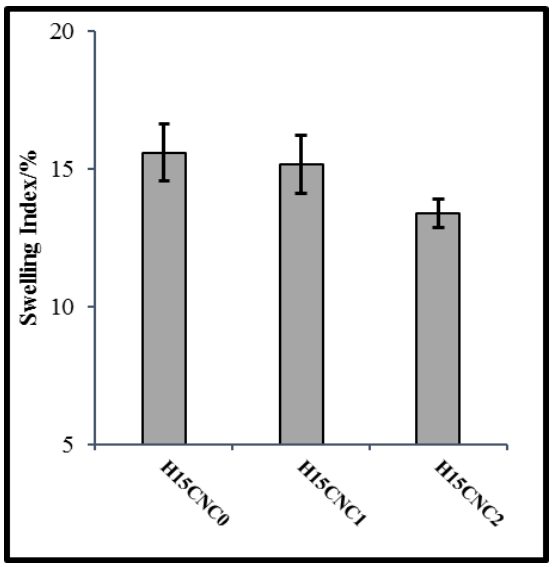

Figure 5.28: Swelling indices for hemp composites. Samples were immersed for 48 h.

5.5.9 Part II - Conclusions

In this investigation, it has been shown that cellulose nanocrystals can be sprayed onto the fibre mats to bind the loose fibres together. The fibre mats possessed an average tensile strength of about 0.11 kNm^{-1} when treated with 2 wt% CNCs in water, whereas those mats treated with 1 wt% and without CNCs possess no measurable tensile strength using a 10 N load cell. It appeared that the addition of CNCs modified the fibre surfaces (CNC coating) as well as filled the gaps between the fibres within the mats (thin CNC films). The tensile strength and Young's modulus of composites with CNC treated fibre mats (2 wt% CNC) increased by about 15 and 16 %, respectively. This indicates that the CNC addition improved the fibre-matrix interfacial adhesion. This was further supported by the lower swelling indices and higher thermal stability obtained for the composites with CNC treated fibre mats compared to those composites without CNC treated fibre mats. At low fibre content, the production method of composites with CNC treated fibre mats by compression moulding was found to be effective and resulted in a good consolidated final product. However, at high fibre contents, the composites displayed very poor consolidation due to the CNC films formed between the fibres. This films are mostly like to act as a barrier, restricting the flow of the molten polymer through the composites. This results in poor fibre wetting and strong declines in the tensile strength and Young's modulus of composites, limiting the use of compression moulding for the composite processing.

6 Chapter Six

Improving polypropylene matrix composites reinforced with aligned fibre mats through high fibre content

6.1 Introduction

The main goal of this study was to improve the mechanical performance of polypropylene matrix composites through high fibre content. Different polymer sheet thicknesses and stacking arrangements were investigated to achieve high fibre content. Interfacial shear strength between the fibre and the matrix was obtained experimentally from which the critical fibre length was determined.

6.2 Materials and Methodology

6.2.1 Materials

The materials used for the production of the fibre mats and composites are described in Chapter 4.

6.2.2 Production of PP/MAPP sheets

PP blended with MAPP were formed into sheets using a Thermo Prism TSE-16-TC extruder (the details are provided in Section 4.2.5) and a Labtech 1201-LTE20-44 twin-screw extruder (Figure 6.1a). The former extruder was equipped with a die spacer of 1.00 mm, whereas the latter had a die spacer of 0.50 mm allowing the production of thinner sheets. The 11 heating zones of the Labtech extruder barrel were set at 155 °C (feed entrance), 165 °C, 165 °C, 165 °C, 165 °C, 170 °C, 170 °C, 170 °C, 170 °C, 170 °C, 170 °C and 170 °C (at exit). The rotating screw speed was set to 45 rpm.

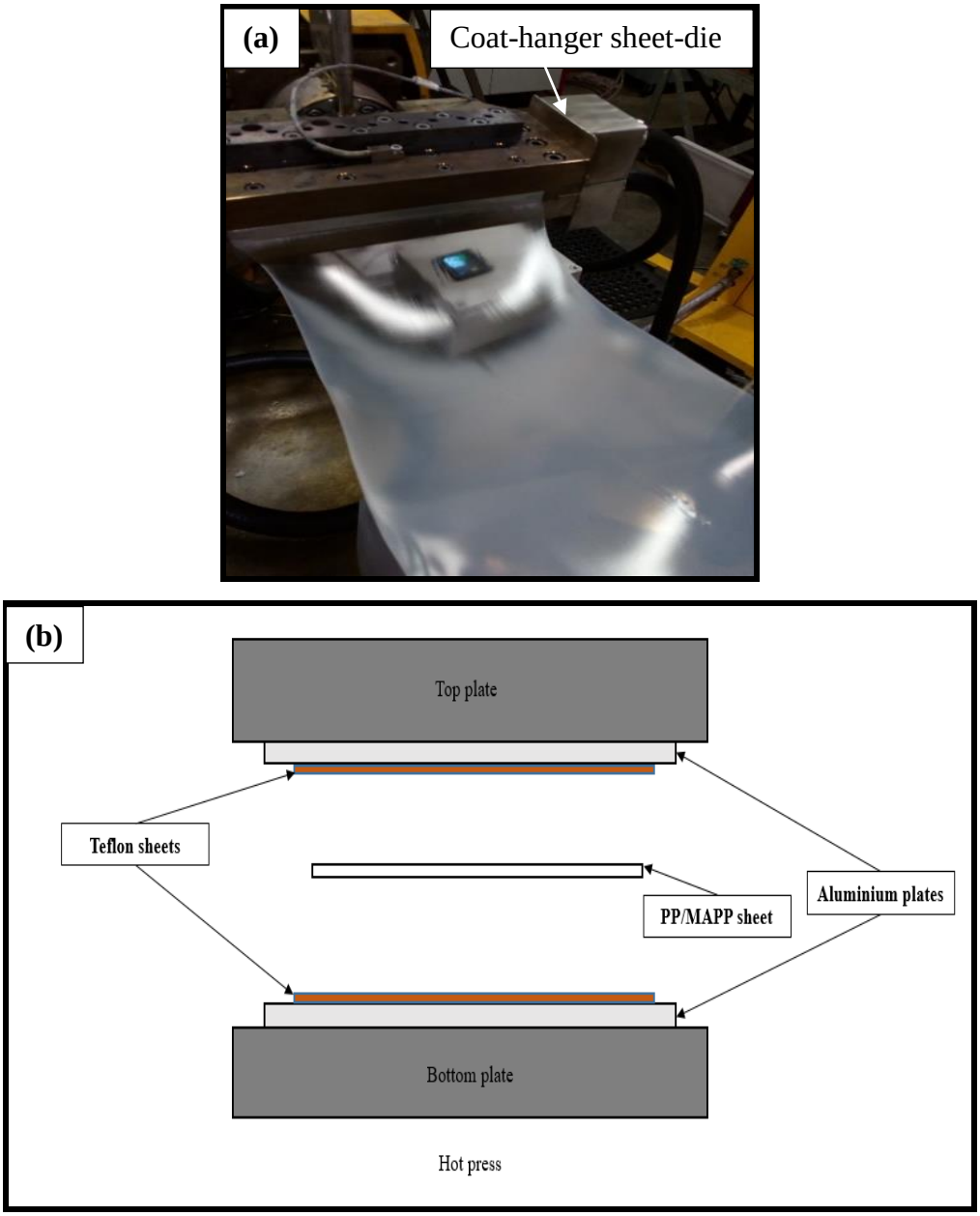

Figure 6.1 (a) The PP/MAPP sheet extrusion using a Labtech twin-screw extruder (b) Schematic representation of reduction of sheet thickness in a hot press.

In order to further reduce the thickness of sheets produced with a die spacer of 0.50 mm, they were pressed between two aluminium plates inside a hot press (Figure 6.1b). The two aluminium plates were lined with Teflon® sheets to avoid polymer sheets adhering to the plates. Based on trial runs, the time (5 minutes) and applied pressure (1.5 MPa) were maintained as constants with temperatures 130, 140 or 150 °C changed to adjust the thickness of the sheets. After cooling down to room temperature, the sheets produced were cut to the size of the mould used for the production of composites (the details are provided in Section 4.2.6). The thicknesses

of these sheets were measured at six different points, as shown in Figure 6.2, using a Vernier calliper. The sheets were then stored in sealed bags for further processing.

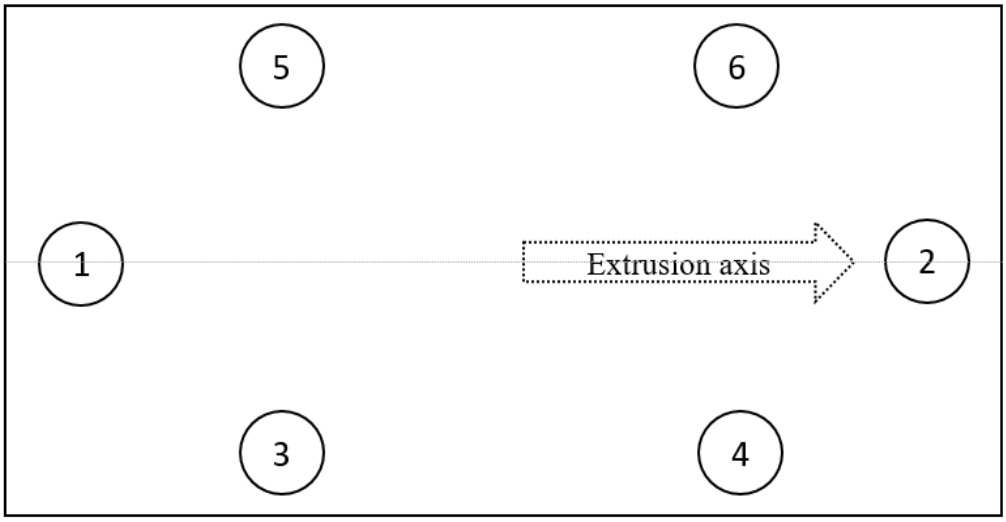

Figure 6.2: Schematic diagram showing different locations from where the measurements were taken out to obtain the average thickness of the sheets.

6.2.3 Fabrication of composites

A series of composites were produced between 30 and 70 wt% fibre contents and tensile tested. Although the production procedures for the composites using hot press were similar to that reported in Chapter 4 and Chapter 5, a slight modification in the hot-pressing procedure was necessary for the production of composites above 50 wt%. The composites were further pressed in the hot press. It has been previously reported that pressing twice could reduce the fibre spring-back in the composite; spring-back is a condition where material partially returns to its original shape due to elastic recovery [5]. This condition often occurs in compression-moulded components when the compaction pressure is released suddenly. To account for this pressing was repeated. After pressing for the first time, composites were allowed to cool under pressure and then pressed a second time at 170 °C for 5 minutes at a pressure of 1 MPa. Table 6.1 represents the abbreviations and stacking arrangements used for composites, respectively.

Table 6.1: Abbreviations and stacking arrangements of polymer sheets (PP/MAPP) and hemp fibre mats in the mould

Samples*	Targeted fibre wt%	PP* sheets No.	Fibre mats No.	Actual fibre wt%	Stacking arrangement from bottom to the top of the mould
H30 - 0.66	30	3	6	29.1	1PP*/3MATS/1PP*/ 3MATS/1PP*
H30 - 0.56		3	6	29.5	1PP*/3MATS/1PP*/3MATS/1PP*
H30 - 0.29		4	6	30.0	1PP*/2MATS/1PP*/2MATS/1PP*/2MATS/1PP*
H30 - 0.24		4	6	31.8	1PP*/2MATS/1PP*/2MATS/1PP*/2MATS/1PP*
H35 - 0.56	35	5	8	34.2	1PP*/2MATS/1PP*/2MATS/1PP*/2MATS/1PP*/2MATS/1PP*
H40 - 0.66	40	3	8	39.4	1PP*/4MATS/1PP*/4MATS/1PP*
H40 - 0.56		5	10	41.2	1PP*/3MATS/1PP*/2MATS/1PP*/2MATS/1PP*/3MATS/1PP*
H40 - 0.29		6	10	41.3	1PP*/2MATS/1PP*/2MATS/1PP*/2MATS/1PP*/2MATS/1PP*/2MATS/1PP*
H45 - 0.56	45	5	12	44.5	1PP*/3MATS/1PP*/3MATS/1PP*/3MATS/1PP*/3MATS/1PP*
H50 - 0.29	50	8	14	50.1	1PP*/2MATS/1PP*/2MATS/1PP*/2MATS/1PP*/2MATS/1PP*/2MATS/1PP*/2MATS/1PP*/2MATS/1PP*
H60 - 0.29	60	10	18	59.9	1PP*/2MATS/1PP*/2MATS/1PP*/2MATS/1PP*/2MATS/1PP*/2MATS/1PP*/2MATS/1PP*/2MATS/1PP*/2MATS/1PP*/2MATS/1PP*/2MATS/1PP*
H70 - 0.29	70	12	22	70.2	1PP*/2MATS/1PP*/2MATS/1PP*/2MATS/1PP*/2MATS/1PP*/2MATS/1PP*/2MATS/1PP*/2MATS/1PP*/2MATS/1PP*/2MATS/1PP*/2MATS/1PP*/2MATS/1PP*

Note the following: PP* = PP/MAPP, MATS = hemp fibre mats produced using DSF. *In the abbreviations 'H' refers to hemp composites, the number following 'H' refers to the nominal weight percentage (wt%) of fibres and the final number refers to the thickness (in mm) of the polymer sheets used in the production of composites.

Initially, the stacking arrangements of polymer sheets and fibre mats in the mould were according to the literature [16]. Although these arrangements successfully produced composites up to 30 wt% fibre content, the production was not successful above 30 wt% due to poor fibre wetting. It is known that reasonable interfacial

bonding between fibre and matrix is required to achieve effective reinforcement as applied stress is transferred from matrix to fibre across the interface. For good interfacial bonding to occur, the matrix should be impregnated fully into the space between the fibres and wet the fibres. Therefore, in the present study, decreasing the overall thickness of fibre mats between two polymer sheets within the stacking arrangements of composites and so decreasing the distance the polymer needs to travel is expected to improve fibre wetting through the composite and therefore improve the tensile properties of the composite. The possible stacking arrangements of composites were determined by the thickness of polymer sheets and fibre content. For instance, Figure 6.3 shows the various stacking arrangements used for the production of composites with 40 wt% fibre content. When polymer sheets with an average thickness of 0.66 mm were used, the stacking arrangements consisted of a maximum of four fibre mats between two polymer sheets (see Figure 6.3a). When polymer sheets with an average thickness of 0.56 mm were used, it was possible to decrease the number of fibre mats to a maximum of three between two polymer sheets (see Figure 6.3b). When polymer sheets with an average thickness of 0.29 mm were used, it was possible to further decrease the number of fibre mats between two polymer sheets from a maximum of three to two (Figure 6.3c). This stacking pattern of two fibre mats between two polymer sheets was repeated depending on the fibre content and produced composites up to 70 wt%.

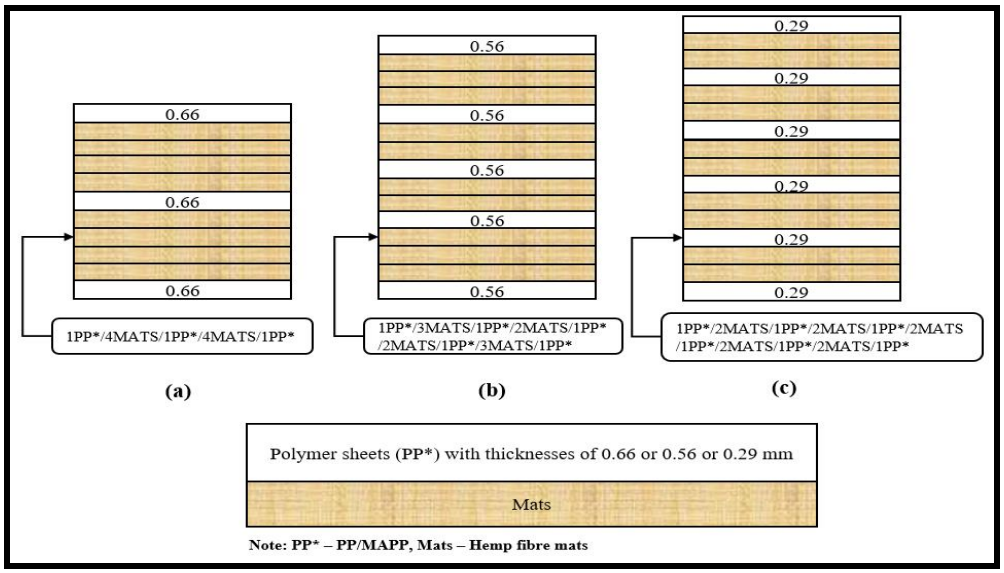

Figure 6.3: Schematic diagram representing various stacking arrangements used for the production of composites with 40 wt% fibre content. The arrangements of fibre mats and the polymer sheets depend on the thickness of the sheets used.

6.2.4 Composite tensile testing

Tensile testing for all composite samples was conducted following the method described in Section 4.2.7.

6.2.5 Assessment of composite morphology

Tensile fracture surfaces of composites were investigated using a Hitachi S4100 field emission scanning electron microscope. The details are described in Section 5.2.5.

6.2.6 Composite flexural testing

Flexural testing (three-point bending) was performed on an Instron-4204 fitted with a 5 kN load cell according to the ASTM D 790-3 (Standard Test Methods for Flexural Properties of Unreinforced and Reinforced Plastics and Electrical Insulating Materials). The crosshead speed and unsupported spans were 1.5 mm/min and 48 mm, respectively. Five test specimens with dimensions of 75 x 12.7 x 3 mm were tested for each batch of samples. The average flexural properties were calculated.

6.2.7 Composite impact testing

Impact testing was carried out according to the EN ISO 179-1 Plastics-Determination of Charpy Impact strength. An advanced universal pendulum impact tester (POLYTEST) with an impact velocity of 2.9 m/s and a hammer weight of 0.475 kg at 22 °C was used. Five test specimens with dimensions of 75 x 10 x 3 mm were tested for each batch of samples.

6.2.8 Composite density and porosity measurement

The density of composites was measured based on ASTM 792-00 (Standard Test Methods for Density and Specific Gravity (Relative Density) of Plastics by Displacement). The immersion fluid used was distilled water. Densities of three specimens with dimensions of 25 x 25 mm were measured for each batch of samples and the average density was obtained. Total porosity of composites was calculated using the equation [36]:

$$V_P = \frac{(\rho_{ct} - \rho_c)}{\rho_{ct}} \qquad (6.1)$$

where:

$$\rho_{ct} = \rho_f v_f + \rho_m v_m \quad (6.2)$$

Such as ρ_{ct} – theoretical density of composites, ρ_f, ρ_m and $v_f v_m$ – densities and volume fractions of fibre and matrix, respectively.

6.2.9 Fibre length and fibre diameter measurement

Fibre length and diameter were measured manually from the scanning electron micrographs of the fibre mats using ImageJ software. A total of 500 fibres were measured from 25 micrographs. The mean fibre length, diameter and fibre length and diameter distributions were reported.

6.2.10 Interfacial shear strength (IFSS) measurement of PP/hemp fibre samples using single fibre pull-out testing

The single fibre pull-out test (SFPO) has become the most popular method for obtaining interfacial shear strength due to its ease of application [218]. In this test, the debonding initiates at the entry point of the embedded fibre and progressively extends along the fibre until the debonding of the fibre finishes. The pull-out force (maximum debonding force) is converted to an apparent IFSS according to the Kelly-Tyson equation [219]. The interfacial shear strength for the maximum debonding forces was calculated using the equation:

$$\tau = \frac{F_{max}}{\pi d l_e} \quad (6.3)$$

where F_{max} is the maximum debonding force, *d* is the diameter of the fibre and l_e is the embedded length.

The single fibre pull-out samples for the measurement of IFSS were prepared according to literature [35, 218]. For the preparation of samples, silicone rubber moulds with nominal dimensions of 12 x 10 x 3 mm were used. A through hole with a 6 mm diameter was punched at the centre from the top side of the mould. In order to insert fibre, a slot with a 2.5 mm depth was cut from the centre of the 12 mm length side of the mould to the edge of the circular hole. Different embedded lengths from 0.25 to 1 mm at 0.25 mm intervals were tested. The mould was flexed to open

the cut such that the desired embedded fibre length could be obtained by drawing the fibre through the cut. The length and average diameter of each embedded fibre was measured under an optical light microscope. The moulds with embedded fibres were then placed on top of an aluminium plate lined with a Teflon sheet (to prevent adhering of polymer onto the plate). The hole at the centre of each mould was filled with 3 mg of granulated PP/MAPP sheets. The single fibre pull-out samples were obtained by placing the ready moulds inside a preheated hot press at 170 °C for 15 minutes (no pressure was applied). The samples were then allowed to cool in air at room temperature.

The pull-out testing was carried out on an Instron-4204 tensile testing machine fitted with a 10 N load cell; the crosshead speed was 0.5 mm/min. The sample was held on the upper jaws. The free end of the fibre was glued onto a cardboard piece. This cardboard piece was held on the bottom jaws. Twenty-five samples were assessed.

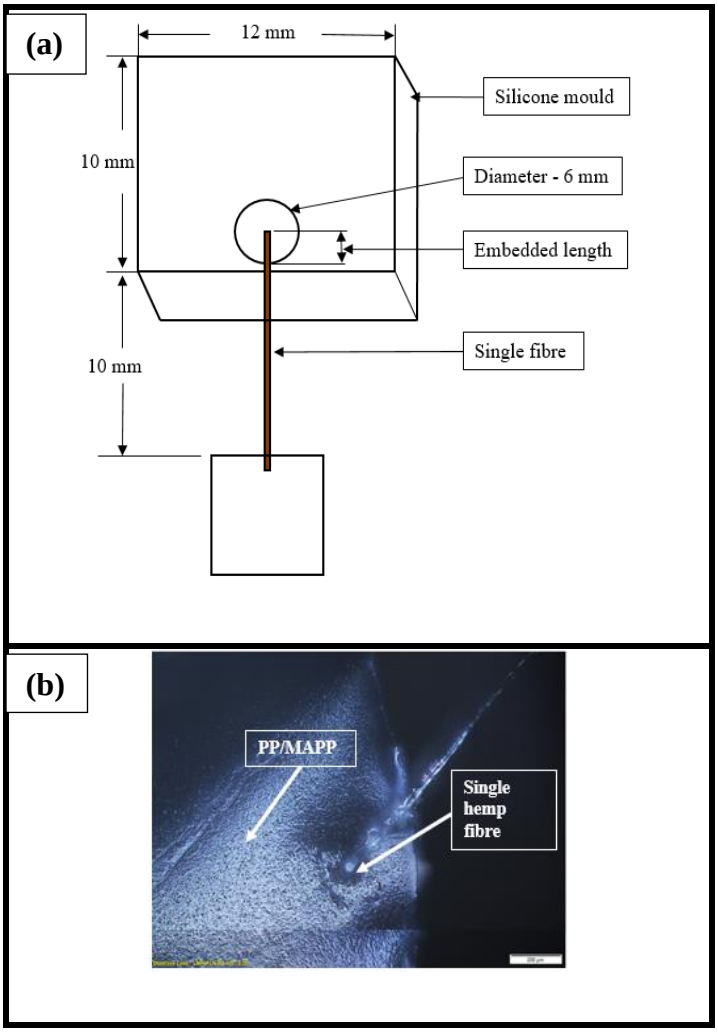

Figure 6.4: (a) Schematic diagram of test specimen for single fibre pull-out test (b) Optical image of single fibre embedded in PP/MAPP matrix (scale bar 200 µm).

6.2.10.1 Determination of critical fibre length

The critical fibre length (L_c) was determined from the average interfacial shear strength obtained from single fibre pull-out testing using the equation found generally in literature [5, 152]:

$$L_c = \frac{\sigma_f \mathrm{d}}{2\tau_i} \tag{6.4}$$

where (σ_f) average fibre strength, (d) average fibre diameter and (τ_i) the interfacial shear strength obtained.

6.3 Results and Discussion

6.3.1 Production of PP/MAPP sheets

As aforementioned, the thickness of each sheet was assessed at six different points (as shown in Figure 6.2). The extruded sheets were slightly thicker (about 23 %) in the middle than at the edges (see Figure 6.5). This could be due to the melt flow pattern of the material through the sheet die [177]. In contrast, after pressing between the aluminium plates, the sheets appeared to be slightly more uniform (about 18 % difference only between the middle and the edges), with small standard deviations observed, as indicated by the error bars.

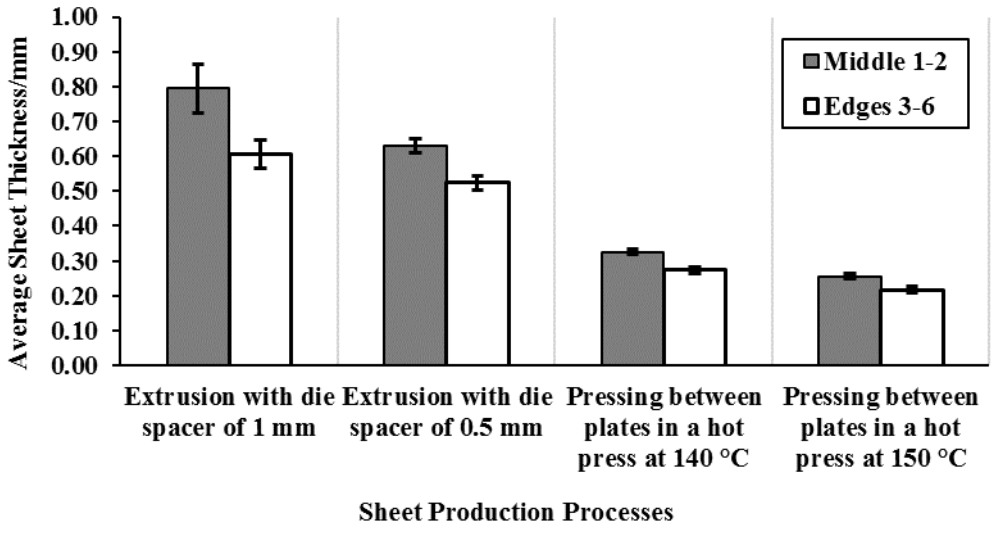

Figure 6.5: Graph displaying the average thicknesses of the sheets along the extrusion axis 1-2 (Middle 1-2) and at the edges 3-6.

Table 6.2 details the overall average thickness of the polymer sheets calculated from the six different points. As expected, after pressing in the hot press, the overall average thickness of the sheets (produced with a die-spacer of 0.50 mm) reduced, although not significantly for 130 °C (confirmed by the Student's t-test). At 160 °C, due to reduced viscosity holes over ~ 40 % were formed within the sheets produced, making these unusable in composites.

Table 6.2: The polymer sheet production processes and the overall average thickness of the polymer sheets. Standard deviations are shown in parentheses

Sheet production processes	Hot press temperature /°C	Overall average sheet thickness/mm
Extrusion using die spacer of 1.00 mm	-	0.66 (0.05)
Extrusion using die spacer of 0.50 mm	-	0.56 (0.06)
Extrusion using die spacer of 0.50 mm + Pressing between the plates in a hot press	a) 130 °C b) 140 °C c) 150 °C d) 160 °C	a) 0.49 (0.03) b) 0.29 (0.04) c) 0.24 (0.02) d) 0.13 (0.06)

6.3.2 Tensile properties of composites

In this investigation, a range of composites was produced using different sheet thicknesses. Generally, it was found that decreasing the overall thickness of fibre mats between two polymer sheets within the stacking arrangements of composites and so decreasing the distance the polymer needs to travel improved the fibre wetting through the composite and therefore improved the tensile strength and Young's modulus of the composites (see Figure 6.6). However, the composites made with polymer sheets of 0.24 mm had the lowest tensile strength and Young's modulus. Although these composites had the least distance the polymer needs to travel (equal with the distance the polymer needs to travel in composites made with polymer sheets of 0.29 mm), the polymer content at the edges was found to be lower compared to other composites, as indicated by the lowest ratio of thicknesses of polymer sheets to the fibre mats at the edges (see Table 6.3) and hence resulted in a weaker composite. It appears from the photographs of these composite surfaces (Figure 6.7a compared to Figure 6.7b) that the polymer content at the edges was

insufficient to bring about reasonable fibre wetting. The SEM micrographs of the tensile fracture surfaces of these composites (Figure 6.8) also indicated poor fibre wetting; there appeared to have large protruding fibres with no evidence of matrix material adhering to their surfaces, unlike other composites in which very few fibres can be observed as the fibres are mostly covered by the matrix material suggesting reasonable fibre wetting. For composites containing approximately same fibre content (30 wt%), the use of different sheet thicknesses did not result in significant differences in composite tensile strength and Young's modulus, except for composites made with polymer sheets of 0.24 mm.

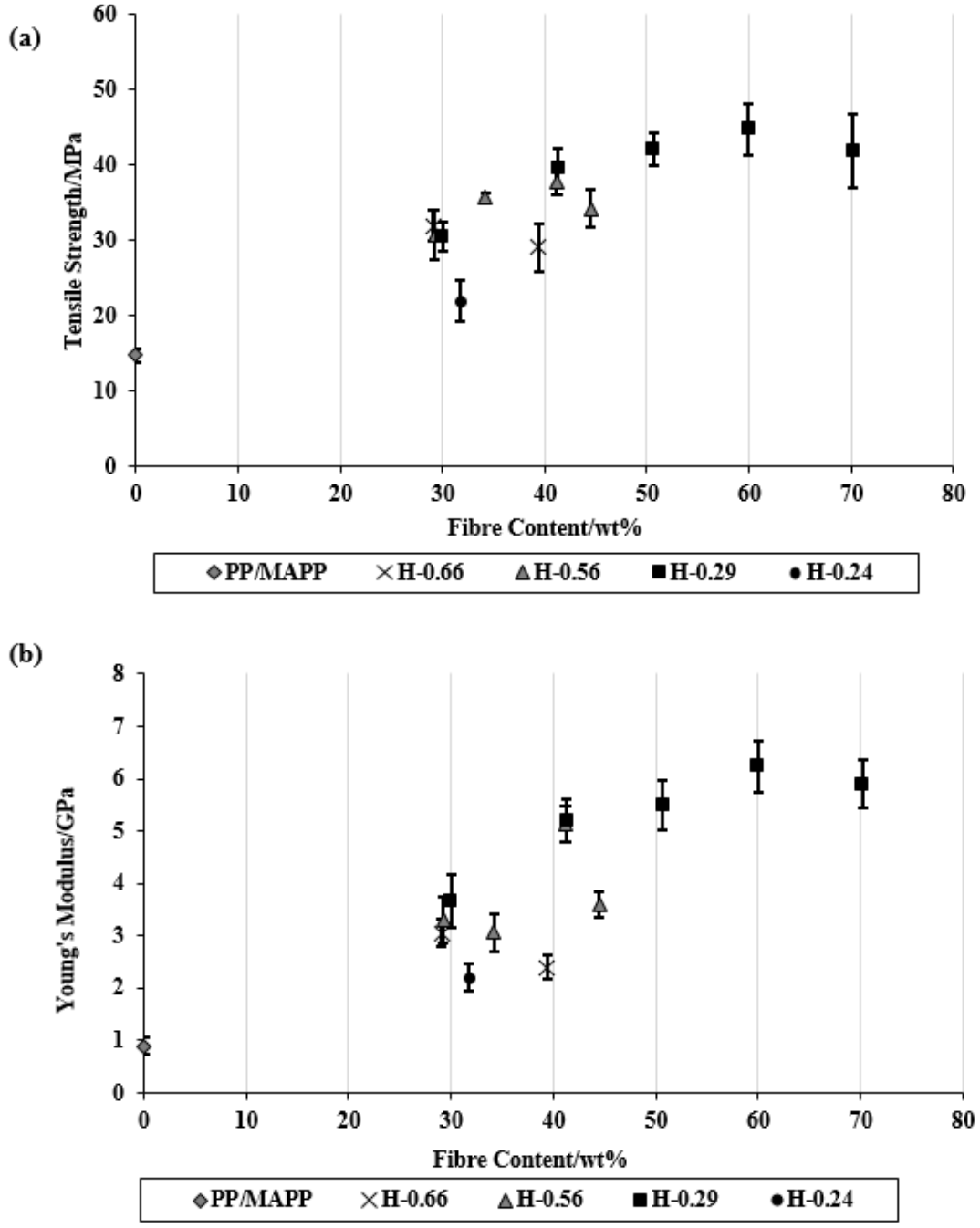

Figure 6.6: Tensile strength and Young's modulus of composites as a function of fibre content.

Table 6.3: Ratio of thicknesses of polymer sheets to fibre mats in composites

Samples*	Average thickness of a fibre mat/mm	Total thickness of fibre mats in composites/mm	Total polymer sheet thicknesses at edges in composites/mm	Total polymer sheet thicknesses at middle in composites	Ratio of thicknesses of polymer sheets to fibre mats at edges in composites	Ratio of thicknesses of polymer sheets to fibre mats at middle in composites
H30 - 0.66	0.80	4.8	1.83	2.40	0.381	0.500
H30 - 0.56		4.8	1.56	1.89	0.325	0.394
H30 - 0.29		4.8	1.08	1.32	0.225	0.275
H30 - 0.24		4.8	0.84	1.08	0.175	0.225
H35 - 0.56		6.4	2.60	3.15	0.406	0.492
H40 - 0.66		6.4	1.83	2.40	0.286	0.375
H40 - 0.56		8.0	2.60	3.15	0.325	0.394
H40 - 0.29		8.0	1.62	1.98	0.203	0.248
H45 - 0.56		9.6	2.60	3.15	0.271	0.328
H50 - 0.29		11.2	2.16	2.64	0.193	0.236
H60 - 0.29		14.4	2.70	3.30	0.188	0.229
H70 - 0.29		17.6	3.24	3.96	0.184	0.225

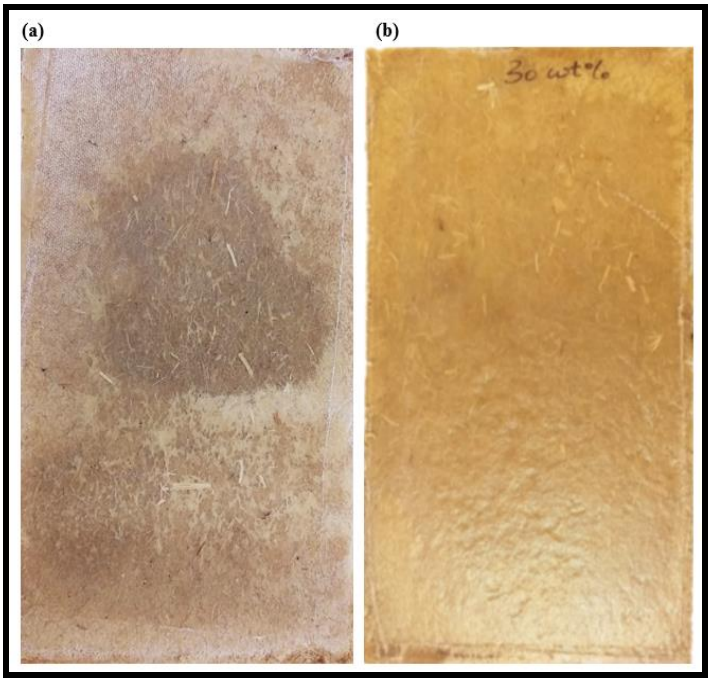

Figure 6.7: Example photographs of the composite surfaces made with polymer sheets of: (a) 0.24 and (b) 0.29 mm.

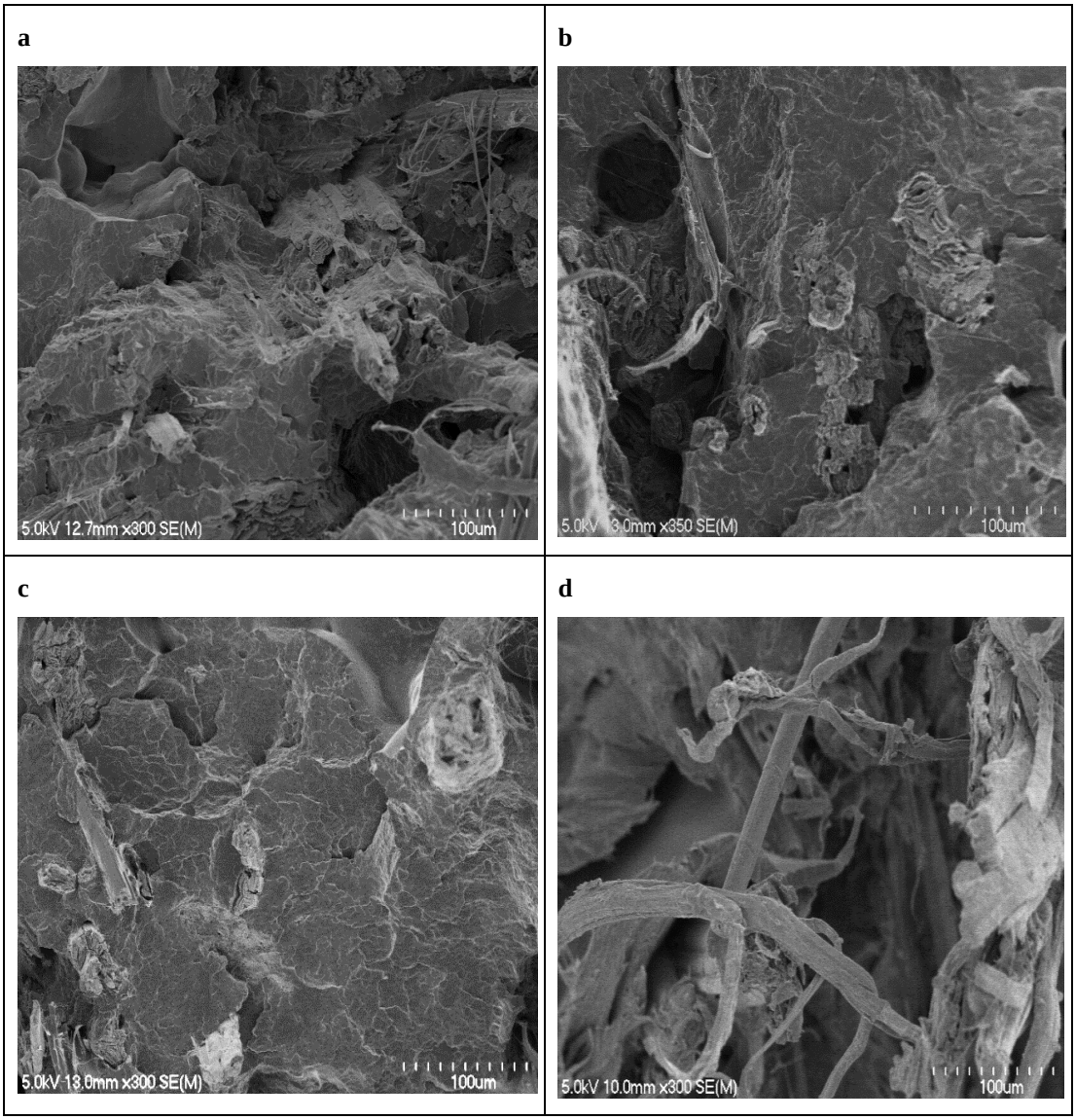

Figure 6.8: Sample scanning electron micrographs of tensile fracture surfaces of composites containing approximately 30 wt% fibre content made with polymer sheets of: (a) 0.66, (b) 0.56, (c) 0.29 and (d) 0.24 mm.

Composites made with polymer sheets of 0.66 mm showed significant decreases in the tensile properties (see Figure 6.6) when the fibre content was increased from 30 to 40 wt%, unlike other composites made with polymer sheets of 0.56 or 0.29 mm which showed significant increases. The use of thinner polymer sheets (0.66 compared to 0.56 or 0.29 mm) made possible decreases in the overall thickness of fibre mats between two polymer sheets within the stacking arrangements of the composites (see Table 6.3). This reduced the distance the polymer needs to travel and improved the fibre wetting. The tensile fracture surfaces of composites made with polymer sheets of 0.66 mm appeared to have large holes (Figure 6.9a) from where the fibres are likely to be pulled out indicating poor fibre wetting, unlike other composites in which fibres are concealed by the matrix (Figure 6.9b and 6.9c). The

composites made with polymer sheets of 0.56 or 0.29 mm did not show significant differences between their tensile properties thought to be due to the similar levels of fibre wetting within these composites (Figure 6.9b compared to 6.9c). However, composites made with polymer sheets of 0.56 mm showed significant decreases in tensile strength and Young's modulus at the fibre content of 45 wt% due to poor fibre wetting (see Figure 6.10a) as a result of large distance the polymer needs to travel (see Table 6.1).

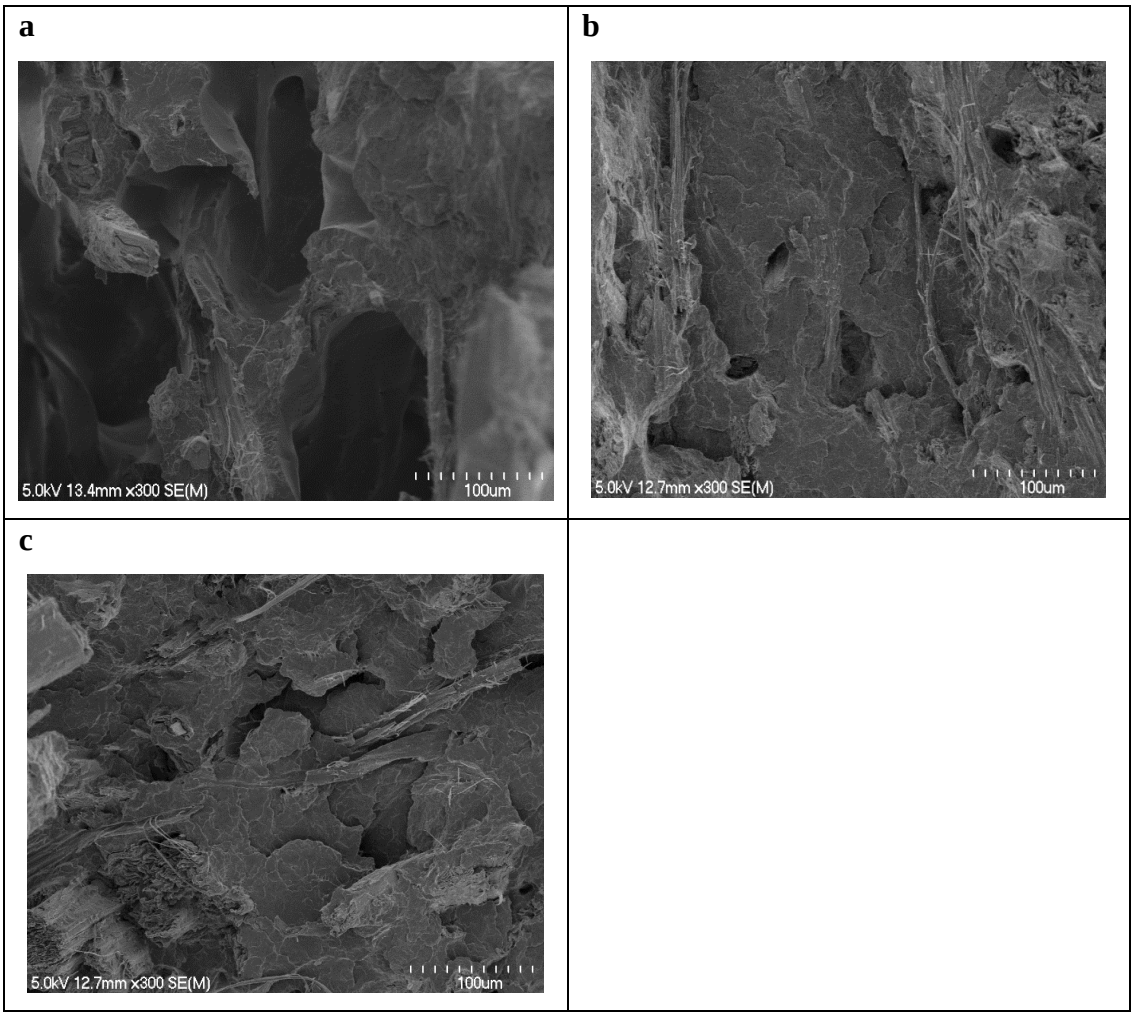

Figure 6.9: Scanning electron micrographs of tensile fracture surfaces of composites containing approximately 40 wt% fibre content made with polymer sheets of: (a) 0.66, (b) 0.56 and (c) 0.29 mm.

Composites made with polymer sheets of 0.29 mm showed progressive increases in tensile strength and Young's modulus with increasing fibre content up to 60 wt%, and thereafter significant decreases. This is thought to be due to the reasonable fibre wetting (Figure 6.10b and 6.10c) throughout these composites as a result of the least distance the polymer needs to travel. However, it should be noted that the composites with fibre contents above 40 wt% were not fully free of defects; a few gaps between

the fibres and the matrix and some voids were visible in the fracture surfaces of these composites. The formation of voids at high fibre content in composites could be due to the evaporation of a greater amount of moisture from the fibres. Similar observations for composites with fibre contents above 40 wt% have been reported elsewhere [5]. Reduction in tensile properties at about fibre content of 70 wt% is thought to be due to insufficient polymer (see Table 6.3) for adequate wetting (Figure 6.10d). The strongest and stiffest composite contained 60 wt% fibre content and had average tensile strength and Young's modulus of 44.8 MPa and 6.2 GPa, respectively, which were 2.9 and 6.5 times higher than those of the control.

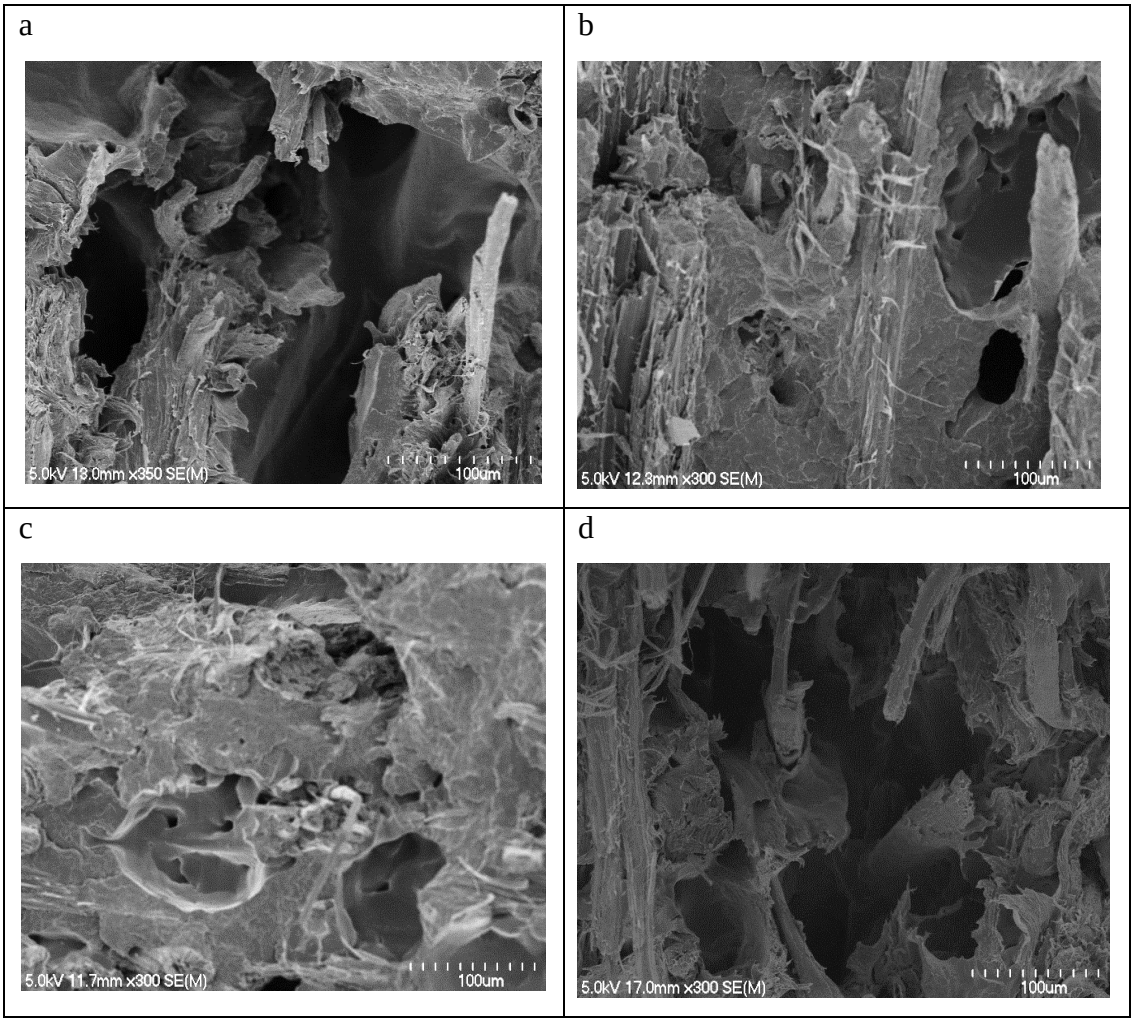

Figure 6.10: Scanning electron micrographs of tensile fracture surfaces of composites containing fibre content of: (a) 45 wt% made with polymer sheets of 0.56 mm, (b), (c) and (d) 50, 60 and 70 wt% made with polymer sheets of sheet thickness of 0.29 mm, respectively.

6.3.3 Flexural properties of composites

Figure 6.11 shows the tensile side view of the fractured flexural samples. As can be seen, the cracks appeared on the tension surfaces of the samples. It was observed during testing that crack propagated to the middle through the sample thickness with no buckling or delamination in composites.

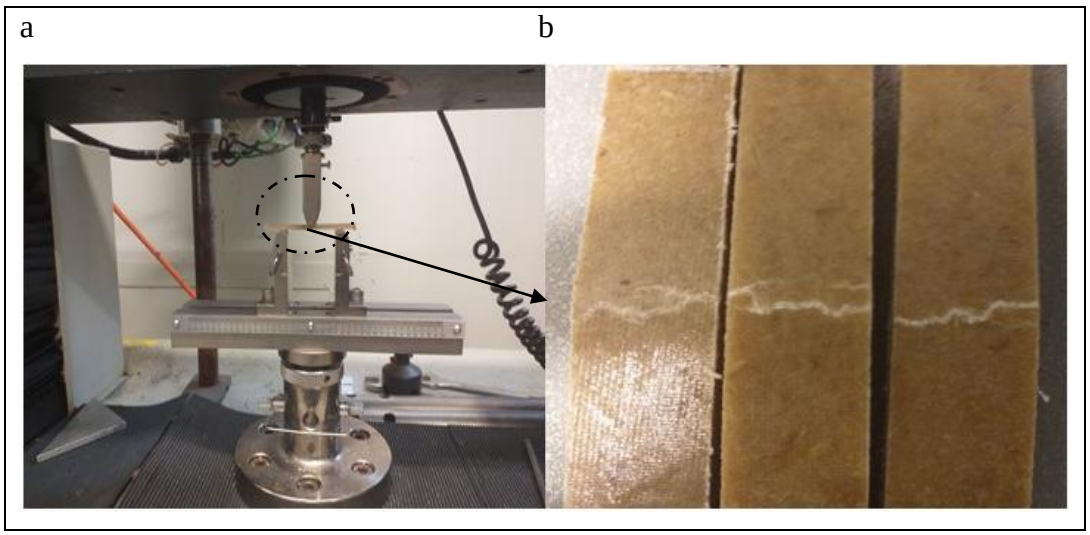

Figure 6.11: (a), (b) Sample picture of flexural testing samples showing the cracks formed from the tensile sides.

The average flexural strength and flexural modulus of the composites with different fibre contents are presented in Figure 6.12. The effect of polymer sheet thicknesses and stacking arrangements on flexural properties appeared to be almost similar to that observed for the tensile properties. It has been previously reported that the fracture micro-mechanics that occurs in the composites under flexural testing is similar to tensile testing [7]. The maximum flexural strength and flexural modulus occurred for composites at the fibre content of about 60 wt% were 97.6 MPa and 3.6 GPa, respectively. At this fibre content, flexural strength and flexural modulus were about 244 % and 256 %, respectively higher than those of the control.

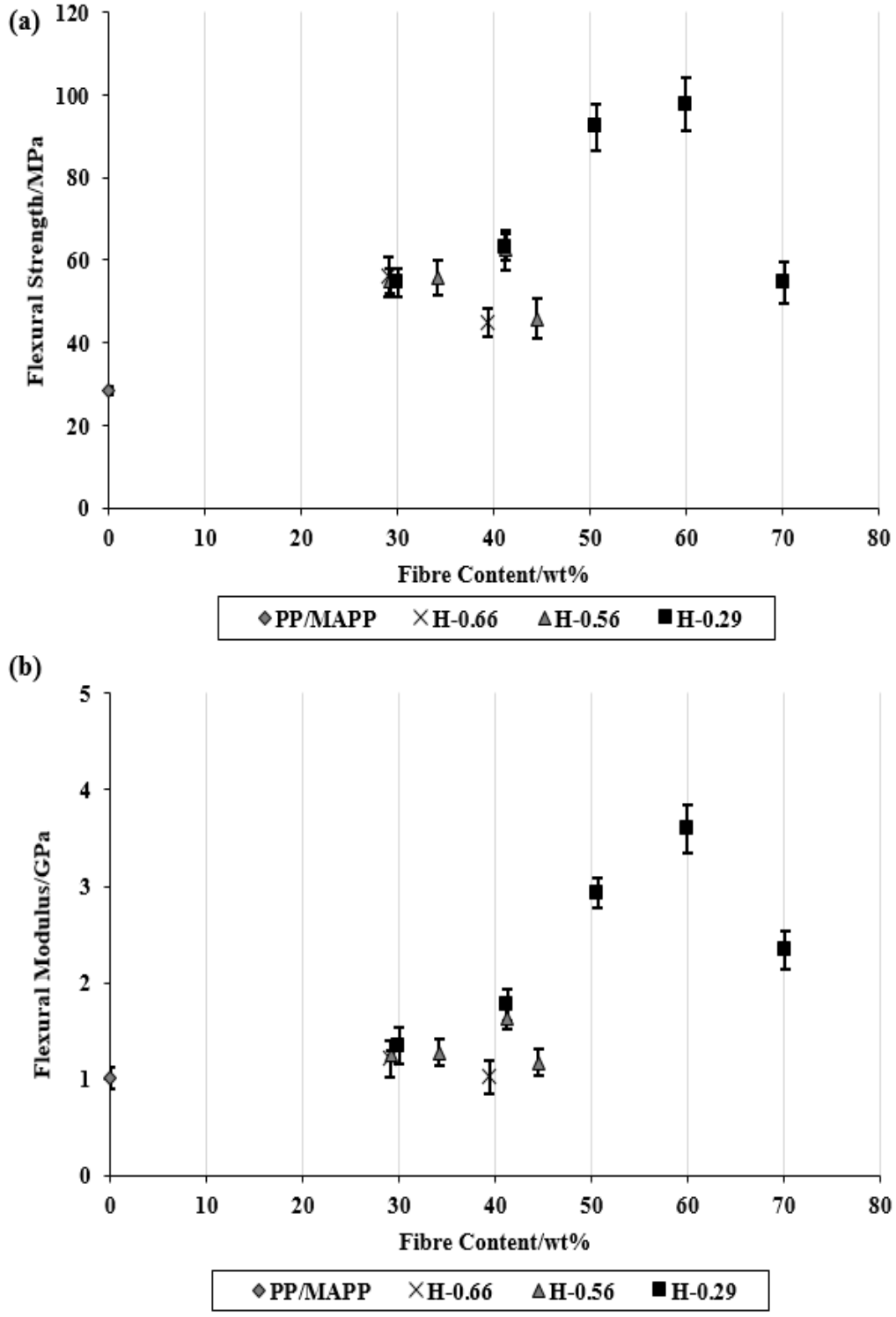

Figure 6.12: (a) Flexural strength and (b) Flexural modulus of composites as a function of fibre content.

6.3.4 Impact strength of composites

The average impact strengths of unnotched control and composite samples are shown in Figure 6.13. It should be noted that the control samples were not broken during the

testing. The impact strength of the control samples decreased drastically with the inclusion of fibres. The reduction in impact strength of thermoplastics such as PP with the inclusion of natural fibres is commonly observed in the literature [2, 4]. However, for the composites, the effect of polymer sheet thicknesses and stacking arrangements on impact strength appeared similar to that observed for the tensile and flexural properties. It has been previously reported that the interfacial bonding between the fibre and matrix plays a vital role in determining the mechanical properties of composites [4].

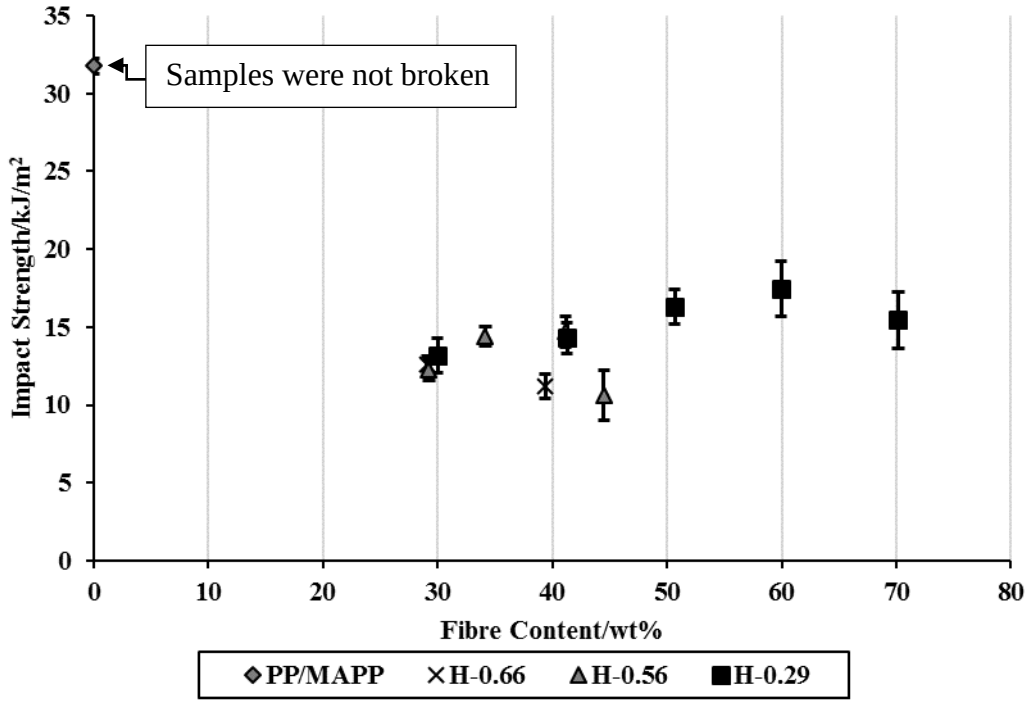

Figure 6.13: The average impact strength of composites as a function of fibre content.

6.3.5 Density and porosity of composites

Both density and porosity of the composites were found to increase with increasing volume fraction of fibres (Figure 6.14). This is due to the fact that the density of fibre being higher than that of the matrix [220]. Typically, significant porosity has been shown by natural fibre composites and has been shown to increase with increasing fibre content [34] [36]. Porosity arises mainly due to the limited interaction between the fibre and the matrix and inclusion of air during processing [4].

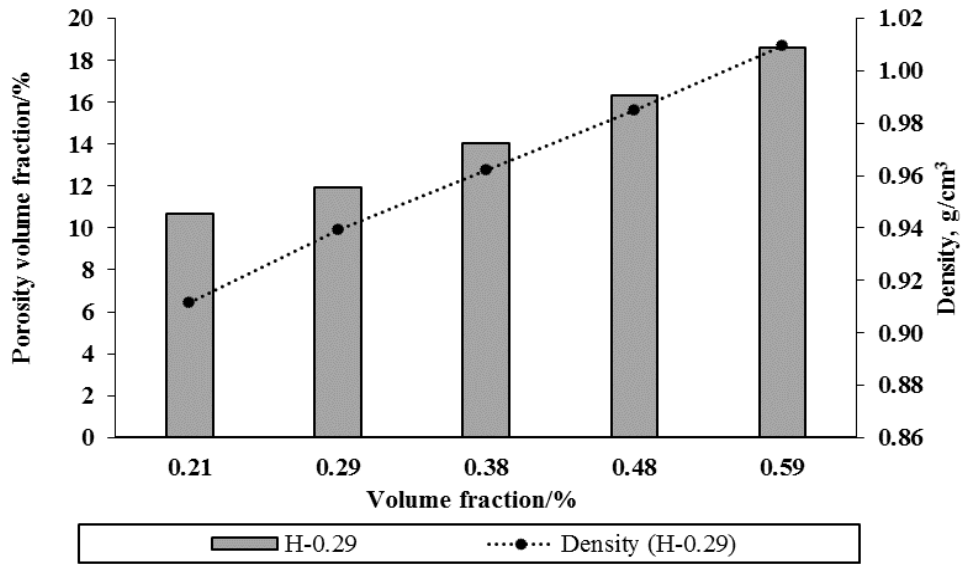

Figure 6.14: Density and porosity of composites as a function of the volume fraction of fibres.

6.3.6 Fibre length and diameter distributions

Both fibre length and fibre dimeter play an important role in determining the strength of the composites. Figure 6.15 and Figure 6.16 represent the fibre length and fibre diameter distribution within the fibre mats. The fibres had an average length and an average diameter of 1.880 mm and 0.051 mm, respectively.

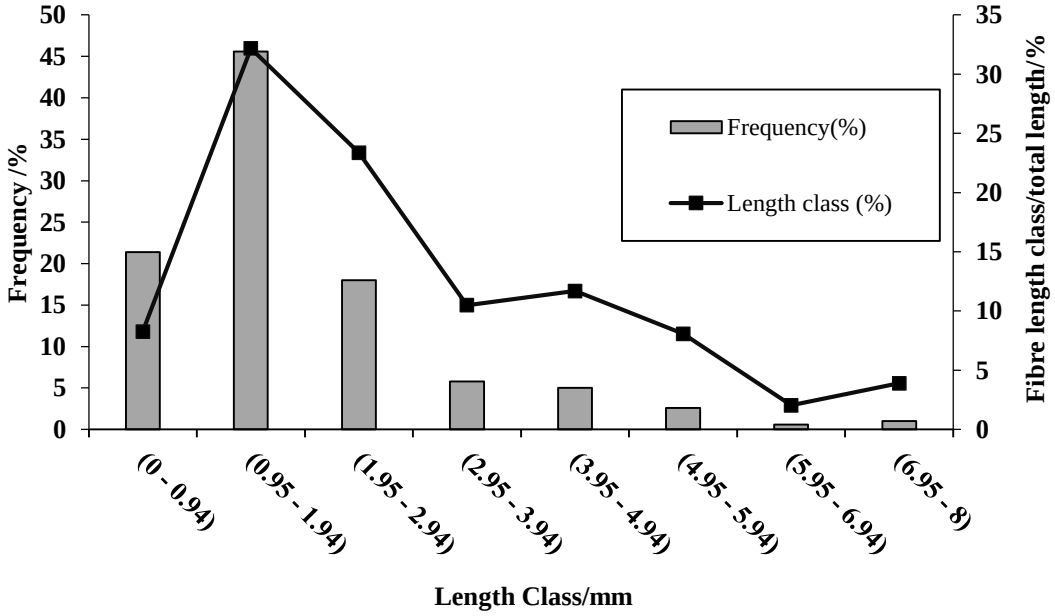

Figure 6.15: Hemp fibre length distribution.

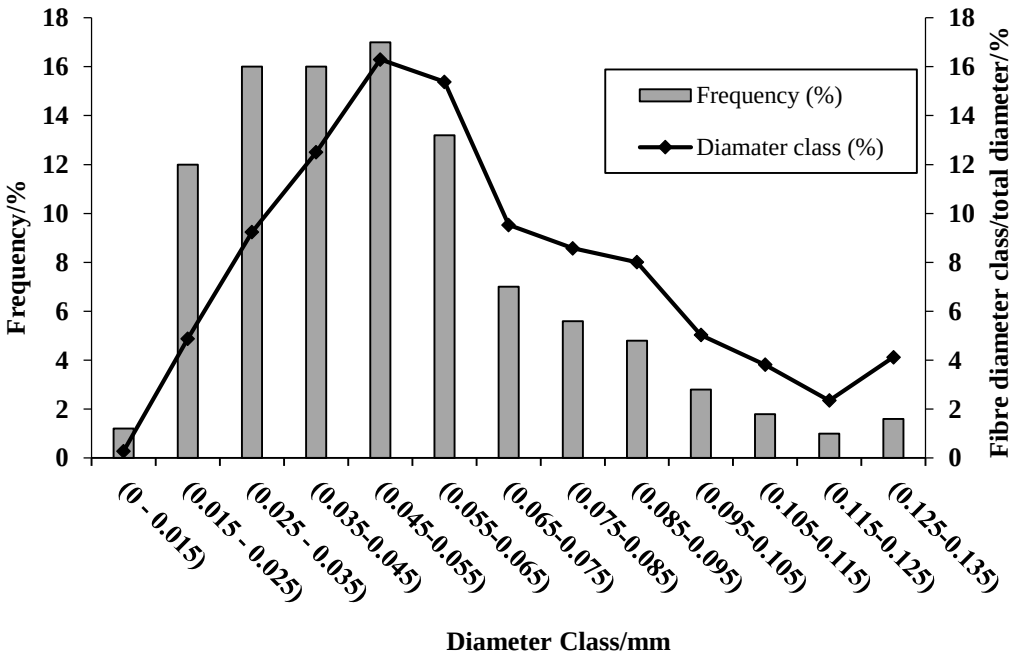

Figure 6.16: Hemp fibre diameter distribution.

6.3.7 Determination of interfacial shear strength and critical fibre length of PP/hemp samples

The average interfacial shear strength (IFSS) value obtained for the PP/hemp samples was 8.7 MPa, indicating a relatively reasonable level of interfacial bonding when compared to the IFSS values of other natural plant fibre thermoplastic composites reported in the literature [4, 54]. For instance, the IFSS value for PP/dew-retted flax samples with MAPP was found to be 11.4 MPa using pull-out testing [221]. An IFSS value of 7.5 MPa was found for PP/flax-duralin samples using micro-bond testing [17]. A higher IFSS value of 15.4 MPa was found for PP/hemp composite samples with alkali treated fibres obtained using single fibre fragmentation testing (SFFT) [4]. In another work, an IFSS value of 12 MPa was found for PP/flax composite samples obtained using the fragmentation test [222]. The higher IFSS values obtained with the fragmentation testing is not surprising as there has been no application of pressure (hot press) in single fibre pull-out testing (SFPO) compared to the fragmentation testing. It has been previously reported that the IFSS values obtained not taking into account the application of pressure could be an underestimation to some degree for the compression moulded composites [35, 54]. This is due to the fact that the use of pressure could help homogeneous matrix adhesion with the fibre surfaces.

The critical fibre length (L_c) determined using the average IFSS obtained by means of single fibre pull-out testing was found to be L_c = 0.85 mm. An almost close value of Lc = 0.83 for a composite containing alkali treated hemp fibre with a matrix of polypropylene has been reported in the literature [54]. Figure 6.17a shows the scanning electron micrographs of hemp fibre surfaces before the SFPO testing. As can be seen, the fibre surfaces appeared to be rough due to the HT alkali treatment, as evidenced by the striations on the surfaces [2]. Figure 6.17b and 6.17c show the fibre surfaces after the SFPO testing. As expected, the fibre surfaces appeared to have reasonable fibre wetting by the PP/MAPP matrix as strong covalent bonds can be formed between the OH groups present on the fibre surfaces and the MA functional group of MAPP [5].

Using the Von Mises yield criterion, the shear stress (τ_m) required to bring about matrix tearing was estimated using the following equation [223, 224]:

$$\tau_m = \frac{\sigma_m}{\sqrt{3}} \qquad (6.3)$$

where, σ_m is the tensile strength of the matrix (PP/MAPP). The average tensile strength of the matrix was found to be 14.8 MPa. Thus, the estimated τ_m based on the above equation was 8.5 MPa. It can be seen that the average IFSS obtained is slightly higher than the estimated τ_m, suggesting that the composites are most likely to fail by matrix tearing, assuming that all the fibres are longer than the critical fibre length. However, in fact, there are a significant proportion of fibres in actual composites which are below the Lc (see Figure 6.15). Therefore, during tensile testing, fibre pulling-out will also occur. Furthermore, the estimated IFSS value is based on the average fibre strength obtained from the single fibre tensile testing. In actual composites, there are a significant proportion of fibres which could have failed at much lower stresses than the average fibre strength.

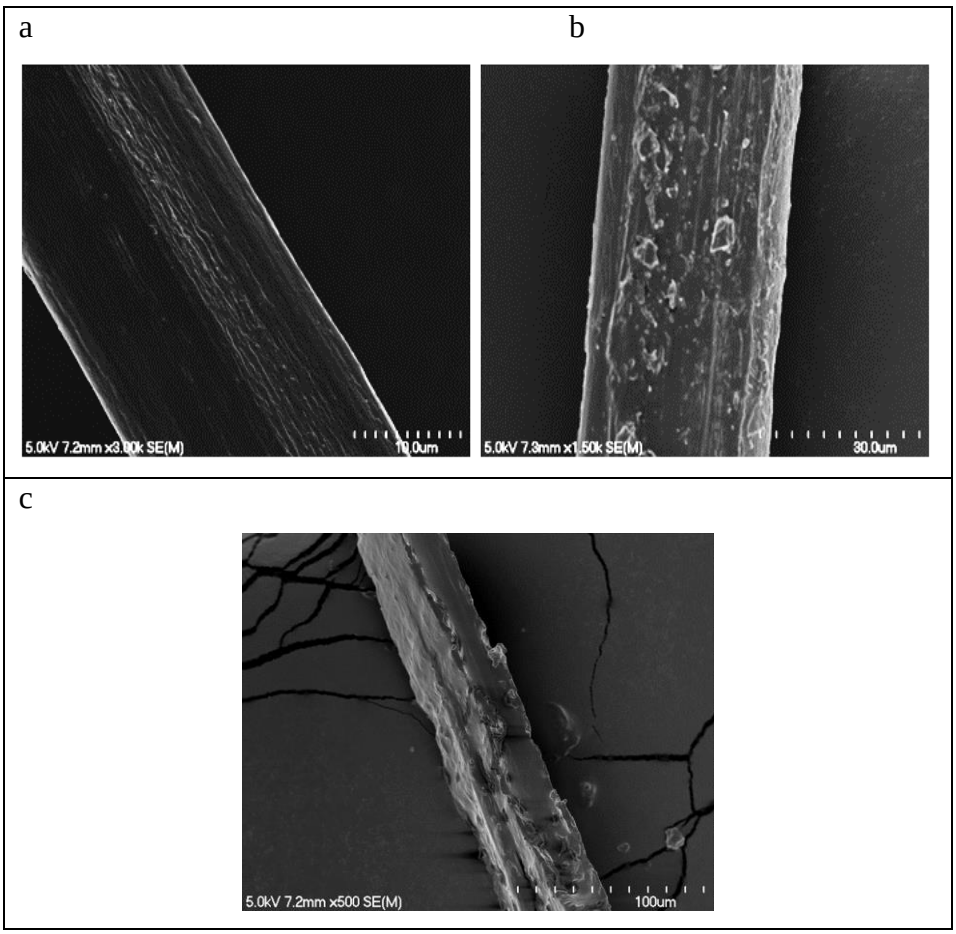

Figure 6.17: Scanning electron micrographs of single hemp fibre surfaces: (a) before single fibre pull-out testing (b), (c) after the pull-out testing.

6.4 Chapter Conclusions

Different polymer sheet thicknesses and stacking arrangements were investigated to improve the mechanical performance of the polypropylene matrix composites through achieving high fibre content. It was found that decreasing the overall thickness of fibre mats between two polymer sheets within the stacking arrangements of composites and so decreasing the distance the polymer needs to travel improved the fibre wetting through the composite and therefore improved the tensile properties of the composite. The maximum mechanical properties (tensile properties, flexural properties and impact strength) of the composites were found at a fibre content of 60 wt%. The tensile strength and Young's modulus of the composites were found to be 44.8 MPa and 6.2 GPa, respectively; the flexural strength and flexural modulus of the composites were found to be 97.6 MPa and 3.6 GPa, respectively and the impact strength of the composites was found to be 18 kJ/m^2.

7 Chapter Seven

Conclusions

7.1 Effects of alkali treatment

Two different alkali treatments (high temperature and ambient temperature) were carried out in order to produce fibre mats from high strength hemp fibres using dynamic sheet forming (DSF). Although the chemical composition of fibres was not directly assessed, from single fibre testing, it was found that the high temperature treatment increased the fibre tensile strength compared to that of untreated fibre, whereas the ambient temperature treatment reduced the fibre tensile strength.

The increase in tensile strength of the high temperature treated fibre can only be explained by the removal of weak components (as supported by FTIR, TGA, SEM and change of diameter) and thus the remaining material is stronger. Furthermore, the removal of weak components from the fibre cell walls could be leading to close packing and alignment of cellulose chains. This was supported by the higher crystallinity index for the fibre after the high temperature alkali treatment compared to untreated fibre. The close compaction could have enhanced the adhesion between cellulose microfibrils, thereby providing better fibre tensile strength towards the loading direction compared to untreated fibres. The ambient temperature treatment also removed some of the weak components (as supported by FTIR, TGA, SEM and change of diameter) and increased the crystallinity index of the fibre, however, resulted in a significant reduction in fibre strength, suggesting that cellulose degradation had occurred during the ambient temperature treatment. This was further supported by the lower crystallinity index for the two-hour ambient temperature treated fibre compared to that of untreated fibre; the lower crystallinity index was most likely due to the increase of amorphous cellulose content as a result of cellulose degradation. Earlier studies have reported that chemical reagents first react with the chain ends at the surface of the crystallites, as they cannot diffuse into the crystalline region, thus limiting crystalline damage to open some of the hydrogen-bonded

cellulose chains. The chemical reagent then diffuses into the crystalline region, reacting with the cellulose and simultaneously generating more amorphous cellulose (cellulose degradation) [225, 226].

Granulation after the high temperature treatment further improved the fibre separation and only this well-separated fibre could be successfully formed as a mat using dynamic sheet forming.

Overall, the high temperature treatment seems best for the production of strong and stiff fibres because the low temperature treatment is most likely to bring about degradation of the crystalline cellulose chains in the microfibrils or bonding between cellulose microfibrils before sufficient removal of weak components from the fibres.

7.2 Effects of nozzle geometry on fibre orientation and assessment of fibre orientation

With the goal of improving the alignment of fibres within the mats produced using DSF, the effect of nozzle geometry (contraction ratio and exit shape) on fibre orientation was investigated. The orientation of fibres within fibre mats were assessed using ImageJ and X-ray diffraction (XRD). Image analysis using ImageJ and XRD analyses supported that reasonable alignment of hemp fibre produced using DSF had occurred. It was found that the contraction ratio is the main nozzle geometry factor influencing orientation compared to the exit shape of a nozzle. Also, the alignment of fibres within the mats was found to increase with the increase in contraction ratio of nozzles, although the improvement was only statistically significant for extreme cases (lowest versus highest contraction ratios of the nozzles which successfully produced sheets). Improved fibre orientation obtained for dynamic sheet forming was indicated by higher values of coherency factor (0.31 compared to 0.23) and Herman's order parameter (0.511 compared to 0.464) for the fibre mats produced using the modified (highest contraction nozzle) compared to those mats produced by the manufacturers nozzle (lowest contraction nozzle).Polypropylene matrix composites reinforced using selected mats (highest and lowest orientated mats) with different fibre contents were tested parallel and perpendicular to the fibre loading direction. It was found that the tensile strengths of the composites made with the fibre mats produced using a nozzle of higher contraction ratio tested parallel to the main fibre alignments direction were higher than those composites made with the fibre mats produced using the current nozzle in

DSF (lowest contraction ratio nozzle). At a fibre content of about 30 wt%, the average tensile strength of the composites made with the highest orientated fibre mats was found to increase by about 11 %.

7.3 Effect of surface treatments on fibre mats produced using DSF

The effect of surface treatments (stearic acid vapour and cellulose nanocrystals) on fibre mats and the potential of these mats as reinforcements in polypropylene matrix composites were evaluated. The stearic acid vapour treatment reduced the hydrophilicity and slightly improved the thermal stability of fibre mats. The CNC treatment was found to bind the loose fibres together within the mats effectively and improved the integrity of fibre mats during handling. Untreated fibre mats were too weak for handling and also below the accuracy limits of the equipment to provide reliable tensile testing data. In contrast, the 2 wt% CNC treatment (CNCs in water) by spraying had improved their tensile strength.

The composites with MAPP exhibited the highest tensile strength. In the absence of MAPP, the composites with fibre mats treated with SA appeared significantly stronger than the composites with alkali treated fibre mats only. This indicates that SA could act as a coupling agent to improve the strengths of the composites, but not as effective as maleic anhydride polypropylene. Although the composites made with a combination of SA and MAPP did not exhibit any additive benefits for tensile strengths, however, the lower standard deviations observed for the composite tensile strengths with the combination of stearic acid and MAPP treatments, as indicated by the error bars, suggest more homogeneous fibre-matrix interactions throughout the composites compared to the other composites. After coupling with MAPP, the tensile strength (increase by about 15 %) and Young's modulus (increase by about 16 %) of composites (15 wt% fibre content) increased with the incorporation of CNC treated fibre mats (treated with 2 wt% CNC in water). However, with increasing fibre and CNC contents, the composites with CNC treated fibre mats showed declines in tensile strength and Young's modulus or no reliable data was acquired for these tensile properties. This is thought to be due to the very poor consolidation of composites in the presence of CNC; the CNC films formed between the fibres hinder the flow of polymers resulting in poor wetting of fibres by the matrix materials thereby decrease in these tensile properties of the composites.

7.4 Effect of sheet thicknesses and stacking arrangements on the mechanical properties of polypropylene matrix composites.

The mechanical performance of composites was improved through increasing fibre content from 30 to 60 wt%. It was found that decreasing the overall thickness of fibre mats between two polymer sheets within the stacking arrangements of composites and so decreasing the distance the polymer needs to travel improved the fibre wetting through the composite and therefore improved the tensile properties of the composite. In this work, a repeating stacking pattern (repetition depends on the fibre contents) with a minimum of only two fibre mats between two polymer sheets (thickness of 0.29 mm) was found to provide the highest mechanical performance for the composites (tensile properties, flexural properties and impact strength). The maximum mechanical properties (tensile properties, flexural properties and impact strength) of the composites were found at fibre content of about 60 wt%. The tensile strength and Young's modulus of the strongest composites were found to be 45 MPa and 6.2 GPa, which is about 3.0 and 6.9 times higher, respectively than that of the control sample (PP/MAPP). At this fibre content, the flexural strength and modulus were found to be 98 MPa and 3.6 GPa, which is about 3.4 and 3.6 times higher, respectively than that of PP/MAPP. The impact strength of the composites at this fibre content was found to be 18 kJ/m^2.

Based on the outcomes, it is believed that the objectives of the research set at the beginning of this thesis have been met upon the completion of this study. It can be conclusively said that the fibres mats produced using DSF can effectively increase the potential of hemp fibres to be used in future applications as a result of improved composite mechanical properties due to improved reinforcement efficiency. Depending on the application, where higher composite tensile properties and dimensional stability are required, the combination of MAPP and stearic acid treatments can be considered.

8 Chapter Eight

Recommendations and Future Works

The research outcomes have set an important platform to improve further the mechanical performance of polypropylene matrix composites reinforced with aligned short hemp fibre mats. Some recommendations for future work have been proposed.

- In this work, hemp fibres were treated to a maximum of only 120 °C with fibre to solution ratio of 1:8. The treatment increased the strength of the fibres, suggesting better packing of cellulose chains occur for high temperature treatment. Also, the treatment resulted in well-separated fibres for the production of fibre mats using dynamic sheet forming. However, further investigations could be carried out to improve the fibre strength and fibre separation further. Effect of higher temperatures and different fibre to solutions ratios on the tensile strength and Young's modulus of the fibres could be further investigated.

- Hemp fibre mats in this work were produced using dynamic sheet forming with constant variables, except nozzle geometry. The influence of other variables such as rotation of the drum, the force of pump and thickness of fibre mats on fibre orientation and composite mechanical properties, could be further investigated. Moreover, as aforementioned, fibre separation should be improved using chemical or mechanical separation methods to make use of nozzles with very high contraction ratios to further improve the orientation of fibres within the mats produced.

- Extending image analysis to three dimensional. Three dimensional imaging of the fibre mats using confocal laser scanning microscopy or X-ray computed tomography (CT) followed by image analysis may be carried out.

- Composites with CNC treated fibre mats were not successfully produced with high fibre contents. Thermosets, such as epoxy, may be trailled for the production of composites as they generally provide better wetting of fibres

compared to thermoplastic such as polypropylene matrix. The alignment of CNCs after spraying could be investigated.

- The mechanical properties of composites using a combination of alkali treatment, coupling agent and surface treatments (SA and CNC treatment) could be investigated. The use of X-ray photoelectron spectroscopy (XPS) and Secondary ion mass spectrometer (SIMS) for surface characterisation after treatments could be carried out to further investigate the effects of treatments

References

1. Parker, G., *Encyclopedia of materials: science and technology.* 2001.
2. Pickering, K., *Properties and performance of natural-fibre composites*. 2008: Elsevier.
3. Gupta, N. and M. Paramsothy, *Metal-and polymer-matrix composites: functional lightweight materials for high-performance structures.* JOM, 2014. **66**(6): p. 862-865.
4. Pickering, K., M.A. Efendy, and T. Le, *A review of recent developments in natural fibre composites and their mechanical performance.* Composites Part A: Applied Science and Manufacturing, 2015.
5. Beckermann, G., *Performance of hemp-fibre reinforced polypropylene composite materials.* 2007.
6. Low, I.-M., *Advances in ceramic matrix composites*. 2018: Woodhead Publishing.
7. Chi, L., S. Lu, and Y. Yao, *Damping additives used in cement-matrix composites: A review.* Composites Part B: Engineering, 2019. **164**: p. 26-36.
8. Matthews, F.L. and R.D. Rawlings, *Composite materials: engineering and science*. 1999: Elsevier.
9. Tanzi, M.C., S. Farè, and G. Candiani, *Foundations of Biomaterials Engineering*. 2019: Academic Press.
10. Smith, P. and J. Yeomans, *Benefits of fiber and particulate reinforcement.* Materials Science and Engineering, 2009. **2**: p. 133-154.
11. Sanjay, M., et al., *Characterization and properties of natural fiber polymer composites: A comprehensive review.* Journal of Cleaner Production, 2018. **172**: p. 566-581.
12. Yan, L., N. Chouw, and K. Jayaraman, *Flax fibre and its composites–A review.* Composites Part B: Engineering, 2014. **56**: p. 296-317.
13. Yu, H., K. Potter, and M. Wisnom. *Aligned short fibre composites with high performance*. in *19th International Conference on Composites Materials. Montreal, Canada: CACSMA.* 2013.
14. Callister, W.D. and D.G. Rethwisch, *Materials science and engineering: an introduction*. Vol. 7. 2007: John wiley & sons New York.
15. Bourmaud, A., et al., *Main criteria of sustainable natural fibre for efficient unidirectional biocomposites.* Composites Part A: Applied Science and Manufacturing, 2019. **124**: p. 105504.
16. Ghazali, M. and A. Efendy, *Bio-composites materials from engineered natural fibres for structural applications*. 2016, University of Waikato.

17. Bos, H.L., *The potential of flax fibres as reinforcement for composite materials*. 2004: Technische Universiteit Eindhoven Eindhoven.
18. Dittenber, D.B. and H.V. GangaRao, *Critical review of recent publications on use of natural composites in infrastructure.* Composites Part A: Applied Science and Manufacturing, 2012. **43**(8): p. 1419-1429.
19. Pervaiz, M. and M.M. Sain, *Carbon storage potential in natural fiber composites.* Resources, conservation and Recycling, 2003. **39**(4): p. 325-340.
20. Peças, P., et al., *Natural fibre composites and their applications: a review*. Journal of Composites Science, 2018. **2**(4): p. 66.
21. Wambua, P., J. Ivens, and I. Verpoest, *Natural fibres: can they replace glass in fibre reinforced plastics?* Composites science and technology, 2003. **63**(9): p. 1259-1264.
22. Brief, L., *Opportunities in natural fiber composites.* Lucintel LLC, Irving (TX), 2011.
23. Carus, M., et al., *Wood-Plastic Composites (WPC) and Natural Fibre Composites (NFC).* Nova-Institute: Hürth, Germany, 2015: p. 16.
24. Ku, H., et al., *A review on the tensile properties of natural fiber reinforced polymer composites.* Composites Part B: Engineering, 2011. **42**(4): p. 856-873.
25. Norman, D.A. and R.E. Robertson, *The effect of fiber orientation on the toughening of short fiber‐reinforced polymers.* Journal of applied polymer science, 2003. **90**(10): p. 2740-2751.
26. Sunny, T., K.L. Pickering, and S.H. Lim. *Alignment of Short Fibres: An Overview*. in *Processing and Fabrication of Advanced Materials-XXV*. 2017.
27. Pickering, K. and M.A. Efendy, *Preparation and mechanical properties of novel bio-composite made of dynamically sheet formed discontinuous harakeke and hemp fibre mat reinforced PLA composites for structural applications.* Industrial Crops and Products, 2016. **84**: p. 139-150.
28. Pickering, K.L. and T.M. Le, *High performance aligned short natural fibre–epoxy composites.* Composites Part B: Engineering, 2016. **85**: p. 123-129.
29. Kabir, M., et al., *Chemical treatments on plant-based natural fibre reinforced polymer composites: An overview.* Composites Part B: Engineering, 2012. **43**(7): p. 2883-2892.
30. Islam, M., K. Pickering, and N. Foreman, *Influence of alkali treatment on the interfacial and physico-mechanical properties of industrial hemp fibre reinforced polylactic acid composites.* Composites Part A: Applied Science and Manufacturing, 2010. **41**(5): p. 596-603.
31. Efendy, M.A. and K. Pickering, *Comparison of harakeke with hemp fibre as a potential reinforcement in composites.* Composites Part A: Applied Science and Manufacturing, 2014. **67**: p. 259-267.
32. Efendy, M.A. and K. Pickering, *Comparison of strength and Young modulus of aligned discontinuous fibre PLA composites obtained experimentally and from theoretical prediction models.* Composite Structures, 2019. **208**: p. 566-573.
33. Efendy, M.A. and K.L. Pickering, *Fibre orientation of novel dynamically sheet formed discontinuous natural fibre PLA composites.* Composites Part A: Applied Science and Manufacturing, 2016. **90**: p. 82-89.
34. Le, T.M. and K.L. Pickering, *The potential of harakeke fibre as reinforcement in polymer matrix composites including modelling of long harakeke fibre composite strength.* Composites Part A: Applied Science and Manufacturing, 2015. **76**: p. 44-53.

35. Islam, M.S., *The influence of fibre processing and treatments on hemp fibre/epoxy and hemp fibre/PLA composites*. 2008, the University of Waikato.
36. Le, T.M., *Harakeke fibre as reinforcement in epoxy matrix composites and its hybridisation with hemp fibre*. 2016, University of Waikato.
37. Lundell, F., L.D. Söderberg, and P.H. Alfredsson, *Fluid mechanics of papermaking.* Annual Review of Fluid Mechanics, 2011. **43**: p. 195-217.
38. Cui, H. and J.R. Grace, *Flow of pulp fibre suspension and slurries: A review.* International Journal of Multiphase Flow, 2007. **33**(9): p. 921-934.
39. Carlsson, A., F. Lundell, and L.D. Söderberg, *Fiber orientation control related to papermaking.* Journal of fluids engineering, 2007. **129**(4): p. 457-465.
40. Bagg, G.E.G., et al., *Process for the manufacture of a composite material having aligned reinforcing fibers*. 1971, Google Patents.
41. Bagg, G.E.G., et al., *Manufacture of composite materials*. 1977, Google Patents.
42. Zafeiropoulos, N., et al., *Engineering and characterisation of the interface in flax fibre/polypropylene composite materials. Part I. Development and investigation of surface treatments.* Composites part A: applied science and manufacturing, 2002. **33**(8): p. 1083-1093.
43. Li, X., L.G. Tabil, and S. Panigrahi, *Chemical treatments of natural fiber for use in natural fiber-reinforced composites: a review.* Journal of Polymers and the Environment, 2007. **15**(1): p. 25-33.
44. Bledzki, A. and J. Gassan, *Composites reinforced with cellulose based fibres.* Progress in polymer science, 1999. **24**(2): p. 221-274.
45. Stamboulis, A., et al., *Environmental durability of flax fibres and their composites based on polypropylene matrix.* Applied Composite Materials, 2000. **7**(5-6): p. 273-294.
46. Mohammed, L., et al., *A review on natural fiber reinforced polymer composite and its applications.* International Journal of Polymer Science, 2015. **2015**.
47. Ho, M.-p., et al., *Critical factors on manufacturing processes of natural fibre composites.* Composites Part B: Engineering, 2012. **43**(8): p. 3549-3562.
48. Piotrowski, S. and M. Carus, *Ecological benefits of hemp and flax cultivation and products.* Nova institute, 2011. **5**: p. 1-6.
49. Thomsen, A.B., et al., *Hemp raw materials: The effect of cultivar, growth conditions and pretreatment on the chemical composition of the fibres*. 2005.
50. Islam, M.S., K.L. Pickering, and N.J. Foreman, *Influence of alkali fiber treatment and fiber processing on the mechanical properties of hemp/epoxy composites.* Journal of Applied Polymer Science, 2011. **119**(6): p. 3696-3707.
51. Saheb, D.N. and J. Jog, *Natural fiber polymer composites: a review.* Advances in polymer technology, 1999. **18**(4): p. 351-363.
52. Wang, B., et al., *Pre-treatment of flax fibers for use in rotationally molded biocomposites.* Journal of reinforced plastics and composites, 2007. **26**(5): p. 447-463.
53. Azwa, Z., et al., *A review on the degradability of polymeric composites based on natural fibres.* Materials & Design, 2013. **47**: p. 424-442.
54. Beckermann, G., *Performance of Hemp-Fibre Reinforced Polypropylene Composite Materials*. 2007, University of Waikato

The University of Waikato: Hamilton, New Zealand.

55. La Mantia, F. and M. Morreale, *Green composites: A brief review*. Composites Part A: Applied Science and Manufacturing, 2011. **42**(6): p. 579-588.
56. Van de Velde, K. and P. Kiekens, *Thermoplastic pultrusion of natural fibre reinforced composites.* Composite structures, 2001. **54**(2): p. 355-360.
57. Rodríguez, E., et al., *Characterization of composites based on natural and glass fibers obtained by vacuum infusion.* Journal of composite materials, 2005. **39**(3): p. 265-282.
58. Puglia, D., et al., *Thermal and mechanical characterisation of Phormium tenax-reinforced polypropylene composites.* Journal of Thermoplastic Composite Materials, 2013: p. 0892705712473629.
59. Holbery, J. and D. Houston, *Natural-fiber-reinforced polymer composites in automotive applications.* Jom, 2006. **58**(11): p. 80-86.
60. Broda, J., et al., *Formation and properties of polypropylene/stearic acid composite fibers.* Textile Research Journal, 2016. **86**(1): p. 64-71.
61. Shahzad, A., *Hemp fiber and its composites–a review.* Journal of Composite Materials, 2012. **46**(8): p. 973-986.
62. Harper, L., et al., *Fiber alignment in directed carbon fiber preforms–a feasibility study.* Journal of Composite Materials, 2008.
63. Vyakarnam, M.N. and L.T. Drzal, *Composite material of aligned discontinuous fibers*. 2000, Google Patents.
64. Yu, H., K. Potter, and M. Wisnom, *A novel manufacturing method for aligned discontinuous fibre composites (High Performance-Discontinuous Fibre method).* Composites Part A: Applied Science and Manufacturing, 2014. **65**: p. 175-185.
65. SUCH, M., C. WARD, and K. POTTER, *Aligned discontinuous fibre composites: a short history.* Journal of Multifunctional Composites, 2014. **2**(3).
66. Bagg, G., M. Evans, and A. Pryde, *The glycerine process for the alignment of fibres and whiskers.* Composites, 1969. **1**(2): p. 97-100.
67. Ericson, M.L. and L.A. Berglund, *Processing and mechanical properties of orientated preformed glass-mat-reinforced thermoplastics.* Composites science and technology, 1993. **49**(2): p. 121-130.
68. *Method and apparatus for separating, aligning, and collecting fibers from a fibrous mass*. 1970, Google Patents.
69. Parratt, N., *Whisker alignment by the alginate process.* Composites, 1969. **1**(1): p. 25-27.
70. Bagg, G.E.G., et al., *Aligning fibres*. 1976, Google Patents.
71. Flemming, T., G. Kress, and M. Flemming, *A new aligned short-carbon-fiber-reinforced thermoplastic prepreg.* Advanced Composite Materials, 1996. **5**(2): p. 151-159.
72. RICHTER, H., *Single fiber and hybrid composites with aligned discontinuous fibres in polymer matrix.* Advances in composite materials, 1980: p. 387-398.
73. Pickering, K. and T.M. Le, *High performance aligned short natural fibre–Epoxy composites.* Composites Part B: Engineering, 2016. **85**: p. 123-129.
74. Carlsson, A., *Near wall fibre orientation in flowing suspensions*. 2009, KTH.
75. Thorp, B.A., *Paper Machine Operations.* Atlanta (third edition): TAPPI Press, 1991: p. 601.
76. Olson, J.A., et al., *Modeling a turbulent fibre suspension flowing in a planar contraction: The one-dimensional headbox.* International Journal of Multiphase Flow, 2004. **30**(1): p. 51-66.

77. Atkins, M.J., *Axial variations and entry effects in a pressure screen*. 2007, The University of Waikato.
78. Duffy, G.G., G. Longdill, and P. Lee, *High-consistency flow of pulp suspensions in pipes.* Tappi [Technical Association of the Pulp and Paper Industry](USA), 1978.
79. Jeffery, G.B., *The motion of ellipsoidal particles immersed in a viscous fluid.* Proceedings of the Royal Society of London. Series A, Containing papers of a mathematical and physical character, 1922. **102**(715): p. 161-179.
80. Joung, C., N. Phan-Thien, and X. Fan, *Direct simulation of flexible fibers.* Journal of non-newtonian fluid mechanics, 2001. **99**(1): p. 1-36.
81. Allan, P., et al., *Shear controlled orientation technology for the management of reinforcing fibres in moulded and extruded composite materials.* Journal of materials processing technology, 1996. **56**(1): p. 272-281.
82. Papathanasiou, T. and D.C. Guell, *Flow induced alignment in composite materials*. 1997: Woodhead publishing.
83. A. Carlsson, L.D.S., and F. Lundell, *Fibre orientation near a wall of a headbox.* Nordic Pulp & Paper Research Journal, 2010. **vol. 25**: p. pp. 204–212.
84. Petrie, C.J., *The rheology of fibre suspensions.* Journal of Non-Newtonian Fluid Mechanics, 1999. **87**(2-3): p. 369-402.
85. Bandhakavi, V.S.S. and C.K. Aidun, *Analysis of turbulent flow in the converging zone of a headbox.* 1999.
86. Lin, J., X. Shi, and Z. Yu, *The motion of fibers in an evolving mixing layer.* International Journal of Multiphase Flow, 2003. **8**(29): p. 1355-1372.
87. Njobuenwu, D.O. and M. Fairweather, *Simulation of inertial fibre orientation in turbulent flow.* Physics of Fluids, 2016. **28**(6): p. 063307.
88. Scholz, M.-S., B. Drinkwater, and R. Trask, *Ultrasonic assembly of anisotropic short fibre reinforced composites.* Ultrasonics, 2014. **54**(4): p. 1015-1019.
89. Joseph, P., K. Joseph, and S. Thomas, *Effect of processing variables on the mechanical properties of sisal-fiber-reinforced polypropylene composites.* Composites science and Technology, 1999. **59**(11): p. 1625-1640.
90. Kalsoom, U., P.N. Nesterenko, and B. Paull, *Recent developments in 3D printable composite materials.* RSC Advances, 2016. **6**(65): p. 60355-60371.
91. Tekinalp, H.L., et al., *Highly oriented carbon fiber–polymer composites via additive manufacturing.* Composites Science and Technology, 2014. **105**: p. 144-150.
92. Stoof, D., K. Pickering, and Y. Zhang, *Fused deposition modelling of natural fibre/polylactic acid composites.* Journal of Composites Science, 2017. **1**(1): p. 8.
93. Leong, Y., et al., *Compression and injection molding techniques for natural fiber composites.* Nat Fibre Compos, 2014: p. 216-232.
94. Cristaldi, G., et al., *Composites based on natural fibre fabrics.* Woven fabric engineering, 2010. **17**: p. 317-342.
95. Kalaprasad, G., et al., *Effect of fibre length and chemical modifications on the tensile properties of intimately mixed short sisal/glass hybrid fibre reinforced low density polyethylene composites.* Polymer international, 2004. **53**(11): p. 1624-1638.
96. Madsen, B. and H. Lilholt, *Physical and mechanical properties of unidirectional plant fibre composites—an evaluation of the influence of porosity.* Composites Science and Technology, 2003. **63**(9): p. 1265-1272.

97. Sawpan, M.A., K.L. Pickering, and A. Fernyhough, *Effect of various chemical treatments on the fibre structure and tensile properties of industrial hemp fibres.* Composites Part A: Applied Science and Manufacturing, 2011. **42**(8): p. 888-895.
98. Beckermann, G. and K.L. Pickering, *Engineering and evaluation of hemp fibre reinforced polypropylene composites: fibre treatment and matrix modification.* Composites Part A: Applied Science and Manufacturing, 2008. **39**(6): p. 979-988.
99. Pickering, K.L., et al., *Interfacial modification of hemp fiber reinforced composites using fungal and alkali treatment.* Journal of Biobased Materials and Bioenergy, 2007. **1**(1): p. 109-117.
100. Drzal, L.T., *Interfaces and interphases.* Composites, AMS Handbook, 2001: p. 169-179.
101. Ragoubi, M., et al., *Impact of corona treated hemp fibres onto mechanical properties of polypropylene composites made thereof.* Industrial Crops and Products, 2010. **31**(2): p. 344-349.
102. Ragoubi, M., et al., *Effect of corona discharge treatment on mechanical and thermal properties of composites based on miscanthus fibres and polylactic acid or polypropylene matrix.* Composites Part A: Applied Science and Manufacturing, 2012. **43**(4): p. 675-685.
103. John, M.J. and R.D. Anandjiwala, *Recent developments in chemical modification and characterization of natural fiber‐reinforced composites.* Polymer composites, 2008. **29**(2): p. 187-207.
104. Panaitescu, D.M., et al., *Influence of hemp fibers with modified surface on polypropylene composites.* Journal of Industrial and Engineering Chemistry, 2016. **37**: p. 137-146.
105. De Rosa, I.M., et al., *Tensile behavior of New Zealand flax (Phormium tenax) fibers.* Journal of Reinforced Plastics and Composites, 2010.
106. Kabir, M., et al., *Effects of chemical treatments on hemp fibre structure.* Applied Surface Science, 2013. **276**: p. 13-23.
107. Oushabi, A., et al., *The effect of alkali treatment on mechanical, morphological and thermal properties of date palm fibers (DPFs): Study of the interface of DPF–Polyurethane composite.* South African Journal of Chemical Engineering, 2017. **23**: p. 116-123.
108. Mishra, S., et al., *Studies on mechanical performance of biofibre/glass reinforced polyester hybrid composites.* Composites Science and Technology, 2003. **63**(10): p. 1377-1385.
109. Mohanty, S., et al., *Effect of MAPP as coupling agent on the performance of sisal–PP composites.* Journal of reinforced plastics and composites, 2004. **23**(18): p. 2047-2063.
110. Mwaikambo, L.Y., N. Tucker, and A.J. Clark, *Mechanical Properties of Hemp‐Fibre‐Reinforced Euphorbia Composites.* Macromolecular Materials and Engineering, 2007. **292**(9): p. 993-1000.
111. Kabir, M., et al., *Tensile properties of chemically treated hemp fibres as reinforcement for composites.* Composites Part B: Engineering, 2013. **53**: p. 362-368.
112. Sreekala, M., et al., *Oil palm fibre reinforced phenol formaldehyde composites: influence of fibre surface modifications on the mechanical performance.* Applied Composite Materials, 2000. **7**(5-6): p. 295-329.
113. Bledzki, A., et al., *The effects of acetylation on properties of flax fibre and its polypropylene composites.* Express Polymer Letters, 2008. **2**(6): p. 413-422.

114. Xie, Y., et al., *Silane coupling agents used for natural fiber/polymer composites: A review*. Composites Part A: Applied Science and Manufacturing, 2010. **41**(7): p. 806-819.
115. Hong, C., et al., *Mechanical properties of silanized jute–polypropylene composites.* Journal of Industrial and Engineering Chemistry, 2008. **14**(1): p. 71-76.
116. Zafeiropoulos, N., C. Baillie, and J. Hodgkinson, *Engineering and characterisation of the interface in flax fibre/polypropylene composite materials. Part II. The effect of surface treatments on the interface.* Composites Part A: Applied Science and Manufacturing, 2002. **33**(9): p. 1185-1190.
117. Zafeiropoulos, N., et al., *An experimental investigation of modified and unmodified flax fibres with XPS, ToF-SIMS and ATR-FTIR.* Journal of Materials Science, 2003. **38**(19): p. 3903-3914.
118. Torres, F. and M. Cubillas, *Study of the interfacial properties of natural fibre reinforced polyethylene.* Polymer Testing, 2005. **24**(6): p. 694-698.
119. Binias, D., W. Binias, and J. Broda, *Formation of polypropylene/stearic acid fibers.* Journal of Applied Polymer Science, 2012. **125**(2): p. 1020-1026.
120. Torres, F. and R. Diaz, *Morphological Characterisation of Natural Fibre Reinforced Thermoplastics(NFRTP) Processed by Extrusion, Compression and Rotational Moulding.* Polymers and Polymer Composites, 2004. **12**(8): p. 705-718.
121. Paul, S.A., et al., *The role of interface modification on thermal degradation and crystallization behavior of composites from commingled polypropylene fiber and banana fiber.* Polymer Composites, 2010. **31**(6): p. 1113-1123.
122. Ross, P., R. Mayer, and M. Benziman, *Cellulose biosynthesis and function in bacteria.* Microbiology and Molecular Biology Reviews, 1991. **55**(1): p. 35-58.
123. Kim, J.-H., et al., *Review of nanocellulose for sustainable future materials.* International Journal of Precision Engineering and Manufacturing-Green Technology, 2015. **2**(2): p. 197-213.
124. Oksman, K., et al., *Review of the recent developments in cellulose nanocomposite processing.* Composites Part A: Applied Science and Manufacturing, 2016. **83**: p. 2-18.
125. Chakrabarty, A. and Y. Teramoto, *Recent advances in nanocellulose composites with polymers: A guide for choosing partners and How to incorporate them.* Polymers, 2018. **10**(5): p. 517.
126. Hubbe, M.A., et al., *Nanocellulose in thin films, coatings, and plies for packaging applications: A review.* BioResources, 2017. **12**(1): p. 2143-2233.
127. Juntaro, J., et al., *Nanocellulose enhanced interfaces in truly green unidirectional fibre reinforced composites.* Composite Interfaces, 2007. **14**(7-9): p. 753-762.
128. Xu, X., et al., *Cellulose nanocrystals vs. cellulose nanofibrils: a comparative study on their microstructures and effects as polymer reinforcing agents.* ACS applied materials & interfaces, 2013. **5**(8): p. 2999-3009.
129. Lee, K.-Y., et al., *Hierarchical composites reinforced with robust short sisal fibre preforms utilising bacterial cellulose as binder.* Composites Science and Technology, 2012. **72**(13): p. 1479-1486.
130. Fortea-Verdejo, M., et al., *Upgrading flax nonwovens: Nanocellulose as binder to produce rigid and robust flax fibre preforms.* Composites Part A: Applied Science and Manufacturing, 2016. **83**: p. 63-71.

131. Lee, K.-Y., et al., *On the use of nanocellulose as reinforcement in polymer matrix composites.* Composites Science and Technology, 2014. **105**: p. 15-27.
132. Pickering, K., et al., *Optimising industrial hemp fibre for composites.* Composites Part A: Applied Science and Manufacturing, 2007. **38**(2): p. 461-468.
133. Enomae, T., Y. Han, and A. Isogai, *Fiber orientation distribution of paper surface calculated by image analysis.* TIANJIN KEJI DAXUE XUEBAO, 2004. **19**: p. 51.
134. Bernasconi, A., F. Cosmi, and P. Hine, *Analysis of fibre orientation distribution in short fibre reinforced polymers: A comparison between optical and tomographic methods.* Composites Science and Technology, 2012. **72**(16): p. 2002-2008.
135. Sun, X., et al., *Measurement and quantitative analysis of fiber orientation distribution in long fiber reinforced part by injection molding.* Polymer Testing, 2015. **42**: p. 168-174.
136. Xue, D., M. Miao, and H. Hu, *Permeability anisotropy of flax nonwoven mats in vacuum‐assisted resin transfer molding.* The Journal of The Textile Institute, 2011. **102**(7): p. 612-620.
137. Schneider, C.A., W.S. Rasband, and K.W. Eliceiri, *NIH Image to ImageJ: 25 years of image analysis.* Nature methods, 2012. **9**(7): p. 671-675.
138. Shah, D.U., et al., *The biocomposite tube of a chaetopterid marine worm constructed with highly-controlled orientation of nanofilaments.* Materials Science and Engineering: C, 2015. **48**: p. 408-415.
139. Rezakhaniha, R., et al., *Experimental investigation of collagen waviness and orientation in the arterial adventitia using confocal laser scanning microscopy.* Biomechanics and modeling in mechanobiology, 2012. **11**(3-4): p. 461-473.
140. Gesellchen, F., et al., *Cell patterning with a heptagon acoustic tweezer–application in neurite guidance.* Lab on a Chip, 2014. **14**(13): p. 2266-2275.
141. Torres-Rendon, J.G., et al., *Mechanical performance of macrofibers of cellulose and chitin nanofibrils aligned by wet-stretching: a critical comparison.* Biomacromolecules, 2014. **15**(7): p. 2709-2717.
142. Dri, F.L., et al., *Anisotropy of the elastic properties of crystalline cellulose I β from first principles density functional theory with Van der Waals interactions.* Cellulose, 2013. **20**(6): p. 2703-2718.
143. Siqueira, G., et al., *Cellulose nanocrystal inks for 3D printing of textured cellular architectures.* Advanced Functional Materials, 2017. **27**(12).
144. Tabet, T.A. and F.A. Aziz, *Cellulose microfibril angle in wood and its dynamic mechanical significance*, in *Cellulose-Fundamental Aspects*. 2013, InTech.
145. Sigalov, G.M., et al., *Method of effective ellipses for digital image analysis of size, shape, orientation, and interparticle distances in polymer blends: application to a study of polyamide 6/polysulfone reactive blending.* Macromolecules, 1997. **30**(25): p. 7759-7767.
146. Püspöki, Z., et al., *Transforms and operators for directional bioimage analysis: a survey*, in *Focus on Bio-Image Informatics*. 2016, Springer. p. 69-93.
147. Kim, S.H., C.M. Lee, and K. Kafle, *Characterization of crystalline cellulose in biomass: basic principles, applications, and limitations of XRD, NMR, IR, Raman, and SFG.* Korean Journal of Chemical Engineering, 2013. **30**(12): p. 2127-2141.

148. Fuchs, C., et al., *Application of Halpin–Tsai equation to microfibril reinforced polypropylene/poly (ethylene terephthalate) composites.* Composite Interfaces, 2006. **13**(4-6): p. 331-344.
149. Landel, R.F. and L.E. Nielsen, *Mechanical properties of polymers and composites*. 1993: CRC press.
150. Krenchel, H., *Fibre reinforcement; theoretical and practical investigations of the elasticity and strength of fibre-reinforced materials.* 1964.
151. Sanadi, A. and M. Piggott, *Interfacial effects in carbon-epoxies.* Journal of materials Science, 1985. **20**(2): p. 421-430.
152. Khalil, H.A., et al., *The effect of acetylation on interfacial shear strength between plant fibres and various matrices.* European Polymer Journal, 2001. **37**(5): p. 1037-1045.
153. Vallejos, M., et al., *Micromechanics of hemp strands in polypropylene composites.* Composites Science and Technology, 2012. **72**(10): p. 1209-1213.
154. Thomason, J., *Micromechanical parameters from macromechanical measurements on glass reinforced polyamide 6, 6.* Composites Science and Technology, 2001. **61**(14): p. 2007-2016.
155. Bernasconi, A., D. Rossin, and C. Armanni, *Analysis of the effect of mechanical recycling upon tensile strength of a short glass fibre reinforced polyamide 6, 6.* Engineering fracture mechanics, 2007. **74**(4): p. 627-641.
156. Beckermann, G., K.J.C.P.A.A.S. Pickering, and Manufacturing, *Engineering and evaluation of hemp fibre reinforced polypropylene composites: Micro-mechanics and strength prediction modelling.* 2009. **40**(2): p. 210-217.
157. Taha, I., L. Steuernagel, and G. Ziegmann, *Optimization of the alkali treatment process of date palm fibres for polymeric composites.* Composite Interfaces, 2007. **14**(7-9): p. 669-684.
158. ASTM, D., *3379-75.* Standard Test Method for Tensile Strength and Young's Modulus for High-Modulus Single-Filament Materials, Annual Book of ASTM Standards,(May 1989), 1986. **8**: p. 128-131.
159. Biagiotti, J., et al., *A systematic investigation on the influence of the chemical treatment of natural fibers on the properties of their polymer matrix composites.* Polymer Composites, 2004. **25**(5): p. 470-479.
160. Zafeiropoulos, N. and C. Baillie, *A study of the effect of surface treatments on the tensile strength of flax fibres: Part II. Application of Weibull statistics.* Composites Part A: Applied Science and Manufacturing, 2007. **38**(2): p. 629-638.
161. Segal, L., et al., *An empirical method for estimating the degree of crystallinity of native cellulose using the X-ray diffractometer.* Textile research journal, 1959. **29**(10): p. 786-794.
162. Roy, A., et al., *Improvement in mechanical properties of jute fibres through mild alkali treatment as demonstrated by utilisation of the Weibull distribution model.* Bioresource technology, 2012. **107**: p. 222-228.
163. Mwaikambo, L.Y. and M.P. Ansell, *Chemical modification of hemp, sisal, jute, and kapok fibers by alkalization.* Journal of applied polymer science, 2002. **84**(12): p. 2222-2234.
164. Ouajai, S. and R. Shanks, *Composition, structure and thermal degradation of hemp cellulose after chemical treatments.* Polymer degradation and stability, 2005. **89**(2): p. 327-335.
165. Knill, C.J. and J.F. Kennedy, *Degradation of cellulose under alkaline conditions.* Carbohydrate Polymers, 2003. **51**(3): p. 281-300.

166. Abraham, E., et al., *Extraction of nanocellulose fibrils from lignocellulosic fibres: a novel approach.* Carbohydrate Polymers, 2011. **86**(4): p. 1468-1475.
167. Chen, W., et al., *Individualization of cellulose nanofibers from wood using high-intensity ultrasonication combined with chemical pretreatments.* Carbohydrate Polymers, 2011. **83**(4): p. 1804-1811.
168. Peng, F., et al., *Comparative study of hemicelluloses obtained by graded ethanol precipitation from sugarcane bagasse.* Journal of agricultural and food chemistry, 2009. **57**(14): p. 6305-6317.
169. Li, Y. and K.L. Pickering, *Hemp fibre reinforced composites using chelator and enzyme treatments.* Composites Science and Technology, 2008. **68**(15): p. 3293-3298.
170. Olsson, A.-M. and L. Salmén, *The association of water to cellulose and hemicellulose in paper examined by FTIR spectroscopy.* Carbohydrate research, 2004. **339**(4): p. 813-818.
171. Le Troedec, M., et al., *Influence of various chemical treatments on the composition and structure of hemp fibres.* Composites Part A: Applied Science and Manufacturing, 2008. **39**(3): p. 514-522.
172. Sun, R., J. Tomkinson, and G.L. Jones, *Fractional characterization of ash-AQ lignin by successive extraction with organic solvents from oil palm EFB fibre.* Polymer Degradation and Stability, 2000. **68**(1): p. 111-119.
173. Methacanon, P., et al., *Properties and potential application of the selected natural fibers as limited life geotextiles.* Carbohydrate Polymers, 2010. **82**(4): p. 1090-1096.
174. Dahiya, J. and S. Rana, *Thermal degradation and morphological studies on cotton cellulose modified with various arylphosphorodichloridites.* Polymer International, 2004. **53**(7): p. 995-1002.
175. Abràmoff, M.D., P.J. Magalhães, and S.J. Ram, *Image processing with ImageJ.* Biophotonics international, 2004. **11**(7): p. 36-42.
176. Yoshiharu, N., et al., *Cellulose microcrystal film of high uniaxial orientation.* Macromolecules, 1997. **30**(20): p. 6395-6397.
177. Kostic, M.M. and L.G. Reifschneider, *Design of extrusion dies.* Encyclopedia of chemical processing, 2006. **10**: p. 633-649.
178. Lewis, D.D.J., *Interlaminar reinforcement of carbon fiber composites from unidirectional prepreg utilizing aligned carbon nanotubes*. 2016, Massachusetts Institute of Technology.
179. Palmieri, V., et al., *Mechanical and structural comparison between primary tumor and lymph node metastasis cells in colorectal cancer.* Soft matter, 2015. **11**(28): p. 5719-5726.
180. Reddy, A.N.K. and D.K. Sagar, *Half-width at half-maximum, full-width at half-maximum analysis for resolution of asymmetrically apodized optical systems with slit apertures.* Pramana, 2015. **84**(1): p. 117-126.
181. Baghaei, B., et al., *Novel aligned hemp fibre reinforcement for structural biocomposites: Porosity, water absorption, mechanical performances and viscoelastic behaviour.* Composites Part A: Applied Science and Manufacturing, 2014. **61**: p. 1-12.
182. Lamour, G., et al., *Contact angle measurements using a simplified experimental setup.* Journal of chemical education, 2010. **87**(12): p. 1403-1407.
183. John, M.J., et al., *Effect of chemical modification on properties of hybrid fiber biocomposites.* Composites Part A: Applied Science and Manufacturing, 2008. **39**(2): p. 352-363.

184. Hernández, Y., et al., *Stearic acid as interface modifier and lubricant agent of the system: Polypropylene/calcium carbonate nanoparticles.* Polymer Engineering & Science, 2019. **59**(s2): p. E279-E285.
185. Zeng, Y.-X., et al., *Preparation and enhancement of thermal conductivity of heat transfer oil-based MoS 2 nanofluids.* Journal of Nanomaterials, 2013. **2013**: p. 3.
186. Huang, L., et al., *Preparation and mechanical properties of modified nanocellulose/PLA composites from cassava residue.* AIP Advances, 2018. **8**(2): p. 025116.
187. Conceição, I.D.d., et al., *Investigation of the Wettability Using Contact Angle Measurements of Green Polyethylene Flat Films and Expanded Vermiculite Clay Treated by Plasma.* Materials Research, 2019. **22**.
188. Zafeiropoulos, N., C. Baillie, and F. Matthews, *A study of the effect of surface treatments on the thermal stability of flax fibres.* Advanced Composites Letters, 2000. **9**(4): p. 096369350000900405.
189. Dányádi, L., J. Móczó, and B. Pukánszky, *Effect of various surface modifications of wood flour on the properties of PP/wood composites.* Composites Part A: Applied Science and Manufacturing, 2010. **41**(2): p. 199-206.
190. Raj, R., et al., *Compounding of cellulose fibers with polypropylene: Effect of fiber treatment on dispersion in the polymer matirx.* Journal of applied polymer science, 1989. **38**(11): p. 1987-1996.
191. Rachini, A., et al., *Comparison of the thermal degradation of natural, alkali‐treated and silane‐treated hemp fibers under air and an inert atmosphere.* Journal of applied polymer science, 2009. **112**(1): p. 226-234.
192. Mofokeng, J.P., et al., *Comparison of injection moulded, natural fibre-reinforced composites with PP and PLA as matrices.* Journal of Thermoplastic Composite Materials, 2012. **25**(8): p. 927-948.
193. Niu, P., et al., *Study on mechanical properties and thermal stability of polypropylene/hemp fiber composites.* Journal of Reinforced Plastics and Composites, 2011. **30**(1): p. 36-44.
194. Bhattacharya, A., J.W. Rawlins, and P. Ray, *Polymer grafting and crosslinking*. 2008: John Wiley & Sons.
195. Jacob, M., S. Thomas, and K. Varughese, *Novel woven sisal fabric reinforced natural rubber composites: tensile and swelling characteristics.* Journal of Composite Materials, 2006. **40**(16): p. 1471-1485.
196. Bardet, R., et al., *Engineered pigments based on iridescent cellulose nanocrystal films.* Carbohydrate polymers, 2015. **122**: p. 367-375.
197. Lee, K.-Y., *Nanocellulose and sustainability: production, properties, applications, and case studies*. 2018: CRC Press.
198. Jordan, J.H., M.W. Easson, and B.D. Condon, *Alkali Hydrolysis of Sulfated Cellulose Nanocrystals: Optimization of Reaction Conditions and Tailored Surface Charge.* Nanomaterials, 2019. **9**(9): p. 1232.
199. Jativa, F., et al., *Confined self-assembly of cellulose nanocrystals in a shrinking droplet.* Soft Matter, 2015. **11**(26): p. 5374-5380.
200. Chieng, B., et al., *Isolation and characterization of cellulose nanocrystals from oil palm mesocarp fiber.* Polymers, 2017. **9**(8): p. 355.
201. Das, D., et al., *STUDIES ON CELLULOSE NANOCRYSTALS EXTRACTED FROM MUSA SAPIENTUM: STRUCTURAL AND BONDING ASPECTS.* CELLULOSE CHEMISTRY AND TECHNOLOGY, 2018. **52**(9-10): p. 729-739.

202. Gu, J., et al., *Isolation of cellulose nanocrystals from medium density fiberboards.* Carbohydrate polymers, 2017. **167**: p. 70-78.
203. Jonoobi, M., et al., *Characteristics of cellulose nanofibers isolated from rubberwood and empty fruit bunches of oil palm using chemo-mechanical process.* Cellulose, 2011. **18**(4): p. 1085-1095.
204. Ciolacu, D., F. Ciolacu, and V.I. Popa, *Amorphous cellulose—structure and characterization.* Cellulose chemistry and technology, 2011. **45**(1): p. 13.
205. Alemdar, A. and M. Sain, *Isolation and characterization of nanofibers from agricultural residues–Wheat straw and soy hulls.* Bioresource technology, 2008. **99**(6): p. 1664-1671.
206. Niu, F., et al., *The characteristic and dispersion stability of nanocellulose produced by mixed acid hydrolysis and ultrasonic assistance.* Carbohydrate polymers, 2017. **165**: p. 197-204.
207. Wei, B., et al., *Surface chemical compositions and dispersity of starch nanocrystals formed by sulfuric and hydrochloric acid hydrolysis.* PloS one, 2014. **9**(2): p. e86024.
208. Ng, H.-M., et al., *Extraction of cellulose nanocrystals from plant sources for application as reinforcing agent in polymers.* Composites Part B: Engineering, 2015. **75**: p. 176-200.
209. Beck, S. and J. Bouchard, *Auto-catalyzed acidic desulfation of cellulose nanocrystals.* Nordic Pulp & Paper Research Journal, 2014. **29**(1): p. 6-14.
210. Agarwal, U.P., *Raman spectroscopy of CNC-and CNF-based nanocomposites.* In: Handbook of Nanocellulose and Cellulose Nanocomposites. John Wiley & Sons: 609-625. Chapter 18., 2017: p. 609-625.
211. Xu, J., et al., *A nitrogen–sulfur co-doped porous graphene matrix as a sulfur immobilizer for high performance lithium–sulfur batteries.* Journal of Materials Chemistry A, 2016. **4**(44): p. 17381-17393.
212. Börjesson, M., et al., *Increased thermal stability of nanocellulose composites by functionalization of the sulfate groups on cellulose nanocrystals with azetidinium ions.* Journal of Applied Polymer Science, 2018. **135**(10): p. 45963.
213. Dai, D., M. Fan, and P. Collins, *Fabrication of nanocelluloses from hemp fibers and their application for the reinforcement of hemp fibers.* Industrial crops and products, 2013. **44**: p. 192-199.
214. Guhados, G., W. Wan, and J.L. Hutter, *Measurement of the elastic modulus of single bacterial cellulose fibers using atomic force microscopy.* Langmuir, 2005. **21**(14): p. 6642-6646.
215. Herrera-Franco, P. and A. Valadez-Gonzalez, *A study of the mechanical properties of short natural-fiber reinforced composites.* Composites Part B: Engineering, 2005. **36**(8): p. 597-608.
216. Papirer, E., et al., *Inverse gas chromatography investigation of the surface properties of cellulose.* Journal of adhesion science and technology, 2000. **14**(3): p. 321-337.
217. Heng, J.Y., et al., *Methods to determine surface energies of natural fibres: a review.* Composite Interfaces, 2007. **14**(7-9): p. 581-604.
218. Sawpan, M.A., K.L. Pickering, and A. Fernyhough, *Effect of fibre treatments on interfacial shear strength of hemp fibre reinforced polylactide and unsaturated polyester composites.* Composites Part A: Applied Science and Manufacturing, 2011. **42**(9): p. 1189-1196.

219. Kelly, A. and a.W. Tyson, *Tensile properties of fibre-reinforced metals: copper/tungsten and copper/molybdenum.* Journal of the Mechanics and Physics of Solids, 1965. **13**(6): p. 329-350.
220. Beg, M.D.H., *The improvement of interfacial bonding, weathering and recycling of wood fibre reinforced polypropylene composites*. 2007, The University of Waikato.
221. Stamboulis, A., C. Baillie, and E. Schulz, *Interfacial characterisation of flax fibre - thermoplastic polymer composites by the pull - out test.* Die Angewandte Makromolekulare Chemie, 1999. **272**(1): p. 117-120.
222. Awal, A., et al., *Interfacial studies of natural fibre/polypropylene composites using single fibre fragmentation test (SFFT).* Composites Part A: Applied Science and Manufacturing, 2011. **42**(1): p. 50-56.
223. Van Hattum, F. and C. Bernardo, *A model to predict the strength of short fiber composites.* Polymer composites, 1999. **20**(4): p. 524-533.
224. Garkhail, S., R. Heijenrath, and T. Peijs, *Mechanical properties of natural-fibre-mat-reinforced thermoplastics based on flax fibres and polypropylene.* Applied Composite Materials, 2000. **7**(5-6): p. 351-372.
225. Sawpan, M.A., *Mechanical performance of industrial hemp fibre reinforced polylactide and unsaturated polyester composites*. 2010, The University of Waikato.
226. Tserki, V., et al., *A study of the effect of acetylation and propionylation surface treatments on natural fibres.* Composites Part A: applied science and manufacturing, 2005. **36**(8): p. 1110-1118.